Tracking the immune changes in children with cancer and multisystem inflammatory syndrome

By Dr Eleni Syrimi

A thesis submitted to the University of Birmingham for the degree of

DOCTOR OF PHILOSOPHY

Institute of Immunology and Immunotherapy

College of Medical and Dental Sciences

University of Birmingham

September 2021

Abstract

How cancer affects the immune system of children, which is different to adults, is unclear and has not been described systematically. Immune-modulating therapies are proving promising novel therapeutic options in adult cancers but their use in paediatric cancers remains limited. A better understanding of the immune system is needed in order to target the right pathways and optimise immunotherapeutic approaches.

Furthermore, the new virus (SARS-CoV2) has led to the development of a novel disease occurring only in children, called multisystem inflammatory syndrome in children (MIS-C). This disease shares many similarities with different inflammatory paediatric conditions (such as Kawasaki Disease (KD) but also many differences. Identifying the immunological changes occurring in MIS-C patients and how these relate to other paediatric inflammatory conditions is important both to understand the pathogenesis of this new disease and inform rational treatment selection.

Through this study, novel NK pathways have been identified in paediatric cancer patients that can potentially be targeted as well as potential new biomarkers. In MIS-C patients a hyper-inflammation state, with activation of both innate and adaptive immunity, was identified. Treatment with intravenous immunoglobulin (IVIG, standard care) administration led to multiple anti-inflammatory changes including the expansion of CD163+ monocytes and production of arginase.

Acknowledgements

I am so grateful to CRUK and Birmingham Children's hospital charity for funding my study here in Birmingham and to all the patients and their families for participating in my study. Thank you so much for this opportunity.

I thank all my supervisors, Dr Graham Taylor, Prof Paul Murray and Prof Pam Kearns for their guidance and encouragement throughout my PhD. I will always be grateful to them for believing in me and pushing me to reach to the end of this incredible journey. I could not have achieved this without their help and support throughout the last four years.

I would also like to thank Tracey Haigh for her ongoing support and guidance in the lab. Special thanks to the associate professor Jonathan Irish who has kindly welcomed me at Vanderbilt University and has shared his knowledge and expertise in multi-dimensional analysis. I would also like to thank Dr Carrie Willcox with for her guidance and advice in the γδ T-cells analysis and Dr Tracey Perry for her ongoing help and support throughout my PhD.

Finally, I am so grateful to my friends and family. My mom, my dad and my brother – for their unconditional love and cheering me up all the time. Damien and Romeo thank you for being so supportive and understanding throughout my final year of PhD. To my close friends you have been there for me when I needed you the most. I feel so blessed to be surrounded by people who love me. I would not have got through it without your constant support and encouragement. Thank you.

Publication arising for this thesis

Syrimi, Eleni, Fennell, Eanna and Richter, Alex G. and Vrljicak, Pavle and Stark, Richard and Ott, Sascha and Murray, Paul G. and Al-Abadi, Eslam and Chikermane, Ashish and Dawson, Pamela and Hackett, Scott and Jyothish, Deepthi and Krishnan Kanthimathinathan, Hari and Monaghan, Sean and Nagakumar, Prasad and Scholefield, Barnaby R. and Welch, Steven and Khan, Naeem and Faustini, Sian and Davies, Kate and Zelek, Wioleta and Kearns, Pamela and Taylor, Graham, The Innate and Adaptive Immune Landscape of SARS-CoV-2-Associated Multisystem Inflammatory Syndrome in Children (MIS-C) From Acute Disease to Recovery. ISCIENCE-D-21-02048. Accepted for publication at *iScience*.

Table of Contents

List of figures

List of tables

Abbreviations

ALCL- Anaplastic large cell lymphoma

AR/RT- Atypical teratoid/rhabdoid tumours

BCR- B-cell receptor

CCL- Chemokine ligand

CK- Creatinine kinase

CMV- Cytomegalovirus

CNS- Central nervous system

COVID-19- Coronavirus Disease 2019

CRP- C- reactive protein

CSF1- Colony stimulator factor 1

CXCL10- C-X-C motif chemokine ligand 10

CyTOF- Cytometry by Time of Flight

EBV- Epstein-barr virus

EDTA- Ethylenediaminetetraacetic acid

EN-RAGE- Extracellular newly identified receptor for advanced glycation end-products binding protein

ES- Ewing sarcoma

FBC- Full blood count

HGF- Hepatocyte growth factor

HFR- High fluorescence ratio

HL- Hodgkin lymphoma

HLA- Human leukocyte antigen

HSC- Hematopoietic stem cells

ICCC-3- International classification of Childhood cancer

IL- Interleukin

IL-1R1- interleukin-18 receptor 1

IL-1RA- Interleukin-1 receptor antagonist

IFN-g- Interferon gamma

IFN0A2- Interferon alpha 2

IP10- interferon gamma-induced protein 10

IVIG- Intravenous Immunoglobulin

KD- Kawasaki disease

KDSS- Kawasaki disease shock syndrome

KIR- Killer immunoglobulin receptor

LBL- Lymphoblastic lymphoma

LFR- Low fluorescence ratio

LIF-R- Leukemia inhibitory factor receptor

MAIT- Mucosal-associated invariant T cells

MCP-1- monocyte chemoattractant protein 1

mDC- myeloid dendritic cells

MDSCs- myeloid derived stem cells

MEM- Marker Enrichment Modelling

MERS- Middle east respiratory syndrome

MFR- Medium fluorescence ratio

MIP-1a- Macrophage inflammatory protein-1a

MIS-C- Multisystem inflammatory syndrome in children

MMI- Median mass intensity

MMP9- matrix metallopeptidase 9

MPO- myeloperoxidase

NHL- Non-Hodgkin Lymphoma

NK- Natural Killer

NT-proBNP- N-terminal pro-brain natriuretic peptide

PAI-1- plasminogen activator inhibitor-1

PBMC- Peripheral blood mononuclear cells

PCA- Principal component analysis

PC- Paediatric Cancer

pDC- plasmacytoid dendritic cells

PH- Paediatric Healthy

PICU- paediatric intensive care unit

PIMS-TS- Paediatric inflammatory multisystem syndrome temporarily associated with COVID-19

PD-1- Programmed cell death protein

PD-L1- Programmed death-ligand 1

PTX3- pentraxin-3

RBP-4- retinol binding protein 4

RNA- Ribonucleic acid

sTNF-R1- soluble receptors of tumour necrosis factor alpha

Tcm- Central memory T-cells

TCR- T cell receptor

Tem- Effector memory T-cells

TEMRA- Terminally differentiated T-cells

Tfh- T follicular helper cells

Th1- T helper 1 cells

Th2- T helper 2 cells

Th17- T helper 17 cells

Th22- T helper 22 cells

TIL- tumour infiltrate lymphocytes

TNFa – Tumour necrosis factor alpha

t-SNE- t-distributed stochastic neighbour embedding

TSS- Toxic shock syndrome

WHO- World health organisation

SARS- Severe acute respiratory syndrome

SARS-CoV-2- Severe acute respiratory syndrome coronavirus 2

sCD40L- soluble CD40 ligand

UMAP- Uniform manifold approximation and projection

WBC- White blood cells

WHO- World Health Organisation

γδ- gamma delta T-cells

CHAPTER 1- Introduction

1.1 Paediatric Immune System

1.1.1 Background

The human immune system has evolved to provide an efficient rapid respond to acute infections and adapt to changes (Simon, Hollander and McMichael, 2015). The adult immune system is relatively stable over time but varies among individuals (Carr *et al.*, 2016). Conversely, the paediatric immune system undergoes several changes over time, adapting regularly to vaccines and pathogens exposure, with the most significant changes occurring during the first two years of life, followed by more subtle changes later on in childhood(Dowling and Levy, 2014; Yu *et al.*, 2018).

The paediatric immune system transitions from an environment of immune tolerance during the foetal period to a sudden exposure to environmental factors at birth (Dowling and Levy, 2014; Yu *et al.*, 2018). This transition renders new born babies more susceptible to infections, particularly bacterial, due to their immature innate immune system (Dowling and Levy, 2014; Yu *et al.*, 2018) and impaired neutrophil functions (Filias *et al.*, 2011). In addition, impaired T helper 17 (Th17) and T helper 1 (Th1) responses also increases susceptibility to pathogens such as Escherichia coli, Listeria monocytogenes and herpes simplex virus (Adkins, 2007; Kollmann *et al.*, 2012). Moreover, the infant's immune system lacks "antigen experience," where in both the T and B cells compartments there are high numbers of naïve and low numbers of memory and effector cells. Therefore, an antigen driven response will take longer to develop (Adkins, 2007) further contributing to a young infant's susceptibility to bacterial and viral infections. During the first 3 months of life, the

infant is dependent on circulating maternal antibodies for immune protection while their immune system matures (Olin *et al.*, 2018).

Young children remain at risk of acute infections from viruses and bacteria, as their immune system continues to develop over time ('Infections in child care centres', 2000). Vaccination programmes have dramatically reduced mortality in children (Allen and Hicks, 2021) as they provide protective immune responses against serious diseases. In addition, encountering different pathogens, results in immunological memory which is considered to be an evolving feature of our immune system providing long lasting protection towards future reinfections (Simon, Hollander and McMichael, 2015; Aranburu *et al.*, 2017). Studies have shown that these immune responses in childhood are relatively uniform but environmental factors are mostly responsible for the person's intra-variability observed (Brodin *et al.*, 2015). Thus, the paediatric immune system has a unique feature, being able to react to novelty, a function that becomes ineffective later in life and particularly in elderly individuals.

The 10,000 Immunomes project (Zalocusky *et al.*, 2018) is a reference dataset for human immunology and provides evidence- based immune references, derived from 10,000 controls, according to age, sex and race. With the incorporation of available datasets from flow and mass cytometry repositories, this study is the largest and most comprehensive study to date for immunome references. However, the paediatric studies included in their analysis were mostly of individuals aged over 10 years of age and therefore not taking into account the first decade of life.

Understanding the developing paediatric immune system is crucial not only for vaccine development but also for understanding the mechanisms underpinning different responses to viruses such as in the case of SARS-CoV-2 (Carsetti *et al.*, 2020) and the development of childhood cancer (Greaves, 2018; Greaves, Cazzaniga and Ford, 2021).To date, undertaking these studies in children has been limited by the small volume of blood and access to these limited samples. In addition, studies have mainly focused on the neonatal period and infancy (Dowling and Levy, 2014; Olin *et al.*, 2018; Lakshmikanth *et al.*, 2020) ignoring the first decade of a child's life, a milestone for the developing immune system. Nevertheless, knowledge of the cellular immune systems, predominantly T, B, Natural Killer (NK) cells and monocytes are important due to their role in tumour surveillance, tumour elimination and defence against infection.

1.1.2 T-Cells

T-cells are part of the adaptive immune system, and their main role is to regulate and orchestrate the immune response (Alberts *et al.*, 2002). Their progenitors, hematopoietic stem cells (HSC) are found in the bone marrow. They give rise to T-cells which then migrate to thymus for further maturation. In the thymus they undergo a differentiation process where mature self-tolerance T-cells are released to the circulation (Alberts *et al.*, 2002). There are two major subsets of T-cells; CD8 and CD4 T cells. CD8 T-cells have mainly a cytotoxic capacity by mediating direct killing whereas the CD4 T-cells act as helper cells, indirectly killing foreign targets and regulating immune responses (Alberts *et al.*, 2002).

T-cell development is not static, but changes with age (Simon, Hollander and McMichael, 2015; Pinti *et al.*, 2016; Zalocusky *et al.*, 2018). T-cell output in the peripheral blood reduces with age as the thymus involute (Salam *et al.*, 2013). Current evidence suggests that the absolute CD8+ and CD4+ T-cell count increases at birth and up to the age of 9-15 months, after which they gradually decrease to adult levels (Schatorjé *et al.*, 2012). In the elderly, the CD4 to CD8 ratio is less than one as CD4+ T-cells reduce in numbers (Pinti *et al.*, 2016). Human CD4+ and CD8+ T-cells have been divided into four differentiation states based on the expression of cell surface proteins CD45RA and chemokine receptor CCR7 (Sallusto *et al.*, 1999): 1) naïve CD45RA+CCR7+ ,2) central memory CD45RA-CCR7+ (Tcm), 3) effector memory CD45RA-CCR7 (Tem) and 4) terminally differentiated CD45RA+CCR7- (TEMRA). CD27 instead of CCR7 has also been used for this subdivision (Hamann *et al.*, 1997).

Phenotypic T-cells changes also occur with age as the immune system encounters different foreign challenges. The main effect of aging in the T-cell compartment is the expansion of the T-cell memory pool and the decreased production of naïve T-cells due to thymic involution (Pinti *et al.*, 2016). More specifically, during the neonatal period, circulating T-cells are mainly naïve recent thymus migrants (Simon, Hollander and McMichael, 2015). Over time the naïve T-cells decrease in frequency and give rise to memory T-cells. In particular, the CD8+ Tem subset increases with age and remains stable once it reaches adult levels (Schatorjé *et al.*, 2012). Furthermore, CD8 Tcm and TEMRA subsets double during the first months of life and then decrease gradually to adult levels(Schatorjé *et al.*, 2012) but, significantly increase again in the elderly (Pinti *et al.*, 2016). The CD4+ Tcm subset has been reported either to remain stable through the years(Schatorjé *et al.*, 2012) or increase with age (Koch *et al.*, 2008; Zalocusky *et al.*, 2018). The CD4 Tem and TEMRA subsets remain very low in numbers throughout life (Schatorjé *et al.*, 2012) however, in cases of cytomegalovirus (CMV) infection an expansion of CD4+ TEMRA has been reported in the elderly (Libri *et al.*, 2011).

These studies have mainly used flow cytometry as a tool to investigate the developing immune system. Flow cytometry is a powerful tool and has evolved to analyse up to 50 markers (Hunka, Riley and Debes, 2020), however these studies were limited by the number of markers measured. As different subsets of T-cells emerge the need for additional markers increases. For example, cytotoxic CD8 T cells are defined by CXCR3 expression and secretion of perforin and granzymes (Charles A Janeway *et al.*, 2001; Oghumu *et al.*, 2015). Moreover, CD4+ T helper cells 1 (Th1) are also defined by CXCR3 expression and secretion of interleukin(IL)-2, tumour necrosis factor alpha (TNFα) and Interferon (IFN-γ) (Mosmann and

Coffman, 1989; Mosmann, 1992; Raphael *et al.*, 2015). T-helper cells 2 (Th2) are defined as CCR4+CCR6- and secretion of IL-4, IL-5 and IL-13 (Mosmann and Coffman, 1989; Mosmann, 1992; Raphael *et al.*, 2015). T-helper cells 17 (Th17) and T-helper cells 22 (Th22) are defined as CCR4+CCR6+ and secrete IL-17 and IL-22 respectively (Aggarwal *et al.*, 2003; Raphael *et al.*, 2015) while T-follicular helper cells (Tfh) are defined as CXCR5+ (Mosmann, 1992). Other T-cell subtypes like mucosal-associated invariant T- (MAIT) cells are defined based on the TCR-va 7.2 expression and are of increasing importance in cancer immunology (Huang *et al.*, 2019). Given the number of markers required to investigate all these different subsets it is now evident scientists are required to harness the power of tools that can provide deeper insights and deep immune phenotype to study the immune system in more detail.

1.1.3 B-cell compartment

B-cells are part of adaptive immunity, and their main role is to produce antibodies against bacterial proteins, polysaccharides and vaccines (Alberts *et al.*, 2002). B-cells are derived from HSCs and develop in the bone marrow where they undergo positive and negative selection for elimination of autoreactive cells (Shlomchik, 2008). They then migrate to the peripheral lymphoid tissues for further development and maturation(LeBien and Tedder, 2008). More specifically, transitional B-cells, having recently exited the bone marrow, migrate to the secondary lymphoid organs for further maturation to naïve B-cells (Sims *et al.*, 2005). Here, naïve B-cells receive a continuous supply of antigen through the circulating lymph(Harwood and Batista, 2010). Once exposed to an antigen, naïve B-cells undergo activation in two ways. The first is a T-cell independent antigen activation (Murphy and Weaver, 2016). This leads to the differentiation of B-cells into short-lived plasmablasts producing IgM antibodies, providing an early antibody response to acute infections (Bromage *et al.*, 2004). The second, is the T-cells dependent activation. In this process the B-cells bind an antigen through their B-cell receptor (BCR), which is then internalised, degraded and re-expressed on the cell surface as peptide bound to major histocompatibility complex (MHC) class II (Blum, Wearsch and Cresswell, 2013). CD4 T-cells and Tfh, bind the MHC-class II and peptide complex through their T-cell receptor (TCR) causing cytokine release and B-cell activation and proliferation(Crotty, 2015). This process is essential for creating both memory B-cells and long-lived plasma cells (Fink, 2012). Memory B-cells remain dormant in the periphery until they encounter the same antigen again (LeBien and Tedder, 2008) while plasma cells are long-lived and produce IgG antibodies for years(Bromage *et al.*, 2004).

The B-cell compartment similarly matures and changes considerably with age and according to the immune status of the host (Piątosa *et al.*, 2010). Overall, absolute numbers of B-cells double during the first month of life and gradually decrease to adult values, whereas in the elderly total B-cells are substantially reduced (Piątosa *et al.*, 2010). In addition, children have a higher proportion of transitional B cells which gradually decreases with age (Piątosa *et al.*, 2010). Based on the expression of cell surface proteins CD27 and IgD, B-cells are divided into four major subsets(Blomberg and Frasca, 2013): naïve (IgD+CD27-), non-switched memory (IgD-CD27+), switched memory (IgD+CD27+) and double negative B-cells (IgD-CD27-). Throughout life, naïve B cells comprise the majority of the B-cell compartment, but this gradually decreases with age. The elderly have a higher proportion of double negative B-cells and less switched memory B-cells compared to children and adults (Pinti *et al.*, 2016). Finally, the population of non-switched and class switched memory B-cells increases during the first decade of life and as children are exposed to more antigens (Piątosa *et al.*, 2010).

1.1.4 Natural Killer (NK) cells

NK cells represent 5-20% of circulating lymphocytes and are part of the innate immune system(Abel *et al.*, 2018). Their role is to kill virally infected cells and malignant cells (Vivier *et al.*, 2008). In addition, they produce key cytokines such as interferon gamma (IFNγ) and tumour necrosis factor alpha (TNFα), mediating immune responses through macrophages and dendritic cells (Abel *et al.*, 2018). NK cells mature in the bone marrow and secondary lymphoid organs (Abel *et al.*, 2018). NK cells undergo education as their inhibitory receptors, such as the killer immunoglobulin-like receptor (KIR) and NKG2A, interact with the major histocompatibility complex MHC-I (He and Tian, 2017). These cells are now deemed self-tolerant and functionally competent.

Little is known about how NK cells change over time. Absolute numbers of NK cells decrease during the first two months of life to reach adult levels (Simon, Hollander and McMichael, 2015). In the neonatal period NK cells ability to elicit cytolytic effect is reduced; this gradually changes with time (Ivarsson *et al.*, 2013; Simon, Hollander and McMichael, 2015) and by 5 months of age it reaches adult levels (Yabuhara, Kawai and Komiyama, 1990).
NK cells can be subdivided into three subsets in order of maturation: $CD56^{bright}CD16-$, $CD56^{dim}CD16-$ and $CD56^{dim}CD16+$ (Cooper, Fehniger and Caligiuri, 2001; Fehniger *et al.*, 2003). The CD56bright NK cell subset is immature, has the capacity to produce cytokines and has low cytotoxic potential (Cooper, Fehniger and Caligiuri, 2001). In the elderly, the CD56bright NK cell subset reduces in frequency, reflecting their decreased production from the bone marrow (Le Garff-Tavernier *et al.*, 2010; Gayoso *et al.*, 2011).

On the other hand, the CD56dim NK cell subset is more cytotoxic and represents the majority of the circulating NK cells (Cooper, Fehniger and Caligiuri, 2001).

The NK maturation process begins in the bone marrow and can be divided into three different stages (figure 1.1). First, the precursor NK cells undergo development processes in the bone marrow until they are ready to exit to the peripheral circulation. During this stage, the NK cells are CD56bright, express high levels of inhibitory receptor NKG2A and activating receptors NKp30, NKp46, NKp80 and do not express killer immunoglobulins-like receptors (KIR) or CD57 (Hamann *et al.*, 2011; Abel *et al.*, 2018). Downregulation of CD56 and expression of CD16 marks the second stage and the transition of the precursor NKs to immature NK cells. The downregulation of CD56 is associated with increased cytotoxic activity and particularly increased anti-tumour cytotoxicity (Abel *et al.*, 2018). Finally, the acquisition of CD57 marks the terminal differentiation stage of NK cells. These cells have the highest cytotoxic potential and sensitivity to stimulation via the Fc receptor CD16 however, possess decreased capacity to proliferate (Lopez-Vergès *et al.*, 2010).

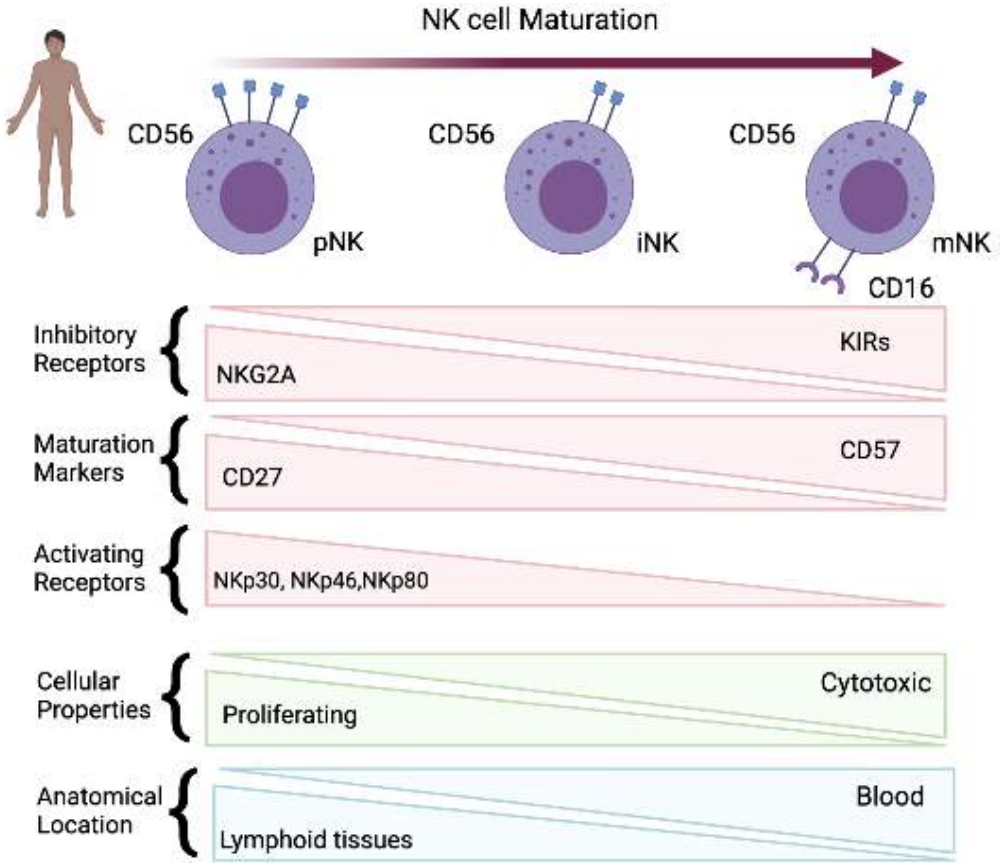

Figure 1-1 NK Cells Maturation process

Human NK cell maturation process is shown with their receptor expression profile. pNK stands for precursor NK cells, iNK stands for immature NK cells and mNK stands for mature NK cells. Figure adapted from Chanvillard *et al.*, 2013 using BioRender.

1.1.5 Monocytes

Monocytes are the largest circulating lymphocytes, represent around 5-10% of the peripheral leukocytes and are part of the innate immune system. They develop from the monoblasts in the bone marrow and are released to the circulation for one to two days after which they migrate to different tissues and differentiate into macrophages (Ziegler-Heitbrock *et al.*, 2010a). They contribute to immune defence and tissue repair through phagocytosis, antigen presentation and cytokine production (Ziegler-Heitbrock *et al.*, 2010a). There are three main circulating subsets based on the expression of CD14 and CD16: classical monocytes are defined as CD14+CD16-, non-classical monocytes are defined as $CD14^{low}$CD16+ and intermediate monocytes are defined as CD14+CD16+ (Ziegler-Heitbrock *et al.*, 2010a).

In general, a newborn's monocytes are immature and exhibit diminished cytokine responses, poor tissue repair and impaired phagocytosis (Simon, Hollander and McMichael, 2015). In addition, there is a paucity of lung macrophages in newborns which resolves a few days after birth (Simon, Hollander and McMichael, 2015). Little is known about how monocytes mature through childhood. However, studies of adults report several dynamic changes in monocytes, particularly for non-classical monocytes which expand in the elderly (Hamann *et al.*, 1997; Sadeghi *et al.*, 1999).

1.2 Paediatric Cancer and Immunotherapies

1.2.1 Paediatric Cancer

Paediatric cancers differ dramatically from adult cancers especially in terms of the epidemiology, biology, cellular origin and response to treatment. Childhood cancers are rare and it is estimated that approximately 1 in 500 children are diagnosed with cancer each year in the developed countries and this figure is expected to rise (Mosmann, 1992). In addition, cancer is the leading cause of death among children aged 1-14 in the UK ("Why children die - research and recommendations,2014," RCPCH). Incidence patterns of these cancers shows a bimodal age-specific pattern with peaks between 1-5 years and 10-14 years of age (figure 1.2,Board et al., 2003). Symptoms vary according to the tumour type, can be non-specific and often resemble those of other common childhood disorders.

The aetiology of cancer in children has puzzled scientists. Ionizing radiation and chemotherapy agents have been associated with a very small number of cases. In addition, several viruses are associated with oncogenesis such as Epstein-barr virus (EBV) with Hodgkin lymphoma(Massini, Siemer and Hohaus, 2009) and polyomaviruses with brain cancer(White *et al.*, 2005). Furthermore, different genetically-driven syndromes predispose to cancer such as Li-Fraumeni syndrome, neurofibromatosis, Bloom Syndrome, Fanconi anaemia and many more(Kliegman RM, S. Geme J, 2019). Overall, paediatric cancer aetiology is thought to be multifactorial with both genetics and environmental factors contributing to cancer development (Greaves, 2018).

An international classification system has been adopted to assign the different types of paediatric tumours into different groups. The 3rd edition of International classification of Childhood cancer (ICCC-3) is now an established classification system used by paediatric pathologists, oncologists and epidemiologists (Steliarova-Foucher *et al.*, 2005). A simplified table has been extrapolated by the ICCC-3 classification and is shown in table 1.

The most common malignancies in children up to the age of 14 in order of prevalence are leukaemia, central nervous system (CNS) tumours, lymphoma, neuroblastoma, Wilms tumour, bone tumours, soft tissue sarcomas, germ cell and gonadal tumours, hepatic tumours and retinoblastoma (figure 1.2, Steliarova-Foucher et al., 2017). On the other hand, for children between 15-19 years old the most common malignancy is lymphoma followed by epithelial tumours and melanoma, leukaemias, germ cell and gonadal tumours, CNS tumours, bone tumours and soft tissue sarcomas(figure 1.2, Steliarova-Foucher et al., 2017).

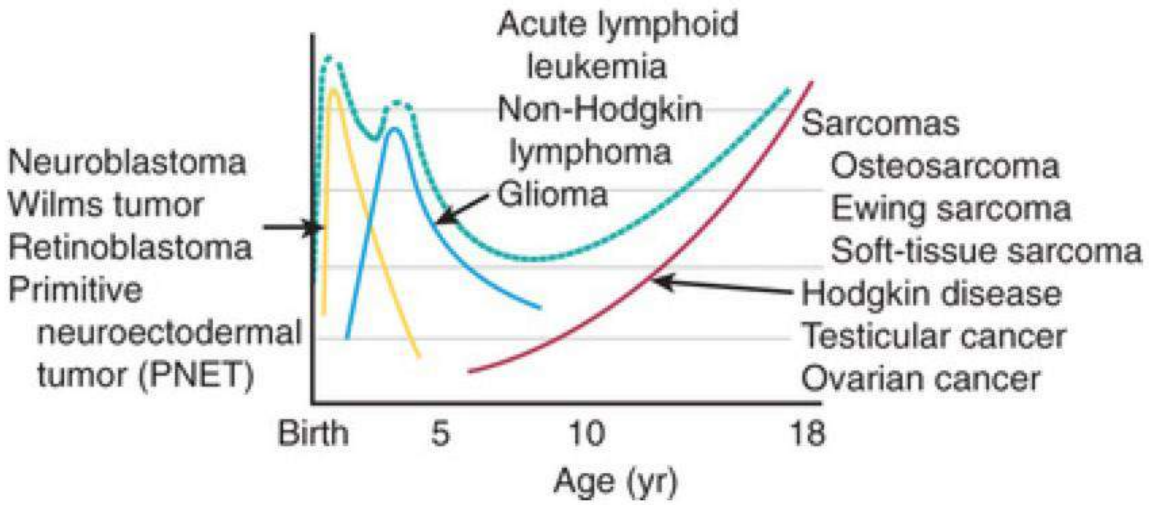

Figure 1-2 General incidence of the most common types of cancer in children by age.

Cumulative incidence of all cancers is shown in dashed line demonstrating the bimodal distribution of the disease. Figure reproduced from the Nelson Textbook of Pediatrics 21st edition.

ICCC-3 Code	*Site*
I.	**Leukaemias, myeloproliferative diseases, and myelodysplastic diseases**
II.	**Lymphomas and reticuloendothelial neoplasms**
III.	**CNS and miscellaneous intracranial and intraspinal neoplasms**
IV.	**Neuroblastoma and other peripheral nervous cell tumours**
V.	**Retinoblastoma**
VI.	**Renal tumours**
VII.	**Hepatic tumours**
VIII.	**Malignant Bone tumours**
IX.	**Soft tissue and other extraosseous sarcomas**
X.	**Germ cell tumours, trophoblastic tumours, and neoplasms of gonads**
XI.	**Other malignant epithelial neoplasms and malignant melanomas**
XII.	**Other and unspecified malignant neoplasm**

Table 1-1 ICCC-3 Code classification for paediatric cancers.

Adapted from the 3rd edition of International classification of Childhood cancer.

1.2.2 Embryonal tumours and paediatric sarcomas

Embryonal tumours occur almost exclusively in young children and arise from undifferentiated cells similar to the ones observed in embryos (Tulla *et al.*, 2015). However, there is no established definition for embryonal tumours and they are mainly divided into non-CNS and CNS tumours. The non-CNS embryonal tumours consist of neuroblastoma, ganglioneuroblastomas, nephroblastoma (Wilm's tumour), retinoblastoma, hepatoblastoma, rhabdoid and some other rare tumours (Willis RA, 1962). The CNS embryonal tumours include medulloblastoma, primitive neuroectodermal tumours (PNETs), medulloepithelioma, and atypical teratoid/rhabdoid tumours (AT/RTs) (Louis *et al.*, 2007).

Survival for embryonal tumours varies according to age of presentation and type of tumour (Tulla *et al.*, 2015). For example, neuroblastoma stage MS spontaneously regress in infants <1 years of age (Brodeur and Bagatell, 2014). On the other hand, survival of patients presenting with neuroblastoma at the age >1 years of age declines significantly(Tulla *et al.*, 2015). In general, the worse prognosis is for patients diagnosed with PNETs and AT/RT and the best prognosis is for patients diagnosed with retinoblastoma (Tulla *et al.*, 2015).

1.2.2.1 Neuroblastoma

Neuroblastoma originates from primitive neural crest cells of the sympathetic nervous system and typically arises in the adrenal medulla or paraspinal ganglia (Aygun, 2018). It occurs mostly in young children <5 years of age and the median age of diagnosis is 22 months of age(Kliegman RM, 2019). Neuroblastoma represents a type of disease that highlights the complexity of the embryonal tumours. Patients presenting with disseminated disease during the first year of age (Stage MS, previously known as 4S) can be treated with observation alone whereas older patients presenting with the same disease burden have poor outcomes despite aggressive multimodal treatment (Maris and Denny, 2002). N-MYC gene amplification occurs in 18-38% of cases and correlates with higher risk for metastatic disease and poor prognosis (Aygun, 2018). Other poor prognostic factors are the loss of 1p,11q,14 q, gain of 17q and DNA ploidy (Bagatell and Cohn, 2016). In addition, neuroblastoma's complex tumour microenvironment further complicates patients' therapeutic response due to its immunosuppressive nature. Several immune escape mechanisms have been described including: downregulation of human leukocyte antigen (HLA) class I and therefore impaired T-cell and NK recognition, secretion of immunosuppressive molecules and recruitment of immunosuppressive cells (Pinto *et al.*, 2015).

Treatment regimens are guided by risk groups and high-risk groups' treatment incorporate high dose chemotherapy with stem cell rescue, surgery, radiotherapy, immune-modulatory therapy and other biological agents(McGinty and Kolesar, 2017). A revolutionary step towards improving outcomes for high risk neuroblastoma patients was the incorporation of

the monoclonal antibody dinutuximab targeting a diasialoganglioside (GD2) to the current conventional treatment regimen and this has increased survival for high-risk patients from 46.5% to 66.5% (McGinty and Kolesar, 2017). Furthermore, early studies suggest that adoptive NK cell therapy in combination with dinutiximab results in meaningful clinical responses in patients with refractory/recurrent neuroblastoma (Federico *et al.*, 2017), suggesting NK therapy should be further explored in neuroblastoma treatment.

1.2.2.2 Nephroblastoma- Wilms tumour

Nephroblastoma (Wilms tumour) originates from the nephrogenic rests, undifferentiated renal mesenchyme, that does not regress and persists postnatally becoming malignant. It occurs mostly in children <5 years old with a peak incident at 2-3 years. It can be unilateral or bilateral in 7% of the cases.

There are several syndromes associated with Wilms tumour such as WAGR syndrome (Wilms tumour, aniridia, genitourinary abnormalities, mental retardation), Denys-Drash syndrome and hemihypertrophy syndrome Beckwith-Wiedemann. A common characteristic of WAGR and Denys-Drash syndromes is loss WT1 gene located at 11p13, which is the first identified Wilms tumour gene. Since then, many other genetic alterations have been described in Wilms tumour such as CTNNB1 mutation affecting the WNT signaling pathway, mutation of p53 and many more.

Treatment involves chemotherapy, surgery and radiotherapy and is risk-adapted. The main aim of treatment is to cure the patient while preserving as much of the renal function as possible. Experimental dendritic cell vaccines targeting WT1 have shown promising results (Shimodaira *et al.*, 2016) however, these results require validation in larger cohorts. Overall, survival for children with Wilms tumour is around 90% and is generally thought to be one the tumours with favourable outcome.

1.2.2.3 Paediatric Sarcomas

Paediatric sarcomas are rare and heterogeneous bone and soft tissue tumours that arise from mesenchymal cells in bones or soft tissues(Anderson *et al.*, 2012). Their prognosis depends on age, stage, tumour site, histology and any underlying molecular events such as chromosomal translocations (Kliegman RM, S. Geme J, 2019). Overall, 5 year survival for paediatric sarcomas has reached a plateau around 60% (Anderson *et al.*, 2012). Due to their rarity, they are understudied cancers.

Rhabdomyosarcoma is the most common soft tissue sarcoma and can be found at any anatomic site (Kliegman RM, S. Geme J, 2019). It occurs in increased frequency in patients with neurofibromatosis and Li-Fraumeni syndrome(McDowell, 2003). It is thought to arise from striated muscle and there are three histological types: the embryonal, botryoid and alveolar. Treatment strategies include surgery, chemotherapy and radiotherapy. Immune checkpoint inhibitors such as CTLA-4 and PD-1 inhibitors are currently being trialled in metastatic rhabdomyosarcoma but preliminary results are not as encouraging (Chen *et al.*, 2019). Other immunotherapies currently being investigated in rhabdomyosarcoma are CAR

T-cells and monoclonal antibody targeting the B7-H3 protein, which has been shown to be present on the surface of many paediatric tumours, however with limited clinical efficacy (Chen *et al.*, 2019).

Osteosarcoma is a bone sarcoma derived from mesenchymal cells and the pathological findings consist of malignant spindle cells associated with malignant formation of osteoid and bone. There are several predisposition syndromes associated with osteosarcoma such as Li-Fraumeni syndrome and Rothmund-Thomson syndrome (Kliegman RM, S. Geme J, 2019). Treatment strategies include chemotherapy and surgery. Immunotherapies such as PD-L1 inhibitors have been used in osteosarcomas but with limited effect (Chen *et al.*, 2021).

Finally, Ewing sarcoma (ES) is an undifferentiated bone sarcoma, arising from mesenchymal cells and is categorized with the primitive neuroectodermal tumours(Kliegman RM, S. Geme J, 2019). Treatment strategies include chemotherapy, surgery and radiotherapy. Immunotherapies have been trialled in ES with limited clinical effect. More specifically, PD-1 or PD-L1 inhibitors have been used in ES but the low mutational burden and the downregulation of HLA class I molecule on the tumour renders these checkpoints ineffective (Morales *et al.*, 2020). Finally, CAR T-cells are currently being trialled in ES however, early phase clinical studies do not show a clinical response perhaps because no specific surface antigen has been identified in ES (Morales *et al.*, 2020).

1.2.2.4 Lymphomas

Lymphoma is the third most common malignancy in children under the age of 14 years and the most common malignancy in adolescents. Lymphomas are categorised as Hodgkin or Non-Hodgkin lymphoma.

Hodgkin lymphoma (HL) is the most common malignancy in adolescents and has been associated with Epstein-Barr virus(Massini, Siemer and Hohaus, 2009). The histological findings are the identification of the Reed-Sternberg cell, a large cell arising from the germinal centre B-cells, surrounded by inflammatory infiltrate cells (Wang *et al.*, 2019). Overall, prognosis is good with an overall survival at 5 years of more than 90% with the current treatment strategies which include chemotherapy and radiotherapy(Kliegman RM, S. Geme J, 2019. Immunotherapy has been used in HL patients with promising results. PD-1 and PD-L1 inhibitors have been used in patients who relapsed with promising results and current studies are investigating introducing this agent as a frontline treatment(Ansell *et al.*, 2015).

Non-Hodgkin lymphoma (NHL) can be divided in three main subtypes: lymphoblastic lymphoma (LBL), mature B-cell lymphoma (Burkitt Lymphoma and diffuse large B-cell lymphoma) and anaplastic large cell lymphoma (ALCL). Most cases of LBL and ALCL cases are T-cell in origin. Treatment and prognosis vary according to the diagnosis and staging. However, the overall survival rate is around 90% (Kliegman RM, S. Geme J, 2019). Immunotherapies are being successfully used in NHL including the monoclonal antibodies

against CD20 (rituximab), CD30 (brentuximab) and CAR T-cells specific for each lymphoma subtype (Neelapu *et al.*, 2020)

1.3 Cancer Immunotherapies in the paediatric oncology setting

We are at the dawn of a new age in cancer treatment with the rapid evolution of immunotherapeutics that exploit the immune system to kill cancer cells. These therapies target the host immune system to either amplify a natural antitumor response or initiate a new immune response (Majzner, Heitzeneder and Mackall, 2017). In adult cancers, the use of immunotherapy is rapidly gaining ground as a more effective and less cytotoxic alternative (Brahmer *et al.*, 2015; Postow *et al.*, 2015; Robert *et al.*, 2015; Brown *et al.*, 2016).

In paediatric oncology, the combination of cytotoxic chemotherapies has improved survival rates over the years, yet significant issues remain. First, for high risk and metastatic disease cure is often unachievable despite aggressive surgical, chemotherapy and radiotherapy combinations (Erdmann *et al.*, 2021). Such patients inevitably relapse and are usually refractory to further treatment. Second, the toxic effects of these treatments remain a significant challenge in the short to medium term despite advances in supportive care. Third, the late effects of cytotoxic treatments, which include secondary cancers, cardiovascular events, and higher risk of infection, remain a significant cause of morbidity and mortality (Lancashire *et al.*, 2010; Reulen *et al.*, 2010; Fidler *et al.*, 2016). It is therefore clear that future research in paediatric oncology should address these issues by identifying novel therapeutics approaches that are more effective, especially in relapse/refractory disease, with less treatment related side-effects and improvement in the long-term

survivor's quality of life. Immunotherapy is an attractive alternative as it offers, in principle, a targeted potent anti-tumour response with less side-effects (Mellman, Coukos and Dranoff, 2011; Majzner, Heitzeneder and Mackall, 2017).

As illustrated previously numerous immunotherapies are being used or investigated in paediatric cancers however, the successes for immune-modulatory therapies observed in adult cancers have not translated into the paediatric setting (Hutzen, Paudel, *et al.*, 2019). The reason behind this is poorly understood, though the fundamental differences of paediatric tumours compared to adult counterparts and their corresponding immune systems are thought to be the cause (Hutzen, Ghonime, *et al.*, 2019). First, paediatric tumours are embryonal in origin with less genetic mutations and therefore lack actionable neoantigens (Marshall *et al.*, 2014; Campbell *et al.*, 2017). Second, the paediatric tumours are thought to be "cold" with little tumour immune infiltrates rendering them unable to respond to immunotherapies (Terry *et al.*, 2020). Lastly, additional complexity stems from the intricacies of the paediatric immune system as stated above.

While there are still significant challenges to address when it comes to immunotherapies in the paediatric cancers, the future of these treatments should be viewed with hope. Novel immunomodulatory drugs are rapidly emerging and rational drug combinations are needed to increase survival and improve the quality of life (Hutzen, Paudel, *et al.*, 2019). This can only be achieved by understanding the molecular processes leading to cancer development and the interplay of the tumour microenvironment with the immune system.

1.4 Multisystem inflammatory syndrome in children associated with Coronavirus Disease 2019 (COVID-19)

1.4.1 Background of SARS-CoV-2

The World Health Organization (WHO) declared coronavirus disease 2019 caused by severe acute respiratory syndrome coronavirus 2 (SARS-CoV-2), as a public health emergency of international concern on the 30th of January 2020 and as a pandemic on the 11th of March 2020 (*WHO Director-General's opening remarks at the media briefing on COVID-19 - 11 March 2020*, 2020; *Statement on the second meeting of the International Health Regulations (2005) Emergency Committee regarding the outbreak of novel coronavirus (2019-nCoV)*, 2020). This novel virus first identified in Wuhan, China rapidly spread around the world affecting millions of people(*COVID-19 Map*, accessed 26 July 2021).

Coronaviruses are single-stranded ribonucleic acid (RNA) viruses that can be transmitted by mammals and birds. The spike (S) protein facilitates viral entry to the host cell via a range of different cellular receptors. Like SARS-CoV, SARS-CoV-2 uses the angiotensin-converting enzyme 2 (ACE2) receptor to infect cells (Wan *et al.*, 2020). The nucleocapsid (N) protein attaches to the viral genome and is involved in the RNA replication while the membrane (M) protein interacts with the N protein to promoting the assembly and exit of the virus from the host cells (Voss *et al.*, 2009; Astuti and Ysrafil, 2020). Finally, the envelope protein facilitates the production, maturation and release of virions(Mohamadian *et al.*, 2021). In humans, several coronaviruses cause mild illness however, over the past decade two newly identified coronaviruses have infected humans causing severe acute respiratory syndrome (SARS) and middle east respiratory syndrome (MERS,Mohamadian *et al.*, 2021).

SARS-CoV-2, as is the case for all human coronaviruses, is transmitted via the respiratory route through droplets that enter the human respiratory epithelial cells (figure 1.3,Nakagawa, Lokugamage and Makino, 2016). The virus then fuses with the endocytotic vesicle and releases its RNA (figure 1.3). Next, virus replication and assembly occur, and infectious virus particles are then released via exocytosis (figure 1.3). In severe cases SARS-CoV-2 migrates to the lower airways causing pneumonia.

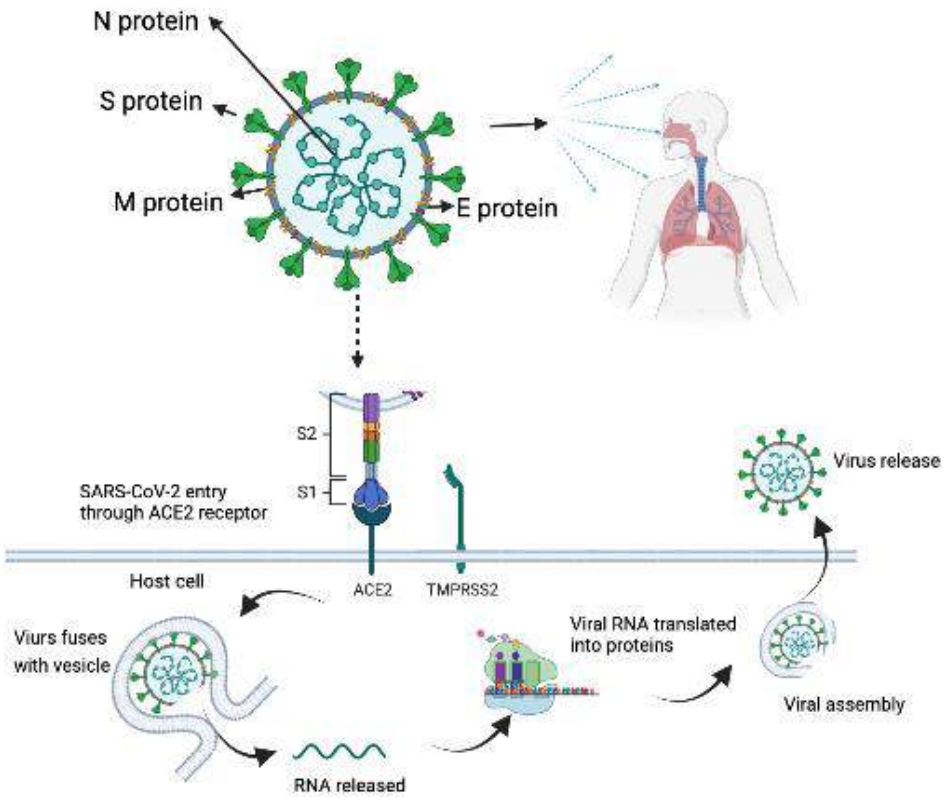

Figure 1-3 SARS-CoV-2 structure, transmission and life cycle.

The spike (S) protein facilitates viral entry to host cell through the angiotensin-converting enzyme 2 (ACE2) receptor. The virus then fuses with vesicle and the SARS-CoV-2 RNA is released intracellularly for replication. Finally, viral assembly occurs and virus is released via exocytosis. Figure produced in BioRENDER.

1.4.2 SARS-CoV-2 in children and research redirection

At the beginning of the COVID-19 pandemic, the general consensus was that SARS-CoV-2 infection in children did not lead to severe disease and in most cases acute infection was either asymptomatic or resulted in mild respiratory symptoms(Castagnoli *et al.*, 2020; Hoang *et al.*, 2020; P.-I. Lee *et al.*, 2020). Many theories emerged as to why this could be the case, including the fact that children have a more active innate immune response, healthier respiratory tracts, are less exposed to environmental factors such as smoking and less vulnerable from co-morbidities such as hypertension (Carsetti *et al.*, 2020; P.-I. Lee *et al.*, 2020). Furthermore, children's ability to produce natural IgM antibodies with broad reactivity and variable affinity has also been suggested as a potential protective mechanism against SARS-CoV-2 (Carsetti *et al.*, 2020).

Subsequently, a rare novel disease in children was reported that was suspected of being linked to SARS-CoV-2 infection. This was called multisystem inflammatory syndrome in children (MIS-C) by WHO (*Multisystem inflammatory syndrome in children and adolescents temporally related to COVID-19*, 2020) or paediatric inflammatory multisystem syndrome temporarily associated with COVID-19 (PIMS-TS) by the Royal College of Paediatrics and Child Health in the UK (Riphagen *et al.*, 2020; *Paediatric multisystem inflammatory syndrome temporally associated with COVID-19 (PIMS) - guidance for clinicians*, 2020). These children presented to hospital several weeks after known exposure to COVID-19 and/or had antibodies against COVID-19 (Riphagen *et al.*, 2020).

During the global pandemic, the research focus was redirected towards COVID-19 research. This resulted in pauses of any non-COVID-19 research activity including cancer research. We, therefore, also re-directed our research towards MIS-C for practical, medical, and intellectual reasons. MIS-C is a rare but dangerous complication of COVID-19. It affects school-aged children and can be life-threatening. It was, therefore, our clinical obligation to offer these patients evidence-based treatments. Using the expertise gained from high-dimensional analysis of paediatric cancer and healthy children, we were well equipped to interrogate the pathogenic processes involved in MIS-C and provide the scientific evidence needed for rational therapy selection. In addition, paediatric cancer and MIS-C lie on the opposite ends of a spectrum of immune functionality. In MIS-C the immune system overcomes numerous tolerance mechanisms to exert inappropriate effector function and causes damage to self-tissue. On the other hand, in cancer the immune system exhibits insufficient effector function and is unable to eliminate the malignant cells. Investigating these two diseases in more detail will therefore provide additional insights on the paediatric immune system and how it responds to these two extremes.

1.4.3 MIS-C and its similarities to Kawasaki Disease

Clinical manifestations of MIS-C resemble other paediatric inflammatory syndromes such as Kawasaki disease (KD), Kawasaki disease shock syndrome (KDSS) and Toxic shock syndrome (TSS) as demonstrated by many studies (Feldstein *et al.*, 2020; Flood *et al.*, 2021). In fact, initial case series reports labelled these children as severe KD (Verdoni *et al.*, 2020). KD is an acute systemic vasculitis affecting medium-size arteries and occurs predominantly in children less than 5 years old (McCrindle Brian W. *et al.*, 2017). Diagnosis is made based on certain diagnostic criteria and must include fever along with the presence of four out of the five following features: rash, peripheral oedema/erythema, non-suppurative conjunctivitis, lymphadenopathy and mucosal change(Kliegman RM, S. Geme J, 2019). KD is the most common cause of acquired heart disease in children due to the cardiac involvement associated with the disease and in particular the risk of formation of large or giant coronary artery aneurysms (CAA, McCrindle Brian W. *et al.*, 2017). This risk is substantially reduced with prompt initiation of treatment with intravenous immunoglobulin (IVIG, McCrindle Brian W. *et al.*, 2017).

MIS-C clinical features vary and include fever, lymphadenopathy, rash, mucosal changes, non-suppurative conjunctivitis, peripheral oedema or erythema, diarrhoea, vomiting, hypotension, cardiac involvement, acute kidney injury and respiratory failure (Ahmed *et al.*, 2020; Castagnoli *et al.*, 2020; Hoang *et al.*, 2020; Hoste, Van Paemel and Haerynck, 2021) . MIS-C is therefore diagnosed in patients presenting with fever, inflammation (based on their laboratory findings), multi-organ failure and clinical features fulfilling full or partial criteria for Kawasaki disease(*Paediatric multisystem inflammatory syndrome temporally associated*

with COVID-19 (PIMS-TS) - guidance for clinicians, 2020) . Clinicians are also asked to exclude other causes that can mimic this condition such as staphylococcal or streptococcal shock syndrome and confirm past SARS-CoV-2 infection with antibody testing. The optimal treatment strategy for MIS-C is unknown and there are no widely accepted guidelines on patient management. Intravenous immunoglobulin (IVIG) is the most commonly used anti-inflammatory agent followed by systemic corticosteroids(Ahmed *et al.*, 2020; Hoste, Van Paemel and Haerynck, 2021) and targeted agents that selectively inhibit the interleukin (IL) IL-6, IL1-b or Tumour Necrosis Factor alpha (TNF-a) pathways in a smaller number of cases (Ahmed *et al.*, 2020; Carter *et al.*, 2020; Consiglio *et al.*, 2020; Diorio *et al.*, 2020; C. Gruber *et al.*, 2020; P. Y. Lee *et al.*, 2020; Henderson and Yeung, 2021; Hoste, Van Paemel and Haerynck, 2021; Rodríguez-Rubio *et al.*, 2021).

Laboratory findings of patients presenting with MIS-C include elevated inflammatory markers (such as C-reactive protein, CRP, erythrocyte sedimentation rate, ESR), high ferritin, lymphopaenia, neutrophilia, hypoalbuminaemia, transaminitis, elevated D-dimers and fibrinogen. In some cases, there is also evidence of acute kidney injury or cardiac involvement through elevated Creatinine kinase (CK), troponin and N-terminal pro-brain natriuretic peptide (NT-proBNP,Ahmed *et al.*, 2020; Castagnoli *et al.*, 2020; Feldstein *et al.*, 2020; Hoang *et al.*, 2020; Hoste, Van Paemel and Haerynck, 2021). MIS-C and KD share similar laboratory findings, but some differences do exist such as lymphopenia being a feature of MIS-C and lymphocytosis for KD. A comparison of the clinical and laboratory findings of MIS-C and KD is shown on table 1.2.

MIS-C	KD
Clinical Characteristics	
Mean age 10-11 years	Mean age 2 years
Fever >38°C	**Fever >38°C for more than 5 days**
Gastrointestinal involvement : Diarrhea and Vomiting or signs of Acute abdomen	Milder gastrointestinal symptoms
Myocardial dysfunction/myocarditis	Coronary artery aneurysms (more severe cardiac features seen in KDSS)
Respiratory Failure	Respiratory involvement is rare
Rash	Rash
Non-suppurative conjunctivitis	Non-suppurative conjunctivitis
Lymphadenopathy	Lymphadenopathy
Peripheral oedema or erythema with desquamation	Peripheral oedema or erythema with desquamation
Mucosal changes	Mucosal changes
Laboratory findings	
High CRP and ESR	Same but not as marked
High Ferritin	Not a feature
High D-Dimers	Only in cases with coronary aneurysms
Hypoalbuminemia	Same
Lymphopenia	Leukocytosis
Neutrophilia	Same
High CK, LDH, troponin, NT-pro-BNP	Normal or mildly elevated
Thrombocytopenia	Thrombocytosis
Evidence of acute kidney injury	Only in severe cases
Transaminitis	Same
SARS-CoV-2 serology positive	SARS-CoV-2 serology negative

Table 1-2 Comparison of MIS-C and KD.

Clinical and laboratory findings are shown for both diseases. In red are the officially diagnostic criteria for KD which includes **fever** with the presence of at least four out of the five principal features. MIS-C : Multisystem inflammatory syndrome in children, KD: Kawasaki disease, KDSS: Kawasaki disease shock syndrome References used for making the table: Masuzawa *et al.*, 2015; Kliegman RM, S. Geme J, 2019; *Paediatric multisystem inflammatory syndrome temporally associated with COVID-19 (PIMS-TS) - guidance for clinicians*, 2020.

1.4.4 Immunology of MIS-C

1.4.4.1 Cytokine profile of MIS-C patients

Several studies evaluated the cytokine profile of MIS-C and KD patients in an attempt to unravel the hyperinflammation immune state of the disease(Carter *et al.*, 2020; Consiglio *et al.*, 2020; C. Gruber *et al.*, 2020; Esteve-Sole *et al.*, 2021). All studies reported an increase in pro- and anti- inflammatory cytokines in both MIS-C and KD patients however, inter-study differences were observed. For example, interferon-gamma (INFγ) and inflammatory cytokines such as interleukin-1 (IL-1) , Interleukin-10 (IL-10), Interleukin-6 (IL-6), Interleukin-8 (IL-8), C-X-C motif chemokine ligand 10 (CXCL10), Macrophage inflammatory protein-1a (MIP-1a), MIP-1b, tumour necrosis factor-a (TNFα) and IL-17 were found to be increased in MIS-C and KD patients by Esteve-Sole *et al.* These findings mainly agree with Gruber *et al.*, Diorio *et al.* and Carter *et al.,* but disagree with Consiglio *et al.*, who reported raised IL-17 as a feature of KD disease alone and normal levels of IL-6 in MIS-C. In addition, interleukin-2 receptor agonist was found to be elevated (Carter *et al.*, 2020; P. Y. Lee *et al.*, 2020) as well chemokines recruiting NK and T cells such as Chemokine ligand-19 (CCL19) and CUB domain-containing protein 1 (CDCP1, Gruber *et al.*, 2020). Likewise, neutrophils and monocytes chemokine ligands (CCL2 and CCL4) as well as EN-RAGE (extracellular newly identified receptor for advanced glycation end-products binding protein) and colony stimulator factor 1 (CSF1) were also raised in MIS-C (C. N. Gruber *et al.*, 2020). Finally, the immunosuppressive soluble molecules such as the programmed death-ligand 1 (PD-L1), leukaemia inhibitory factor receptor (LIF-R), hepatocyte growth factor (HGF) and interleukin-18 receptor 1 (IL-18R1) were also increased in MIS-C probably as a compensation response to inflammation (C. N. Gruber *et al.*, 2020). In summary, studies

reported a consistent upregulation of both pro- and anti-inflammatory cytokines in MIS-C cases which resembles KD disease in some studies but differs in others.

1.4.4.2 Adaptive and innate immunity of MIS-C patients

A smaller number of studies assessed cellular immunity in MIS-C patients and two compared MIS-C patients to KD. Using flow cytometry Carter *et al.*, 2020, demonstrated that MIS-C patients compared to healthy counterparts, had decreased frequencies of CD4, CD8, γδ T-cells and B-cells but increased plasmablasts. Similar results were also identified by other groups (C. N. Gruber *et al.*, 2020; P. Y. Lee *et al.*, 2020; Vella *et al.*, 2021). Carter *et al.*, 2020, has also described innate and adaptive immune activation in MIS-C patients and in particular for the CD4+CCR7+ and γδ T-cells, neutrophils and monocytes. Moreover, Consiglio *et al.* using also flow cytometry, identified high frequencies of CD4 central and effector memory T-cells and low frequencies of T follicular helper (Tfh) in MIS-C patients but not in KD (n=3). Vella *et al.* also using flow cytometry, identified increased proliferation and activation of both CD4 and CD8 T-cells subsets, and particular the CX3CR1+CD8+ T-cells, but interestingly did not report any changes in the Tfh cells in MIS-C patients when compared to COVID-19 paediatric patients. Lastly, performing mass cytometry on nine MIS-C patients Gruber *et al.* reported activation of non-classical monocytes and neutrophils in both MIS-C and KD but did not observe any phenotypic changes in T-cells or B-cells. Overall, the immune analysis of MIS-C patients showed a marked immune activation of both adaptive and innate immunity however, the heterogeneity of patients, the small numbers of patients and conflicting data make it difficult to draw firm conclusions regarding the immunological processes of MIS-C.

1.5 Advances in immune-monitoring technology

Flow cytometry is a powerful immunological tool that analyses single cells as they flow past single or multiple lasers (McKinnon, 2018). Each cell is analysed for their light scatter and one or more fluorescence parameters(McKinnon, 2018). Light scatter measured in the forward or side directions relative to the lasers can assess the size of the cell and its granularity (McKinnon, 2018). Measuring fluorescence parameters requires staining of cells with fluorescence conjugated antibodies either on the surface of the cells or intracellularly. A great challenge with multiple fluorescence parameters is the need for compensation between fluorochromes. This is required because when fluorochromes are excited they emit photons within a range of wavelengths that overlap with the wavelengths emitted by other fluorophores causing cells to falsely appear double positive ('An Introduction to Spectral Overlap and Compensation Protocols in Flow Cytometry', 2016). This technology undoubtedly helped advance the immunological field and has evolved over the last decades leading to experiments with the possibility of assessing 50 markers on a single cell (Hunka, Riley and Debes, 2020). However, a downside of this advancement is the amount of compensation controls that are needed to correct for spectral overlap (McKinnon, 2018).

Our tools for probing the immune system have now improved dramatically and have advanced to the recent development of Cytometry by Time of Flight (CyTOF) which can analyse millions of cells and measure over 50 immune markers per cell and the amount of markers are increasing with metal isotopes availability (Bandura *et al.*, 2009). Cells are labelled with heavy metal ion-conjugated antibodies and detected using time-of-flight mass

spectrometry(McKinnon, 2018). A key advantage of CyTOF is that it enables a large numbers of markers to be measured using only a single low-volume sample, such as the small blood samples available from paediatric patients(Lai *et al.*, 2015). Another emerging method allowing unlimited amount of markers to be measured on a single cell is the cellular indexing of transcriptomes and epitopes by sequencing (CITE-seq, Stoeckius *et al.*, 2017). Using oligonucleotide-labelled antibodies, this method integrates measurements of both cellular proteins and transcriptomes into a sequencing based readout of single cells achieving a more detailed characterization of cellular phenotypes(Stoeckius *et al.*, 2017).

Despite the increase in the number of parameters there are many challenges to address including identifying the optimal way to visualize and interpret the high-dimensional data generated (Kimball *et al.*, 2018). Therefore, computational approaches, such as dimensionality reduction and clustering algorithms are needed to allow the true power of the technique to be harnessed. Accordingly, several analysis pipelines have been developed, moving away from Boolean gating strategies traditionally used to analyse flow cytometry data, to gain new biological insights (Kimball *et al.*, 2018).

The first step of high-dimensional data analysis is dimensionality reduction and visualisation of the data in a two-dimension space. In the case of mass cytometry data, nonlinear dimensionality reduction techniques are needed to avoid overrepresentation of the data (Becht *et al.*, 2019) that might be caused with linear dimensionality reduction tools such as principal component analysis (PCA). A commonly used tool is viSNE, an algorithm that uses a t-distributed stochastic neighbour embedding (t-SNE) to distribute the high-dimensional data into a two-dimension map(Maaten and Hinton, 2008; Kimball *et al.*, 2018). The

resulting t-SNE plots consist of two axis tSNE1 and tSNE2 where cells are distributed based on a continuum of their marker expression and phenotypically similar cells are often located close to each other forming “islands”. Users can identify cellular phenotypes by colouring the maps with different markers, look for variations between individuals and gain a quick overview of the cellular differences between experimental groups(Kimball *et al.*, 2018). t-SNE has the ability to expand low density areas and ignore global relationships (Becht *et al.*, 2019) making it easier to gate on less abundant populations. However, disadvantages of using t-SNE include the slow computational time and inability to represent large datasets (van Unen *et al.*, 2016). A new algorithm called uniform manifold approximation and projection (UMAP), has emerged to try and address these issues as the run time for this tool is much shorter while preserving the global structure of the data (McInnes *et al.*, 2018; McInnes, Healy and Melville, 2020). UMAP also produces two-dimension plots consisting of two axis, UMAP1 and UMAP2, enabling users to interpret the data much easier.

The next step involves clustering populations of interest through unsupervised learning algorithms. Clustering on the original data is not ideal due to the curse of dimensionality, instead clustering on reduced dimensions is preferred (Björklund *et al.*, 2016). Commonly used algorithms include SPADE and FlowSOM (Bruggner *et al.*, 2014; Van Gassen *et al.*, 2015). FlowSOM is an unsupervised technique organizing the data in self-organising maps (SOMs) followed by hierarchical clustering of cells into meta-clusters(Van Gassen *et al.*, 2015). The investigator defines the number of clusters (k) required for meta-clustering. FlowSOM can reveal how markers behave on cells ensuring that all subsets in the dataset are identified correctly(Van Gassen *et al.*, 2015). SPADE is different, as it partitions all the data into many hierarchically organized clusters, reflecting all dimensions, into a branched

tree structure (Levine *et al.*, 2015). This structure recapitulates the cellular hierarchy that links related cell types, making this algorithm superior for identifying rare populations (Levine *et al.*, 2015). However, SPADE is much slower especially when dealing with larger dataset and therefore, FlowSOM has been the preferred clustering tool for many CyTOF users.

In summary, a pipeline of analyses are required for mass cytometry data analysis which includes a dimensionality reduction tool and a clustering algorithm, chosen by the investigators based on their computational skills, the ability to extract data for testing different hypotheses and the speed by which figures can be generated(Kimball *et al.*, 2018).

1.6 Hypothesis and Aims

Hypothesis: The paediatric immune signatures in paediatric cancer and MIS-C have not been described systematically previously and they are important as they could be therapeutically targeted.

My overarching aim is to investigate how cancer and MIS-C affects the paediatric immune system.

The specific aims of this thesis are:

1. Describe the differences in key immune subsets in the blood of paediatic cancer patients compared to healthy children.
2. Investigate the function of specific immune cells that are shown to be affected in cancer patients.
3. Describe the differences in key immune subsets in the blood of patients presenting with a new paediatric inflammatory disease (MIS-C) compared to healthy children.
4. Describe the differences in key immune subsets following the standard of care for MIS-C patients.

To achieve this, I will apply high dimensional immune characterisation of the peripheral blood of cancer patients before standard of care therapy, comparing them to age and sex matched healthy volunteers. Blood samples from MIS-C patients before and after treatment will be similarly assessed and compared to healthy children. Therefore, my work will provide the data needed for the rational incorporation of new immunotherapies into current treatment protocols for both cancer and MIS-C patients. Graphical abstracts for the results chapters are provided in figures 1.4 and 1.5.

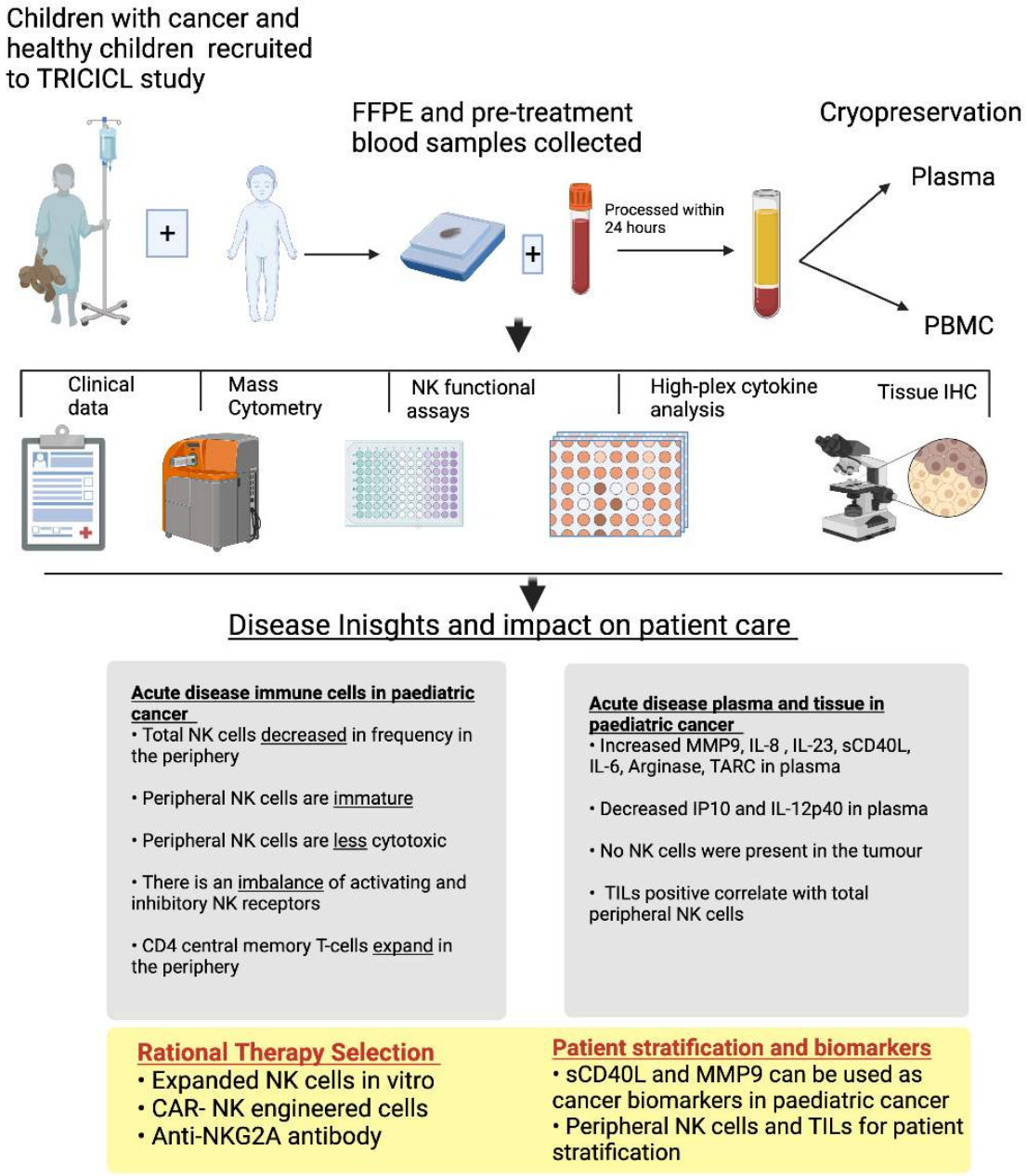

Figure 1-4 Graphical abstract for chapters three and four.

FFPE: Formalin fixed paraffine embedded, PBMC: Peripheral mononuclear blood cells, NK: Natural killer, IHC: Immunohistochemistry,TILs: Tumour infiltrate lymphocytes, MMP9: Matrix metalloproteinase 9, IL: Interleukin, sCD40L: soluble CD40 ligand, TARC: thymus and activation regulated cytokine, IP10: Interferon γ-induced protein 10, IL-12p40: Inteleukin-12 p40 monomer, CAR-NK: Chimeric antigen receptors NK. Figure produced in BioRENDER.

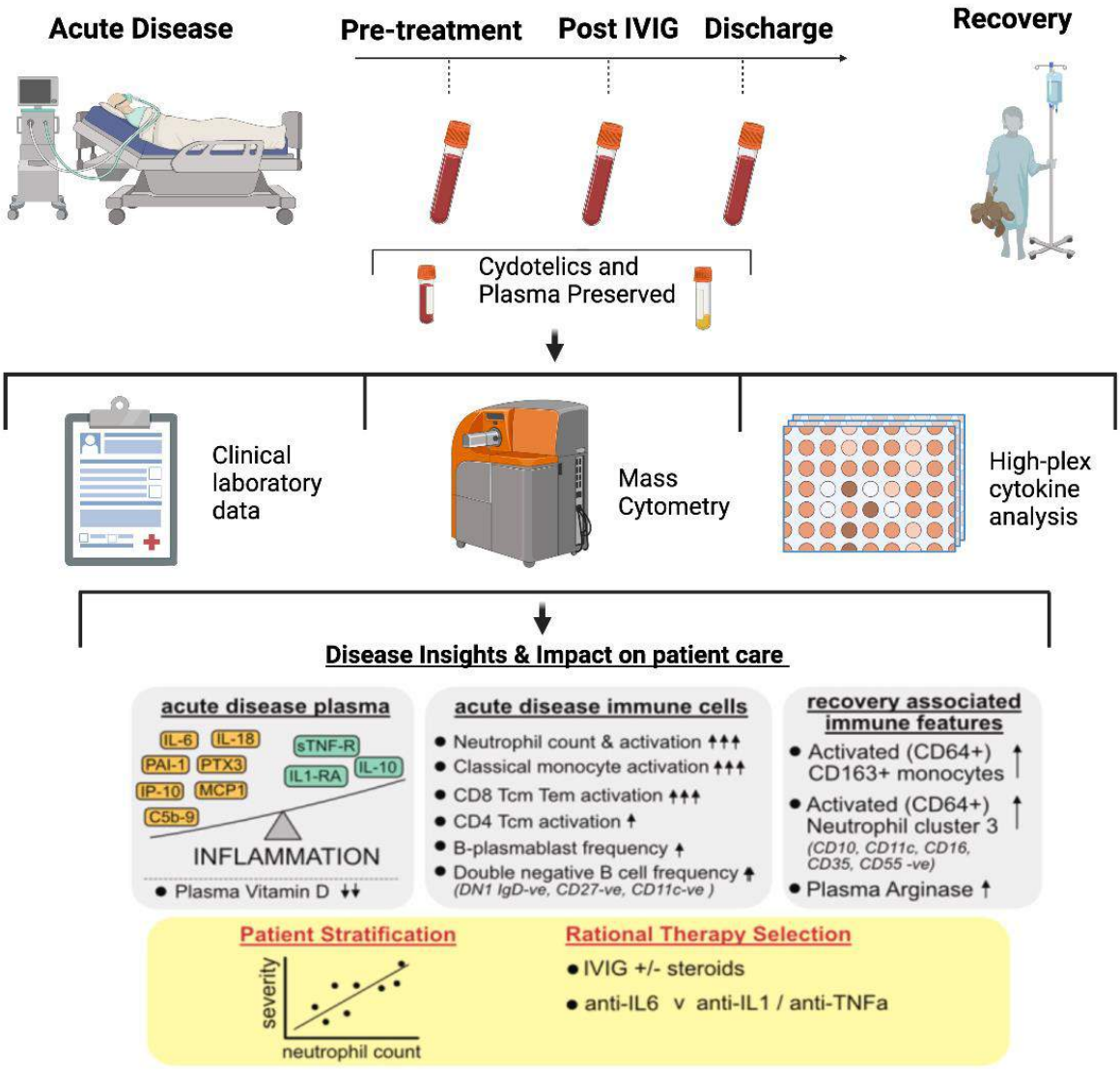

Figure 1-5 Graphical abstract for chapter five.

IVIG: Intravenous Immunoglobulin, IL: Inteleukin. Figure produced in BioRENDER.

CHAPTER 2 - Material and Methods

2.1 Tissue culture media and reagents

- RPMI-1640- Roswell Park Memorial Institute- 1640 medium supplemented with 2mM L-glutamine (Sigma)
- Phosphate-Buffered Saline (PBS)-Sigma
- Interleukin-2- IL-2 (Peprotech)
- Penicillin-streptomycin solution (Gibco)
- Lymphoprep (Stemcell Technologies)
- Foetal calf serum- FCS (Gibco)
- Dimethyl suplhoxide- DMSO (Sigma)
- Freezing medium A: RPMI 1640 containing 60% FCS
- Freezing medium B: 80% FCS and 20% DMSO
- Cell Stain Media (CSM) buffer: PBS and 0.5% of FCS and 0.02% of sodium azide
- Iridium Intercalator: 2,5µl of Fluidigm stock solution into 10ml of CSM-S (CSM + 0.02% of saponin)
- MACS buffer: 0.5% BSA and 2mM EDTA in PBS
- Culture media: RPMI, 10% Foetal Bovine Serum, Penicillin 50U/ ml and streptomycin 50U/ml

2.2 Processing of samples from patients and healthy children

2.2.1 Sample preparation and cryopreservation

Peripheral blood from patients and healthy children were collected in vacutainer tubes containing Ethylenediaminetetraacetic acid (EDTA). Blood volumes sampled varied according to age and followed the World Health Organisation (WHO) guidance for safe sampling in child health research (Howie, 2011). For a single blood draw the following limits were kept: up to max 5 ml (age 0–4 yr); 10 ml (age 5–9 yr); 15 ml (age 10–14 yr); 30 ml (age ≥ 15 yr). Samples were delivered at the University of Birmingham within 24 hours of collection.

<u>Cancer patients and healthy children</u>

Samples were transferred to the University of Birmingham laboratories for processing. Blood was diluted 1:1 with warm RPMI media and then added into a 50ml SepMate tube (Stem Cell Technologies) containing 15ml of Lymphoprep. For smaller samples (blood volume less than 5 ml) 15ml SepMate tubes were used with 4ml of Lymphoprep. Samples were centrifuged for 10 minutes at 1200 g with the brake on. Plasma (2.5mls) was carefully removed from the top of the tube, being careful not to disturb the peripheral blood mononuclear cell (PBMC) layer and transferred into a new 15ml tube for further processing and storage.

PBMCs were poured off (in no longer than 2 seconds) into a new 50ml tube and counted using a haemocytometer. RPMI media was added (5-10ml) and a low-speed centrigugation

at 300g was performed for 8 minutes to isolate the PBMCs and remove platements. After discarding the platelets, the PBMC pellet was resuspended and a number of aliquots cryopreserved according to the ealier PBMC count. Cryopreservation was performed by resuspending the PBMCs with equal volumes of freezing media A and B, transferring the cells into 1ml cryovials, placing these into a room temperature Mr Frosty freezing container (Nalgene) to allow slow cooling at a rate of 1 degree per minute placing the Mr Frosty chamber into a -80°C freezer for at least four hours. PBMC samples were transferred to liquid nitrogen for long-term storage, typically the day after processing but within a maximum of one week.

After PBMC processing was completed, the plasma that had been collected earlier was centrifuged at 1200g for 10 minutes with brake on. Four 500µl aliquots were immediately transferred into 1ml cryovials and stored at -80 °C.

MIS-C patients and healthy children

In addition to the PBMC and plasma isolation protocol mentioned above, whole blood was also frozen using Cytodelics whole blood stabiliser. Equal amount of blood and Cytodelics stabiliser were added to a cryogenic vial and mixed well by inverting the vial 10-15 times. The sample was incubated in room temperature for 10 minutes and then transferred to -80 °C. The numbers of aliquots were determined according to the total blood volume received at the laboratory.

2.2.2 Recovery of cryopreserved cells

PBMC recovery

Cryovials were placed from liquid nitrogen storage into a 37°C water bath. Once thawed the cells were transferred into a 15ml tube and RPMI-1640 + 10% FCS added. PBMCs were collected by centrifugation at 350 g for 5 minut4s with brake on. The supernatant was discarded, and cells were resuspended with 5-10 ml of appropriate media. Cells were then counted using a haemocytometer and used for experiments.

Cydotelics whole blood sample recovery

The manufacturer's cell recovery protocol was followed. Samples were first thawed in a 37°C water bath and fixed using Cytodelics fixation buffer for 15 minutes. Then 2 ml of the Cytodelics red blood cell lysis buffer was added for a further 10-20 minutes until the solution was no longer turbid. The samples were then centrifuged at 400 g with brake on for 5 minutes. The supernatant was aspirated, 2 ml of Cytodelics wash buffer was added and the sample was centrifuged for 5 minutes at 400 g with brake on. Finally, the supernatant was aspirated, and cells were resuspended in appropriate media for further experiments.

2.3 Mass cytometry panel design and optimisation

The initial goal from the immune analysis of the paediatric cancer discovery cohort was to characterise the immune signatures of children with cancer. We therefore developed a broad immunophenotyping panel capturing the majority of the immune subsets. Supporting information of this panel is provided in Table 2.1 containing an array of immune cell lineage markers. Following the results from the paediatric cancer discovery cohort further two panels were developed and applied in the paediatric cancer discovery cohort (Table 2.2) and validation cohort (Table 2.3) for in-depth immunophenotyping of the NK cells. Finally, for the MIS-C patients we used the scRNAseq data (Syrimi *et al.*, 2021) as a guide to develop a focused mass cytometry panel interrogating both the innate and adaptive immunity (Table 2.4). The paediatric cancer panels were applied to patients PBMCs while the MIS-C panel was applied to Cydotelics preserved blood.

Optimal panel design maximises signal and minimizes interference by carefully pairing mass antibody markers with mass channels based on the marker intensity, the sensitivity of channel and crosstalk between mass channels(Takahashi *et al.*, 2017). Taking that into account we carefully assigned markers for low- and high- abundance antigens as per the Fluidigm panel design guidance. The majority of these antibodies were obtained in a conjugate format from Fluidigm while the remaining antibodies were conjugated manually. Antibody titration was performed using 0.5µl or 1µl antibody per 100µl of cell suspension containing $1{,}5x10^6$ cells. The optimal titre for each antibody was assessed by the ability to securely detect positive from negative cells against signal spill-over into other mass channels

(Gullaksen *et al.*, 2019). Antibody titration was performed at the same conditions as the final experiment to ensure proper signal intensity allowing population definition.

To avoid batch effects, all the samples were thawed and stained together, using the same antibody master mix and running all the samples on the CyTOF within 48 hours (as per Fluidigm guidance). In addition, using a barcoding approach (this step was used only for the Paediatric Cancer cohorts and not for the MIS-C) multiple samples were stained together in one tube optimizing data acquisition speed and efficiency as it constitutes a single sample run on the CyTOF (Schuyler *et al.*, 2019). To further avoid batch effects, we randomised patients' samples to different barcodes avoiding inter-barcoding variability. To facilitate comparison across batches and when able to we included a technical replicate in each barcode set as a biologically constant reference or an anchor sample from a single donor processed the same way (Schuyler *et al.*, 2019).

Metal	Marker	Clone	Source
89Y	CD45 (BC)	HI30	Fluidigm
114 Qdot	CD45 (BC)	HI30	Biolegend
115In	CD45 (BC)	HI30	Biolegend
141Pr	CD31	WM59	Biolegend
142Nd	CD57	HCD57	Fluidigm
143Nd	CD38	HIT2	Biolegend
144Nd	CD8	SK1	Biolegend
145Nd	CD4	RPA-T4	Fluidigm
146Nd	IgD	IA6-2	Fluidigm
147Sm	CXCR3	G025H7	Biolegend
148Sm	CD16	3G8	Fluidigm
149Sm	CD127	AO19D5	Fluidigm
150Nd	OX40	ACT35	Fluidigm
151Eu	CCR6	G034E3	Biolegend
152Sm	TCR-gd	11F2	Fluidigm
153Eu	CCR4	L291H4	Biolegend
154Sm	CD73	AD2	Biolegend
155Gd	PD1	EH12.2H7	Fluidigm
156Gd	CD45RA	HI100	Biolegend
158Eu	CD33	WM53	Fluidigm
159Tb	CD161	HP-3G10	Fluidigm
160Gd	CD39	A1	Fluidigm
161Dy	ICOS	C398.4A	Biolegend
162Dy	CD27	L128	Fluidigm
163Dy	CD56	NCAM16.2	Fluidigm
164Dy	CD95	DX2	Fluidigm
165Ho	CD19	HB19	Fluidigm
166Er	CD24	ML5	Fluidigm
167Er	CCR7	G043H7	Biolegend
168Er	CXCR5	J252D4	Biolegend
169Tm	CD25	2A3	Fluidigm
170Er	CD123	6H6	Biolegend
171Yb	CD5	UCHT2	Biolegend
172Yb	CD11c	3.9.	Biolegend
173Yb	CD3	UCHT1	Biolegend
174Yb	HLA-DR	L243	Fluidigm
175Lu	CD14	M5E2	Fluidigm
176Yb	TCR va7.2	3C10	Biolegend
194-198Pt	CD45 (BC)	HI30	Biolegend
209Bi	CD11b	ICRF44	Fluidigm

Table 2-1 Generic panel one used for the paediatric cancer patients and healthy children.

Barcodes are indicated as BC.

Metal	Marker	Clone	Source
115In	CD45 (BC)	HI30	Biolegend
141Pr	Gamma-delta 2	123R3	Milteny
142Nd	CD57	HCD57	Fluidigm
144Nd	CD8	SK1	Biolegend
145Nd	CD4	RPA-T4	Fluidigm
147Sm	CXCR3	G025H7	Biolegend
148Sm	CD16	3G8	Fluidigm
149Sm	CD127	AO19D5	Fluidigm
151Eu	CCR6	G034E3	Biolegend
152Sm	CD27	M-T271	
153Eu	CX3CR1	2A91	Biolegend
154Sm	TIGIT	A15153G	Biolegend
155Gd	PD1	EH12.2H7	Fluidigm
156Gd	CD45RA	HI100	Biolegend
159Tb	NKp30	Z25	Fluidigm
160Gd	Gamma-delta 1	REA173	Milteny
162Dy	NKp46	BAB281	Fluidigm
163Dy	CD56	NCAM16.2	Fluidigm
164Dy	CD95	DX2	Fluidigm
165Ho	1^{O} NKG2C-PE 2^{O} Anti-PE	134591, PE2	R&D Biosystems & Fluidigm
166Er	NKG2D	ON72	Fluidigm
167Er	CCR7	G043H7	Biolegend
168Er	CXCR5	J252D4	Biolegend
169Tm	NKG2A	Z199	Fluidigm
170Er	CD161	HP3610	Biolegend
171Yb	DNAM	DX11	Fluidigm
173Yb	CD3	UCHT1	Biolegend
175Lu	CD14	M5E2	Fluidigm
176Yb	TCR-va 7.2	3C10	Biolegend
194Pt	CD45 (BC)	HI30	Biolegend
198Pt	CD45 (BC)	HI30	Biolegend
209Bi	CD11b	ICRF44	Fluidigm

Table 2-2Mass cytometry panel used to characterise the NK cells phenotype in the first paediatric patient cohort.

Barcodes are indicated as BC.

Metal	Marker	Clone	Source	Metal	Marker	Clone	Source
89Y	CD45 (BC)	HI30	Fluidigm	161Dy	ILT3	ZM4.1	Biolegend
106Cd	CD45 (BC)	HI30	Biolegend	161Dy	ILT5	222821	R&D Systems
110Cd	CD45 (BC)	HI30	Biolegend	161Dy	ILT4	42D1	Fluidigm
111Cd	CD38	HIT2	Biolegend	162Dy	NKp44	P44-8	Biolegend
112Cd	CCR2	K036C2	Biolegend	162Dy	NKp46	BAB281	Fluidigm
114Cd	CD8a	SK1	Biolegend	163Dy	CXCR4	12G5	Biolegend
115In	CD57	HNK-1	Biolegend	163Dy	CXCR3	G025H7	Fluidigm
116Cd	CD36	5-271	Biolegend	164Dy	CD161	HP3G10	Fluidigm
141Pr	CD3	UCHT1	Fluidigm	165Ho	KIR2DS4	179315	R&D Systems
142Nd	CD19	HIB19	Fluidigm	166Er	NKG2D	ON72	Biolegend
143Nd	CD45RA	HI100	Fluidigm	167Er	KIR3DL1	DX9	Fluidigm
144Nd	CD69	FN50	Fluidigm	167Er	KIR3DL2	539304	R&D Systems
145Nd	CD4	RPA-T4	Fluidigm	168Er	CD127	A019D5	Fluidigm
146Nd	KIR2DL1/S1/ S3/S5	HP-MA4	Biolegend	169Tm	NKG2A	Z199	Fluidigm
147Sm	CXCR1	42705	R&D Systems	170Er	CD122	Tu27	Fluidigm
147Sm	CXCR2	5E8/CXCR2	Fluidigm	171Yb	CD226	DX11	Fluidigm
148Nd	CD14	RMO52	Fluidigm	172Yb	CX3CR1	2A9-1	Fluidigm
149Sm	CD25	2A3	Fluidigm	173Yb	KIR2DL2/L3	DX27	Fluidigm
150Nd	CD27	LG.3A10	Fluidigm	173Yb	KIR2DL5	UP-R1	Miltenyi Biotec
151Eu	KIR2DL1/S5	143211	R&D Systems	174Yb	CD94	HP-3D9	Fluidigm
152Sm	ILT1	337902	Biolegend	175Lu	PD-1	EH12.2H7	Fluidigm
153Eu	CXCR5	RF8B2	Fluidigm	176Yb	KIR2DL4	181703	R&D Systems
154Sm	TIGIT	MBSA43	Fluidigm	194Pt	CD45 (BC)	HI30	Biolegend
154Sm	TIM3	F38-2E2	Fluidigm	195Pt	CD45 (BC)	HI30	Biolegend
155Gd	CD56	B159	Fluidigm	196Pt	CD45 (BC)	HI30	Biolegend
156Gd	ILT2	GHI/75	Fluidigm	198Pt	KIR2DL2/L3 /S2/S4	180704	R&D Systems
158Gd	ILT2/LIR6	586326	R&D Systems	209Bi	CD16	3G8	Fluidigm
159Tb	NKp80	239127	R&D Systems				
160Gd	CXCR6	K041E5	Fluidigm				

Table 2-3 Mass cytometry panel used to characterise the NK cells phenotype in the second paediatric patient cohort.

Barcodes are indicated as BC.

Metal	Marker	Clone	Source
89Y	CD41/42a61	A2A9/6 & REA209	Biolegend & Miltenyi
106Cd	CD16	3G8	Biolegend
110Cd	CD14	RMO52	Beckman Coulter
113Cd	CD2	TS1/8	Biolegend
114Cd	CD8	SK1	Biolegend
115In	CD57	HCD57	Biolegend
116Cd	CD36	5-271	Biolegend
139La	FCeR1	AER-37	Biolegend
141Pr	CD45	HI30	Fluidigm
142Nd	CD19	HIB19	Fluidigm
144Nd	CD32	FUN-2	Biolegend
145Nd	CD4	RPA-T4	Fluidigm
146Nd	IgD	IA6-2	Fluidigm
147Sm	CD11c	5-HCL-3	Biolegend
148Nd	CD69	REA824	Miltenyi
149Sm	CD64	10.1	Biolegend
150Nd	CD62L	DREG56	Biolegend
151Eu	CD123	6H6	Biolegend
155Gd	CD45RA	HI100	Fluidigm
156Gd	CD177	MEM-166	Biolegend
159Tb	CD86	IT2.2	Biolegend
160Gd	CD39	A1	Fluidigm
161Dy	CD163	GHI/61	Biolegend
162Dy	CD55	IS11	Biolegend
163Dy	CD56	NCAM16.2	Fluidigm
164Dy	CD95	DX2	Biolegend
166Er	CD35	E11	Biolegend
167Er	CD27	L128	Fluidigm
168Er	CD10	H10a	Biolegend
169Tm	CD25	2A3	Fluidigm
173Yb	CD3	UCHT1	Biolegend
174Yb	CD40	HB14	Biolegend
175Lu	CXCR4	12G5	Fluidigm
176Yb	CD63	H5C6	Biolegend
194Pt	CD66b	6/40c	Biolegend
195Pt	CD235	HI264	Biolegend
196Pt	CD38	HIT2	Biolegend
198Pt	HLA-DR	L243	Biolegend

Table 2-4 Mass cytometry panel used to immune characterise the MIS-C patients and healthy children.

2.4 Mass cytometry staining protocol

Metal conjugated antibodies were either purchased from Fluidigm or were prepared in house using Maxpar antibody labelling reagents according to the manufacturer's protocol (Fluidigm). An equal number of cells from each individual were stained. Two broad approaches were used. Experiments analysing samples from cancer patients (and the appropriate healthy controls) used barcoding to allow samples from multiple individuals to be stained in a single tube. Cells from each individual were transferred into separate FACS tubes and staiend with a CD45 specific antibody conjugated with one of a range of different metals. PBMCs from cancer patients and paediatric healthy children were barcoded using a batch randomisation scheme to avoid bias. Cells were washed twice with cell-stained media (CSM) buffer at 350G. Different CD45-specific metal conjugated antibodies were added to the different tubes and incubated for 20 minutes at room temperature. Cells were then washed in CSM and combined together for phenotypic staining. Experiments analysing samples from MIS-C patients did not use barcoding and cells from a single individual were stained in separate tubes.

Staining for phenotypic markers was performed as follows. A master-mix of antibodies was prepared by adding the appropriate pre-tested and titrated quantities of antibodies into filtered CSM buffer. Fc receptors were blocked by adding 5ul FcX block (Biolegend) to cells for 10 minutes followed by 50µl of the surface staining antibody cocktail for 30 minutes at room temperature. For experiments analysing PBMCs, live dead rhodium stain was added for a further 10 minutes. Live dead stain was not used in experiments analysing Cytodelics preserved whole blood samples, as recommended by the manufacturer. Finally, cells were

washed twice with CSM at 350 g then resuspended in 1ml of freshly prepared 1.6% paraformaldehyde (PFA) and left overnight. The following day, cells were centrifuged at 1000g for 5min then incubated with 500µl of iridium intercalator (Fluidigm) solution for a minimum of one hour. Cells were analysed using a Fluidigm Helios mass cytometer at an acquisition rate less than 500 events per second. Immediately prior to acquisition cells were washed once in CSM and twice in deionised water then filtered through a 70µm cell strainer. Four element calibration beads (Fluidigm) were added to the cells for data normalisation using the Helios data acquisition software. Normalised data were uploaded to Cytobank for further analysis including de-barcoding, manual and automated analysis.

2.5 Data quality control

The aim of data quality assessment was to detect whether the intrasample variations were due to instrument variations rather than biological causes. Changes in instrument performance could lead to gradual loss of detector sensitivity, built up of debris or changes in the ionization efficiency (Lee and Rahman, 2019). It is therefore crucial to monitor the changes during sample acquisition and perform data quality control before proceeding to any further data analysis. First, EQ bead normalisation was performed as recommended to correct for both short- and long- term signal fluctuations (Lee and Rahman, 2019). Then multiple acquisitions of single samples were combined through concatenation process. Normalization and concatenation of the FCS files were performed by the UOB mass cytometry technical specialist using the Fluidigm CyTOF software.

Second, the signal stability was assessed for each FCS file. The EQ bead and non-EQ beads populations were identified and for each of these populations time vs any measured parameter was plotted, and the slope was calculated. In general, a slight negative slope was generally accepted as it reflects the gradual loss of instrument sensitivity over time(Lee and Rahman, 2019). A steeper slow for both beads and cells can indicate a rapid loss of instrument sensitivity while a stepper slope for the cells alone could indicate sample degradation(Lee and Rahman, 2019). These samples should be flagged for quality issues but, in our study no sample with an abnormal slope was identified (figure 2.1). Transient spikes in signal intensity indicates micro-clogs during acquisition and these time windows were excluded from the analysis (figure 2.2) and could be misinterpreted as false positive signals (Lee and Rahman, 2019). Lastly, Samples with less than 100,000 cells were excluded from any further analysis as they were considered blank or of poor quality.

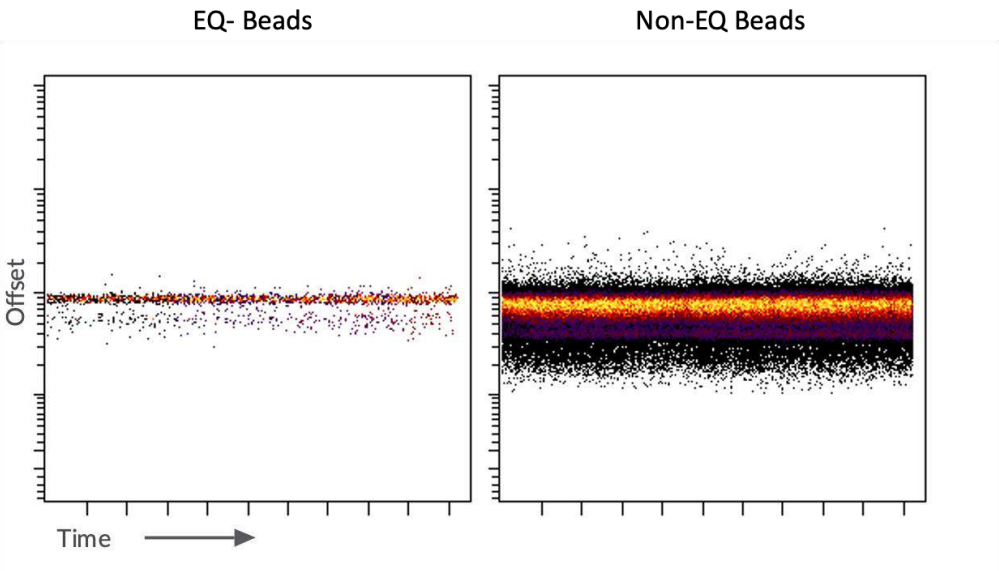

Figure 2-1 Data quality control of mass cytometry assessing the slope using time vs any parameter.

This is an example of assessing the time slope during the quality control step. It is evident there is no drop of the signal throughout this acquisition.

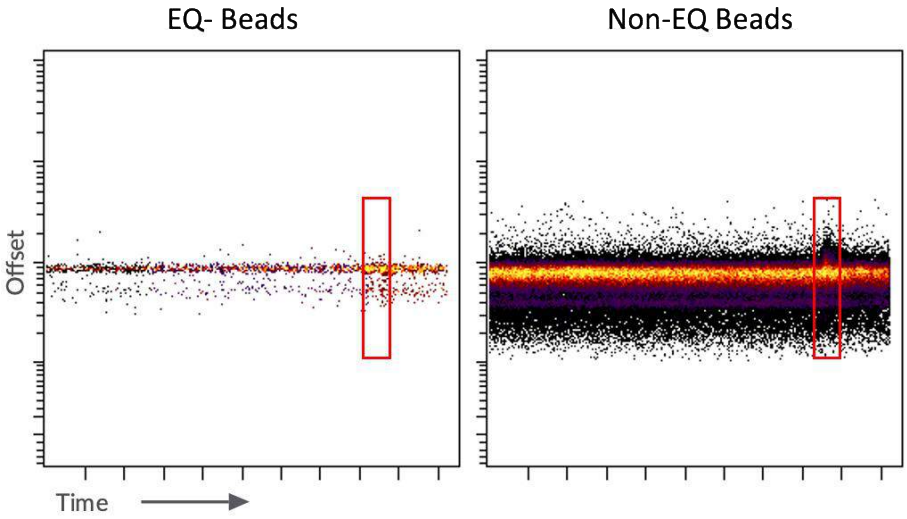

Figure 2-2 Data quality control of mass cytometry assessing the slope using time vs any parameter.

This is an example of assessing the time slope during the quality control. There is a transient spike in signal intensity for both beads and non-beads. This time window annotated with a red box was excluded from the analysis.

2.6 Data analysis pipeline

Bead normalised data were analysed using mainly the Cytotbank software. Singlet cells were identified using the gaussian parameters- residual, offset, centre and width- as per the "Recommendations for use of gaussian discrimination parameters" publication by Fluidigm. Samples were then debarcoded, down sampled to equal number of cells per sample and FCS files from patients or healthy donors concatenated on separated FCS files for illustration purposes.

Dimensionality reduction was then performed in Cytobank using the viSNE implementation of t-distributed stochastic neighbour embedding (t-SNE, Maaten and Hinton, 2008). It is a well-established tool utilized for analysis and display of high-dimensional data into a two-dimensional space (Kimball *et al.*, 2018). Identifying where the different cell types and phenotypes are located on the plot relies on the user's biological knowledge and is facilitated by colouring the t-SNE plots with different parameters. This is particular useful for gaining an overview of different cellular phenotypes across different islands, identifying inter-individual variation and gaining insights into cellular changes between groups(Kimball *et al.*, 2018). Due to the stochastic nature of the algorithm, two independent runs on the same dataset will give two different plots which vary in terms of island location and therefore, it is not possible to directly compare two viSNE plots that were performed separately. In cases where the user wishes to validate workflows, replicate their work in different dataset or analyse larger dataset with limited computer power then setting the same number of seed for each viSNE run will generate similar plots with the islands kept in relatively similar locations. An alternative tool used for dimensionality reduction is UMAP

(Becht *et al.*, 2019). UMAP works similarly to t-SNE, with the difference that it preserves the topological structure of the high-dimensional representation (Becht *et al.*, 2019). UMAP was performed using the UWOT package and robust linear modelling performed using the MASS package in R version 3.5.3.

Manual gating of high-dimensional data can be very subjective and suffers from the potential of operational bias. In addition, to interrogate a dataset of a 40-marker mass cytometry panel a user would require 780 biaxial plots (Nx(N-1))/2, N=number of markers). It is evident that applying traditional biaxial plots in these datasets is insufficient and efforts to reduce such burdens have given rise to unsupervised approaches that partition cell population according to the natural structure of the dataset (Liu *et al.*, 2019). Therefore, a clustering tool was then utilised to identify different cellular clusters within the datasets. In this study FlowSOM (Gassen *et al.*, 2015) or Spade (Qiu *et al.*, 2011) were the chosen unsupervised tools. FlowSOM has been assessed as the top-performing unsupervised tool in terms of stability, precision, coherency of clustering results and speed (Liu *et al.*, 2019). Heatmaps can be generated to assess the phenotype of each cluster. SPADE on the other hand, preserves cellular progression and hierarchies thus, it can facilitate biological discoveries including the identification of rare cell types (Qiu *et al.*, 2011). Lastly, marker enrichment modelling (MEM) is an algorithm that objectively describes cells by generating a machine-readable quantitative label (Diggins *et al.*, 2017). MEM is useful for identifying cellular phenotypic differences between health and disease. It was performed in R using v3.0 of the code downloaded from GitHub.

Despite the disadvantages of manual gating, 2D biaxial plots were utilized alongside unsupervised techniques to further interrogate the data and analysing specific immunological populations of interest.

In summary, a high-dimensional data analysis pipeline include: 1) data quality control, 2) identification of live singlet cells and when applicable debarcoding and concatenation, 3) a dimensionality reduction tool, 4) a clustering tool and 5) 2D biaxial plot to interrogate specific immune subsets. Overall, the choice of tool will depend on the question a user would like to answer. A graphical illustration of the data analysis pipeline is shown in figure 2.3.

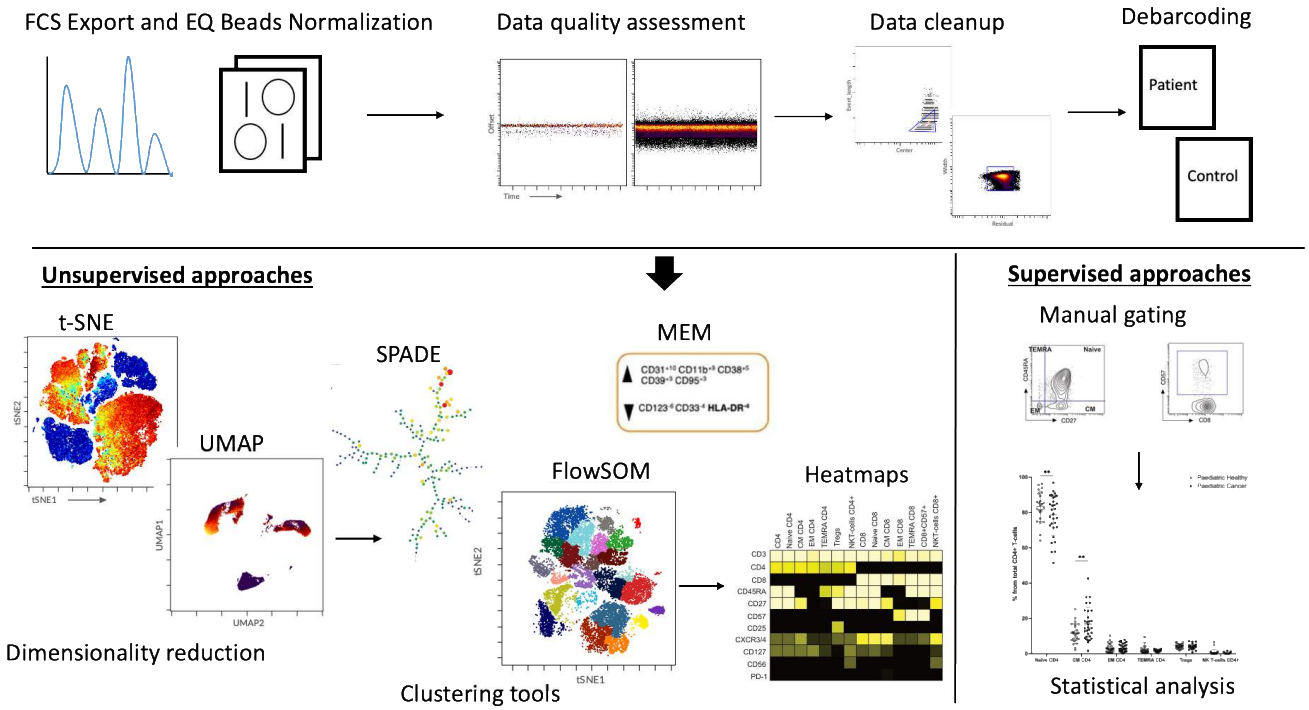

Figure 2-3 Graphical illustration of the data analysis pipeline

2.7 Fluorescent flow cytometry staining protocol and panels used

Fluoescent flow cytometry was used to characterise NK cells and γδ T-cell in a subset of paediatric cancer patients and healthy children using panels of antibodies shown in Table 2.5 and 2.6. Cell surface staining was performed by adding pre-tested and titrated antibodies and incubating for 30 minutes in the dark at 4°C. The cells were then washed once with MACS buffer and intracellular fixation reagent (eBioscience) added as per manufacturer protocol for an hour in the dark at 4°C. Cells were then washed twice with permeabilization buffer and pre-tested and titrated intracellular antibodies were added and incubated for further 30 minutes in the dark at 4°C. Finally, cells were washed twice with permeabilization buffer and resuspended in MACS buffer. BD CompBead anti-mouse (BD Biosciences) were used for compensation according to the manufacturer's recommendation. Samples were analysed on a BD LSRII flow cytometer and data analysed in Cytobank or BD FACS DIVA software.

Fluorochrome	Antibody	Clone	Source
e450	CD3	SK7	eBioscience
APC	CD56	CMSSB	eBioscience
PeCyC7	CD16	eBioCB16	eBioscience
Percpcy5.5	CD57	QA17A04	Biolegend
FITC	CD107a	H4A3	Biolegend
AF700	TNF-a	Mab11	Biolegend
PE	INF-g	4S.B3	Biolegend
APC-Cy7	CD19	HIB19	eBioscience
APC-Cy7	CD14	6ID3	eBioscience
APC-Cy7*	Live-Dead		Biolegend
PeCy7	perforin	dG9	eBioscience
PE-texas red	granzyme b	GB11	Invitrogen

Table 2-5 Fluorescent flow cytometry antibody panel used for further NK cell characterisation in paediatric cancer and paediatric healthy.

*e-Fluor 780 live dead stain was detected on the APC-Cy7 detector.

Fluorocrome	Antibody	Clone	Source
BV510	live/dead	Zombie Aqua	BioLegend
BV421	CD3	UCHT1	BioLegend
BV650	CD8	SK1	BD Biosciences
FITC	Vd1	REA173	Miltenyi
PE	Vd2	123R3	Miltenyi
PE-Cy5	Vg9	IMMU 360	Beckman Coulter
PE Dazzle 594	CD27	M-T271	BioLegend
BV711	CD45RA	HI100	BD Biosciences
BV605	CD45RO	UCHL1	BioLegend
APC Fire 750	CD161	HP-3G10	BioLegend
AF647	Hobit	Sanquin-Hobit/1	BD Biosciences
PE-Cy7	Perforin	B-D48	BioLegend
BV786	Tbet	O4-46	BD Biosciences

Table 2-6 Fluorescent flow cytometry antibody panel used for γδ T-cell characterisation of paediatric cancer patients and paediatric healthy.

This panel was created by Dr Carrie Willcox.

2.8 NK functional assays

NK cytotoxicity assay

The cytotoxicity of NK cells was determined by measuring their capacity to kill the erythroleukemia cell line K562. PBMCs were recovered and incubated overnight in culture media with 200IU/ml IL-2 (Peprotech). K562 cells were CFSE labelled (CFSE tacking kit,Biolegend) following the manufacturer's instructions. Cells from each donor were co-cultured with CFSE labelled K562 correcting for the NK frequency differences observed for each donor and the effector to target ratios were defined. Cells were cultured at 37^{o}C in cell culture media overnight. The following day, cells were recovered, washed once with PBS and incubated for 10 minutes with efluor 780 live dead stain (ebioscience) in the fridge. Cells were then washed once and resuspended in MACS buffer. Counting beads (ebioscience) were added to the sample and data acquired using a BD LSR-II flow cytometer. Cytotoxicity was calculated using the formula cytotoxicity= [(expected live target cells - live target cells)/ expected live target cells] x100.

NK cell degranulation assay

NK cell degranulation was measured similarly to NK cytotoxicity. PBMCs were recovered and incubated overnight in culture media containing IL-2. The following day cells were co-cultured with K562 cells with defined NK:K562 cell ratios. Anti-CD107a-FITC antibody (Biolegend) was added at the beginning of the assay at 1ul/well for an hour. Monensin and brefeldin A (Biolegend) were then added to the assay as per manufacturer's instructions. At the end of the incubation cells were stained with fluorescent labelled antibodies (table 2.7). Cells were then fixed and permeabilized using the eBioscience fixation and permeabilization kit and

intracellular staining for INF-g and TNF-a performed as per manufacturer's instructions. Samples were then acquired on an LSR-II flow cytometer and data analysed in Cytobank.

Fluorochrome	Antibody	Clone	Source
APC	CD3	SK7	eBioscience
BV510	CD56	NCAM16.2	BD Bioscience
Percpcy5.5	CD57	QA17A04	Biolegend
PE-Cy7	CD16	eBioCB16	eBioscience
APC-Cy7	Live-Dead		Biolegend
APC-Cy7	CD14	61D3	Invitrogen
APC-Cy7	CD19	HIB19	BD Biosciences
PE	INF-γ	4S.B3	Biolegend
AF700	TNF-a	MAb11	BD Biosciences

Table 2-7 NK cells degranulation assay fluorescent panel.

NK expansion assay

A minimum of 500,000 PBMCs were resuspended in culture media consisted of RPMI/5% human albumin serum/ 1000IU/ml IL-2 /1% Penicillin-streptomycin solution. Cells were placed in a 48 wells plate at 500,000 cells per well. Culture media was replaced every three days. NK cells were cultured in vitro for 12-14 days. Cytotoxic capacity of the cultured NK cells was then assessed as per the NK cytotoxicity protocol above.

2.9 Cytomegalovirus (CMV) IgM and IgG Elisa

Plasma was tested for CMV IgM and IgG antibodies via a semiquantitative ELISA following the manufacturer's protocol (Table 2.8). Photometric measurement of the colour intensity was determined using a microplate reader at a wavelength of 450nm and data were analysed in Microsoft Excel.

Elisa	Catalogue Number	Source
CMV IgG Elisa	EI 2570-9601 G	EUROIMMUN
CMV IgM Elisa	EI 2570-9601M	EUROIMMUN

Table 2-8 CMV IgM and IgG ELISA assays

2.10 MHC class I chain-related gene A (MICA) and UL16 binding portien-2 (ULBP2) ELISA

The concentration of MICA, ULBP-2 or MMP9 (Table 2.9) was measured in plasma samples using sandwich ELISAs following the manufacturer's protocol. Photometric measurement of the colour intensity was determined using a microplate reader at a wavelength of 450nm and data were analysed in Microsoft Excel.

ELISA	Catalogue Number	Source
Human MICA	DY1298	R&D Systems
Human ULBP-2	DY1300	R&D Systems
Human MMP9	A668	Antibodies.com

Table 2-9 MICA, ULBP2 and MMP9 ELISA

2.11 Human myeloperoxidase (MPO) instant ELISA

The concentration of MPO (Table 2.10) was measured in plasma samples using an instant sandwich ELISA following the manufacturer's protocol. Photometric measurement of the colour intensity was determined using a microplate reader at a wavelength of 450nm and data were analysed in Microsoft Excel.

Elisa	Catalogue Number	Source
Human MPO	BMS2038INST	ThermoFisher Scientific

Table 2-10 MPO Elisa

2.12 Arginase activity assay

The enzymatic activity of arginase in plasma samples was measured using an arginase activity assay kit (Table 2.11) following the manufacturer's protocol. Photometric measurement of the colour intensity was determined using a microplate reader at a wavelength of 430nm and data were analysed in Microsoft Excel. The arginase activity of a sample was determined using the following equation:

$$Arginase = \frac{(A430)sample - (A430)blank}{(A430)standard - (A430)water} \times \frac{(1mM \times 50 \times 10^3)}{(V \times T)}$$

T= Reaction time

V= Sample volume (µl) added to well

1mM= Concentration of urea standard

50= reaction volume (µl)

10^3= mM to µM conversion factor

Assay	Catalogue Number	Source
Arginase enzymatic activity	MAK112	Sigma-Aldrich

Table 2-11 Arginase activity assay

2.13 Cytokine Array

Plasma cytokine levels were measured using the human XL Cytokine array kit and the human soluble receptor array hematopoietic panel (both R&D Systems) following the manufacturer's instructions. This assay was used for explorative purposes. In order to identify as many altered molecules as possible, samples from three patients were combined together to produce pooled samples for two age groups: children with cancer <3 years old (C12,C16 and C21) and children with cancer >10 years of age (C06,C10 and C15). Similarly, healthy paediatric children were used as controls: children <3 years old (HV06,HV11,HV18 and HV26) and children >10 years of age (HV13,HV20,HV30 and HV34). ChemiDoc MP imaging system (BioRad) was used to acquire images of the arrays for quantification. The images were analysed using ImageLab software (BIO-RAD).

2.14 Cytokine bead assays

The concentration of cytokines in plasma samples was measured using the LEGENDplex multi-analyte flow assay kits from Biolegend (Table 2.12). The manufacturer's instructions were followed. Samples were acquired using a BD LSR FORTESSA X-20 cytometer and data analysis performed using BioLegend LEGENDplex data analysis software.

Assay kit	Catalogue Number	Source
Human Inflammation panel 1	740809	BioLegend
Human Inflammation panel 2	740776	BioLegend
Human Macrophage/Microglia	740503	BioLegend

Table 2-12 LEGENDplex assay panels

2.15 Immunohistochemistry

FFPE sections of patients with available written legal guardian consent were stained at Birmingham Children's Hospital pathology department for CD45, CD56 and CD57. Slides were scanned and analysed using the Aperio eSlide manager software.

2.16 Further data analysis and statistical testing

For the paediatric cancer cohorts GraphPad Prism v9 was used for statistical testing for all experiments. The detail of each statistical test is provided in each figure legend. For the MIS-C study the data and statistical analysis was performed in R using the lm, PCAtools, marixStats and matrixTests packages. The detail of each statistical test is provided in each figure legend. The correlation matrix was produced in R using publicly available code

downloaded from GitHub (Wherry research group, University of Pennsylvania). All graphs were prepared using ggplot2 in R v.4.0.3 or Prism v9 (GraphPad Software).

P values were considered as significant if <0.05 and false discovery rate (FDR) was set at <0.05.

CHAPTER 3- Immune perturbations of children with cancer

3.1 Introduction

It has been suggested that the immune system regulates cancer development through a process called “cancer immunoediting” (Dunn, Old and Schreiber, 2004). During this dynamic process the immune system has three key immunological features. First during the elimination phase, also known as cancer immunosurveillance, NK and T-cell responses eradicate the developing cancer cells (Dunn, Old and Schreiber, 2004). It has been suggested that the release of cytokines by the growing tumour cells activates the innate and adaptive immune system which then triggers a cascade of events leading to tumour elimination(Mittal *et al.*, 2014). If this process is successful, then there is no progression to the second phase. However, if some cancer cells do survive then they enter into equilibrium. During this phase, the immune system exerts persistent selection pressure on the cancer cells and they have to undergo through genetic changes to adapt. The end result of this phase is a new formation of malignant cells with reduced immunogenicity that allows them to move on to the final phase. In the escape phase, cancer cells can outgrow the immune system, allowing them to expand into tumours and become clinically detectable. This phase is associated with the creation of an immunosuppressive tumour microenvironment further enabling tumour growth, invasion and metastatic dissemination. Understanding the immunological mechanisms that lead to immune escape gave rise to several immunotherapies that harness the immune system to overcome the immunosuppressive tumour microenvironment and eradicate cancerous cells (Zhao *et al.*, 2019). These therapies had very promising results in adults’ cancers(Zhao *et al.*, 2019).

Turning to paediatric cancers, despite advances in chemotherapy and radiotherapy, paediatric malignancies remain one of the leading causes of death by disease in children and younger adults(Cunningham, Walton and Carter, 2018). In addition, the late effects of chemo- and radiotherapies can permanently impair the quality of life of the survivors in the future(Grabow *et al.*, 2018). It is therefore not surprising the increased interest in incorporating immunotherapies in the landscape of paediatric cancer therapies, as they offer an attractive more specific and less cytotoxic alternative. However, for immuno-modifying agents, the clinical response observed in adults with cancer did not translate into the paediatric cancer patients (Hutzen, Paudel, *et al.*, 2019). The reason behind this is not fully understood however, paediatric cancers are fundamentally different from those of adults. For example, paediatric tumours have fewer somatic mutations and therefore are less immunogenic due to the lack of actionable neoantigens(Campbell *et al.*, 2017) .

Furthermore, the paediatric immune system is not fully functional and gradually matures to that of an adult by encountering pathogens and vaccinations(Dowling and Levy, 2014). These differences in both the paediatric immune system and paediatric cancer biology could perhaps explain the difference in responses observed with immune-modulatory therapies. Therefore, understanding the role of the paediatric immune system in cancer is crucial to identify optimal immune-targeted treatment strategies for these patients.

The aim of this chapter was to characterise the immune system of children with cancer at the time of diagnosis and before any treatment was administered and compare this to that of healthy children.

3.2 Cohort Demographics

3.2.1 Ethical statement and patient recruitment

All patient samples were obtained at Birmingham Children's Hospital (BCH) as part of a study (TrICICL) approved by the South of Birmingham Research Ethics Committee (REC: 17/WM/0453, IRAS: 233593). Samples from seven healthy children (aged 12 years) were obtained via the Coronavirus Immunological Analysis study approved by North West - Preston Research Ethics Committee (REC: 20/NW/0240, IRAS: 282164). Written informed consent was obtained from all participants' legal guardians. All laboratory experiments were conducted at the University of Birmingham (UoB).

3.2.2 Patient Characteristics

Between April 2018 and March 2021, 51 children with a range of cancer diagnoses were recruited from BCH. Research samples were obtained from paediatric cancer patients before any disease modifying treatment was administered and processed at UOB within 24 hours. In addition, 33 aged-matched children without cancer were also recruited. These patients were attending BCH for routine surgical procedures, for example orchidopexy or endoscopy foreign body removal, and were screened through a questionnaire to ensure they were healthy with no underlying conditions. The analyses were performed in two different cohorts. The first one was used as a discovery cohort while the other one was used as a validation cohort. Key demographic information is summarized in Tables 3.1 and 3.2. There was no difference in the age distribution between paediatric healthy (PH) and paediatric cancer (PC) cohorts (figure3.1).

Paediatric Healthy

Study Number	Age	Gender
HV01	37m	Female
HV05	12m	Male
HV06	17m	Female
HV11	19m	Male
HV12	72m	Female
HV13	170m	Female
HV14	20m	Female
HV15	22m	Male
HV16	78m	Male
HV18	15m	Male
HV20	110m	Female
HV21	74m	Female
HV22	42m	Male
HV25	77m	Male
HV26	12m	Female
HV28	35m	Male
HV30	126m	Male
HV34	174m	Female
HV37	54m	Female

Paediatric Cancer

Study Number	Age	Gender	Disease
C01	79m	Female	Rhabdomyosarcoma
C02	73m	Male	Burkitt's lymphoma
C03	36m	Female	Neuroblastoma
C04	167m	Female	Hodgkin's disease
C05	58m	Male	Wilms
C06	187m	Female	Rhabdomyosarcoma
C07	122m	Male	Hodgkin's disease
C08	20m	Male	Neuroblastoma
C09	17m	Female	Rhabdoid tumour
C10	145m	Female	Burkitt's lymphoma
C11	17m	Male	Neuroblastoma
C12	22m	Female	Pilomyxoid astrocytoma
C14	179m	Female	Ewing's sarcoma
C15	187m	Male	Hodgkin's disease (non classical NHPHL)
C16	12m	Male	Neuroblastoma
C18	36m	Female	Hepatoblastoma
C19	12m	Male	Nephroblastomatosis
C20	73m	Male	Hodgkin's disease
C21	34m	Male	Burkitts lymphoma
C22	75m	Female	Parameningeal Rhabdomyosarcoma

Table 3-1 First cohort demographics.

Demographic data for the paediatric healthy donors and paediatric cancer patients. The diagnosis for each patient is also shown. Age is provided in months.

Paediatric Healthy

Study Number	Age	Gender
HV04	16m	Female
HV07	7m	Male
HV11	19m	Male
HV12	72m	Female
HV13	170m	Female
HV14	20m	Female
HV15	22m	Male
HV16	78m	Male
HV19	51m	Male
HV21	74m	Female
HV23	30m	Male
HV24	137m	Female
HV25	77m	Male
HV27	109m	Male
HV30	126m	Male
HV31	11m	Male
HV37	54m	Female
HV38	153m	Male
HV39	147m	Female
HV40	155m	Male
HV41	154m	Male
HV42	150m	Male
HV43	155m	Male
HV44	124m	Male

Paediatric Cancer

Study Number	Age	Gender	Disease
C23	56m	Female	Wilms
C24	172m	Female	Hodgkins Disease
C25	29m	Male	Neuroblastoma
C26	167m	Female	Osteosarcoma
C27	179m	Male	Hodgkins Disease
C28	59m	Male	Rhabdomyosarcoma
C29	51m	Male	Rhabdomyosarcoma
C30	189m	Female	Ewings sarcoma
C31	176m	Male	Hodgkins Disease
C32	118m	Male	Hodgkins Disease
C33	130m	Female	Ewings sarcoma
C34	47m	Female	Wilms
C35	183m	Male	Osteosarcoma
C36	19m	Female	Wilms
C37	38m	Female	Wilms
C38	32m	Male	Embryonal supratentorial tumour
C39	143m	Male	Osteosarcoma
C40	163m	Female	Hodgkins Disease
C41	162m	Male	Mixed Germ Cell Tumour
C42	149m	Male	Rhabdomyosarcoma
C44	87m	Male	B-cell Lymphoma
C45	189m	Male	Hodgkins Disease
C46	86m	Male	Rhabdomyosarcoma
C47	4m	Female	Rhabdoid tumour
C48	170m	Male	Hodgkins disease
C49	188m	Female	Rhabdoid tumour
C50	88m	Female	Hepatoblastoma
C51	65m	Male	Rhabdomyosarcoma
C52	152m	Male	Rhabdomyosarcoma
C53	158m	Female	Osteosarcoma
C54	169m	Female	Ewings sarcoma

Table 3-2 Second cohort demographics.

Demographic data for the paediatric healthy donors and paediatric cancer patients. The diagnosis for each patient is also shown. Age is provided in months.

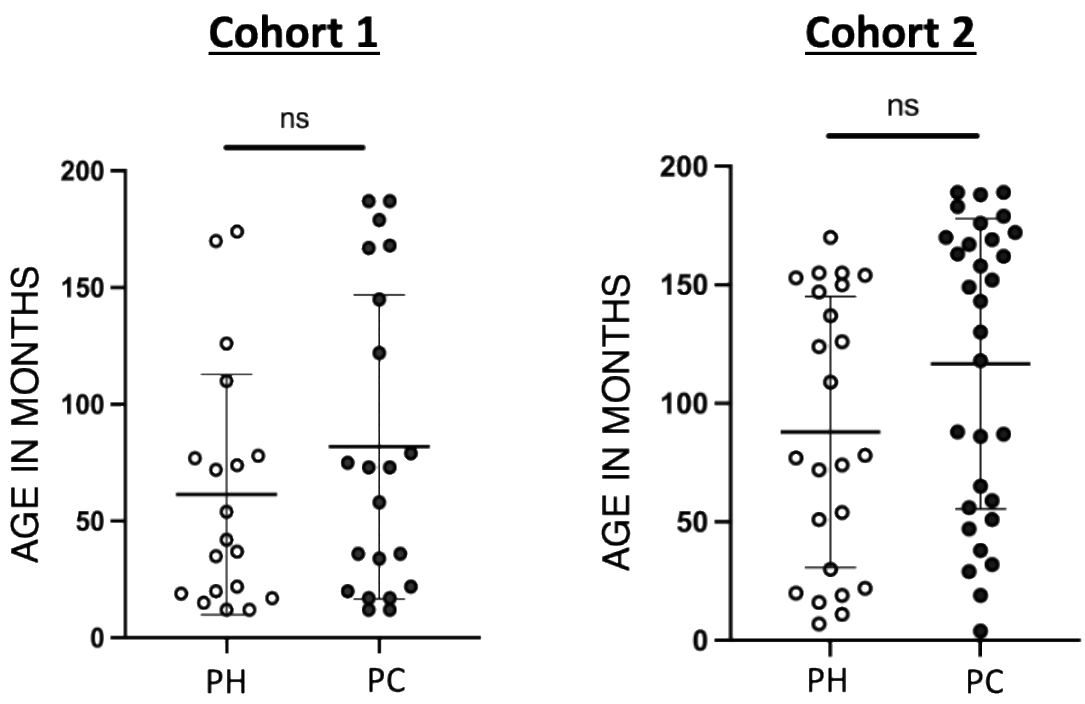

Figure 3-1 Age distribution for paediatric healthy (PH) and paediatric cancer (PC).

The age distribution is shown for the 2 cohorts. Error bars show mean +/-1 standard deviation. There was no significant difference in age between the two groups (unpaired t-test).

3.3 Clinical laboratory data of paediatric cancer patients

3.3.1 Anaemia is the presenting feature of paediatric cancer patients

Pre-treatment full blood count (FBC) data taken at the time of diagnosis were collected for all cancer patients, with the exception of patient C26 for whom data were not available. The most important parameters are shown in figure 3.2A. Haemoglobin was low in 76% of the cancer patients. This is consistent with adult cancer studies that reported cancer-related anaemia at the time of diagnosis reported to be secondary to cytokines released by the tumour causing bone marrow suppression (Bokemeyer, Oechsle and Hartmann, 2005). In contrast, total white blood cells (WBC) were abnormal in 14% of the cancer patients, with the majority presenting with higher rather than lower WBC values. Platelet counts were abnormal in 38% of patients and were always higher than reference values. This phenomenon has also been described in adult cancers as a paraneoplastic abnormality that promotes tumour growth and metastasis through a variety of cytokine release (Lin, Afshar-Kharghan and Schafer, 2014). Focusing on WBC subsets, 26% of the patients presented with neutrophilia. Lymphocytes on the other hand, were either normal (74%) or low (26%). Finally, monocytes were increased in 30% of the patients. Interestingly, there was no distinct pattern regarding these alterations, which were present in both solid tumours and lymphomas. However, when we tracked the different parameters at the level of individuals it was evident that patients tended to have either lower or higher values in all parameters (figure 3.2 B).

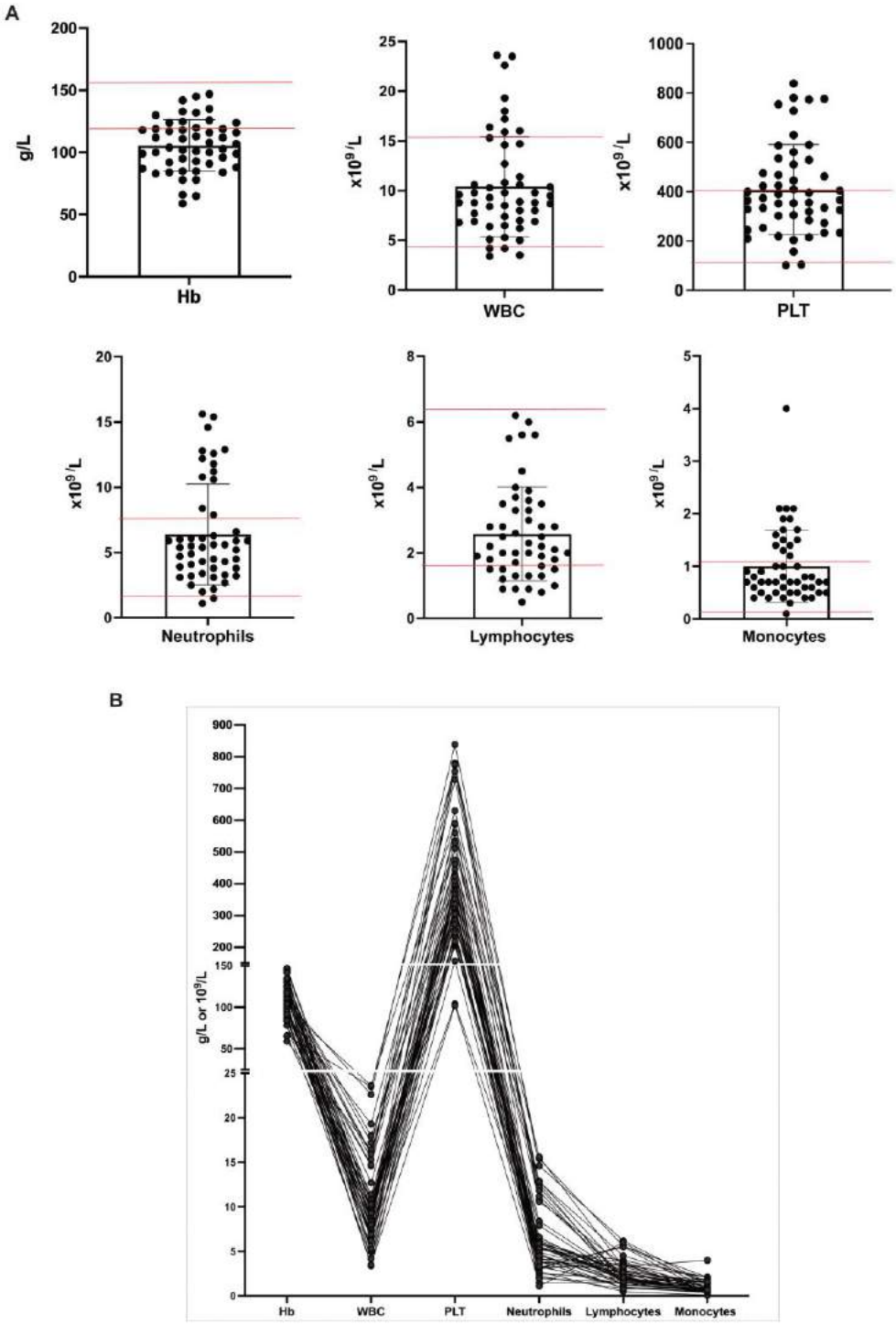

Figure 3-2 Clinical laboratory data for cancer patients.

(A) Haemoglobin (Hb), White Blood Cells (WBC), Platelets (PLT), Neutrophils, lymphocytes and monocytes values are shown for each individual and the mean with SD is also shown. The red lines represent the lowest and highest values within the normal range for each parameter. Individuals outside of these lines are considered to have an abnormal value. (B) All values taken together and mapped for each individual.

3.3.2 Increased reticulocyte indices in paediatric cancer patients indicates release of immature reticulocyte by the bone marrow

Paediatric cancer samples arrived and were processed at our lab within 24 hours of sample collection. During peripheral blood mononuclear cells (PBMC) isolation some paediatric patients' samples had marked differences in appearances compared to the healthy ones. (figure 3.3). In particular, the lymphocyte layer of samples from paediatric cancer patients was blood stained suggesting red blood cells (RBC) contamination. This made us postulate that these RBCs were of low density for them to float on the density layer with lymphocytes. We, therefore, hypothesized that they could be immature RBCs.

To investigate this further, we performed reticulocyte indices analysis (Wollmann *et al.*, 2014) on a subset of patients and healthy children (figure 3.4). Standard reticulocyte count was not different between healthy and cancer patients however a trend towards higher reticulocyte count was observed in cancer patients. Using the Sysmex technology reticulocytes were further analysed based on their RNA content and classified into three groups according to their fluorescence intensity: low fluorescence ratio (LFR), medium fluorescence ratio (MFR), and high fluorescence ratio (HFR). The fluorescence intensity is proportional to the amount of RNA contained in the reticulocytes and their degree of maturation therefore, higher fluorescence ratio correlates with more immature reticulocytes (Wollmann *et al.*, 2014). MFR and HFR were significantly increased while LFR significantly decreased in paediatric cancer patients suggesting these cells were more immature. In summary, higher counts of immature reticulocytes were released into the periphery of paediatric cancer patients. These results require validation in larger cohorts.

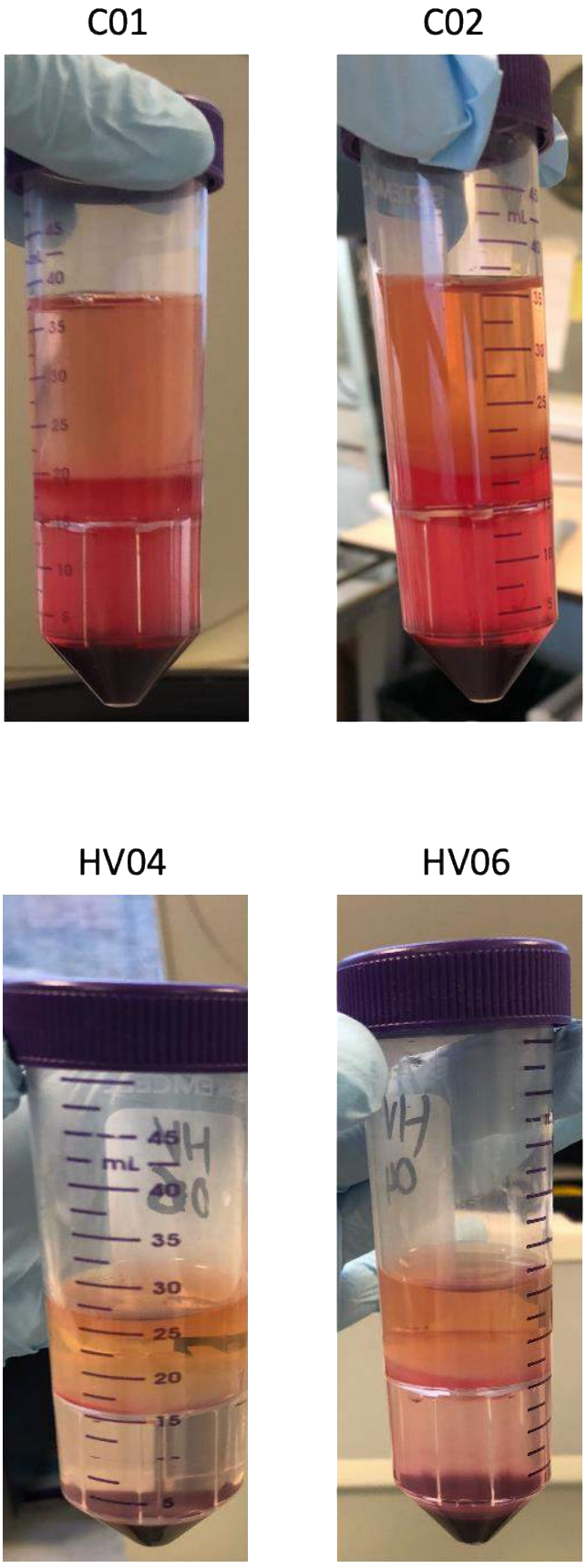

Figure 3-3 Lymhoprep preparation for paediatric cancer and paediatric healthy children.

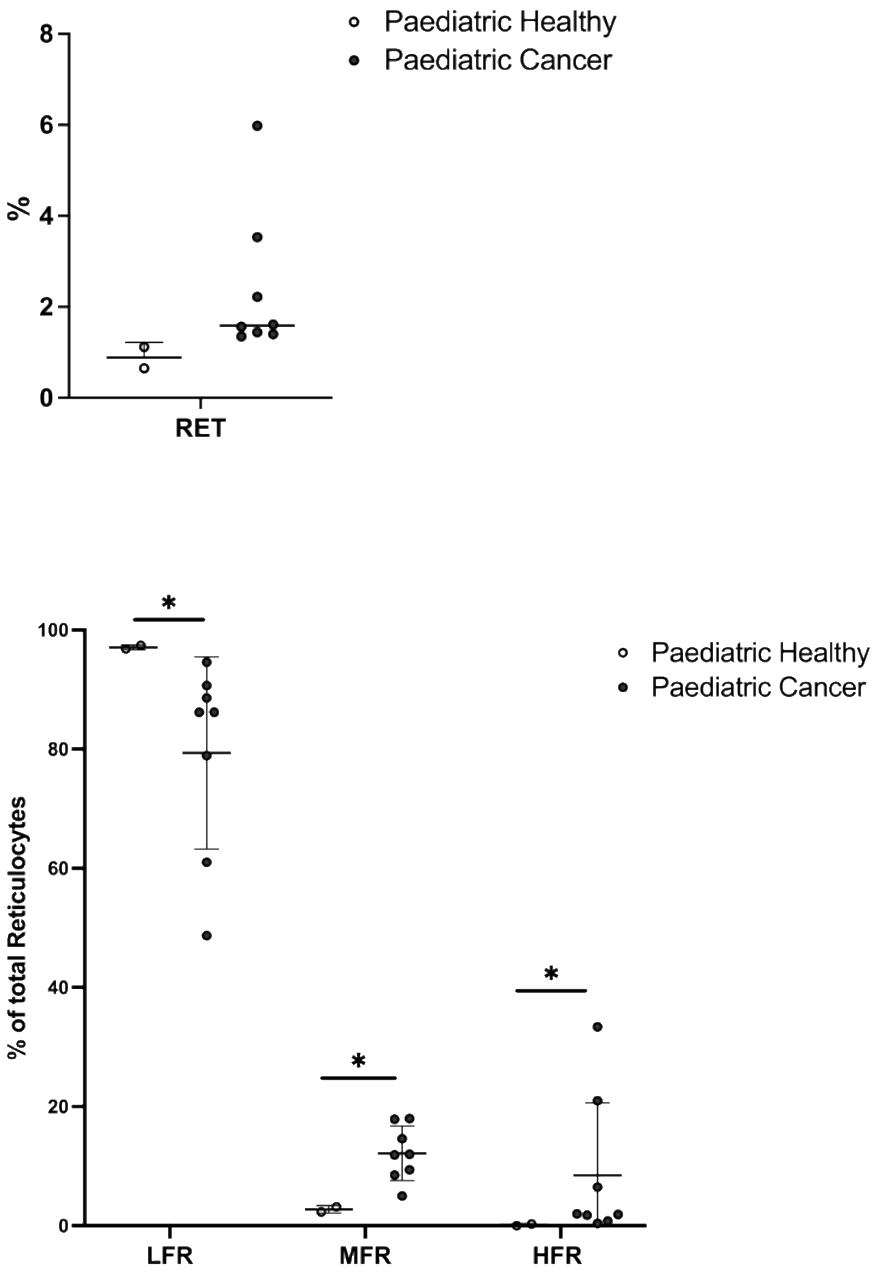

Figure 3-4 Immature reticulocytes are increased in paediatric cancer patients.

Reticulocyte percentage (RET), low fluorescence ratio (LFR), medium fluorescence ratio (MFR), and high fluorescence ratio (HFR) are shown for paediatric healthy and paediatric cancer patients. Error bars show the mean +/- 1 standard deviation. P values were calculated using Wilcoxon ranked sum tests with false discovery rate at 5% and correction using the Benjamini-Hochberg method. Significant results are indicated: * $p<0.05$, ** $p<0.01$, *** $p<0.001$.

3.4 Mass Cytometry Analysis show marked NK deficit in paediatric cancer patients

3.4.1 NK cells are decreased in paediatric cancer patients

To explore in more detail the immune changes in children with cancer, peripheral blood mononuclear cells (PBMCs) from 20 children diagnosed with a variety of childhood cancers (Table 3.1) and 19 age-matched healthy children were analysed using a 38-marker mass cytometry panel. Samples from paediatric cancer patients were taken at the time of diagnosis and before any treatment was administered. For visualisation purposes flow cytometry standard (fcs) files from patients and healthy children were concatenated into two separate files using equal numbers of cells from each individual (4751 cells).

To get an overview of the dataset, manual gating of CD3-CD19- and CD3+CD19+ populations were performed (figure 3.5A). These populations were then configured using the UMAP dimensionality reduction package(McInnes *et al.*, 2018). Based on their linear marker expression we were able to identify the main immune subsets: Monocytes, NK cells, CD4, CD8, γδ, MAIT and B-cells (figure 3.6). The UMAP plots of paediatric healthy and cancer showed clear differences in the distributions of innate immune cells with monocytes increased and NK cells decreased in paediatric cancer patients (figure 3.5B).

Next, the frequency of the main immune subsets for each individual were examined. Equal numbers of CD45+ cells (4.751 cells) from paediatric cancer patients, healthy children and concatenated fcs files were configured using the ViSNE implementation in Cytobank. Gating on the tSNE projection of the data was preferred as this produced better separation of low

abundance cell populations like γδ and Mait T-cells (Becht *et al.*, 2019). The main immune subsets were therefore, identified on the t-SNE maps using their linear markers as follows: CD3+CD4+ T-cells, CD3+CD8+ T-cells, CD3+TCRγδ+ T-cells, CD3+TCRVa7.2 MAIT T-cells, CD19+ B-cells, CD56+ NKs cells and CD14+ Monocytes (figure 3.7).

Analysing the cell frequency for each individual revealed that patients had a significantly lower frequency of NK cells ($p=0.0035$) and a trend for increased monocytes (figure 3.8). The frequency of T and B cell subsets were not significantly different (figure 3.8).

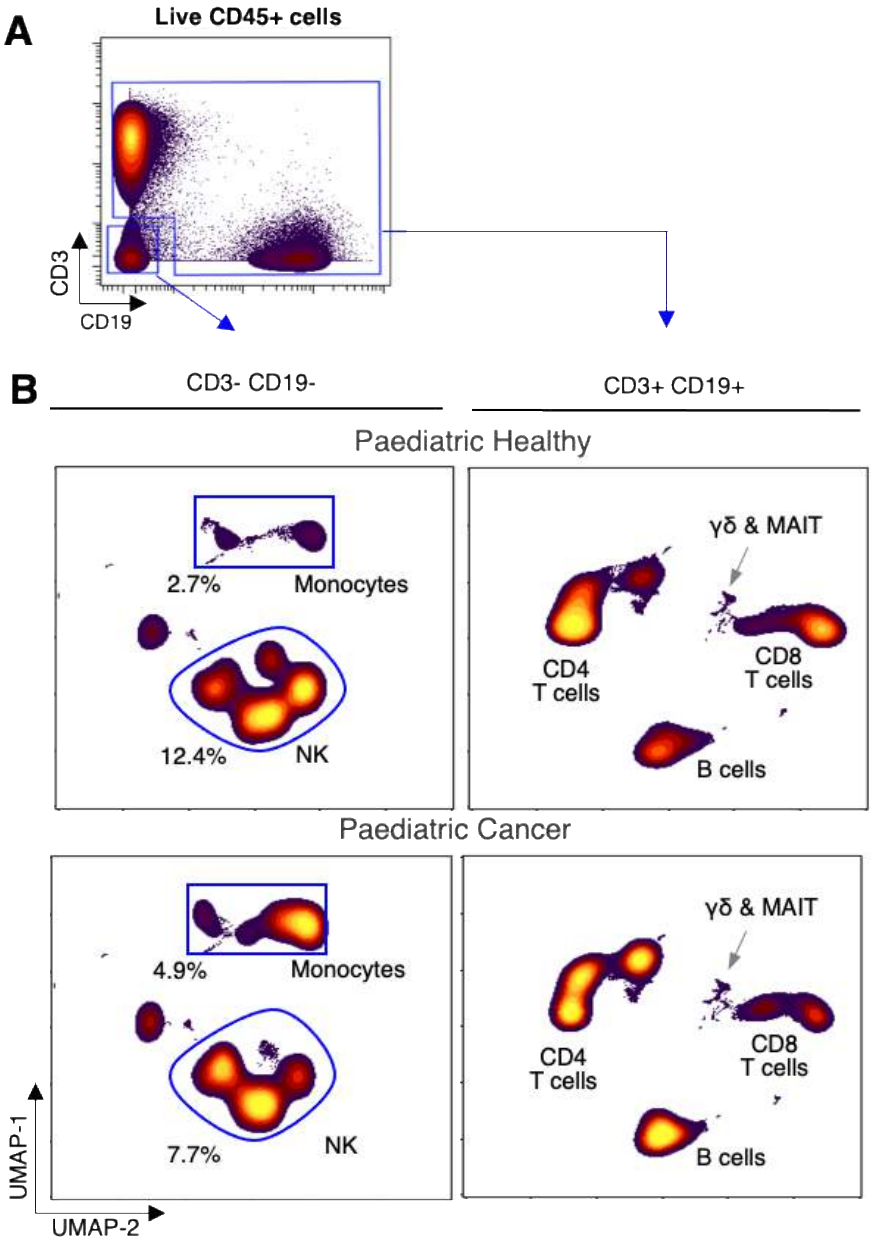

Figure 3-5 UMAP plots of both innate and adaptive immune cells in paediatric healthy and cancer.

(A) Manual gating strategy used to split immune cells into CD3-CD19- and CD3+Cd19+subsets. (B) Concatenated fcs files for both paediatric healthy (n=19) and paediatric cancer patients (n=20) were analysed by UMAP dimensionality reduction. The frequency and identify of main immune subsets is shown.

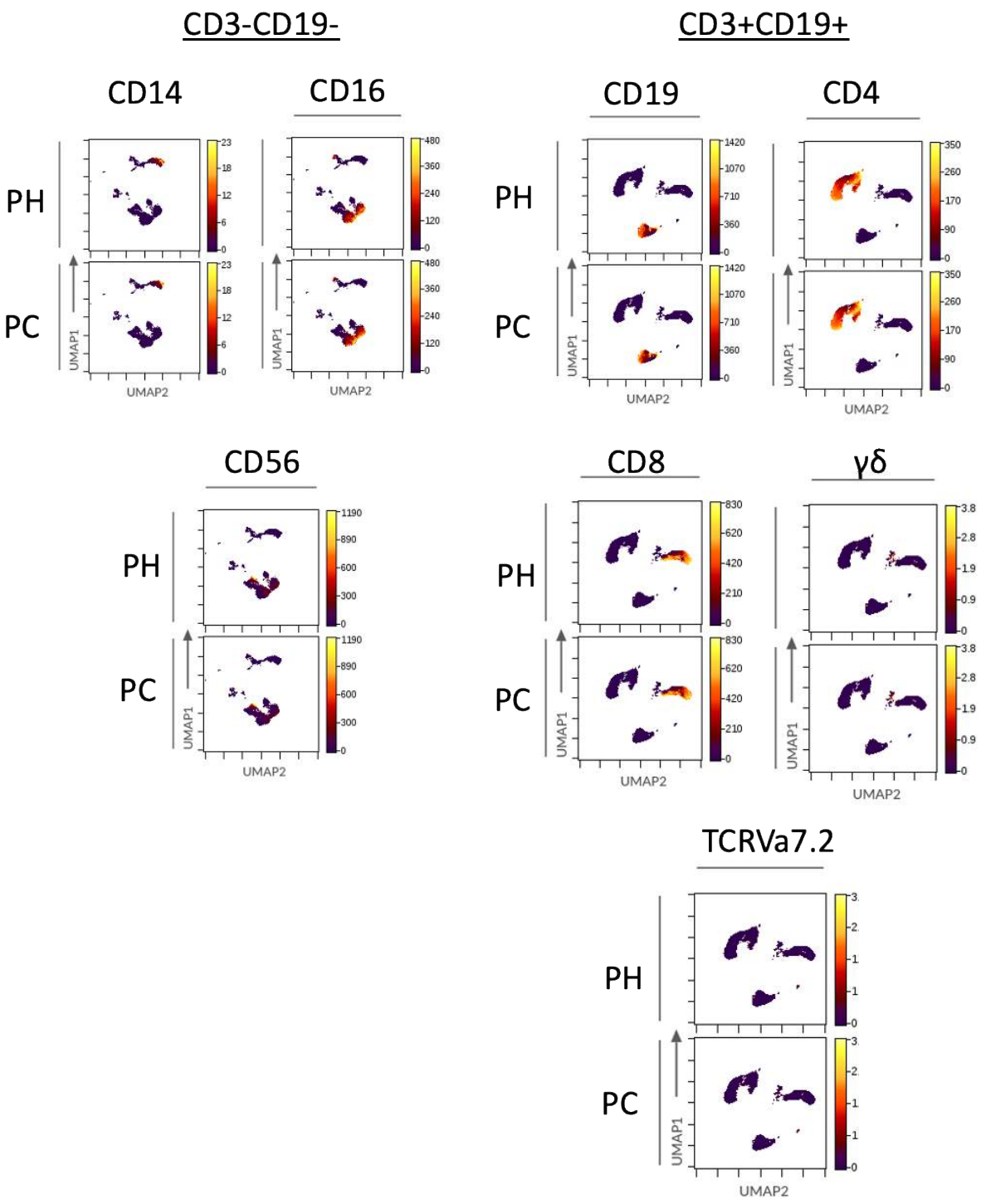

Figure 3-6 Linear marker expression shown for the main immune subsets.

Marker expression of the main immune subsets is shown for Peadiatric Healthy (PH) and Paediatric Cancer (PC) on the UMAP plots.

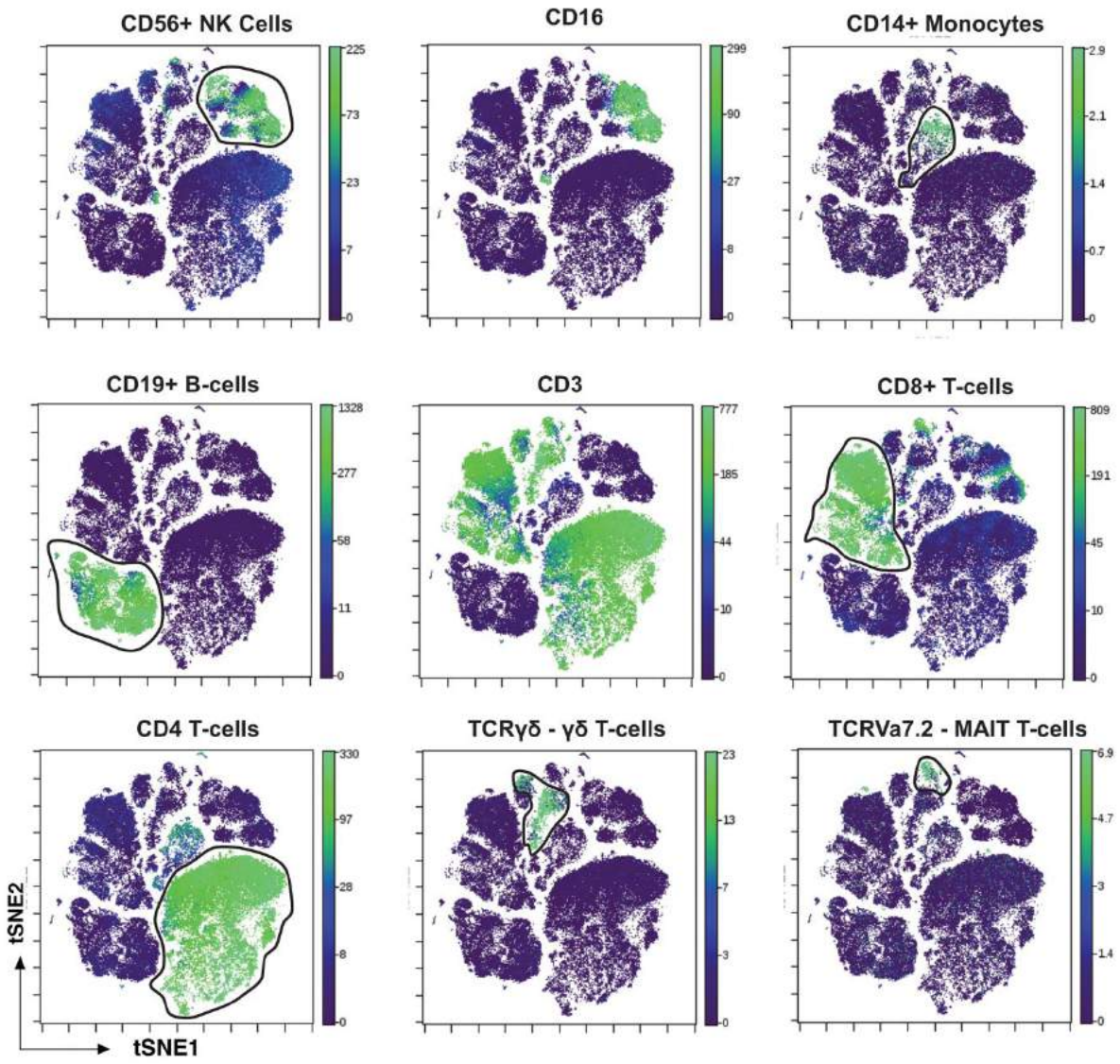

Figure 3-7 Gating strategy for data analysis.

Gating strategy used to separate total immune cells into subsets for analysis. Each subset is determined by the indicated marker. Intensity of staining is represented by colour, with levels shown on the right-hand side of each plot. This illustration was performed using the paediatric healthy concatenated files.

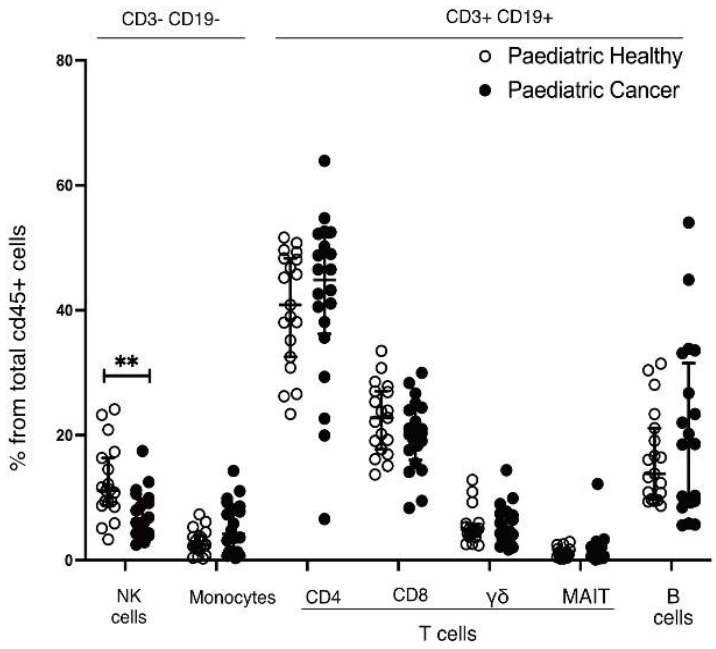

Figure 3-8 Frequency of the main immune subsets at the level of individual.

Frequency of the main immune subsets for all healthy children (open symbols) and cancer patients (closed symbols) expressed as a percentage of total CD45+ cells. Error bars show the mean +/- 1 standard deviation. P values were calculated using Wilcoxon ranked sum tests with false discovery rate at 5% and correction using the Benjamini-Hochberg method. Significant results are indicated: * $p<0.05$, ** $p<0.01$, *** $p<0.001$.

3.4.2 Analysis of NK subsets show an increase of CD56^{bright} CD16- NK cells and decrease of CD57+ NK cells in paediatric cancer patients

Having demonstrated the decrease in frequency of the NK cells in the paediatric cancer patients, NK phenotypic changes were next examined. Classical NK differentiation markers CD56 and CD16 (Cooper, Fehniger and Caligiuri, 2001) were used to separate NK cells into three distinct subsets: CD56^{bright}CD16-, CD56^{dim}CD16- and CD56+CD16+(figure 3.9A). Analysis of these subsets for individuals showed that cancer patients possessed higher frequencies of the CD56^{bright}CD16- NK cells, a subset that is considered to be immature (Caligiuri, 2008, figure 3.9C). Particularly, this was 1.4-fold higher in cancer patients compared to healthy children. Assessing the subset overlay on the t-SNE map created from the CD56+ NK cells, it was evident this subset was more prominent in the paediatric cancer patients (figure 3.9B).

Next, a range of NK phenotypic markers expression was examined on total NK cells. Paediatric cancer patients had higher proportions of NK cells expressing markers associated with NK immaturity CD25, CD27, CD127 and HLA-DR (Lee, Fragoso and Biron, 2012, 2012; Scoville, Freud and Caligiuri, 2017; Erokhina *et al.*, 2018, p. , figure 3.9D). Accordingly, markers of maturity CD45RA and CD57(Lopez-Vergès *et al.*, 2010; Krzywinska *et al.*, 2016) were lower in paediatric cancer patients (figure 3.9D). There were no differences in the proportion of NK cells bearing the adhesion molecule CD11b(Somersalo *et al.*, 1992), the adhesion molecule and ectoenzyme CD38 nor CD161(Kurioka *et al.*, 2018; Le Gars *et al.*, 2019), markers expressed by pro-inflammatory NK cells. There was also no difference in the expression of CXCR3 which is required for NK tumour recruitment(Wendel *et al.*, 2008). Interestingly, cancer patients possessed higher levels of NK cells expressing CCR7, a

chemokine receptor that is thought to be acquired in response to IL-18 rich environment and it is thought to promote NK migration to lymphoid tissues (Pesce *et al.*, 2016). Finally, the expression of the immune checkpoint inhibitor PD-1 was examined(Barrow and Colonna, 2019). PD-1 is expressed on a minority of mature NK cells and in adult cancer patients was found to be increased(Niu *et al.*, 2020, p. 1). In contrast, our data showed that paediatric cancer patients had a significant lower frequency of PD-1 positive NK cells compared to healthy children.

We then examined whether the expression of each phenotypic marker was similar or different in all three NK subsets (figure 3.10). CXCR3 expression was significantly lower in the first subset ($CD56^{bright}$CD16-) of cancer patients. In the second subset ($CD56^{dim}$CD16-), markers of maturity CD45RA and CD57 as well as CD38 and CD161 were also significantly lower in paediatric cancer, while in the third and most mature subset (CD56+CD16+), CD57 expression was also noted to be significantly lower in disease. In summary, these results indicate that the increased expression of the immature receptors noted in the total NK cells of paediatric cancer patients, was driven by the expansion of the $CD56^{bright}$ NK subset. On the other hand, the decreased expression of the NK mature receptors was driven primarily by the NK subsets 2 and 3.

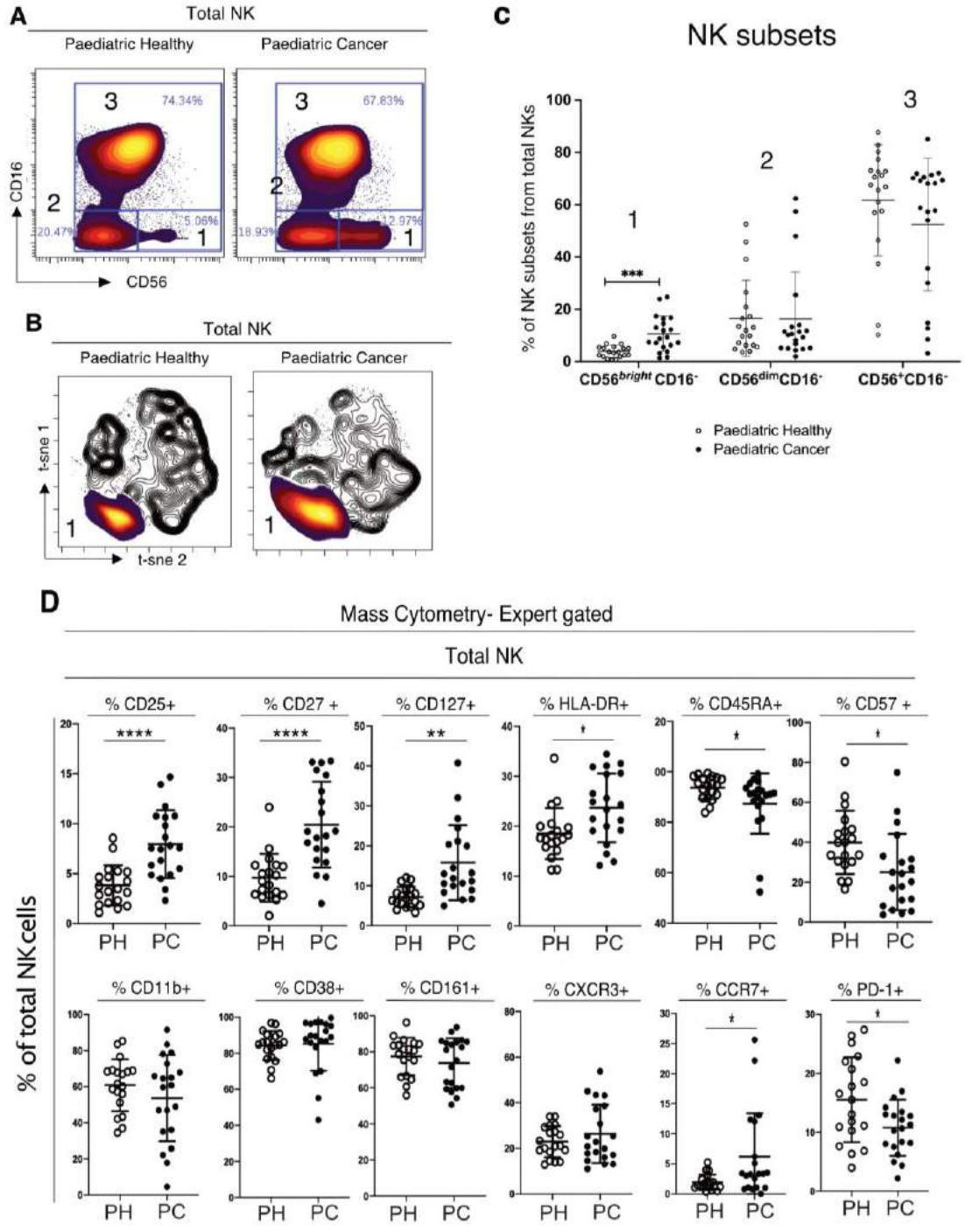
A
Total NK
Paediatric Healthy
Paediatric Cancer
CD16
CD56
74.34%
67.83%
B
Total NK
Paediatric Healthy
Paediatric Cancer
t-sne 1
t-sne 2
C
NK subsets
% of NK subsets from total NKs
CD56bright CD16-
CD56dim CD16-
CD56+CD16-
Paediatric Healthy
Paediatric Cancer
D
Mass Cytometry- Expert gated
Total NK
% of total NK cells
% CD25+
% CD27 +
% CD127+
% HLA-DR+
% CD45RA+
% CD57 +
% CD11b+
% CD38+
% CD161+
% CXCR3+
% CCR7+
% PD-1+
PH
PC

Figure 3-9 Immature NK cells are increased in frequency in paediatric cancer patients.

(A) Biaxial plots of concatenated FCS files from healthy children (n=19) and cancer patients (n=20). Total NK cells were manually gated using CD16 and CD56 expression to delineate NK cells into four canonical differentiation subsets. In order of maturity: subset 1 ($CD56^{bright}CD16^{-}$), 2 ($CD56^{dim}CD16^{-}$), 3 ($CD56^{+}CD16^{+}$. The proportion of NK cells in each subset is shown on each plot. B) Heat plots of cell density from subset 1 were overlaid on black and white contour tSNE plots of total NK cells from paediatric healthy donors (left panel) and cancer patients (right panel). C) Frequency of each NK subset, expressed as a percentage of total NK cells per individual. (D) Mass cytometry analysis of paediatric cancer patients and paediatric healthy showing percentage of total NK cells positive for the indicated markers. The mean +/- 1 standard deviation is shown. P values were calculated using Wilcoxon ranked sum tests with false discovery rate at 5% and correction using the Benjamini-Hochberg method. Significant results are indicated: * $p<0.05$, ** $p<0.01$, *** $p<0.001$.

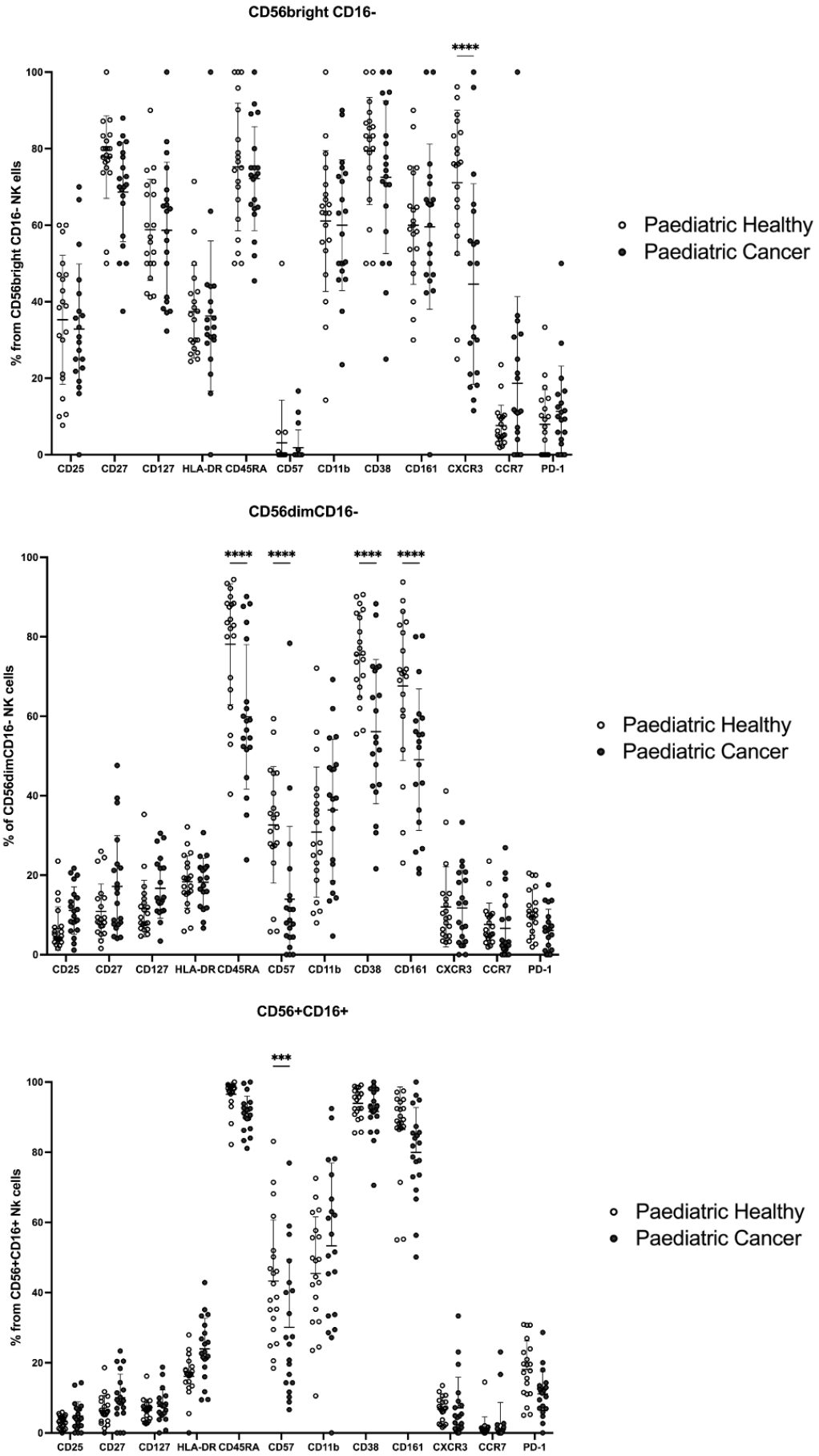
CD56bright CD16-
% from CD56bright CD16- NK ells
****
CD25 CD27 CD127 HLA-DR CD45RA CD57 CD11b CD38 CD161 CXCR3 CCR7 PD-1
Paediatric Healthy
Paediatric Cancer
CD56dimCD16-
% of CD56dimCD16- NK cells
**** **** **** ****
CD25 CD27 CD127 HLA-DR CD45RA CD57 CD11b CD38 CD161 CXCR3 CCR7 PD-1
Paediatric Healthy
Paediatric Cancer
CD56+CD16+
% from CD56+CD16+ Nk cells
***
CD25 CD27 CD127 HLA-DR CD45RA CD57 CD11b CD38 CD161 CXCR3 CCR7 PD-1
Paediatric Healthy
Paediatric Cancer

Figure 3-10 Phenotypic markers shown in all 3 NK subsets.

Frequency of NK cells within each of the four NK subsets (defined using CD16 and CD56) showing the percentage of cells positive for each of the indicated markers. The error bars show the mean +/- one standard deviation. P values were calculated using Wilcoxon ranked sum tests with false discovery rate at 5% and correction using the Benjamini-Hochberg method. Significant results are indicated: * $p<0.05$, ** $p<0.01$, *** $p<0.001$.

3.4.3 HLA-DR expression is decreased in paediatric cancer patients' monocytes.

Turning now to monocytes, a trend towards increased abundance of monocytes in paediatric cancer patients, was seen in both mass cytometry data (figure 3.8) and absolute counts data (figure 3.2). Using CD14 and CD16 to delineate the main monocyte subsets(Ziegler-Heitbrock *et al.*, 2010a) —classical monocytes (CM, CD14+ CD16-), transitional monocytes (TM, CD14+CD16+ and non-classical monocytes (NCM, CD14-CD16+) —we found patients' monocytes contained a significant higher proportion of TM (3.11A and B).

Next, Marker Enrichment Modelling (MEM) (Diggins *et al.*, 2018), an algorithm that quantifies the enriched features of a cell population was applied in order to determine whether the monocytes were also altered in phenotype. This analysis showed monocytes from healthy children were positively enriched for HLA-DR (▲HLA-DR^{+6}) whereas monocytes from paediatric cancer patients were negatively enriched (▼HLA-DR^{-4}, figure 3.12A). Differences in monocyte HLA-DR levels were confirmed by measuring the HLA-DR median mass intensity on total monocytes gated from each individual (Figure 3.12B). Finally, comparing HLA-DR levels on each monocyte subset, we observed HLA-DR levels on CM to be

significantly lower for paediatric cancer patients compared to healthy children (Figure 3.12B). In summary, monocytes alterations were observed in paediatric cancer patients with the expansion of TM and overall decreased HLA-DR expression in total monocytes and more specifically CM.

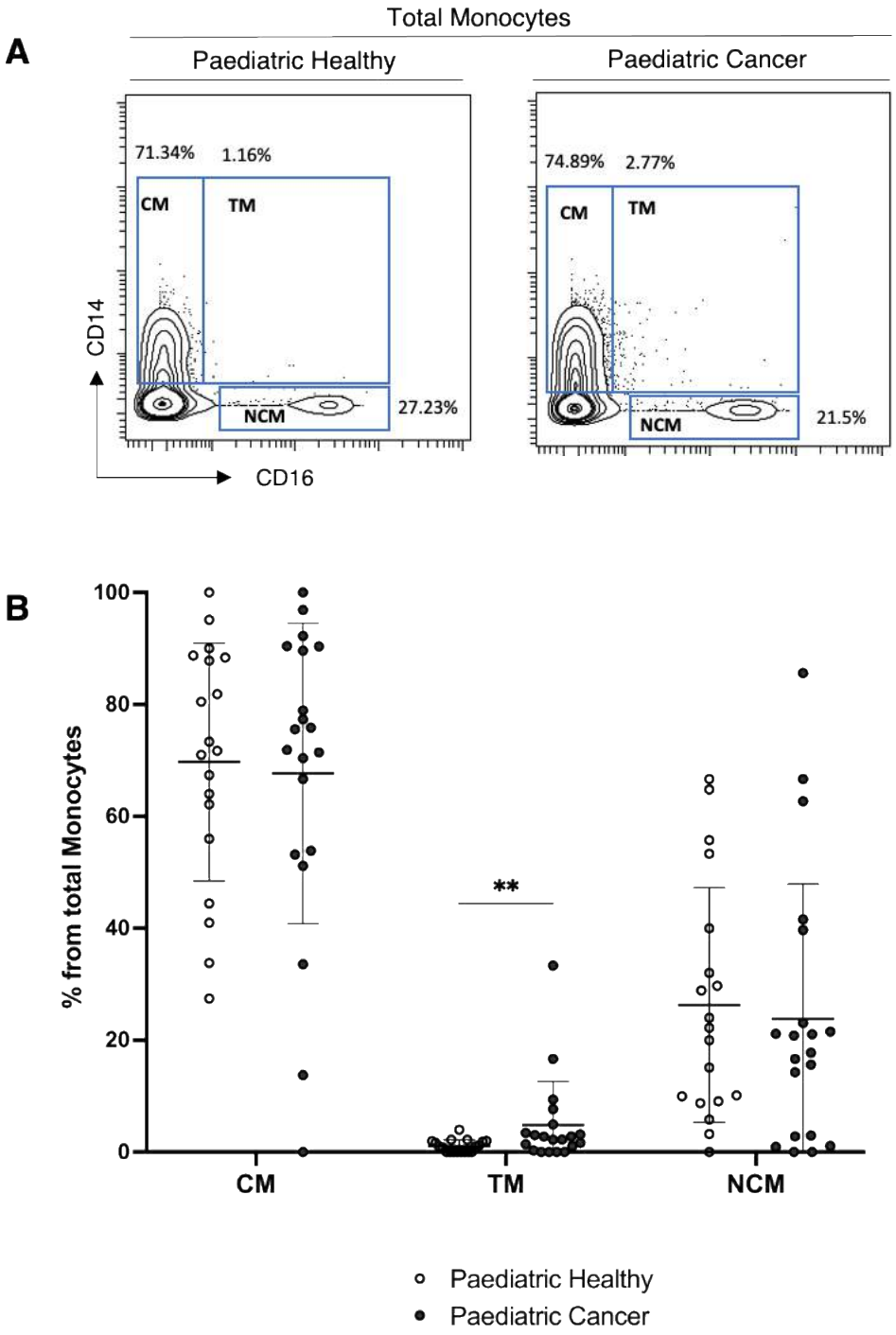

Figure 3-11 Transitional Monocytes are expanding in paediatric cancer patients.

(A) Manual gating strategy for monocytes subsets shown for paediatric healthy and paediatric cancer patients. (B) Frequency of each monocyte subset shown at the level of each individual. The error bars show the mean +/- one standard deviation. P values were calculated using Wilcoxon ranked sum tests with false discovery rate at 5% and correction using the Benjamini-Hochberg method. Significant results are indicated: * $p<0.05$, ** $p<0.01$, *** $p<0.001$.

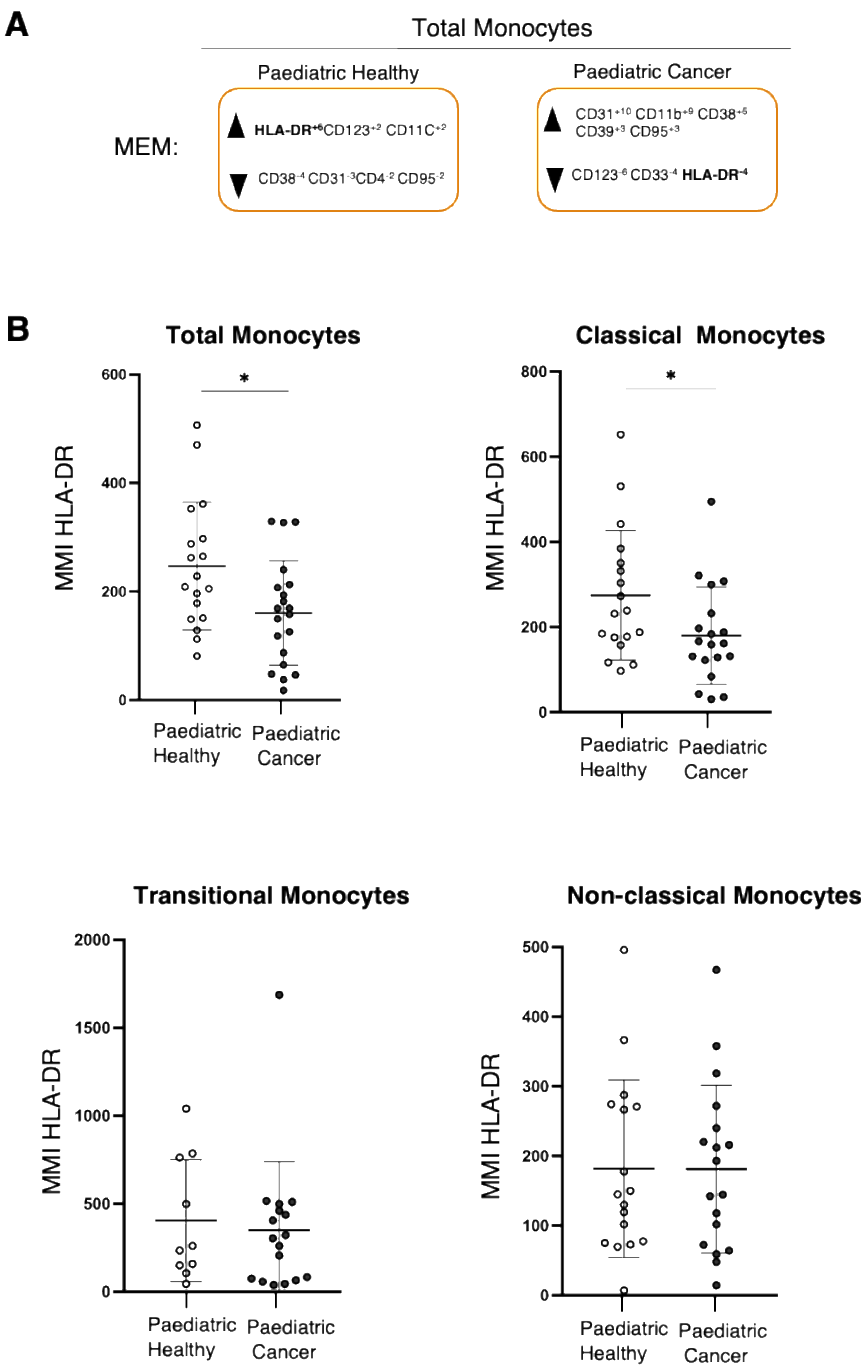

Figure 3-12 Monocytes in paediatric cancer patients have decreased expression of HLA-DR.

(A) Results of Marker enrichment modelling (MEM) of total monocytes. (B) Median mass intensity (MMI) of HLA-DR on total monocytes, classical monocytes, transitional monocytes and non-classical monocytes shown for each individual. Note for some donors the MMI could not be calculated due to the absence of some subsets. The error bars show the mean +/- one standard deviation. P values were calculated using Wilcoxon ranked sum tests with false discovery rate at 5% and correction using the Benjamini-Hochberg method. Significant results are indicated: * $p<0.05$, ** $p<0.01$, *** $p<0.001$.

3.4.4 Phenotypical changes are observed in B-cells of paediatric cancer patients

Moving on to B-cells, there was no significant difference in the frequency of total B-cells between paediatric cancer patients and paediatric healthy (figure 3.8). To investigate whether differences existed in the B-cell subsets(Blomberg and Frasca, 2013; Cossarizza *et al.*, 2019) manual gating of the main subsets was performed as follows: Plasmablasts ($CD27^{high}CD38^{high}$), Non-switch memory B-cells (IgD+CD27+), Class-switch memory B-cells (IGD-CD27+), Naïve B-cells (IgD+Cd27) and double negative B-cells (IgD-CD27-, figure 3.13A). No difference in frequency was observed in the B-cell subsets between paediatric cancer patients and paediatric healthy children (figure 3.13B).

Next, heatmaps were generated of B-cells and their subsets, in order to investigate the phenotypical differences of B-cells in paediatric cancer patients and paediatric healthy children (figure 3.14A). Overall, several B-cells markers were decreased in paediatric cancer patients including: CXCR5, CD73, CD39 and CCR6. This decrease of marker expression was only significant for CXCR5 and CCR6 and was not driven by one particular B-cell subset, as it was seen in both memory and the naïve B-cells subsets (figure 3.14B).

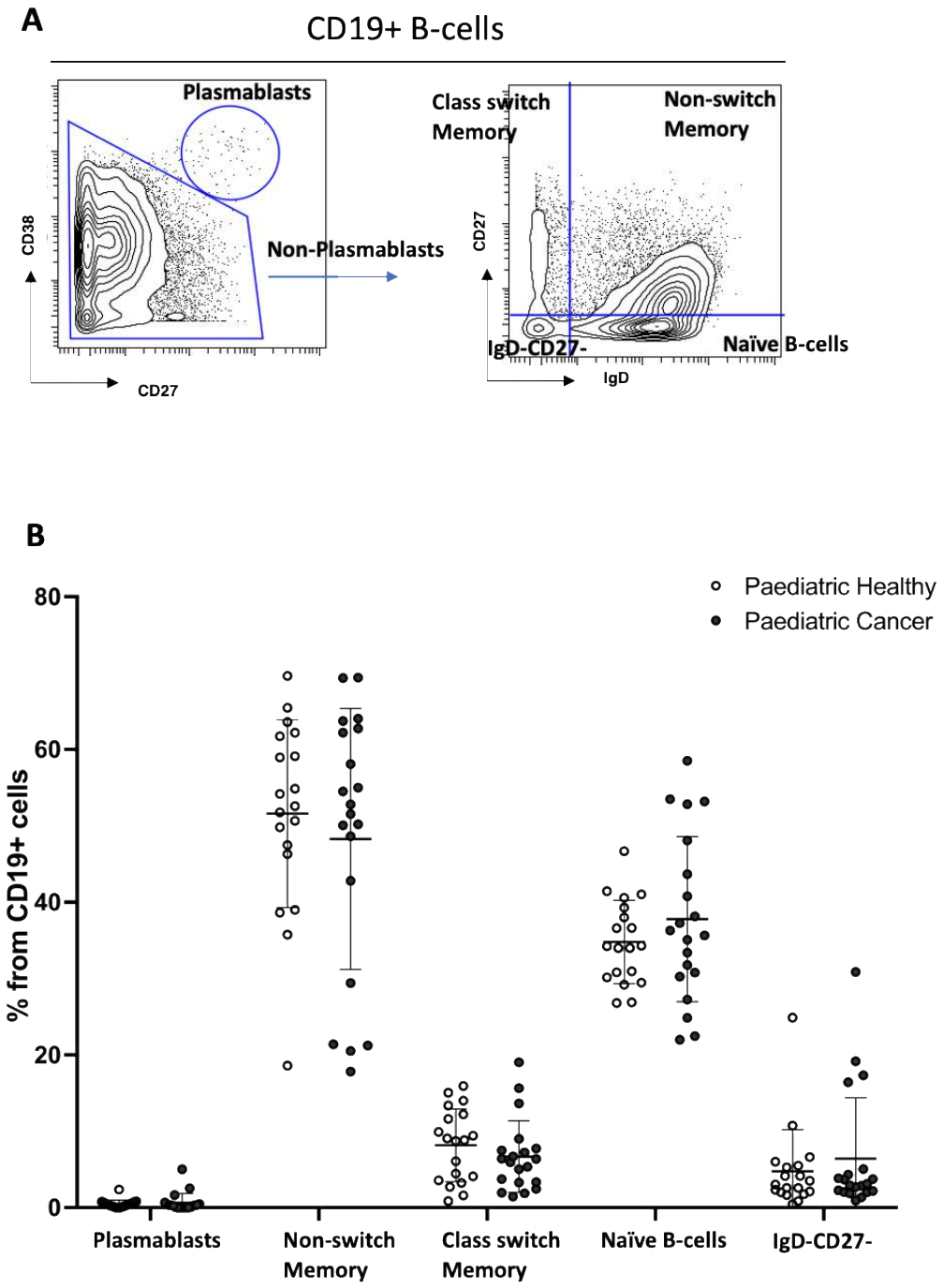

Figure 3-13 B-cells are not altered in frequency in paediatric cancer patients.

(A) Gating strategy for the main B-cells subsets. (B) Frequencies of main B-cells subsets shown at the level of individual. The error bars show the mean +/- one standard deviation. P values were calculated using Wilcoxon ranked sum tests with false discovery rate at 5% and correction using the Benjamini-Hochberg method. No significant results are not indicated.

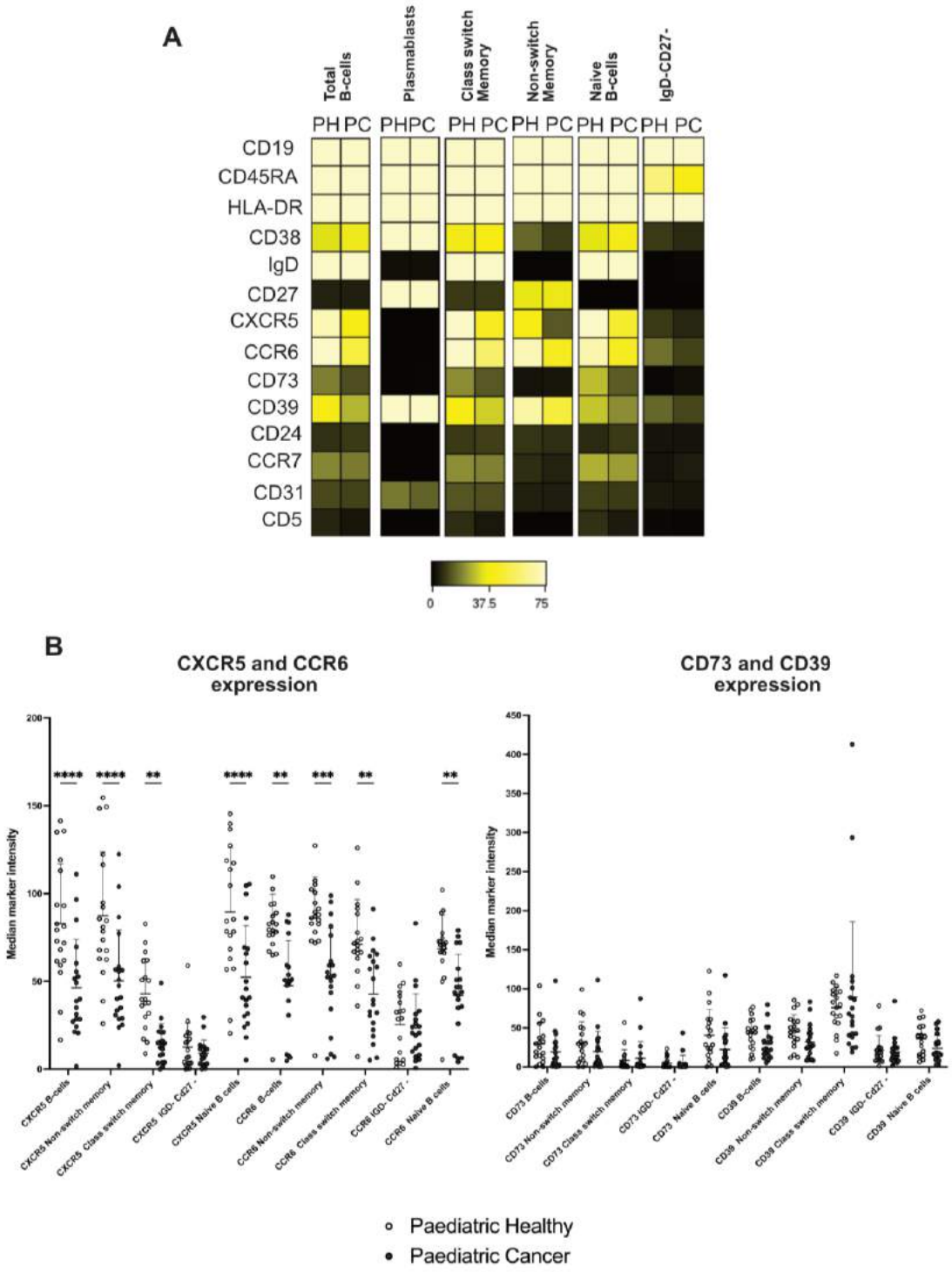

Figure 3-14 B-cells of cancer patients have decreased expression of CXCR5 and CCR6.

(A) Heatmaps of total B-cells and main B-cells subsets are shown. Each row is a marker, and each column is the concatenated fcs files for paediatric healthy (PH) and paediatric cancer (PC) for the relevant population. The median marker intensity for each marker is shown from 0 to 75. (B) Median marker intensity calculated for each B-cell subset at the level of each individual. The error bars show the mean +/- one standard deviation. P values were calculated using Wilcoxon ranked sum tests with false discovery rate at 5% and correction using the Benjamini-Hochberg method. * p<0.05, ** p<0.01, *** p<0.001, **** p<0.0001

3.4.5 CD4+ T-cells are more differentiated in paediatric cancer patients

Next, T-cells were explored in more detail. First, manual gating was performed using the canonical markers CD45RA and CCR7 (Sallusto *et al.*, 1999)to divide CD4 and CD8 T-cells into naïve (CCR7+CD45RA+), central memory (Tcm, CCR7+CD45RA-), effector memory (Tem, CCR7-CD45RA-) and terminally differentiated effector memory (TEMRA, CCR7-CD45RA+, figure 3.15A). Marked differences were observed in the CD4+ subpopulations. Paediatric cancer patients had lower frequencies of naïve CD4 with concomitant increases in Tcm, Tem and TEMRA T-cells compared to healthy children (figure 3.15B). Assessing next the remaining T-cells subsets no differences were observed in Tregs, NK T-cells or activated T-cells (figure 3.15B). We did, however, identify differences in the Tregs subsets A (CD45RA+CCR4-) and B (CD45RA-CCR4+,Kordasti *et al.*, 2016), with subset A decrease and subset B increase in paediatric cancer patients (3.15C). Furthermore, increased T-cell differentiation is known to be associated with prior cytomegalovirus (CMV) infection in adults and particularly elderly (Khan *et al.*, 2002). To investigate whether this increase in cancer patients was due to prior CMV infection, CMV IgG and IgM Elisa was performed from plasma of both paediatric healthy and paediatric cancer patients. There was no association of prior CMV infection and increased T-cell differentiation (figure 3.16).

To further evaluate differences in T-cell phenotype, t-SNE dimensionality reduction was performed on all CD3+ cells using equal numbers of cells from each individual (3100 cells per individual). Marked differences in the spatial cell distributions were observed between paediatric cancer patients and healthy children (Figure 3.17A). Next, unsupervised FlowSOM clustering was used to assign T-cells into 40 meta-clusters (Figure 3.17B). Expression levels

of key phenotypic markers on each meta-cluster are presented in Figure 3.17C as separate heatmaps for the 19 healthy control children (left panel) and 20 paediatric cancer patients (right panel) alongside fold difference of meta-cluster frequencies (middle panel). Visually comparing the two heatmaps, there was little difference in the marker expression for each meta-cluster apart from the low CXCR3 expression noted on the memory CD4 and CD8 T-cells subsets of paediatric cancer patients. This was confirmed when the median marker intensity expression was extracted for the CD4 and CD8 subsets for each individual (figure 3.18). This unsupervised approached confirmed the manual gated data as naïve CD4 were present at higher frequency in healthy children while Tem and TEMRA CD4 were present at higher frequency in paediatric cancer patients. Furthermore, FlowSOM analysis provided additional insights. The most important differences in T-cell frequency between patients and controls were for metacluster 35 (Th1 CD4+ T-cells based on CXCR3 expression), metacluster 22 (Th2 CD4+ T-cells based on CCR4+ CCR6-) and metacluster 30 (Th17 CD4+ T-cells based on CCR4+CCR6+). Frequencies of both were increased in patients. To confirm these results manual gating of Th1, Th2 and TH17/22 T-cells was performed (figure 3.19A). Assessing the frequency of each subset at the level of individuals showed that paediatric cancer patients had increased frequencies of Th17/22 T-cells(Mosmann *et al.*, 1986; Peck and Mellins, 2010) but no changes were observed in Th1 or Th2 T-cell subset (figure 3.19B).

Finally, patients had an increased frequency of gamma delta (γδ) T-cells (meta-clusters 8 and 9). In collaboration with Dr Carrie Willcox and using a fluorescent cytometry panel, we found this increase was solely due to effector Vδ1 γδ T-cell cells (figure 3.20A-C) a subset with adaptive immunobiological properties(Davey *et al.*, 2017). In addition, the innate-like

Vδ2 γδ T cells were of similar frequency in patients and controls although there was a clear difference in phenotype, with levels of perforin lower in patients' cells (figure 3.20D).

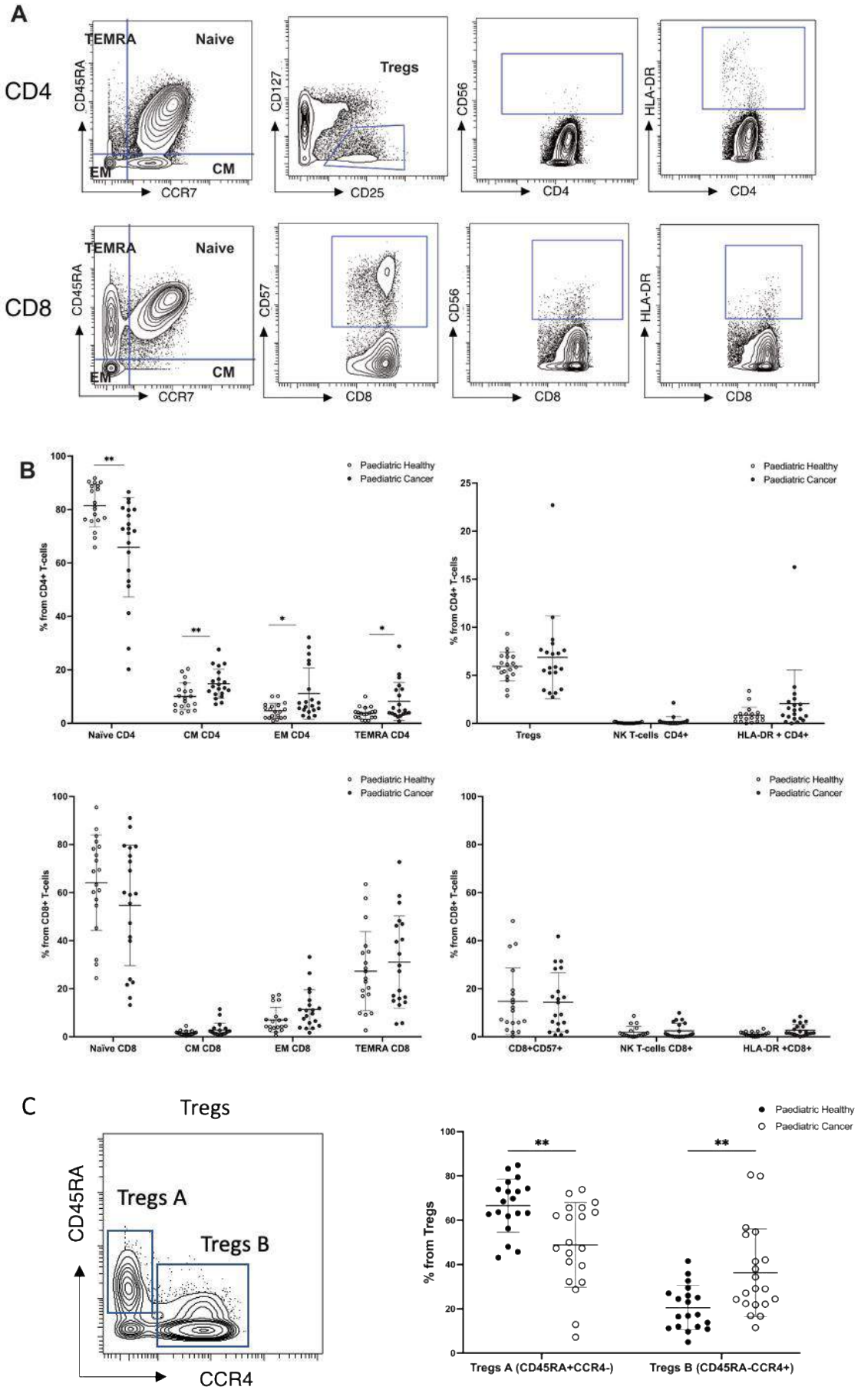
A
CD4
TEMRA
Naive
CD45RA
EM
CM
CCR7
Tregs
CD127
CD25
CD56
CD4
HLA-DR
CD4
CD8
TEMRA
Naive
CD45RA
EM
CM
CCR7
CD57
CD8
CD56
CD8
HLA-DR
CD8
B
Paediatric Healthy
Paediatric Cancer
% from CD4+ T-cells
Naïve CD4
CM CD4
EM CD4
TEMRA CD4
Tregs
NK T-cells CD4+
HLA-DR + CD4+
% from CD8+ T-cells
Naïve CD8
CM CD8
EM CD8
TEMRA CD8
CD8+CD57+
NK T-cells CD8+
HLA-DR +CD8+
C
Tregs
CD45RA
Tregs A
Tregs B
CCR4
% from Tregs
Tregs A (CD45RA+CCR4-)
Tregs B (CD45RA-CCR4+)

Figure 3-15 CD4 T-cell differentiation is observed in paediatric cancer patients.

A) Gating strategy for the main CD4 and CD8 subsets. (B) The frequency of each subset gated in (A) is shown at the level of each individual for both paediatric healthy and paediatric cancer. The error bars show the mean +/- one standard deviation. P values were calculated using Wilcoxon ranked sum tests with false discovery rate at 5% and correction using the Benjamini-Hochberg method. Significant results are indicated: * $p<0.05$, ** $p<0.01$, *** $p<0.001$.

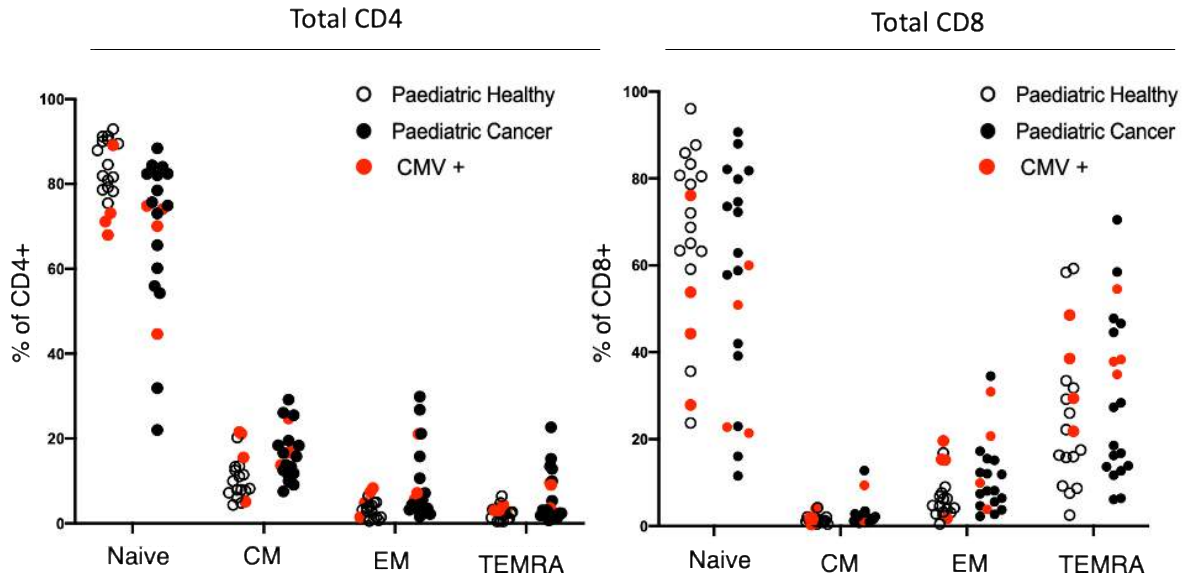

Figure 3-16 CMV is not associated with the increase CD4 differentiation observed in paediatric cancer patients.

The frequency of CD4+ and CD8+ T cells subsets (Naïve; CM, Central Memory; EM, Effector Memory and TEMRA, T effector memory CD45RA revertant) is shown for individuals as a percentage of total CD4+ or CD8+ T cells. Donors that tested positive for cytomegalovirus IgM or IgG antibodies are coloured red.

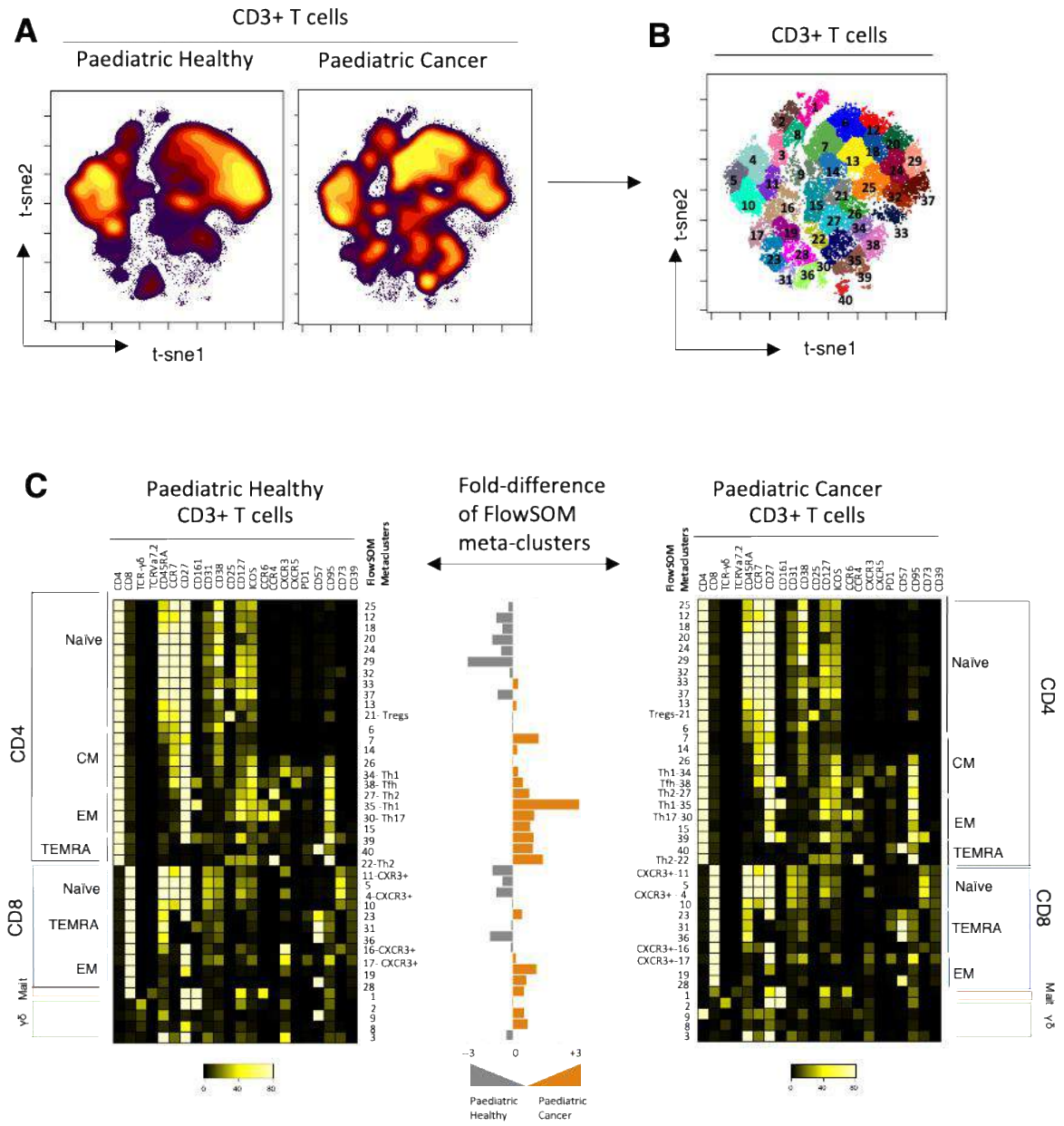

Figure 3-17 Unsupervised FlowSOM analysis of CD3+ T-cells reveals marked differences in the frequencies of T cell subsets in paediatric cancer patients relative to age matched controls.

A) Results of tSNE dimensionality reduction performed on CD3+ cells from concatenated fcs files from patients and healthy children assessing the differences on the spatial cell distributions in the two-dimensional space. (B) Unsupervised clustering (FlowSOM) of T-cells was performed based on their spatial orientation on the tSNE axis, generating 40 meta-clusters. C) The expression of markers for each meta-cluster is shown on heatmaps generated for paediatric healthy donors (left panel) and paediatric cancer patients(right panel). The fold difference of the meta-clusters abundance between healthy donors and cancer patients is shown in the centre panel.

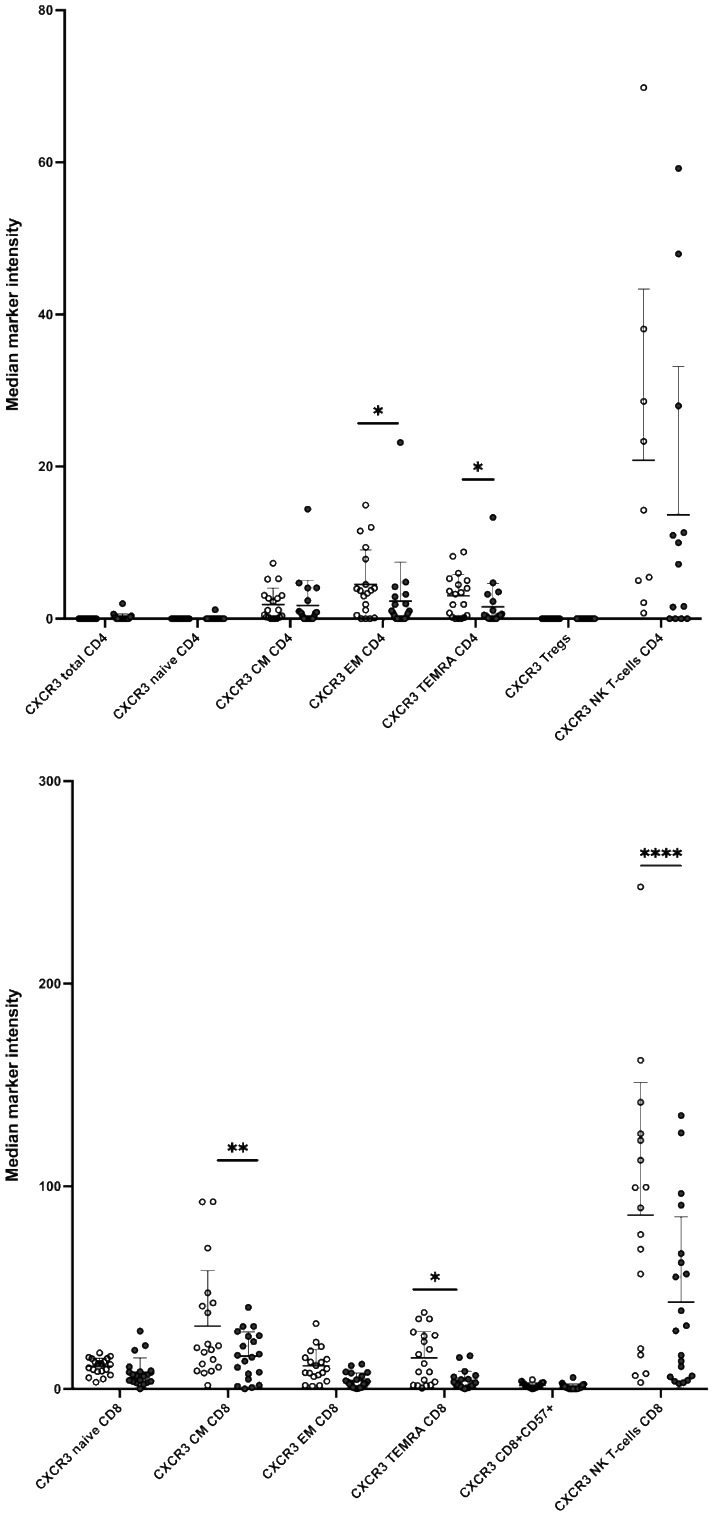

Figure 3-18 CXCR3 expression is decreased in CD4 and CD8 memory subsets.

Median marker intensity is shown for each CD4 and CD8 subset at the level of each individual. The error bars show the mean +/- one standard deviation. P values were calculated using Wilcoxon ranked sum tests with false discovery rate at 5% and correction

using the Benjamini-Hochberg method. Significant results are indicated: * p<0.05, ** p<0.01, *** p<0.001.

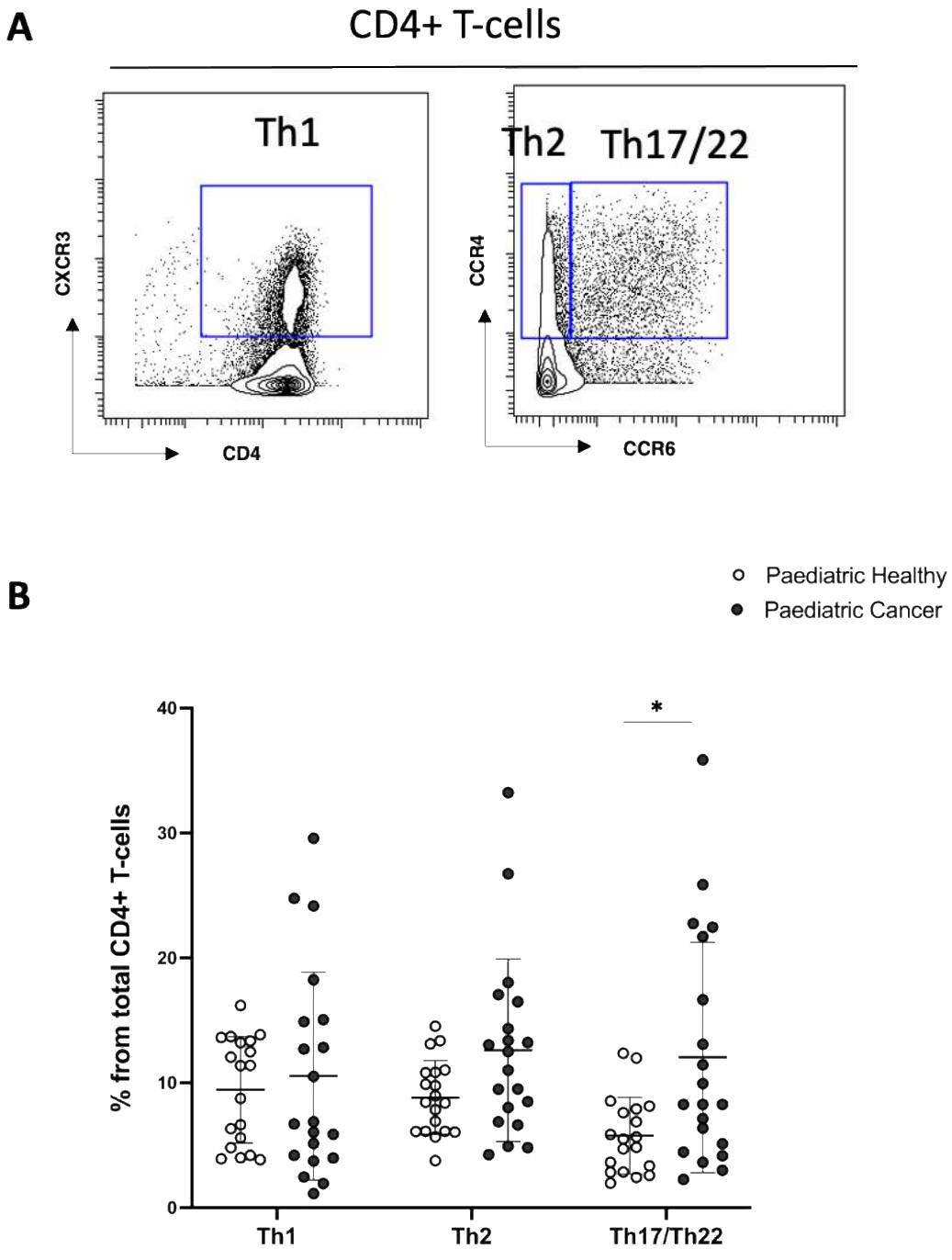

Figure 3-19 Th17/Th22 expand in paediatric cancer patients.

(A) Gating strategy for Th1, Th2, Th17/22. (B) Frequency of subsets gated in (A) show at the level of individual for paediatric healthy (PH) and paediatric cancer (PC). The error bars show the mean +/- one standard deviation. P values were calculated using Wilcoxon ranked sum tests with false discovery rate at 5% and correction using the Benjamini-Hochberg method. Significant results are indicated: * p<0.05, ** p<0.01, *** p<0.001.

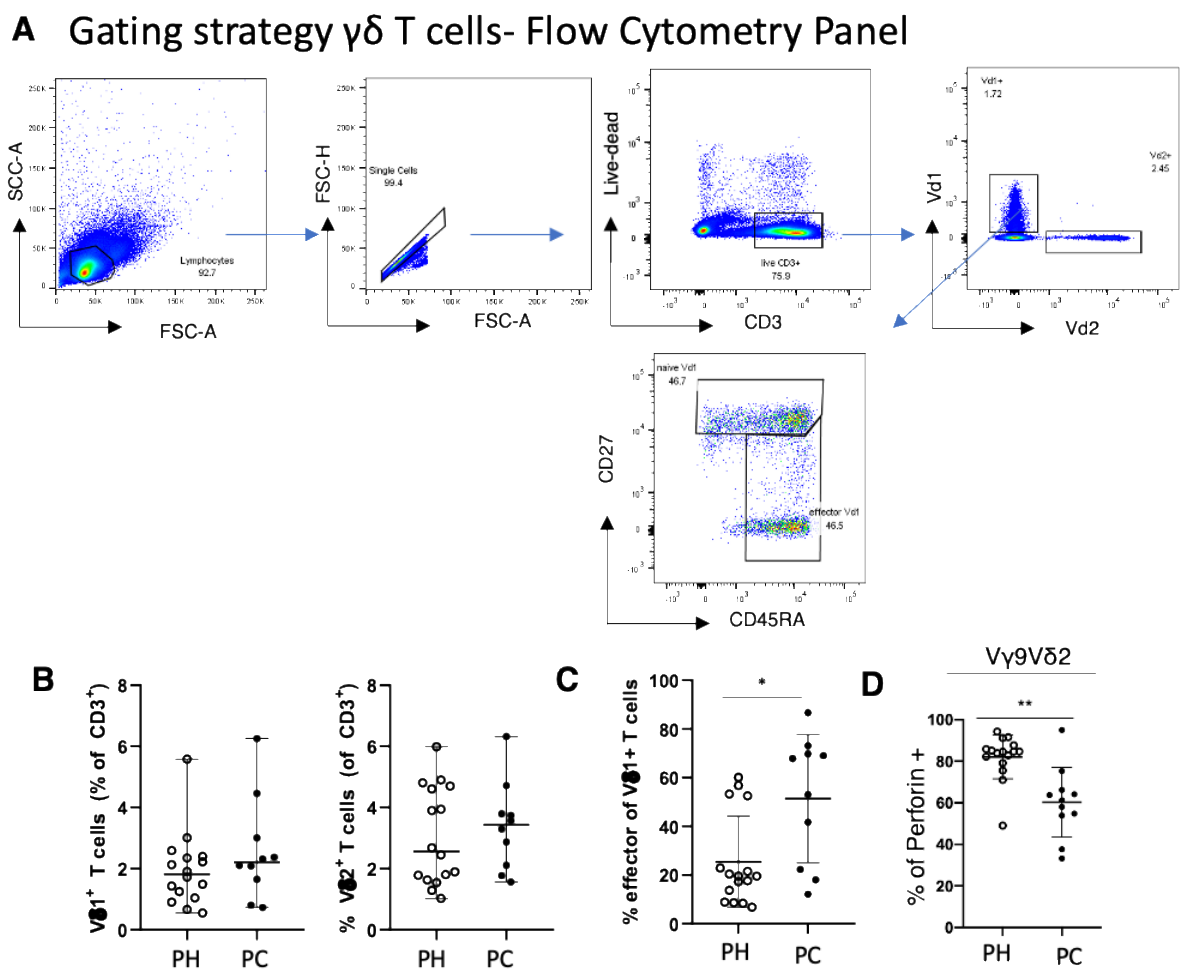

Figure 3-20 Effector Vδ1 γδ T-cell cells expanding in paediatric cancer patietns.

(A)Gating strategy used to investigate gamma delta T cells and naïve and effector delta 1 (Vd1) T cells using a fluorescent flow cytometry antibody panel. B) Frequencies of Vd1 and Vd2 (gamma delta 2) T-cells for individuals expressed as a percentage of CD3+ T cells. C) Frequency of effector Vd1 T-cells (CD45RA+CD27-) is shown for individuals and is expressed as a percentage of total Vd1 T-cells. D) Frequency of perforin positive Vγ9Vδ2 T-cells is shown at the level of individuals and is expressed as a percentage of total Vγ9Vδ2. The error bars show the mean +/- one SD. P values were calculated using Wilcoxon ranked sum tests with false discovery rate at 5% and correction using the Benjamini-Hochberg method. Significant results are indicated: * p<0.05, ** p<0.01, *** p<0.001.

3.5 Mass cytometry from further 30 paediatric cancer patients confirms the immune perturbations identified from the initial discovery cohort

3.5.1 Main immune cell analysis confirms the NK changes observed in paediatric cancer patients

To validate the immune changes observed previously in the discovery cohort of the 20 paediatric cancer patients, we analysed a further 30 patients and compared them to age matched healthy children (table 3.2, figure 3.1). To do this, a new mass cytometry panel was designed in order to validate the results and further analyse the NK cells in more detail. Samples from paediatric cancer patients were similarly taken at the time of diagnosis and before any treatment was administered. For visualisation purposes flow cytometry standard (fcs) files from patients and healthy children were concatenated into two separate files and t-SNE dimensionality reduction was performed on all CD45+ cells using equal numbers of cells from each individual (11,549 cells). Manual gating of major subsets was then performed as demonstrated in figure 3.21A. Immune analysis of the main cells from paediatric cancer patients and heathy children confirmed the NK findings identified in the discovery cohort, with NK cells being significantly decreased in paediatric cancer patients (figure 3.21B).

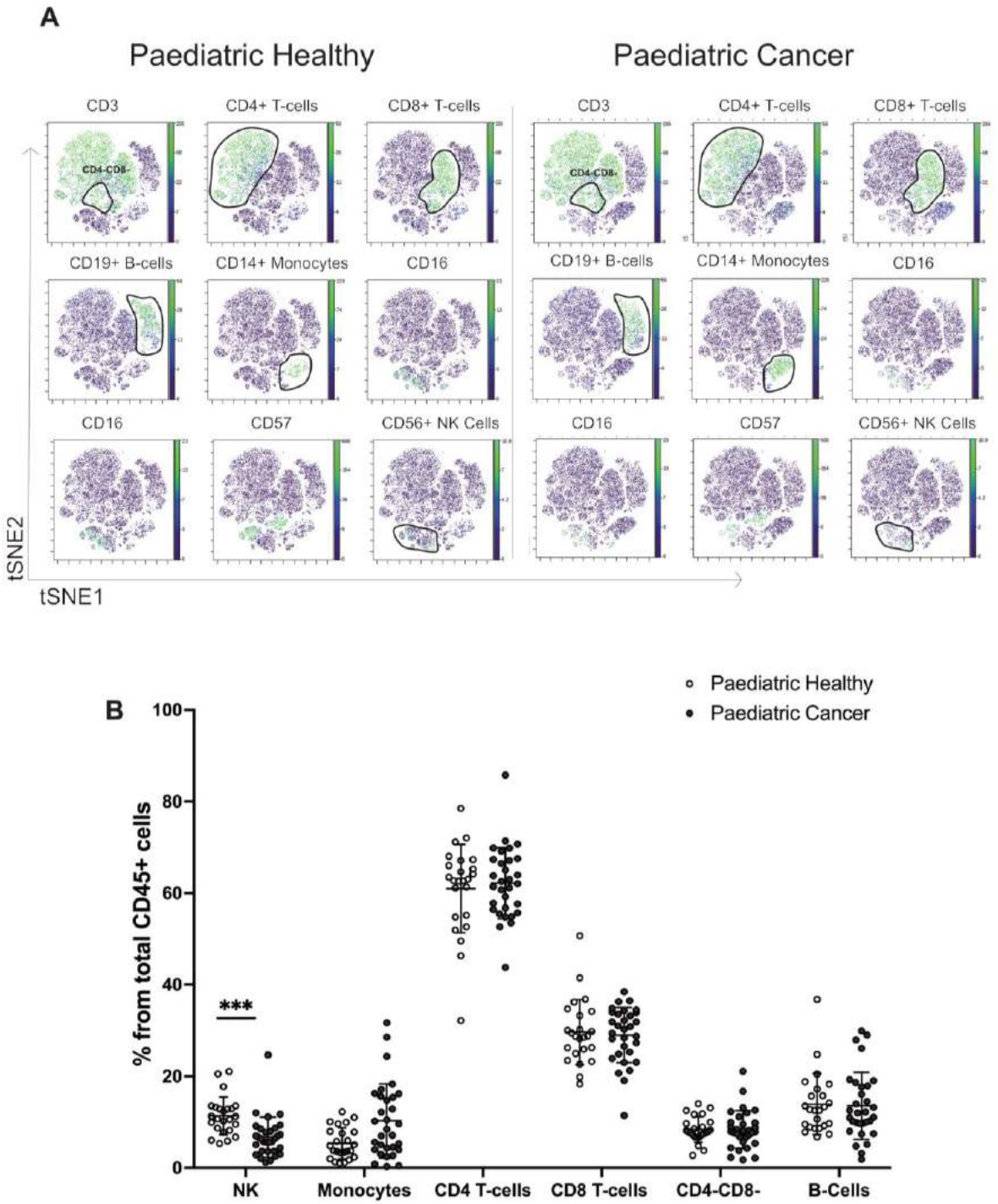

Figure 3-21 NK cells are reduced in frequency in paediatric cancer patients (validation cohort)

(A) T-sne maps of concatenated fcs files from paediatric healthy and paediatric cancer patients shown with the gating strategy for the main immune subsets. (B) Frequencies of the main immune cell subsets shown at the level of each individual for both paediatric healthy and paediatric cancer patients. The error bars show the mean +/- one SD. P values were calculated using Wilcoxon ranked sum tests with false discovery rate at 5% and correction using the Benjamini-Hochberg method. Significant results are indicated: * $p<0.05$, ** $p<0.01$, *** $p<0.001$.

3.5.2 NK subsets analysis confirms the increase of CD56^{bright} CD16- NK cells and decrease of CD57+ NK cells in paediatric cancer patients

Next, we investigated the NK subsets in more detail. Manual gating of the three main subsets was performed using the canonical NK markers CD56 and CD16 (figure 3.22A). Analysis of the frequencies of the three NK subsets at the level of each individual confirmed the expansion of the CD56^{bright}CD16- NK subset in the paediatric cancer cohort. Furthermore, similar analysis for a range of NK phenotypic markers was performed (figure 3.23). Paediatric cancer patients had higher proportions of NK cells expressing markers associated with immature NK cells (CD27 and CD127) and lower proportions of NK cells expressing markers associated with mature NK cells (CD45RA and CD57, figure 3.23). There were no differences in the proportion of NK cells expressing CD38, CD161 or CXCR3/4. There was also no difference in the expression of PD-1.

We then sought to examine the expression of each phenotypic marker for each NK subset (figure 3.24). In the first subset (CD56^{bright}CD16-) CXCR3/4 expression was significantly lower in the paediatric cancer patients. In the second subset (CD56^{dim}CD16-) and third subset (CD56+CD16+) only CD57 was significantly lower in paediatric cancer. Collectively, these results confirm the findings identified in the discovery cohort with NK cells not only being decreased in frequency but also more immature. This is supported by the expansion of CD56^{bright}CD16- subset in paediatric cancer patients, the increased expression on total NK cells of markers associated with immaturity and decreased expression of markers associated with mature NK cells predominantly in subsets two (CD56^{dim}CD16-) and three (CD56+CD16+).

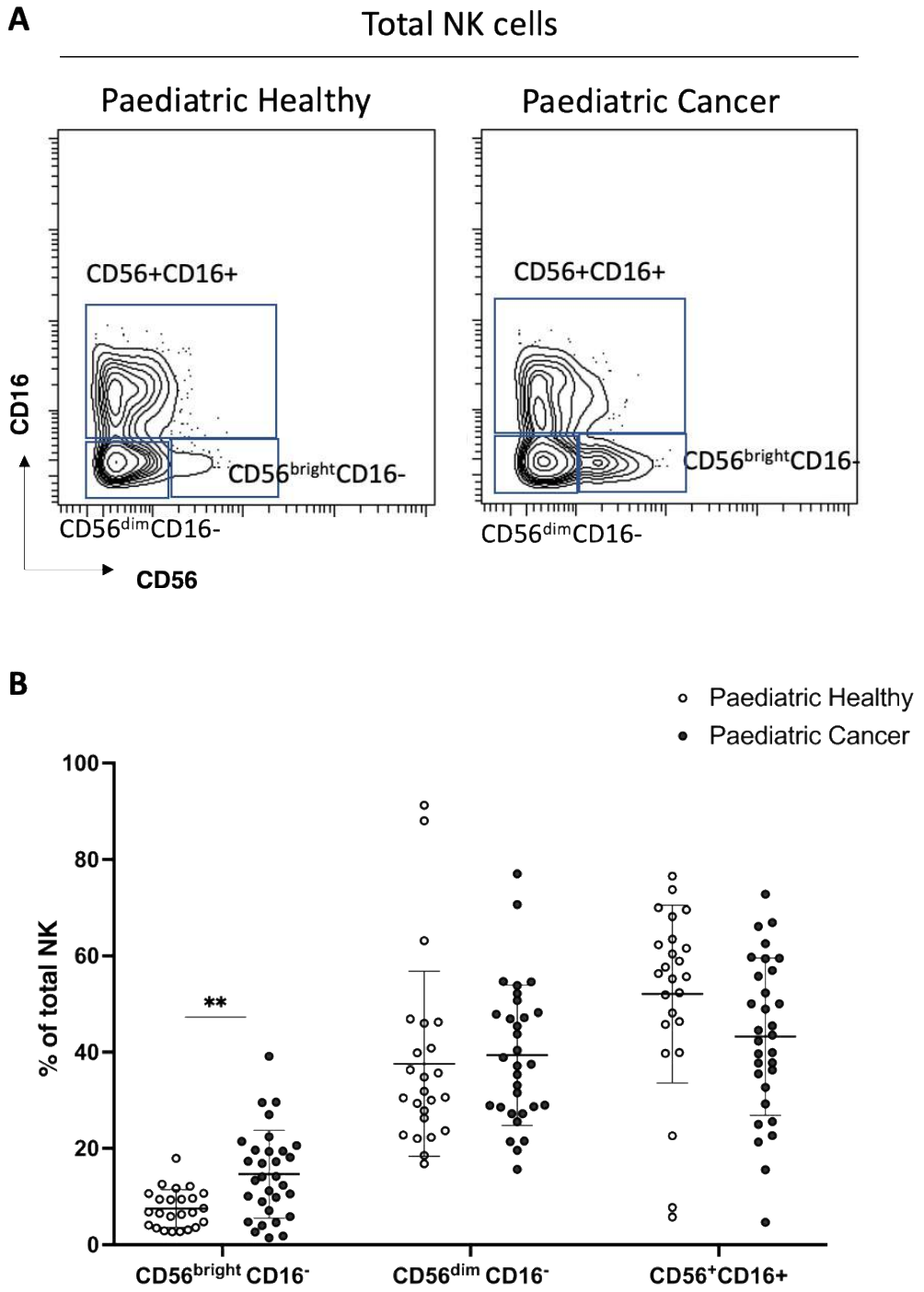

Figure 3-22 CD56brightCD16- NK subset expands in paediatric cancer patients.

(A) Gating strategy for the three NK subsets in paediatric healthy and paediatric cancer patients. (B) Frequency of each NK subset shown on the level of individual for paediatric healthy and paediatric cancer patients. The error bars show the mean +/- one SD. P values were calculated using Wilcoxon ranked sum tests with false discovery rate at 5% and correction using the Benjamini-Hochberg method. Significant results are indicated: * $p<0.05$, ** $p<0.01$, *** $p<0.001$.

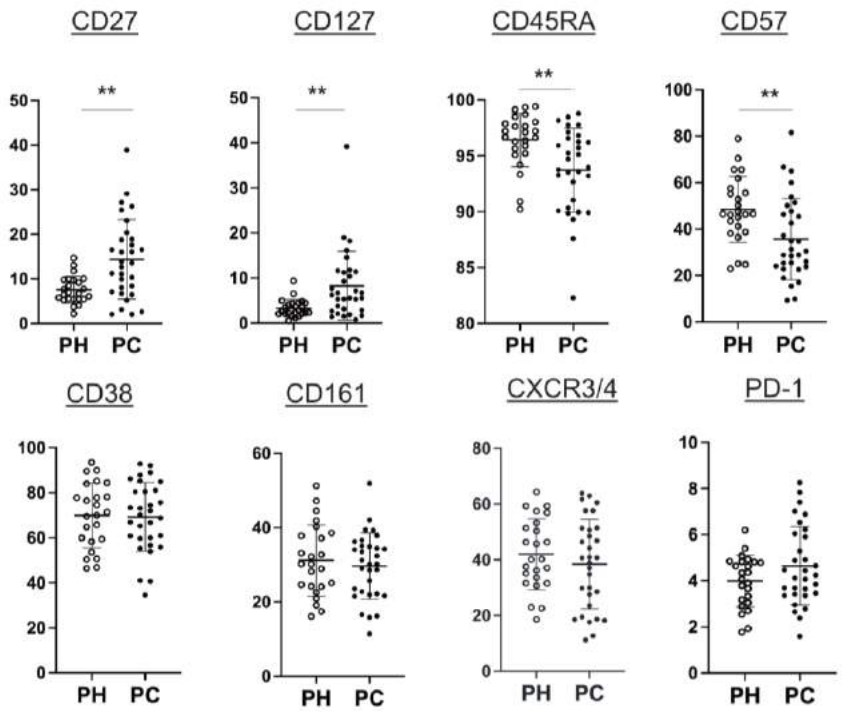

Figure 3-23 NK cells in paediatric cancer are more immature.

(A) Mass cytometry analysis of paediatric cancer patients and paediatric healthy showing percentage of total NK cells positive for the indicated markers. The mean +/- 1 standard deviation is shown. P values were calculated using Wilcoxon ranked sum tests with false discovery rate at 5% and correction using the Benjamini-Hochberg method. Significant results are indicated: * $p<0.05$, ** $p<0.01$, *** $p<0.001$.

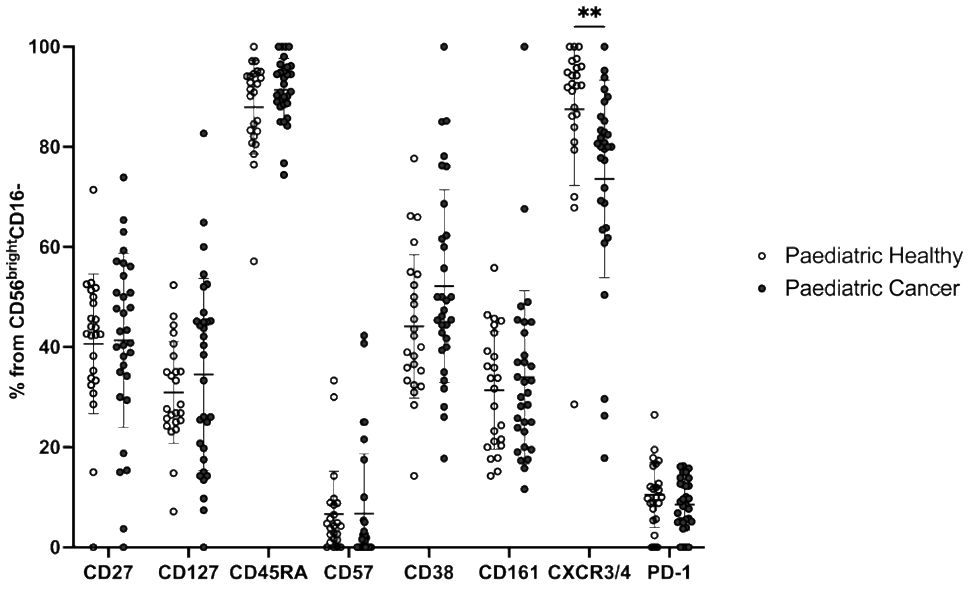
**
% from CD56brightCD16-
100
80
60
40
20
0
CD27
CD127
CD45RA
CD57
CD38
CD161
CXCR3/4
PD-1
Paediatric Healthy
Paediatric Cancer

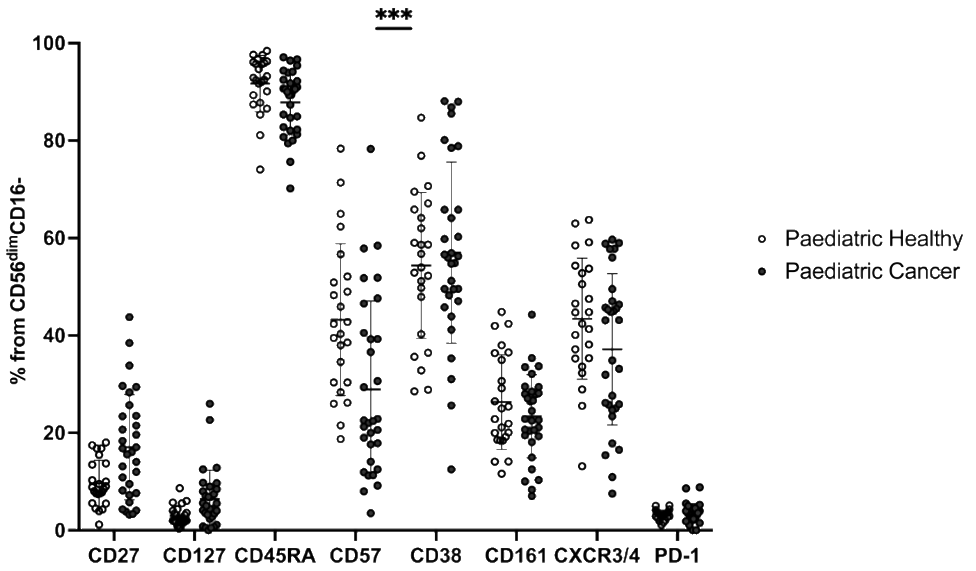
***
% from CD56dimCD16-
100
80
60
40
20
0
CD27
CD127
CD45RA
CD57
CD38
CD161
CXCR3/4
PD-1
Paediatric Healthy
Paediatric Cancer

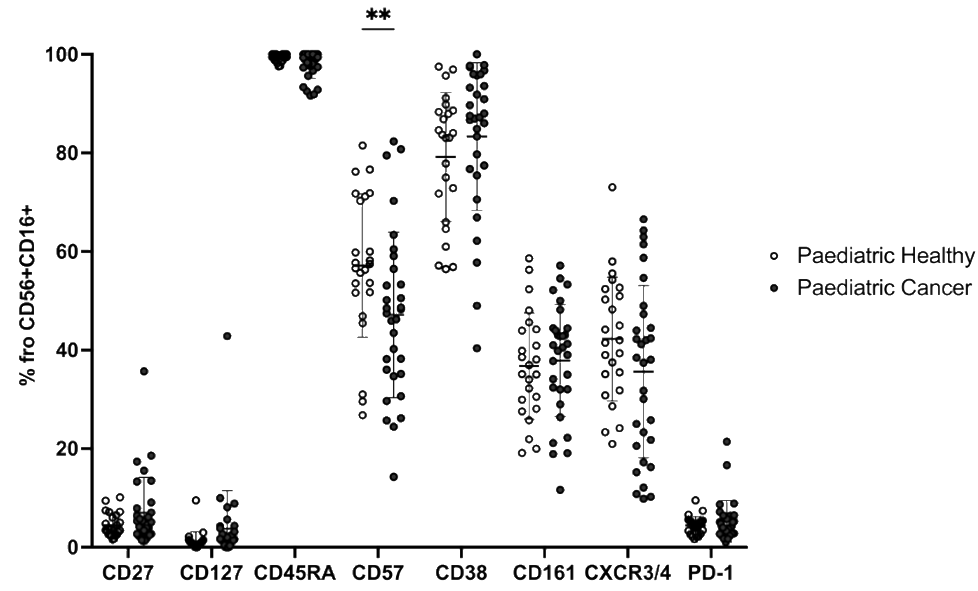
**
% fro CD56+CD16+
100
80
60
40
20
0
CD27
CD127
CD45RA
CD57
CD38
CD161
CXCR3/4
PD-1
Paediatric Healthy
Paediatric Cancer

Figure 3-24 Phenotypic markers shown in all 3 NK subsets.

Frequency of NK cells within each of the four NK subsets (defined using CD16 and CD56) showing the percentage of cells positive for each of the indicated markers. The error bars show the mean +/- one standard deviation. P values were calculated using Wilcoxon ranked sum tests with false discovery rate at 5% and correction using the Benjamini-Hochberg method. Significant results are indicated: * $p<0.05$, ** $p<0.01$, *** $p<0.001$.

3.5.3 Non-classical monocytes are decreased in paediatric cancer patients

Turning now to monocytes, a trend towards higher monocyte counts was identified when the full blood count data were investigated however, the mass cytometry analysis on the discovery cohort revealed no differences in the total monocyte frequency between paediatric cancer patients and healthy children. Furthermore, analysis of the monocyte subsets in the discovery cohort revealed the expansion of transitional monocytes in the paediatric cancer patients. To validate these results manual gating of the three monocytes subsets was performed in the validation cohort using the canonical monocytes markers CD14 and CD16 (figure 3.25A). Non-Classical monocytes were significantly decreased in paediatric cancer patients and no differences were observed in the frequencies of classical or transitional monocytes (figure 3.25B). These results differ from the findings observed in the discovery cohort suggesting further investigation of monocytes subsets is needed in larger cohorts.

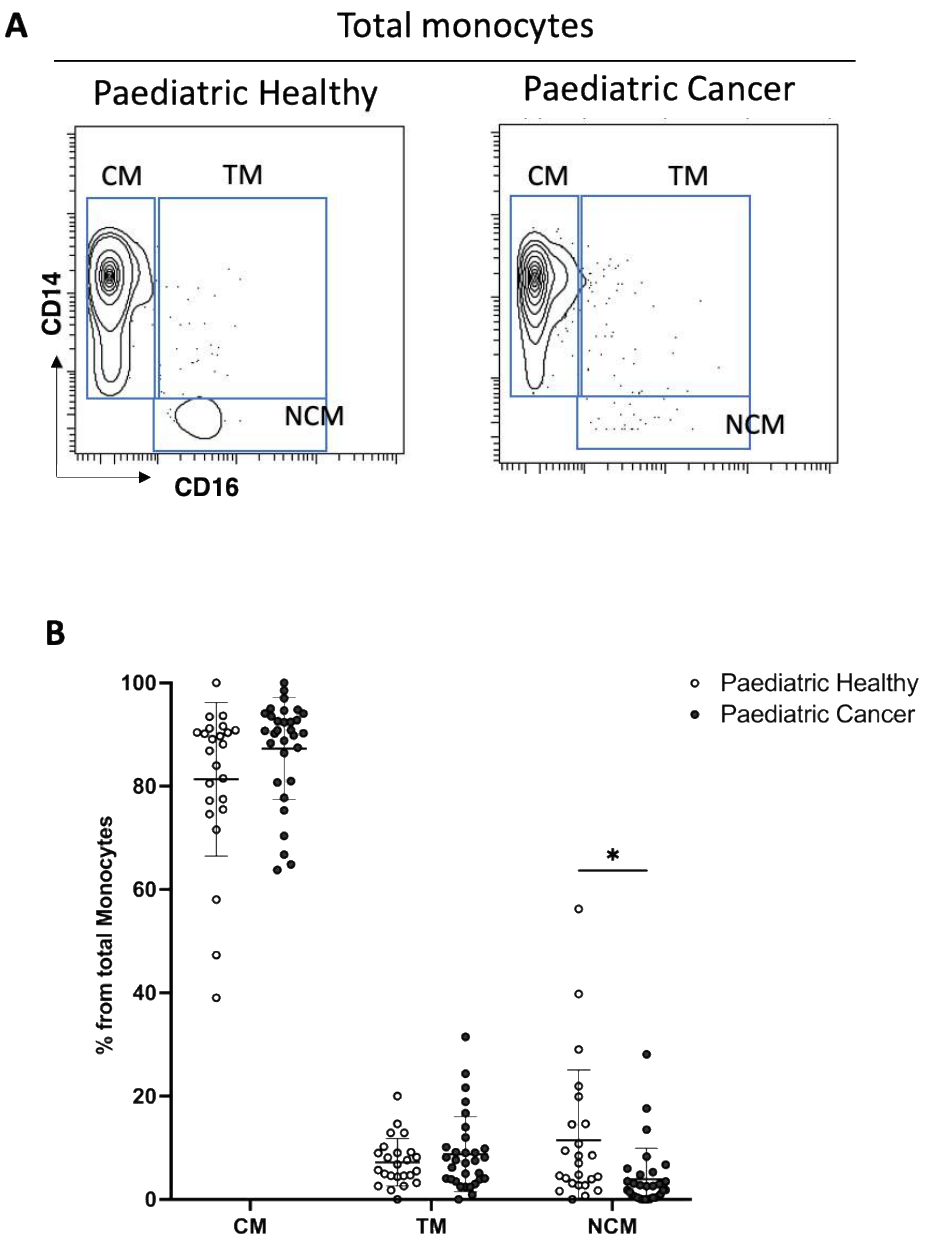

Figure 3-25 Non-classical monocytes are reduced in frequency in paediatric cancer patients.

(A) Gating strategy for three main monocytes subsets in paediatric healthy and paediatric cancer patients. (B) Frequencies of the three monocytes subsets shown at the level of each individual. The error bars show the mean +/- one standard deviation. P values were calculated using Wilcoxon ranked sum tests with false discovery rate at 5% and correction using the Benjamini-Hochberg method. Significant results are indicated: * $p<0.05$, ** $p<0.01$, *** $p<0.001$.

3.5.4 T-cells analysis of the validation cohort confirms the CD4 T-cells differentiation observed in paediatric cancer patients.

Finally, as demonstrated in the discovery cohort, CD4 T-cells were more differentiated in the paediatric cancer patients. To validate these results, manual gating of the main CD4 and CD8 T-cell subsets was performed as demonstrated in figure 3.26. Using the canonical markers CD45RA and CD27, CD4 and CD8 T-cell subsets were gated as: Naïve (CD45RA+CD27+), Tcm (CD45RA-CD27+), Tem (CD45RA-CD27-) and TEMRA (CD45RA+CD27-). Moreover, Tregs (Liu *et al.*, 2006)were gated as $CD25^{high}CD127^{low}$ while NK T-cells(Chan *et al.*, 2013) were gated as CD8+CD56+ and CD4+CD56+. Analysis of the CD8+ T-cell subsets at the level of each individual showed no differences between paediatric healthy and paediatric cancer patients. On the other hand, within the CD4+ T-cells subsets, Tcm were expanded in paediatric cancer patients with concomitant decrease of CD4+ Naïve T-cells (figure 3.27). Lastly, heatmaps were generated to investigate whether the CXCR3 expression was similarly decreased on the T-cells of paediatric cancer patients (figure 3.28). Indeed, the CXCR3/4 marker intensity was decreased in both CD4 and CD8 memory subsets as well as the NK T-cells of the paediatric cancer patients (figure 3.28). Collectively, the analysis of T-cells in the validation cohort confirms the results identified in the paediatric discovery cohort with CD4+ T-cells being differentiated and CXCR3 expression decreased in memory CD4 and CD8 subsets.

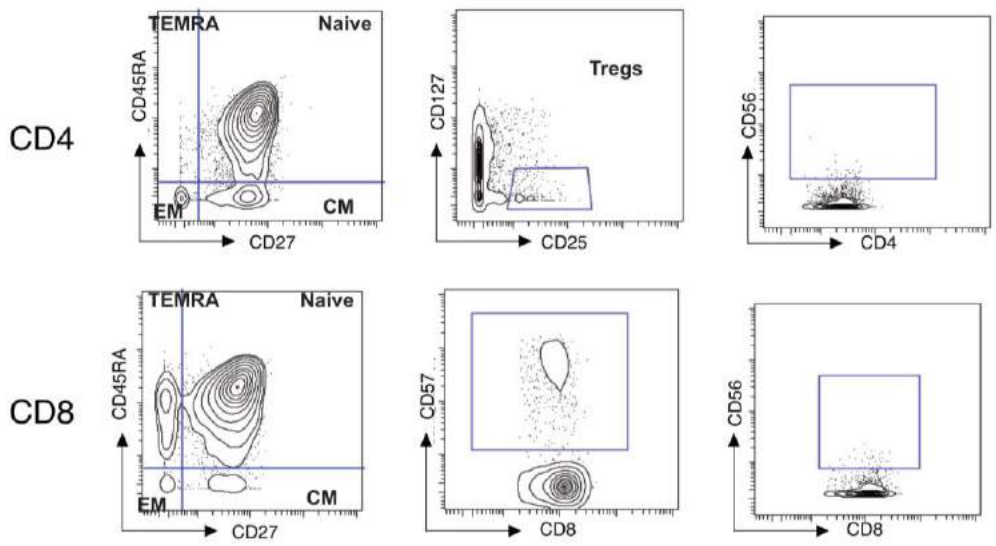

Figure 3-26 Gating strategy for T-cells.

Gating strategy shown for the main CD4+ and CD8+ T-cells subsets.

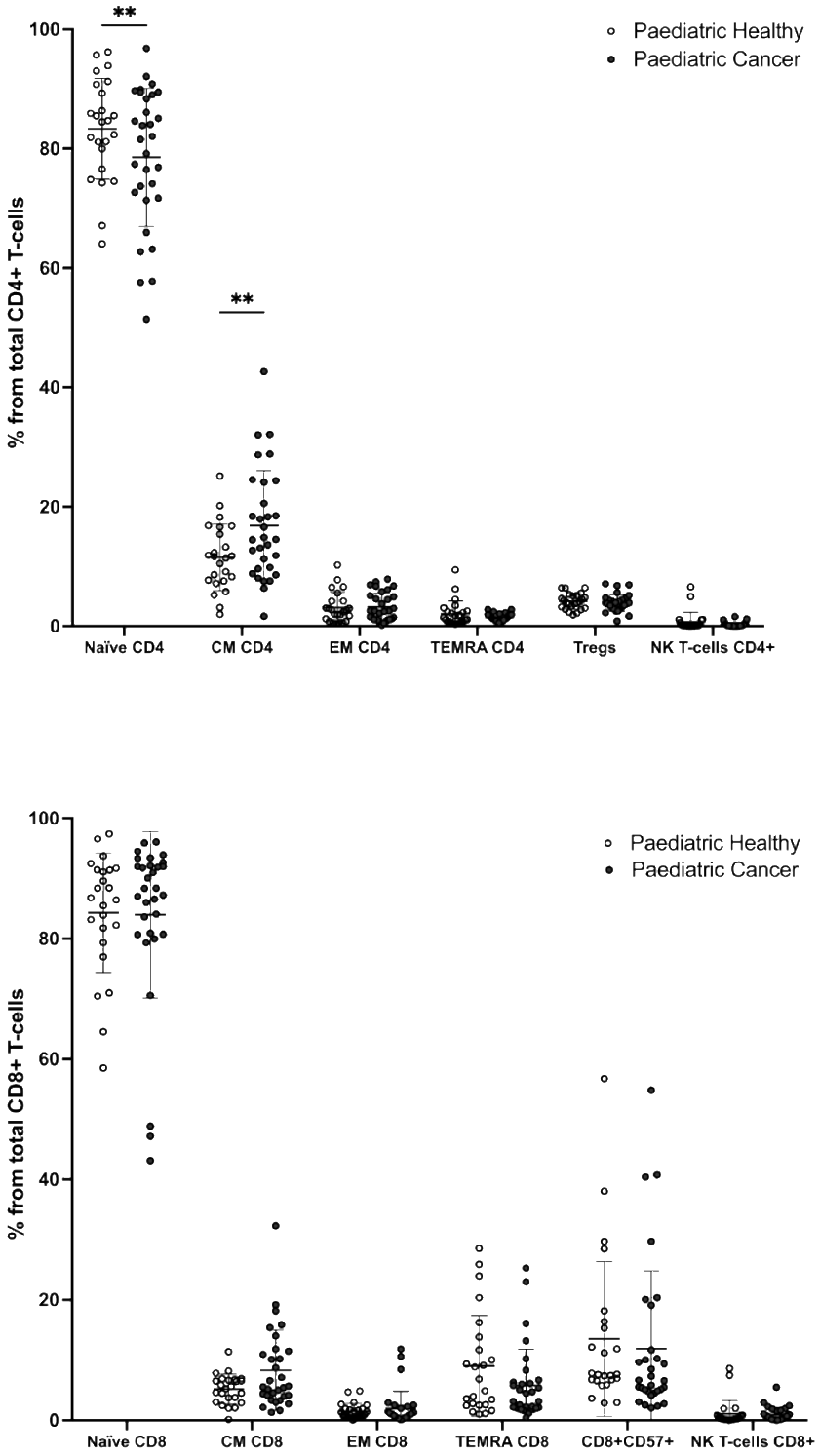

Figure 3-27 CD4+ central memory expansion with concomitant decrease of CD4+ Naïve T-cells is seen in paediatric cancer patients.

Frequencies of the main CD4 and CD8 T-cells subsets (as gated in figure 3.23) is seen at the level of each individual for paediatric healthy and paediatric cancer patients. The error bars show the mean +/- one standard deviation. P values were calculated using Wilcoxon ranked sum tests with false discovery rate at 5% and correction using the Benjamini-Hochberg method. Significant results are indicated: * $p<0.05$, ** $p<0.01$, *** $p<0.001$.

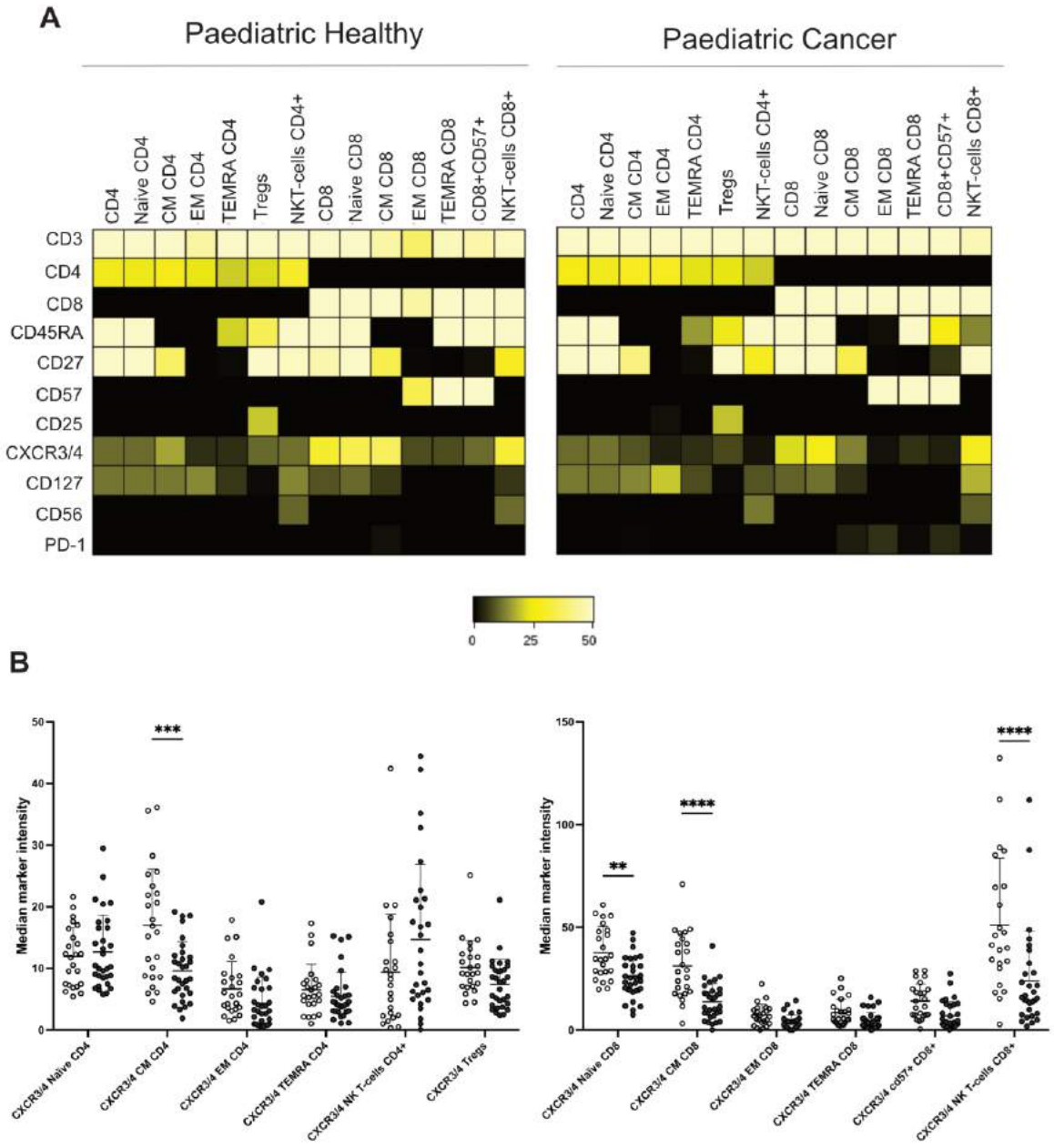

Figure 3-28 CXCR3/4 expression is decreased in the T-cells of paediatric cancer patients.

(A)Heatmaps of total CD4, CD8 and their main subsets are shown. Each row is a marker, and each column is a population. These heatmaps have been generated from the concatenated fcs files of paediatric healthy (PH) and paediatric cancer (PC) patients. The median marker intensity for each marker is shown from 0 to 50. (B) CXCR3/4 marker intensity is shown at the level of individual for each CD4 and CD8 subsets. The error bars show the mean +/- one standard deviation. P values were calculated using Wilcoxon ranked sum tests with false discovery rate at 5% and correction using the Benjamini-Hochberg method. Significant results are indicated: * p<0.05, ** p<0.01, *** p<0.001.

3.6 Subgroup analysis of paediatric cancer patient's explorative data

Deep immune profiling of 51 paediatric cancer patients identified important differences in NK and T-cells. The most important results identified in this study were the decreased frequency of total NK cells, the expansion of the $CD56^{bright}$ CD16- NK subset and also the expansion of the CD4+ Tcm subset. To explore whether these abnormalities were associated to a particular disease, we analysed separately the patients with the six most frequent paediatric malignancies: Hodgkin Lymphoma, Osteosarcoma, Neuroblastoma, Wilms tumour, Rhabdomyosarcoma and Ewing's sarcoma (figure 3.29). Even though this analysis is explorative due to the small number of patients with each malignancy, it was evident that these results were not driven by a certain disease or certain individuals. Overall, the sarcomas had the most significant decrease of total NK cells and expansion of the $CD56^{bright}$ NK subset and the CD4+ Tcm subset. In summary, these results suggest a pan-cancer effect in the paediatric immune system rather than a disease specific response however, further studies are needed to validate these findings.

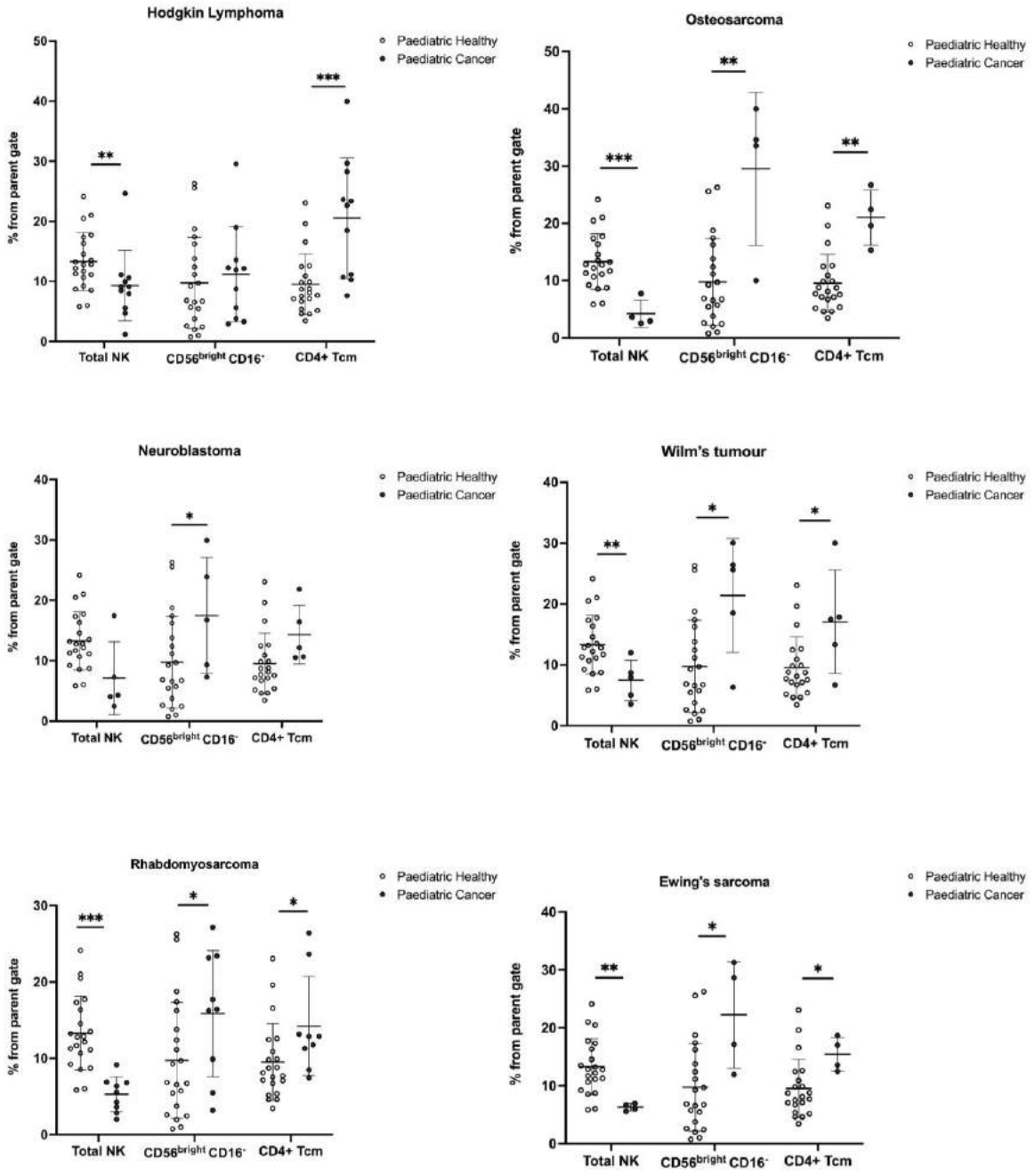

Figure 3-29 Subgroup analysis of the most important results in the six most common paediatric cancers.

Total NK cells, CD56^{bright}CD16- NK cells and CD4 Tcms were analysed for each individual for the six most common paediatric cancers as shown. The error bars show the mean +/- one standard deviation. P values were calculated using Wilcoxon ranked sum tests with false discovery rate at 5% and correction using the Benjamini-Hochberg method. Significant results are indicated: * $p<0.05$, ** $p<0.01$, *** $p<0.001$.

3.7 Conclusions

Immunotherapies can harness the immune system to overcome the immunosuppressive tumour microenvironment and eradicate the malignant cells(Lin and Okada, 2016). Numerous immunotherapeutic agents have shown promising results in adult cancers as these treatments are more effective and less cytotoxic than chemotherapy (Hodi *et al.*, 2010; Sundar *et al.*, 2015). Therefore, immunotherapy could be a great therapeutic candidate for paediatric cancer patients but how to apply them effectively in this patient population requires further exploration. The field is still in its infancy however, preliminary data suggest that the success seen in adults has not translated into paediatric cancers and the reason behind this is not fully understood(Hutzen, Paudel, *et al.*, 2019). We do know that paediatric tumours are fundamentally different from those of adults. For example, most paediatric tumours are embryonal in origin with low mutational burden and therefore lack actionable neoantigens (Wedekind *et al.*, 2018) . In addition, the developing paediatric immune system differs dramatically from that of adults (Dowling and Levy, 2014) and these aberrations could also explain the differences seen in the immune responses to immunotherapies. Thus, understanding the paediatric immune system in both health and cancer could provide useful insights into the immune system of children with cancer and identify key pathways that can potentially be targeted.

In this study we performed a deep immune analysis of 51 cancer patients and 33 age matched healthy children in order to characterise the paediatric immune system of children with cancer. First, using a discovery cohort of 20 cancer patients and 19 age matched healthy children, the main immune cells (NK, monocytes, B-cells and T-cells) were analysed.

Notable differences were identified in the paediatric cancer patients' NK cell and T-cell populations. More specifically, the NK cells of paediatric cancer patients were reduced in frequency and more immature. In addition, T-cells (and particular CD8+ T-cells) had decreased CXCR3 expression and CD4+ T-cells were more differentiated in the paediatric cancer cohort. These results were subsequently confirmed by performing a deep immune analysis in a discovery cohort of an additional 31 cancer patients and 24 age matched healthy children. NK and T-cell responses are crucial in the elimination phase of cancer development as they are involved in eradication of malignant cells (Dunn, Old and Schreiber, 2004). In addition, in tumour bearing mice, CD4+ T-cells were rapidly induced after tumour growth and suppressed anti-tumour CD8+ T-cell responses (Boer *et al.*, 2005). Therefore, even if these cells are indeed tumour specific this does not imply they will generate an effective immune response. In contrary, these cells could contribute to uncontrolled tumour growth. Our results are consistent with the dogma of cancer immunoediting and indicate that that these aberrations seen in paediatric cancer patients are perhaps a way of cancer escaping the defence mechanisms provided by the paediatric immune system.

Embryonal tumours are the most common paediatric tumours and frequently lack HLA-I expression rendering them effective targets for NK cells(Bernards, Dessain and Weinberg, 1986; Borthwick *et al.*, 1988; Raffaghello *et al.*, 2007; Pfeiffer *et al.*, 2011). Indeed, many studies have shown that these tumours can be effectively targeted and eradicated in vitro by NK cells(Bernards, Dessain and Weinberg, 1986; Borthwick *et al.*, 1988; Castriconi *et al.*, 2004; Raffaghello *et al.*, 2007; Pfeiffer *et al.*, 2011). It is, therefore, crucial to understand the role of NKs cells in the context of paediatric tumours. We observed a decrease in frequency

of the NK cells in the periphery that was not disease specific. This could be due to NK migration in the tumour sites however, there was no difference in the expression of the CXCR3 receptor which has been shown to be responsible for NK migration in the tumour sites(Wendel *et al.*, 2008). Given that the NK cells lifespan is two weeks(Zhang *et al.*, 2007), An alternative explanation is that the NK homeostasis is affected. This is supported by the increase of the proportion of the $CD56^{bright}$ NK cells seen in paediatric cancer patients. This subset is considered to be immature and is usually found in the bone marrow where it matures to $CD56^{dim}$ prior to its release to the circulation(Michel *et al.*, 2016). However, occasionally this subset can be found in the periphery as they migrate to secondary lymphoid organs for complete maturation(Michel *et al.*, 2016). Furthermore, several studies reported expression of CCR7, CXCR3 and CXCR4 on this particular subset indicating tropism to the lymphoid tissues(Martín-Fontecha *et al.*, 2004; Pesce *et al.*, 2016, p. 7). Interestingly CCR7, CXCR3 and CXCR4 were all decreased in the $CD56^{bright}$ population of paediatric cancer patients. It is therefore possible that these cells are migrating to secondary lymphoid organs for maturation however they are lacking receptors crucial for lymphoid tissue entry. In addition, several adult cancers have identified increased circulating $CD56^{bright}$ NK cells, and this has been linked to poor prognosis(de Jonge *et al.*, 2019). Nevertheless, the fact that the majority of patients present with anaemia accompanied by immature reticulocytes (high reticulocyte indices- MFR, HFR) along with the abundance of the immature NK subset ($CD56^{bright}$CD16-) in their periphery, suggest that the bone marrow is under stress through perhaps the cancer itself. It has been suggested that cancer can regulate the bone marrow microenvironment through different cytokines and catecholamines in order to promote pro-tumorigenic effects such as growth and therapy resistance (Hanns *et al.*, 2019). Further studies investigating the role and the function of the bone marrow microenvironment in the

context of paediatric solid tumours are needed as this could provide a rationale for more targeted therapies.

CD4+ T-cells play a pivotal role in development and sustainment of effective anti-tumour immunity as they are the orchestrators for several immune responses either directly through providing help to CD8 cytotoxic cells or mediating responses indirectly through cytokines release and antibody production (Tay, Richardson and Toh, 2021). Interestingly, CD4+ Tcm were expanded in paediatric cancer patients. We were not able to demonstrate whether these were antigen specific and future studies are needed to identify their specificity. If these cells are indeed tumour specific and are not able to enter the tumour sites perhaps due to the decreased expression of CXCR3 observed in several subsets of T-cells, then identifying ways to increase their accessibility in the tumour could be beneficial. This however needs to be addressed with caution. As mentioned earlier the expansion of CD4+ in tumour bearing mice was associated with a suppressor phenotype that prevented effective cytotoxic lymphocyte mediated antitumour immunity(Boer *et al.*, 2005). The effect of these suppressive CD4+ T-cells was reversed after treatment with antigen presenting cells- activating agents such as anti-CD40 signalling(Boer *et al.*, 2005). Therefore, further functional studies are needed to interrogate the role of the expanded CD4+ Tcm in paediatric cancer and identify ways to therapeutically target them. In addition, even though no differences in the total Tregs were observed, there were obvious phenotypic Treg differences, with the expansion of Tregs subset B (CCR4hi) and the reduction of Tregs subset A(CD45RAhi) in paediatric cancer patients. Interestingly, the Treg subset B has been suggested to be more suppressive and proliferating when investigated in the context of aplastic anaemia(Kordasti *et al.*, 2016; Lim *et al.*, 2020). If we were to use the Tregs

phenotype as a barometer of immunosuppression, then the expansion of Treg subset B in paediatric cancer could indicate the presence of a more suppressive immune environment further attributing to the argument that the CD4 Tcm expansion could also bear a suppressive phenotype. Furthermore, CXCR3 expression on T-cells of cancer patients has been linked with better outcome as CXCR3 is mediating the recruitment of activated Th1 cells to areas of inflammation as well as the migration of cytotoxic CD8+ to tumour sites (Winter *et al.*, 2007; Kuo *et al.*, 2018). Interestingly, in our cohort the decreased CXCR3 expression was more prominent in the CD8+ T-cells rather than CD4+ T-cells suggesting that CD8+ T-cells are more likely to be excluded from tumour entry. Overall, the role of CXCR3 in tumour recruitment of effector T-cells, the CD4+ Tcm and the Treg subset B expansion in paediatric cancer requires further investigation in larger studies as they could be potentially therapeutically targeted or utilized for disease monitoring.

Our mass cytometry panels were not designed to investigate B-cells or monocytes in detail however, we did identify some interesting phenotypic changes in these two important subsets. B-cells and their main subsets were not altered in frequency however, CXCR5 and CCR6 expression were both decreased in naïve and memory B-cells. B-cells migrate to lymphoid tissues and bone marrow through several key ligands including CXCR5 and CCR6 (Stein and Nombela-Arrieta, 2005; Okada and Cyster, 2006). CXCR5 has been extensively studied in B-cells and is thought to play a crucial role in humoral responses by directing B-cell to the germinal centres light zone and facilitating B-cell activation (Allen *et al.*, 2004; Sáez de Guinoa *et al.*, 2011, p. 13). On the other hand, CCR6 expression has been linked to B-cell migration in areas of inflammation (Geherin *et al.*, 2012). In paediatric cancer patients, both CXCR5 and CCR6 expression were found to be decreased in naïve and

memory B-cells subsets. The reduced expression of CXCR5 could prevent the B-cells, and particularly the naïve B-cells, from entering the light germinal centre zone and therefore affecting the development of memory specific B-cells. Furthermore, the lack of CCR6 could prevent B-cells, and particularly memory B-cells from entering areas of inflammation such as the tumour microenvironment, thus further preventing effective tumour immune responses. These results require validation in larger cohorts, however identifying ways to target CXCR5 and CCR6 could enhance immune responses by developing memory specific B-cells and facilitating tumour entry. Lastly, no differences in the frequencies of monocytes or their subsets were observed however, paediatric cancer patients showed a trend towards increased total monocytes. Investigating the HLA-DR expression in the monocytes of paediatric cancer patients, it was evident that total monocytes and in particular classical monocytes were less enriched for HLA-DR. The HLA-DR^{lo} monocytes are thought to be immunosuppressive and negatively affect cancer immunotherapies (Mengos, Gastineau and Gustafson, 2019). Further studies are needed to investigate the role of HLA-DR^{lo} monocytes in paediatric cancer as this could be therapeutically targeted and perhaps a potential biomarker candidate.

In summary, high dimensional single cell analysis of pediatric cancer patients revealed important immune changes and particular in NK and T-cell subsets. Overall, these results could provide a rational basis for developing and selecting immunotherapies for pediatric cancer patients and improving strategies for future trials. Our patient cohorts included a range of different solid tumours and patients with a broad age range and within these cohorts our results did not appear to be disease or age specific.

CHAPTER 4- NK characterisation in children with cancer

4.1 Introduction

In the previous chapter, high dimensional analysis of the immune system of paediatric cancer patients revealed important changes in the NK cells. More specifically, the paediatric cancer patients had decreased frequency of total NK cells and expansion of the $CD56^{bright}$ NK subset. Cancer associated changes in NK cells have been previously reported in adult cancer patients (Carrega *et al.*, 2008; Mamessier *et al.*, 2013). First, even though no changes were observed in the NK cell frequency, these studies also noted an expansion of the $CD56^{bright}$ NK subset in patients (Carrega *et al.*, 2008; Mamessier *et al.*, 2013). Second, NK cells isolated from these patients had less cytotoxic potential against malignant cells (Mamessier *et al.*, 2013). Third, NK cells from the tumour microenvironment had an imbalance of activating and inhibitory NK receptors and this could perhaps explain their inability to exert direct cytotoxicity against primary tumour cells (Mamessier *et al.*, 2013). Furthermore, tumours can evade the immune system by secreting immunosuppressive cytokines (Hasmim *et al.*, 2015). It has been shown that cytokines play a crucial role in the immune evasion phase (Dunn, Old and Schreiber, 2004) and further understanding of the interactions between cells and cytokines is crucial for future immune-therapeutic approaches.

Lastly, systemic immunity is important, but understanding the tumour is also highly relevant. In contrast to adult cancers, paediatric cancers are thought to be poorly infiltrated by immune cells. It is therefore important to investigate the paediatric tumour

microenvironment and more specifically the immune infiltrates to better understand the tumour's immune evasion strategies and further inform future therapeutic strategies. Given the decrease observed in the NK frequency at the periphery of paediatric cancer patients an intriguing question raised is whether these NK cells have migrated into the tumour sites.

Therefore, the aims of this chapter are a) to perform a detailed characterisation of the NK cell receptors of NK cells isolated from the peripheral blood of paediatric cancer patients and compare this to healthy children, b) investigate the cytotoxic potential of NK cells isolated from the peripheral blood of paediatric cancer patients and compare this to healthy children, c) perform cytokine analysis of plasma from paediatric cancer patients and healthy children and finally, d) perform immunohistochemistry analysis of immune infiltrates in paediatric tumours.

4.2 Characterising NK receptor expression in paediatric cancer patients

4.2.1 Exploratory analysis of the discovery cohort reveals increased NKG2A expression on NK cells from paediatric cancer patients

To explore the NK cell phenotype in more detail a separate NK-focused mass cytometry panel was used to describe the NK receptors on NK cells from six paediatric cancer patients and six healthy children (all selected from the initial discovery cohort from whom surplus cells were available). The expression of the inhibitory receptor NKG2A (Pegram *et al.*, 2011) was significantly increased on total NK cells from paediatric cancer patients (figure4.1 A and B). No difference in the frequency of cells positive for the activating receptors NKG2D, NKp46, NKp30 or DNAM1 was observed (Pegram *et al.*, 2011, Figure 4.1 B). Examining each NK subset described in chapter 3 in turn, the expression of NKG2A was interestingly increased on the mature cytotoxic NK subset 3 (CD56+CD16+, figure 4.1C).

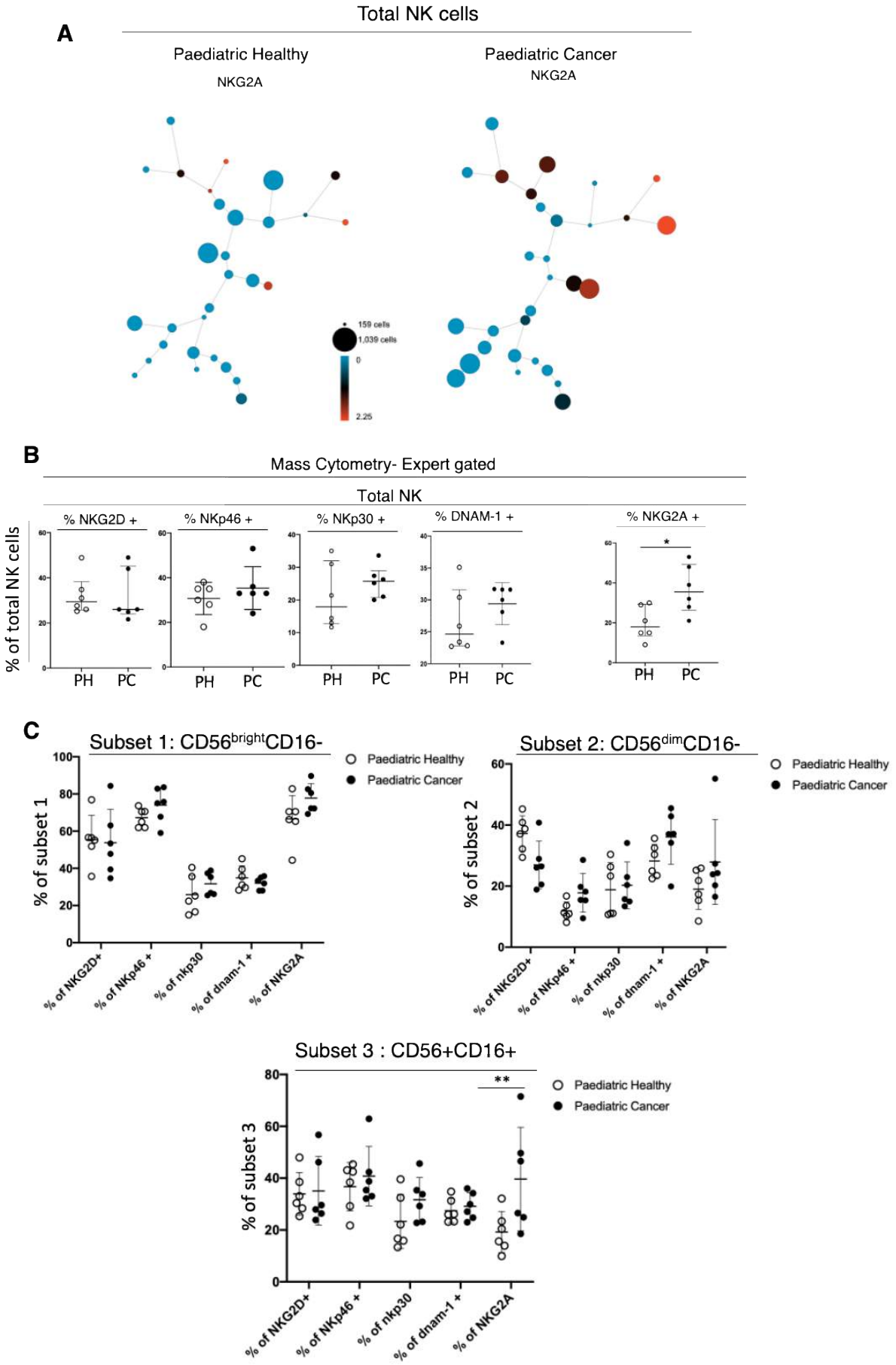
A
Total NK cells
Paediatric Healthy
NKG2A
Paediatric Cancer
NKG2A
159 cells
1,039 cells
0
2.25
B
Mass Cytometry- Expert gated
Total NK
% of total NK cells
% NKG2D +
% NKp46 +
% NKp30 +
% DNAM-1 +
% NKG2A +
PH
PC
C
Subset 1: CD56brightCD16-
Subset 2: CD56dimCD16-
Subset 3 : CD56+CD16+
Paediatric Healthy
Paediatric Cancer
% of subset 1
% of subset 2
% of subset 3
% of NKG2D+
% of NKp46 +
% of nkp30
% of dnam-1 +
% of NKG2A
*
**

Figure 4-1 The expression of the inhibitory receptor NKG2A increased in mature NK cells of paediatric cancer patients.

(A) Total NK cells were clustered using the SPADE algorithm in Cytobank. Spade nodes are coloured by the level of NKG2A expression. Size of each node reflects the numbers of cells. The concatenated fcs files are shown for the 6 healthy children and the 6 cancer patients(B) Additional mass cytometry analysis investigating activating and inhibitory NK receptors. Paediatric healthy (PH, n=6); paediatric cancer (PC, n=6). (C) Frequency of NK cells within each of the three NK cell subsets (subset 1: $CD56^{bright}CD16-$, subset 2: $CD56^{dim}CD16-$, subset 3: CD56+CD16+) showing the percentage of cells positive for each NK receptor analysed. The mean +/- SD is shown. Significant results are indicated: * $p<0.05$, ** $p<0.01$, *** $p<0.001$. The results of Wilcoxon ranked sum tests with false discovery rate correction using the Benjamini-Hochberg method are shown.

4.2.2 Detailed NK receptor analysis in the validation cohort confirms the increase of NKG2A expression and further reveals a decreased expression of activating KIRs and NKp30/80 on NK cells of paediatric cancer patients.

Next, NK cells from paediatric cancer patients (n=31) and healthy children(n=24) of the validation cohort, were analysed using a NK focussed panel. Dimensionality reduction was performed to characterise total NK cells manually gated as per Figure 3.21A. Performing t-SNE on NK cells from 31 patients and 24 controls (1000 NK cells per individual) showed distinct distributions of cells in the contour plots (Figure 4.2A). This difference was driven by the increased frequency of the $CD56^{bright}$ NK cells (figure 4.2B) and the decreased frequency of the CD57+ NK cells in paediatric cancer patients (figure 4.2B). Unsupervised clustering was then performed using FlowSOM (figure 4.2C). Analysis of clusters generated showed that the frequency of cluster 7 ($CD56^{bright}CD16-$) was significantly increased and cluster 5 (CD57+) was significantly decreased in paediatric cancer patients (figure 4.2D and 4.2E). Finally, heatmaps of the NK clusters were generated and comparison of paediatric cancer patients and healthy children revealed that the expression of killer cell immunoglobulin-like

(KIR) receptors was lower in clusters 4,6 and 8 in paediatric cancer patients and NKG2A increased in metacluster 10 (figure 4.2D).

To explore these changes in more detail, total NK cells were manually gated (using a square gate drawn on biaxial plots of CD56 versus markers shown in 4.4) and surface expression of inhibitory and activating NK receptors was measured for each donor (figure 4.4). Interestingly, the activating receptors NKp30 and NKp80 (Moretta *et al.*, 2001) were decreased while the inhibitory receptor NKG2A (Pegram *et al.*, 2011) was increased on the NK cells of paediatric cancer patients (figure 4.3). The median marker intensity (MMI) of NKG2A was extracted and assessed in all NK metaclusters, total NK and the three NK subsets (figure 4.3). The NKG2A MMI for Metaclusters 10 and 8 (CD56+CD16-) was higher in paediatric cancer patients (figure 4.3B). Similar results were observed when the NKG2A MMI was assessed in the three NK subsets, as patients had higher NKG2A MMI on the mature NK subsets $CD56^{dim}$CD16- and CD56+CD16+(figure 4.3C).

Furthermore, a detailed analysis of the killer cell immunoglobulin-like receptors (KIR) was performed. This was challenging as some of the commercially available antibodies can bind to more than one molecule nevertheless, important changes were identified. The KIR2DL1/KIR2DS1/KIR2DS3/KIR2DS5 expression was significantly decreased on the NK cells of paediatric cancer patients (figure 4.4). This decrease did not appear to be due to the inhibitory KIR2DL1(Hilton *et al.*, 2015) or activating KIR2DS5(Della Chiesa *et al.*, 2008), as their expression was similar to healthy children (figure 4.4), but due to the decrease of the activating KIR2DS1 and/or KIR2DS3(Ivarsson, Michaëlsson and Fauriat, 2014). Furthermore, a significant decrease of the expression of the KIR2DL2/KIR2DL3/KIR2DS2/KIR2DS4 was also

seen on the NK cells of paediatric cancer patients (figure 4.4). Again, this decrease was not due to the inhibitory KIR2DL2 and KIR2DL3 (figure 4.4) but due to the activating KIR2DS2 and KIR2DS4(Ivarsson, Michaëlsson and Fauriat, 2014). Finally, investigating the NK receptors in each NK subset (figure 4.5) the increase of NKG2A and decrease of KIR2DL2/KIR2DL3/KIR2DS2/KIR2DS4 were significant for the $CD56^{dim}CD16$- subset but not for the other two subsets. Overall, the deep immune NK analysis of paediatric cancer patients from the validation cohort, confirmed the increased frequency of $CD56^{bright}$ NK subset in paediatric cancer patients described in chapter 3 and further revealed an altered balance of NK receptors.

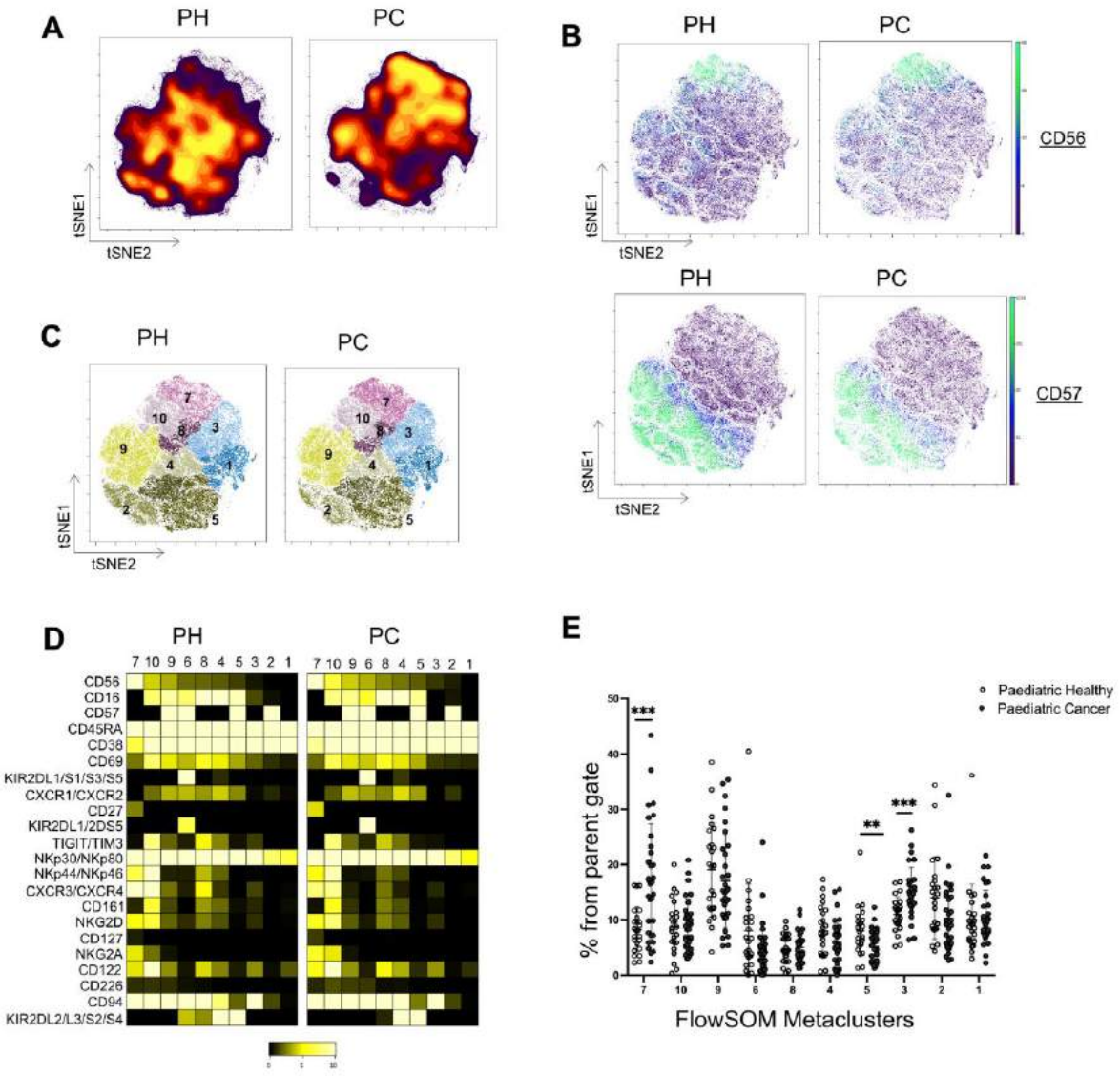

Figure 4-2 Phenotypic changes identified in paediatric cancer patients.

(A) t-SNE contour plots of total NK cells from concatenated fcs files of paediatric healthy (PH, n=24) and paediatric cancer (PC, n=31) individuals. (B) CD56 and CD57 expression on total NK cells demonstrated on the t-sne maps for PH and PC. (C) FlowSOM analysis of total NK cells using 10 metaclusters. (D) Heatmaps generated for all 10 metaclusters (columns) for PH and PC using the median metal intensity from 0 to 10 of each marker (rows). (E) Frequency of each metacluster identified in C now shown at the level of each individual. The mean +/- SD is shown. Significant results are indicated: * $p<0.05$, ** $p<0.01$, *** $p<0.001$. The results of Wilcoxon ranked sum tests with false discovery rate correction using the Benjamini-Hochberg method are shown.

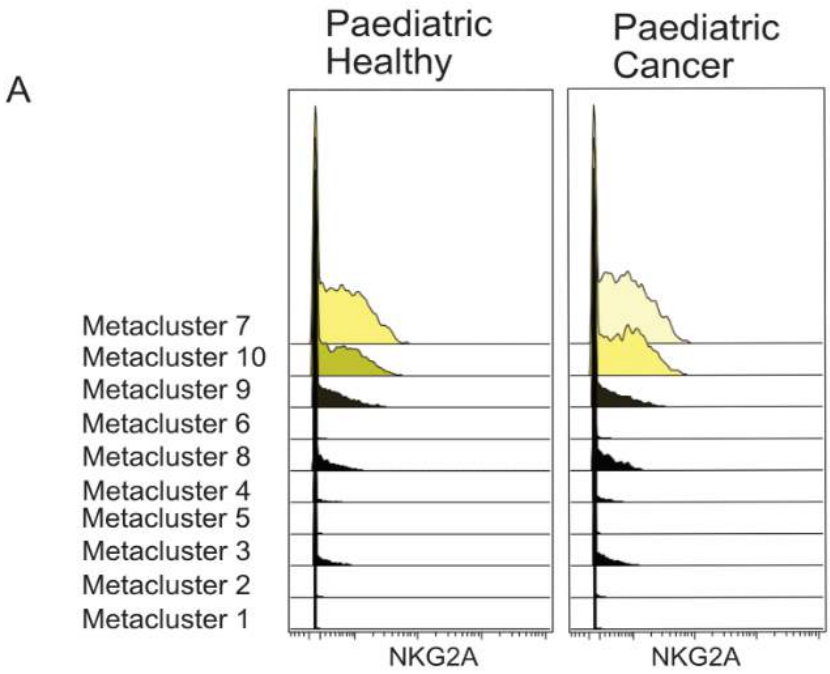
A
Paediatric Healthy
Paediatric Cancer
Metacluster 7
Metacluster 10
Metacluster 9
Metacluster 6
Metacluster 8
Metacluster 4
Metacluster 5
Metacluster 3
Metacluster 2
Metacluster 1
NKG2A
NKG2A

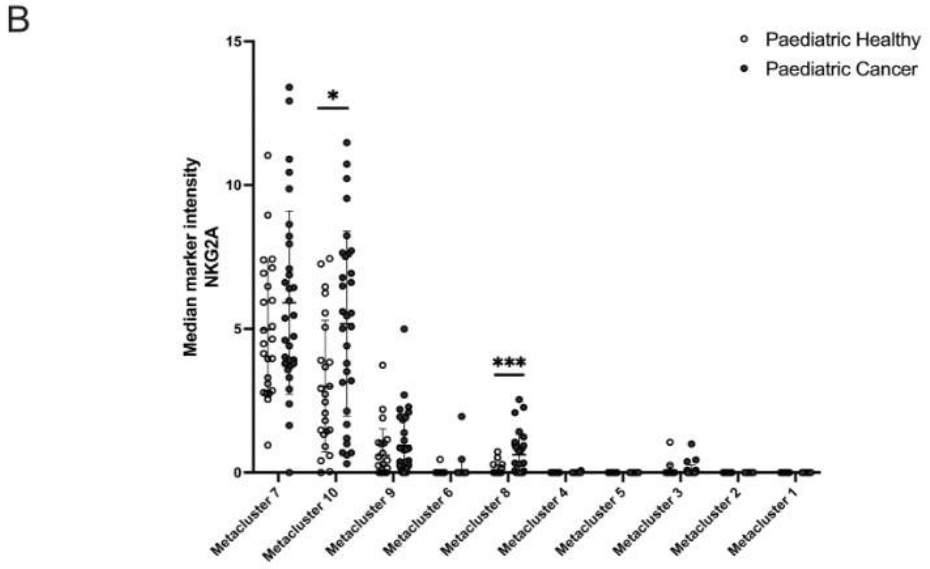
B
Paediatric Healthy
Paediatric Cancer
Median marker intensity NKG2A
15
10
5
0
*
***
Metacluster 7
Metacluster 10
Metacluster 9
Metacluster 6
Metacluster 8
Metacluster 4
Metacluster 5
Metacluster 3
Metacluster 2
Metacluster 1

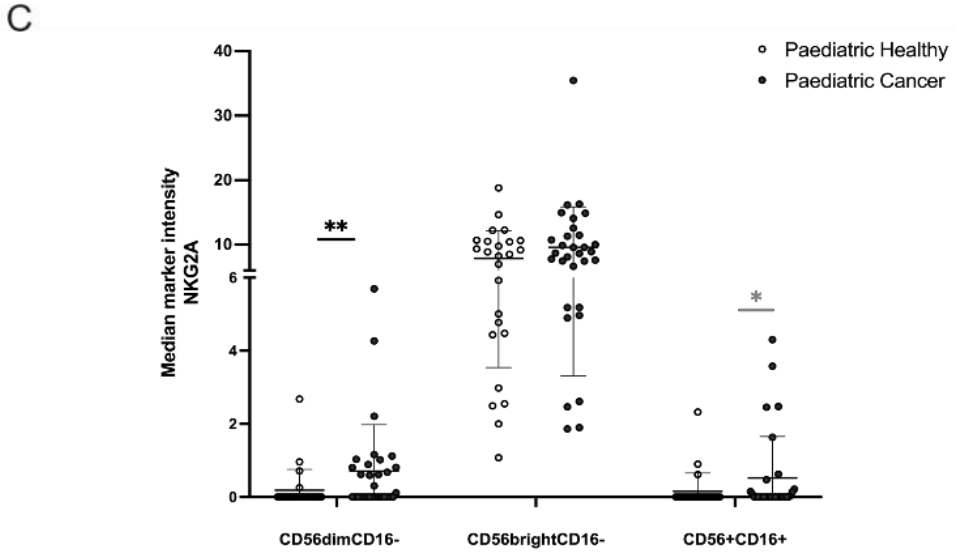
C
Paediatric Healthy
Paediatric Cancer
Median marker intensity NKG2A
40
30
20
10
6
4
2
0
**
*
CD56dimCD16-
CD56brightCD16-
CD56+CD16+

Figure 4-3 NKG2A expression is increased in paediatric cancer patients.

(A)Histograms of concatenated fcs files showing the expression of NKG2A for the metaclusters in figure 4.2. (B+C) Median Marker intensity of NKG2A is shown at the level of each individual for paediatric healthy and paediatric cancer. In (B) the metaclusters in figure 4.2 and in (C) the three NK cells subsets were investigated. The mean +/- SD is shown. Significant results are indicated: * $p<0.05$, ** $p<0.01$, *** $p<0.001$. The results of Wilcoxon ranked sum tests with false discovery rate correction using the Benjamini-Hochberg method are shown. In grey are statistical significant results with FDR >5%.

NK Receptors

Activating Receptors

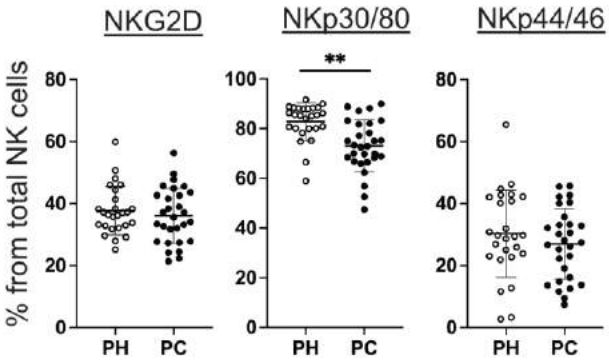

Inhibitory Receptors

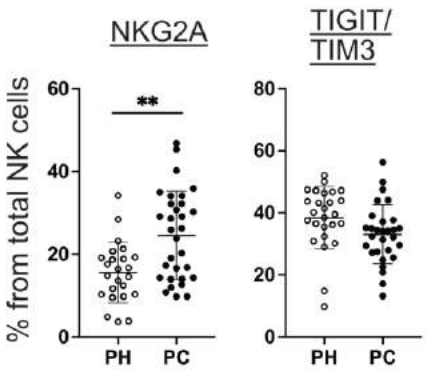

KIR Receptors

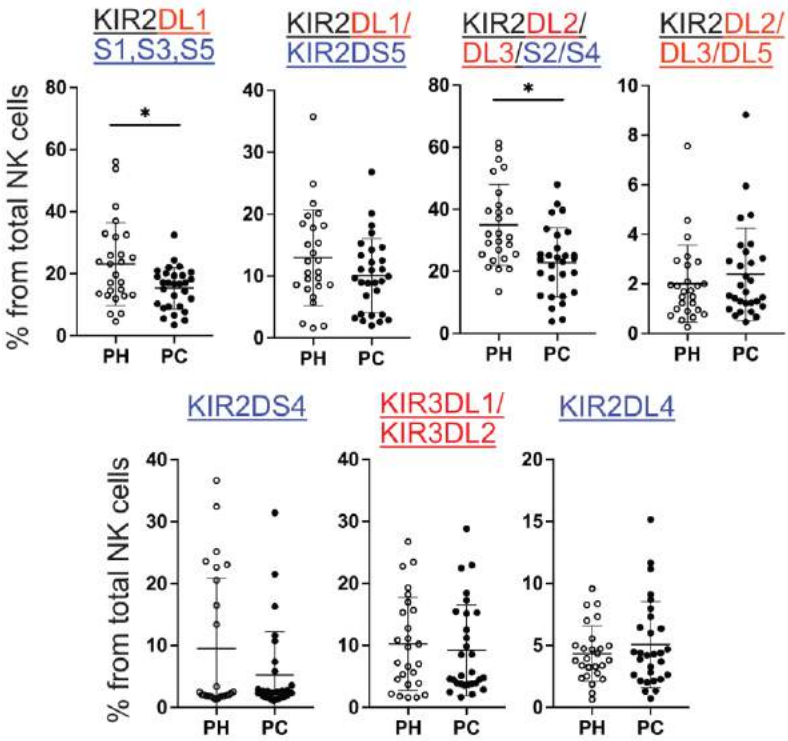

Figure 4-4 NK receptors analysis reveals an imbalance of activating and inhibitory receptors in paediatric cancer patients.

Manual gated data from total NK cells shown at the level of individual for each NK receptor. The mean +/- SD is shown. Significant results are indicated: * $p<0.05$, ** $p<0.01$, *** $p<0.001$. The results of Wilcoxon ranked sum tests with false discovery rate correction using the Benjamini-Hochberg method are shown. For KIR receptors activating receptors are shown in blue while inhibitory receptors are shown in red.

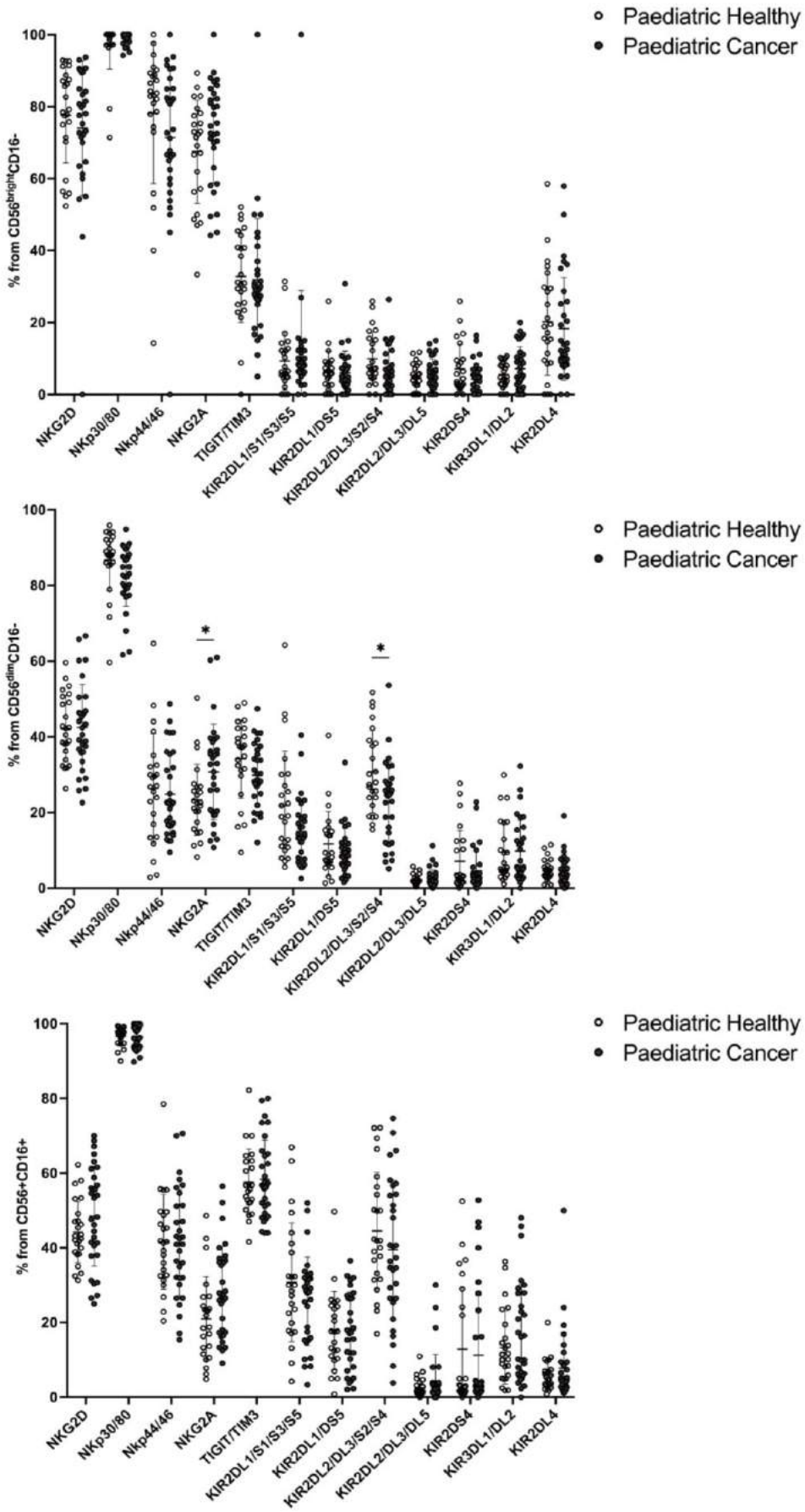
Paediatric Healthy
Paediatric Cancer
% from CD56brightCD16-
% from CD56dimCD16-
% from CD56+CD16+
100
80
60
40
20
0
*
NKG2D
NKp30/80
Nkp44/46
NKG2A
TIGIT/TIM3
KIR2DL1/S1/S3/S5
KIR2DL1/DS5
KIR2DL2/DL3/S2/S4
KIR2DL2/DL3/DL5
KIR2DS4
KIR3DL1/DL2
KIR2DL4

Figure 4-5 NK receptors analysis for each NK subset separately at the level of individual.

The mean +/- SD is shown. Significant results are indicated: * p<0.05, ** p<0.01, *** p<0.001. The results of Wilcoxon ranked sum tests with false discovery rate correction using the Benjamini-Hochberg method are shown.

4.3 NK cells functional assays

4.3.1 NK cells from paediatric cancer patients have fewer cytotoxic granules

The ability of NK cells to kill tumour cells is mainly dependent upon their cytotoxic potential (Bassani *et al.*, 2019) and can be divided in to three main stages . First, the NK cells recognise the target cell and the signal from activating receptors shifts the balance towards activation (Topham and Hewitt, 2009). NK cells then form an immune synapse with the target cell, followed by secretion of perforin and granzyme B into the target cell cytoplasm (Ambrose *et al.*, 2020). This leads to cleavage of different targets by granzymes inducing cell death (Lieberman, 2003; Trapani and Bird, 2008). Given the significant role of perforin and granzyme in mediating NK cytotoxicity, fluorescent flow cytometry was used to measure levels of the intracellular cytotoxic effector molecules perforin and Granzyme-B in NK cells of paediatric cancer patients and healthy children.

Data obtained using mass cytometry and fluorescent cytometry has previously been shown to be comparable (Gadalla *et al.*, 2019). Nevertheless, I validated the NK gating strategy of the three main NK subsets described in chapter 3 ($Cd56^{bright}$CD16-, $CD56^{dim}$CD16- and CD56+CD16+) and compared the two technologies with no differences identified (figure 4.6 A and B). Flow cytometry was then used to measure the intracellular quantity of perforin and granzyme B in NK cells from six cancer patients and five healthy children (all selected

from the discovery cohort, figure 4.6 C and D). Paediatric cancer patients had a significantly lower proportion of total NK cells positive for perforin or granzyme B (Figure 4.6C). Examining each subset in turn provided two important insights. First, the proportion of cells positive for perforin and granzyme varied markedly for each subset: low for subset 1, higher for subset 2 and highest for subset 3, finding consistent with the NK maturation process(Krzewski and Coligan, 2012). Second, for each subset there was no difference in the percentage of NK cells positive for perforin or granzyme B between patients and controls. Therefore, the difference observed in the total NK cells is due to the different proportion of NK subsets present in patients and controls rather than differences for each subset (Figure 4.6 D).

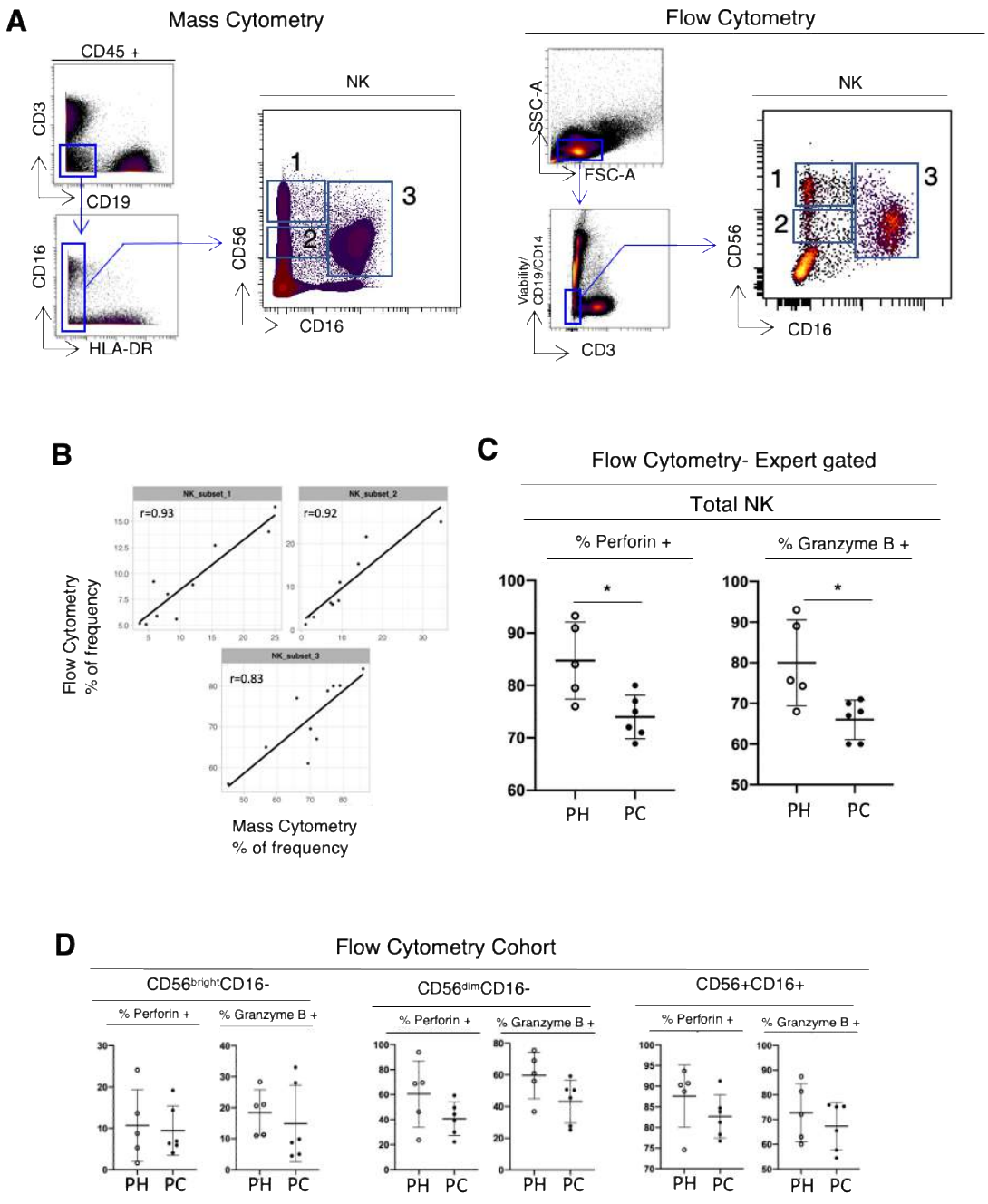

Figure 4-6 Paediatric cancer patients' NK cells have fewer cytotoxic granules compared to healthy children.

(A) Comparison of NK subsets using mass cytometry and flow cytometry. (B) Correlation of NK cells between mass cytometry and flow cytometry. (C) The percentage of total NK cells positive for perforin and Granzyme B is shown for paediatric healthy (PH). and paediatric cancer (PC) patients. (D) The percentage of NK subsets 1 (CD56brightCD16-), 2 (CD56dimCD16-) and 3 (CD56+CD16+) positive for perforin and Granzyme B is shown for paediatric healthy (PH) and paediatric cancer (PC). The mean +/- SD is shown. Significant results are indicated: * p<0.05, ** p<0.01, *** p<0.001. The results of Wilcoxon ranked sum tests with false discovery rate correction using the Benjamini-Hochberg method are shown.

4.3.2 NK cytotoxicity against K562 cells is decreased in paediatric cancer patients

Next, the cytotoxicity of total NK cells against the standard K562 cancer cell line (Nagel, Collins and Adler, 1981) was evaluated. NK cells from five paediatric cancer patients and five age-matched healthy children were assessed at different effector to target ratios (figure 4.7A). Ratios were adjusted to correct for the lower frequency of NK cells observed in paediatric cancer patients. Results from these assays showed that, consistent with their lower levels of perforin and granzyme B, NK cells from paediatric cancer patients were less cytotoxic (Figure 4.7A). The exception was patient C19, who showed similar levels of cytotoxicity to their age-matched control (Figure 4.7B). Interestingly, this patient had a pre-malignant diagnosis of nephroblastomatosis rather than an established malignancy.

An alternative explanation could be that NK cells in patients are less able to recognise K562 cells or are less capable of being activated. To exclude these possibilities the ability of NK cells to degranulate, determined by CD107a surface display, was evaluated. CD107a (lysosomal-associated membrane protein-1) is a lysosomal membrane protein that, in cytotoxic immune cells such as CD8 T-cells and NK cells, is also present in the membrane of cytotoxic granules. When triggered to induce cytotoxicity, CD107a is transported with the cytotoxic granule and displayed on the surface to protect the NK cell from self-lysis (Cohnen *et al.*, 2013). Display of CD107a on the surface of immune cells is therefore used to measure degranulation as a surrogate of cytotoxicity (Penack *et al.*, 2005). Following co-culture with K562 cells, NK cells from patients and controls showed equivalent levels of CD107a positivity (Figure 4.7C). Furthermore, production of interferon-gamma and TNF-a were equivalent

(Figure 4.7C). Collectively, these data show that NK cells from patients were not impaired in their ability to recognise and respond to K562 cells.

Therefore, the impairment of K562 killing by NK cells from patients likely reflects the lower levels of mature cytotoxic NK cells present in paediatric cancer patients' blood. If this was the case, then restoring natural levels of mature NK cells should reverse the defect. To test this hypothesis, NK cells from patient C08 and their age-matched counterpart, healthy donor HV11, were cultured with IL-2 for 14 days then tested for K562 cytotoxicity. Following culture NK cells from the patient exhibited greater cytotoxicity than the control cells, showing that the reduced NK cell cytotoxicity common in paediatric cancer patients is reversible (Figure 4.7D).

Finally, we examined whether soluble NKG2D ligands MICA and ULBP2 in the plasma of paediatric cancer patients might inhibit NK function, as has been reported for adult cancer patients (Molfetta *et al.*, 2017).Unexpectedly, paediatric cancer patients had significantly lower plasma concentrations of MICA and ULBP2 compared to healthy children (figure 4.8). In summary, our results demonstrate that NK cells from paediatric cancer patients had less cytotoxic potential against K562 cells and this was due to the decreased expression of perforin and granzyme in the total NK cell population of paediatric cancer patients that arises due to the decreased proportion of mature cytotoxic NK cells in their blood. Importantly, this deficit in NK cytotoxicity was reversible when NK cells are cultured in vitro with a clinically validated IL-2 protocol (Fernández *et al.*, 2021).

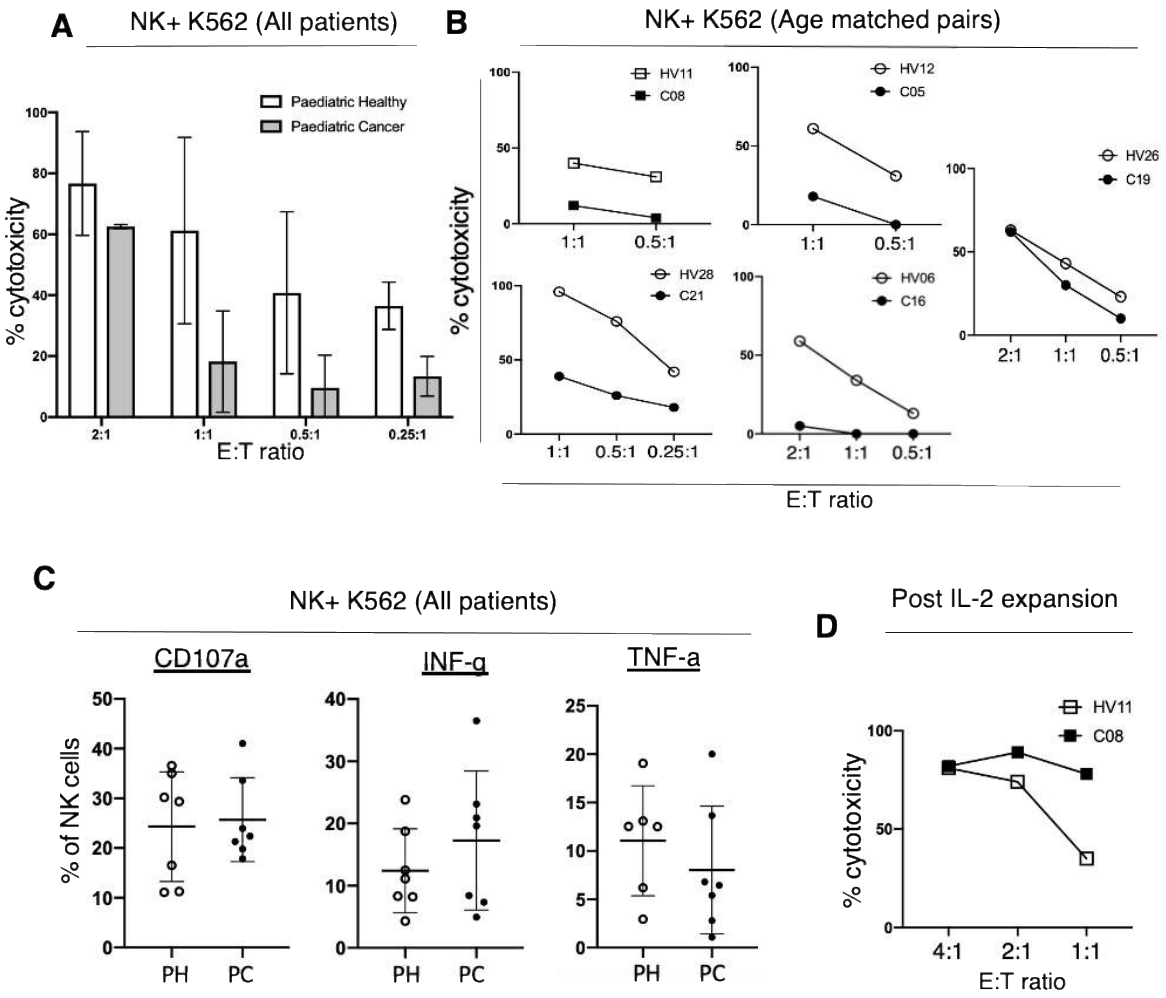

Figure 4-7 NK cells from cancer patients showed decreased cytotoxicity but not decreased recognition of K562 target cells.

(A) Combined results of K562 cytotoxicity assays for five patients and five age matched control donors performed at the indicated NK effector to K562 target ratio. Mean cytotoxicity +/- 1 standard deviation is shown. 9B) Results from panel A now showing each patient and their age matched control. (C) Flow cytometry analysis of NK cells from seven paediatric healthy donors (PH) and seven paediatric cancer patients (PC), which include patients analysed in A and B, measuring degranulation by CD107a as well cytokine production. Error bars shown mean +/- 1 standard deviation. (D) K562 cytotoxicity assay performed using NK cells from patient C08 and their age matched control HV11 using NK cells expanded in vitro with IL-2 for 14 days. E:T indicates the effector: target ration used.

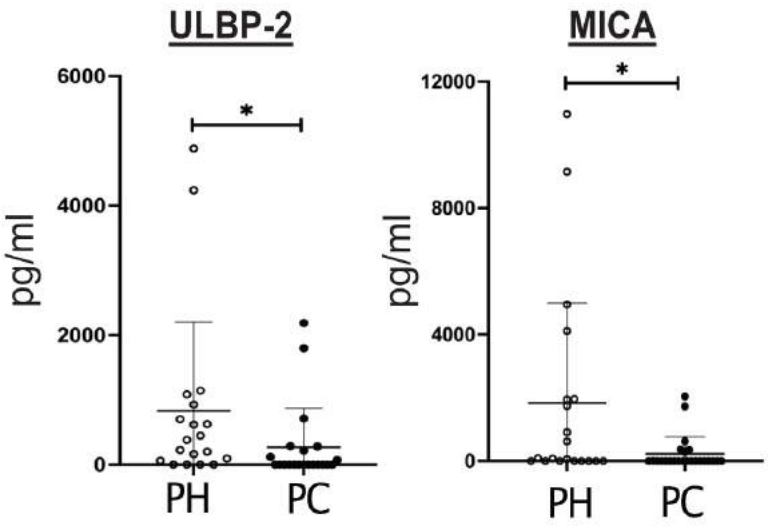

Figure 4-8 ULBP-2 and MICA are decreased in the plasma of paediatric cancer patients.

Results of ELISAs measuring NKG2D ligands ULBP-2 or MICA is shown for paediatric healthy (PH) and paediatric cancer (PC) patients. The mean +/- SD is shown. Significant results are indicated: * $p<0.05$, ** $p<0.01$, *** $p<0.001$. Mann-Whitney tests were used to compare paediatric healthy and paediatric cancer patients.

4.4 Cytokines profile analysis of paediatric cancer patients reveals elevated concentration of cytokines linked to tumour progression and metastasis.

Next, analysis of the cytokine profile of paediatric cancer patients and healthy children was performed. First, explorative cytokine analysis was performed on a subset of paediatric cancer patients (n=6) and healthy children (n=8) using a cytokine array capable of detecting 200 cytokines. The strategy here was to perform an initial broad survey of cytokines to identify key molecules altered in patients for subsequent analysis. As the array can only measure a small number of samples plasma was pooled together into four groups: i) three younger paediatric cancer patients <5 years old, ii) three older paediatric cancer patients >5 years old, iii) four younger healthy children <5 years old and iv) four older healthy children >5 years old. The assay was performed as per manufacture's protocol for each group and pixel density was determined. Figure 4.9 shows scans of the cytokine arrays, with molecules that were significantly increased in abundance in cancer patients relative to healthy children. These include the plasminogen activator inhibitor-1(PAI-1) which is associated with tumour progression(Li *et al.*, 2018), the retinol binding protein 4 (RBP4) which has been linked to tumour development (Berry, Levi and Noy, 2014) and matrix metallopeptidase 9 (MMP9) which is linked to tumour progression(Huang, 2018). Interestingly, dipeptidyl peptidase IV (DPPIV), which is associated with advanced disease in adults with colorectal cancer (De la Haba-Rodríguez *et al.*, 2002), was decreased in paediatric cancer patients. A detailed breakdown of cytokines that were differentially abundant is provided in Appendix 1 and 2. To validate these results, key molecules of interest were then measured in unpooled plasma samples from 43 paediatric cancer patients and 19 healthy children.

Direct comparison of cytokine levels between paediatric cancer patients and healthy children showed statistically significant differences for 7 out of the 29 soluble plasma proteins (figure 4.10A). Specifically, the paediatric cancer patients had statistically significant raised levels of cytokines linked to tumour progression and metastasis such as MMP9 (Huang, 2018), Interleukin 8 (Bakouny and Choueiri, 2020,IL-8), Interleukin 23 (Yan, Smyth and Teng, 2018, IL-23) and soluble CD40 ligand (Chung and Lim, 2014, sCD40L). Moreover, cytokines reported to exert anti-tumour effects, such as-interferon gamma inducible protein 10 (IP-10, Enderlin *et al.*, 2009, IP-10) and human interleukin 12 p40 subunit (IL-12p40, Lasek, Zagożdżon and Jakobisiak, 2014, IL12p40) were significantly decreased in paediatric cancer patients (Figure 4.10). Finally, tumour promoting cytokines interleukin 6 (Kumari *et al.*, 2016, IL-6), Arginase (Grzywa *et al.*, 2020) and thymus- and activation-regulated chemokine also known as CC chemokine ligand 17 (TARC, Korbecki *et al.*, 2020,TARC) were also elevated in paediatric cancer patients however, when corrected for multiple comparisons, this increase was no longer significant.

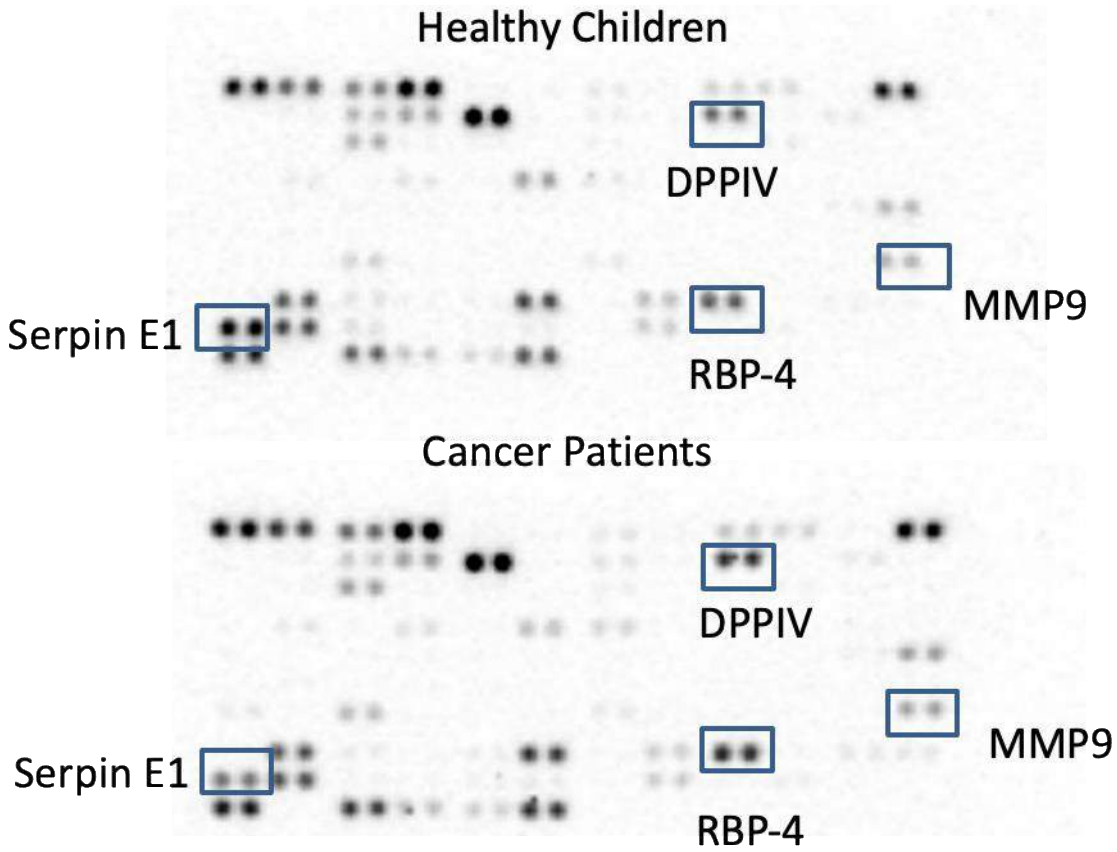

Cytokines	Mean value intensity Healthy	Mean value intensity Cancer	Fold Change	P value
PAI-1	117.5	62.61	-0.46	<0.001
RBP-4	93.07	74.07	-0.20	<0.001
MMP-9	22.77	29.72	0.31	<0.001
DPPIV	86.95	59.46	-0.31	<0.001

Figure 4-9 Cytokine array analysis for paediatric cancer patients (younger group <5 years) and healthy children.

The pixel density arrays are shown for paediatric healthy and paediatric cancer patients annotating in boxes the four most significant cytokines. The table shows the mean value intesity of each cytokine for healthy and cancer patients as well as the fold changes. Statistical analysis was performed using unpaired t-test correcting for multiple comparisons. P values are provided.

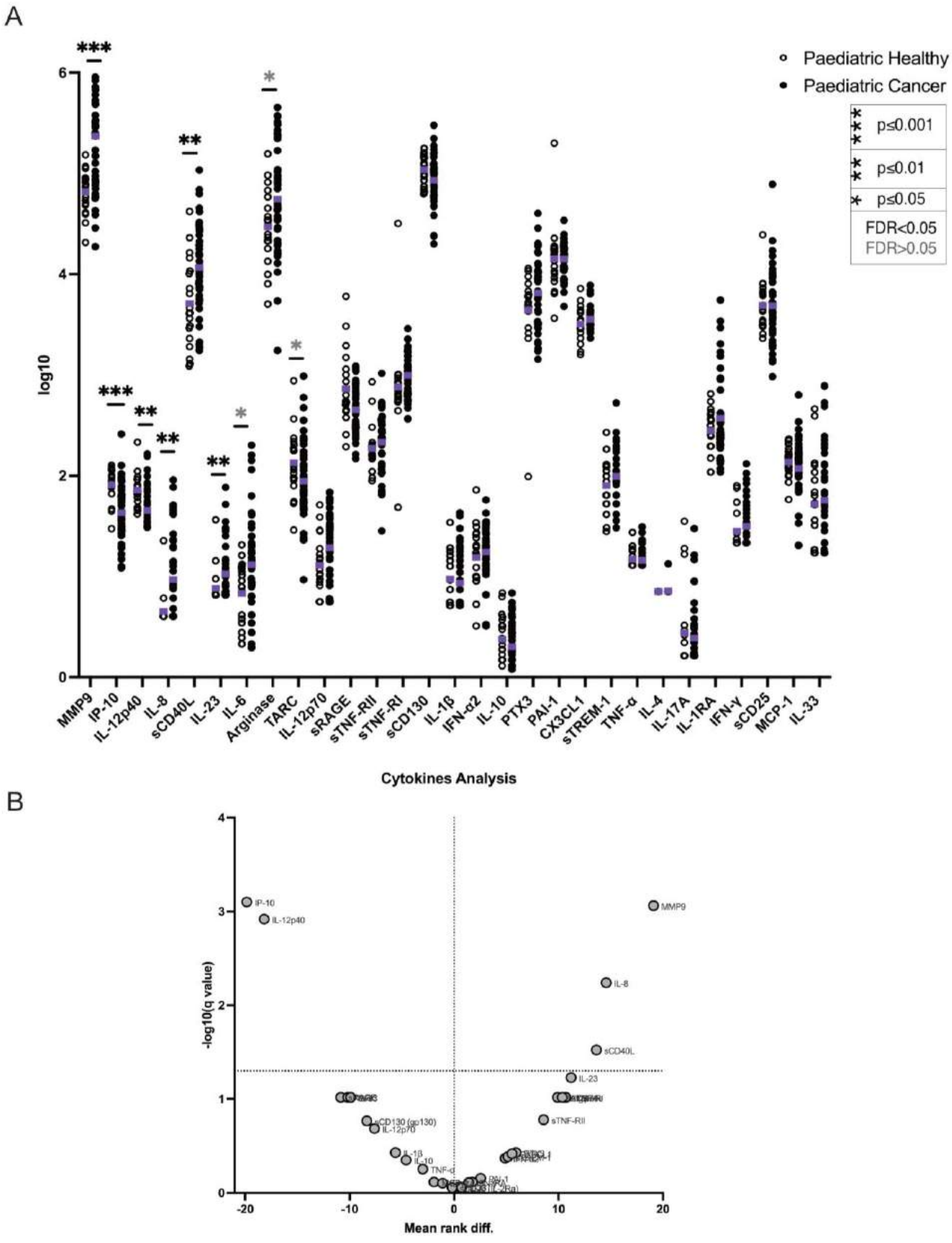

Figure 4-10 Cytokine profile of paediatric cancer patients.

(A) Levels of cytokines in plasma of 43 paediatric cancer patients and 19 healthy children. Results of Wilcoxon rank-sum tests comparing the frequency of each cluster in healthy children and cancer patients are indicated by: * p<0.05, ** p<0.01, *** p<0.001. Non-significant results are not shown, and black p value symbols indicate significant results after 5% false discovery rate correction using the Benjamini-Hochberg method. Purple line indicates the mean of the results. (B) Volcano plot generated for all the cytokines analysed. The values plotted on the x axis represent the difference between the means of paediatric healthy and paediatric cancer patients' values (x=0, no difference). The values plotted on the Y axis represent the minus logarithm of the q value generated by the multiple comparison analysis.

4.5 Analysis of tumour infiltrating lymphocytes revealed that low NK cell abundance in the periphery was not due to NK migration in the tumour sites.

Finally, to investigate whether the decreased frequency of total NK cells in the periphery was due to their migration to the tumour site we accessed our patients' diagnostic biopsies and determined the intratumoral expression of CD45, CD56 and CD57 by performing immunohistochemistry staining analysis. We were able to access samples for only a limited number of patients (n=4) due to constraints of ethical consent. Three patients had malignancy (neuroblastoma and Wilm's tumour) and one had WAGR syndrome and was diagnosed with premalignant nephroblastomatosis, a precursor for the development of Wilm's tumour (Grattan-Smith, 2011). Paediatric cancers frequently express NCAM1 protein (CD56) that is the standard marker to identify NK cells in the blood (Sebire *et al.*, 2005). Therefore, while we stained tissues for CD56, we also used CD45 to identify all lymphoid cells and CD57 to identify cytotoxic NK cells. The percentage of the tumour infiltrate lymphocytes (TIL) and NK cells was assessed by the consultant pathologist at Birmingham Women's and Children's hospital who reviewed and reported all the slides.

As expected, tumour cells showed positive CD56 staining (figure 4.11). CD45 staining varied between patients and was used to measure the percentage of TIL. Neuroblastoma patient

C11 had the highest percentage of TILs (45%), WAGR patient C19 had 10%, Wilm's patient C05 had 5% and Wilm's patient C16 had <1% (figure 4.12). Although the neuroblastoma sample contained a high frequency of CD45+ lymphoid cells only 1% of these were CD57 positive. These results indicate that the TILs in the tumour microenviroment of these four paediatric cancer patients were not NK cells. Finally, correlation analysis was performed comparing the total percentage of CD56 from the PBMCs (total % of NK cells) and the CD45 percentage in the tumour (% of TILs) for the same four patients (figure 4.12). This analysis showed that the number of TILs was linearly correlated with the number of total NK cells in the periphery suggesting that the highest number of circulating NK cells in the periphery the higher the number of TILs. In summary, immunohistochemistry analysis of TILs showed that these cells were not NK in origin suggesting the decrease of total NK cells seen in the periphery of paediatric cancer patients was most likely not due to their migration in the tumour sites. These results should be interpreted with caution given the small number of patients and validation is needed in larger cohorts.

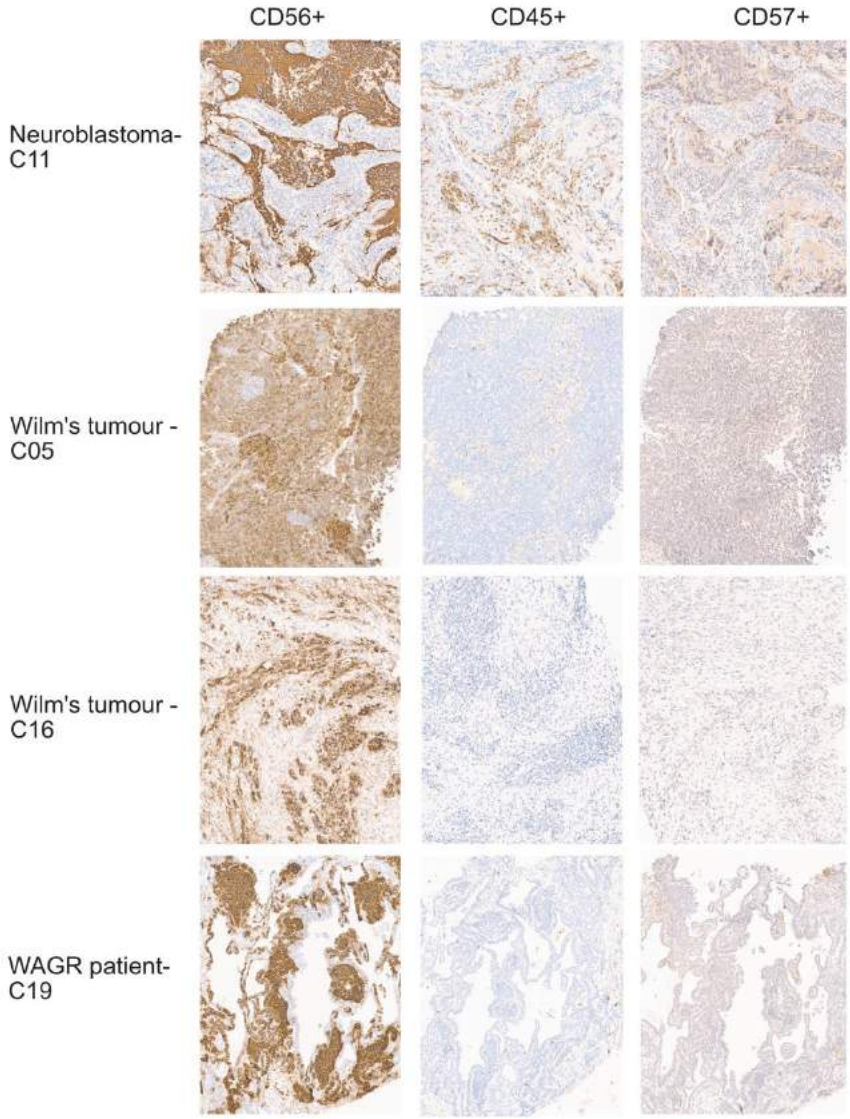

Figure 4-11 Immunohistochemistry analysis of paediatric tumours staining for CD56, CD45 and CD57.

Antibody staining was validated by the consultant pathologist using healthy lymphoid tissue.

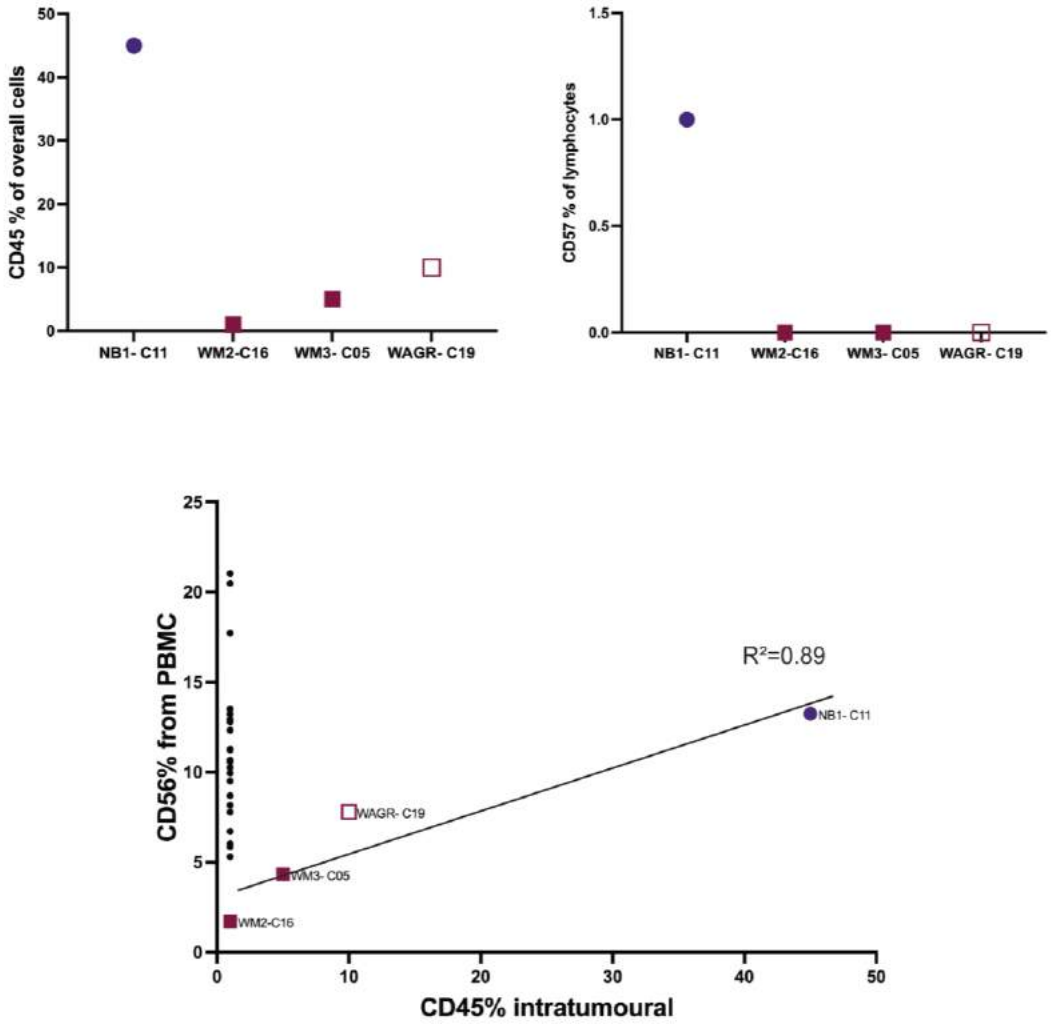

Figure 4-12 TILs percentage at the level of each individual.

Graphs one and two indicate the percentage of CD45+ and CD57+ in the tumour microenviroment as determined by the consultant pathologist at the BWCH. The third graph shows the correlation of the CD56% cells in the periphery and the intratumoural CD45%. In black dots the CD56% for healthy children is shown. R^2 has been calculated using the simple linear regression model, p value= 0.05.

4.6 Conclusions

The main aim of this chapter was to perform a detailed characterisation of the NK cells in paediatric cancer patients. First, an unsupervised analysis of total NK cells in the discovery cohort, confirmed the findings described in chapter 3 with paediatric cancer patients having an increased frequency of $CD56^{bright}$ NK cells compared to age matched counterparts. Next, we investigated whether the decrease in NK cell frequency noted in the periphery of paediatric cancer patients was due to them migrating to the tumour site. Few NK cells (1% of TILs) were identified in the tumour of one patient. This suggests that NK cell entrapment in the tumour site is unlikely to explain the deficit in the periphery. There was also a positive correlation between total NK cells in the periphery with non-NK TILs in the tumour. This could perhaps indicate that a higher percentage of total NK cells reflect a more functional immune system with cells able to migrate to tumour sites and TILs could perhaps be used in future studies for patient stratification. However, as this was only investigated in four patients, larger studies are needed to compare both tumour microenvironment and peripheral blood and validate these results.

Whether an NK cell activates depends on competing signalling from a large range of activating and inhibitory receptors. We therefore characterized the NK receptors in more detail. Interestingly, a significant imbalance was identified for both activating and inhibitory NK receptors in paediatric cancer patients. More specifically, the inhibitory NK receptor NKG2A (Pegram *et al.*, 2011) was increased, and the activating NK receptors NKp30/80 (Moretta *et al.*, 2001), KIR2DS1/3 and KIR2DS2/4(Ivarsson, Michaëlsson and Fauriat, 2014) were decreased in cancer patients. This imbalance of receptors was similar for all NK subsets

with the exception of the the expression of NKG2A and KIR2DS2/4 on the $CD56^{dim}$ NK subset. This imbalance could perhaps reflect a failure in NK cell development and education. It has been described that NK cells undergo education in order for them to be licensed as fully functional cells that are inhibited from killing human leukocyte antigen (HLA) positive healthy cells therefore, acquiring self-tolerance (Yokoyama and Kim, 2006). The self-specific inhibitory KIRs recognize the HLA class I and render the NK cells hyporesponsive, avoiding potential autoreactivity (Kärre, 2002). In addition, NKG2A recognizes the non-classical HLA-E molecule and inhibits the function of NK cells (Le Dréan *et al.*, 1998). Therefore, a prerequisite for NK cells to become fully licensed and functional is to express self-specific inhibitory receptors (He and Tian, 2017). This process is followed by several maturation stages (figure 1.9 from intro) which includes gradual loss of the NKG2A receptor and acquiring CD57 and KIRs (Goodridge, Önfelt and Malmberg, 2015). Interestingly, our results indicate that the NK cells of paediatric cancer patients are licensed given the increased expression of inhibitory receptor NKG2A however, are not mature yet given their decreased expression of certain activating KIRs and CD57. On the other hand NK cells cytotoxicity is controlled by a combination of inhibitory and activating receptors (Kumar, 2018). Therefore, the imbalance of NK receptors seen in paediatric cancer patients could be a mechanism of which the cancer cells evade the immune responses by NK cells or could reflect the increased frequency of the immature NK subset $CD56^{bright}$ seen in the cancer patients.

Given that NKG2A plays a central role in limiting NK cell function, blocking this molecule would be expected to increase the NK cell activity. It has been successfully targeted in adult cancer patients with a monoclonal antibody called monalizumab(Creelan and Antonia, 2019). The antibody binds on the NKG2A receptor blocking its interaction with HLA-E which then

leads to NK activation and secretion of granzymes and perforins to the target cell(Haanen and Cerundolo, 2018). Therefore, a prerequisite for the antibody to work is the expression of NKG2A on the NK cells and HLA-E on the tumours. Our data show NK cells in paediatric cancer patients express more NKG2A and HLA-E has been described to be present in some embryonal tumours such as neuroblastomas (Zhen *et al.*, 2016). However, the majority of NK cells in paediatric cancer patients are immature therefore adding this blockade by itself might not be the answer if they lack molecules such as perforin and granzyme B. Nevertheless, NKG2A was found to be higher in the mature NK subsets of patients thus, future studies including monalizumab as a monotherapy or combination therapy could be beneficial for paediatric cancer patients.

Next, lysis of K562 cells by NK cells from four of the five patients tested was significantly reduced with no difference in the NK degranulation or cytokine production. Interestingly, patient C19 had a pre-malignant condition, and their NK cytotoxicity was not altered. Furthermore, this was also associated with decreased NK levels of perforin and granzyme B in paediatric cancer patients. In adult cancer patients, tumour cells have been shown to secrete NK ligands that bind to NK cell receptors inhibiting their function (Haanen and Cerundolo, 2018). We explored whether this mechanism might also occur in paediatric patients, focusing on soluble ULBP2 and soluble MICA. We detected both ligands, but concentrations were lower in paediatric cancer patients suggesting this was not the mechanism of decreased NK cytotoxicity. Therefore, the decrease in NK cytotoxicity observed for patients is likely to be due to the lower NK levels of perforin and granzyme-B and the decreased proportion of mature NK cells, particularly CD57+ cells that are the strongest mediators of cytotoxicity. We cannot rule out that the alterations seen in the activating and inhibitory NK receptors could

also attribute to the reduced NK cytotoxicity. However, K562 cells lack the HLA-E molecule that inhibits NK function via NKG2A (Monaco *et al.*, 2011) suggesting the increased expression of NKG2A seen in paediatric cancer patients is unlikely to be the cause of decreased K562 killing. Finally, the observation that the one patient with normal NK cytotoxicity had nehproblastomatosis, a pre-malignant disease, rather than cancer suggests compromised NK cytotoxicity may not occur until later in the disease process. This finding requires validation in larger cohort studies.

Finally, moving on to cytokine profile analysis several key alterations were identified. First, IL-23 was found to be increased in paediatric cancer patients. This cytokine has been described to suppress innate immunity, promoting tumour development and metastases (Teng *et al.*, 2010). Second, IL-8 was found to be increased in paediatric cancer patients. IL-8 is thought to act as a chemoattractant molecule for neutrophils and myeloid derived stem cells (MDSCs) promoting an immunosuppressive tumour microenvironment and favouring tumour progression(David *et al.*, 2016). In addition, increased levels of IL-6 and IL-8 have been implicated in reduced NK cytotoxicity through STAT3 signalling which suppressed NKp30 on NK cells, and has been associated with poor overall survival (Wu *et al.*, 2019). Interestingly, both of these cytokines were increased in the periphery of paediatric cancer patients, and we also detected decreased expression of the activating receptor NKp30 as well as reduced NK cytotoxicity. Further studies investigating the link of IL-6 and IL-8 with the NK cells are needed as this could be potentially therapeutically targeted. Currently there are two IL-8 neutralising antibodies which in preclinical studies have proven to reduce invasion, angiogenesis and increase tumour cell apoptosis in melanoma bearing mice (Huang *et al.*, 2002).

The cytokine analysis provided additional insights into paediatric cancer biology. We identified sCD40L to be increased in paediatric cancer patients. Elevated levels of sCD40L may have an immunosuppressive role in cancer patients by decrease of tumour cell apoptosis, increase tumour cell proliferation, inducing angiogenesis, immunosuppressive cytokines and increasing the frequency of immunosuppressive cells (Huang *et al.*, 2012). Therefore, this can also be a novel therapeutic target for paediatric cancer patients. Similarly, MMP9 has also been linked to tumour progression, migration and angiogenesis and has been used as a cancer biomarker in several types of cancer (Huang, 2018). MMP9 could therefore be used as potential novel cancer biomarker and future studies could investigate whether MMP9 inhibitors can be used in paediatric cancer patients.

In summary, the NK cells isolated from the periphery of paediatric cancer patients are decreased in frequency, more immature, less cytotoxic and have an imbalance of activating and inhibitory receptors. The decreased NK cytotoxicity observed was reversible in one patient whose their NK cells were expanded in a clinically validated IL-2 protocol indicating that this could be therapeutically targeted perhaps through expanded NK cells, chimeric antigen receptor (CAR)- engineered NK cells or anti-NKG2A antibody. Furthermore, IL-8 could also be potentially targeted in paediatric cancer patients as this could also reverse the NK cytotoxicity. Finally, sCD40L and MMP9 could be used as potential cancer biomarkers in paediatric cancer patients.

CHAPTER 5- The immune landscape of multisystem inflammatory syndrome in children

5.1 Introduction

The analysis of the immune perturbations in children with cancer as described in chapter 3 and 4, provided us with the expertise to investigate a novel paediatric hyperinflammatory syndrome, called Multisystem Inflammatory Syndrome in Children (MIS-C, (Riphagen *et al.*, 2020). This syndrome occurs in children after primary infection with SARS-CoV-2, the viral cause of coronavirus disease 2019. New MIS-C cases usually present 4-6 weeks after primary SARS-Cov-2 infection in the community(Feldstein *et al.*, 2020; Godfred-Cato *et al.*, 2020). Children with MIS-C present with fever and/or mucocutaneous, cardiac, gastrointestinal, and respiratory system involvement(Ahmed *et al.*, 2020; Riphagen *et al.*, 2020; Whittaker *et al.*, 2020; Hoste, Van Paemel and Haerynck, 2021). In severe cases patients can present with evidence of single or multi-organ failure manifesting with hypotension, cardiac dysfunction and life-threatening shock (Ahmed *et al.*, 2020; Riphagen *et al.*, 2020; Whittaker *et al.*, 2020; Hoste, Van Paemel and Haerynck, 2021). MIS-C shares clinical characteristics with several other paediatric inflammatory conditions such as toxic shock syndrome (TSS), macrophage activation syndrome (MAS) and Kawasaki disease (KD,Consiglio *et al.*, 2020; Lee *et al.*, 2020). The optimal treatment strategy of MIS-C is yet to be established and currently children are being treated with a range of anti-inflammatory medications that have been deployed from KD or adult COVID protocols(*Paediatric multisystem inflammatory syndrome temporally associated with COVID-19 (PIMS) - guidance for clinicians*, no date).

The aims of this chapter were to: 1) characterise the immune alterations occurring acutely in children with MIS-C and compare these to KD and healthy children and 2) describe the immune responses occurring with current MIS-C treatment strategies.

5.2 Cohort Demographics

5.2.1 Ethics statement and patient recruitment

All patient samples were obtained at Birmingham Children's Hospital as part of an ethical approved study (TrICICL) by the South of Birmingham Research Ethics Committee (REC: 17/WM/0453, IRAS: 233593). Samples from seven healthy children (aged 12 years) were obtained via the Coronavirus Immunological Analysis study approved by North West - Preston Research Ethics Committee (REC: 20/NW/0240, IRAS: 282164). Written informed consent was obtained from all participants' legal guardians. All experiments were conducted at the University of Birmingham.

5.2.2 Patient characteristics

Due to the complexity of the disease and the input required from the multidisciplinary team, patients from the West Midlands region were transferred to Birmingham Women and Children's hospital, a tertiary level paediatric hospital. Between April and October 2020, 16 children meeting the MIS-C diagnostic criteria established by the Royal College of Paediatrics and Child Healthy (RCPCH) and 2 children meeting the criteria for KD were recruited to the TrICICL study (Table 5.1). Half of the MIS-C cases occurred four weeks after SARS-CoV-2 cases were detected in the local community while the rest of the cases accumulated over the next few months (Figure 5.1A). All MIS-C patients were over 5 years

of age (Figure 5.1B), from an ethnic minority and tested positive for the combined anti-IgG, IgA and IgM SARS-CoV-2 antibodies (Table 5.1). In contrast, the two KD patients were under 5 years of age and tested negative for the combined anti-IgG, IgA and IgM SARS-CoV-2 antibodies (Table 5.1).

Treatment strategies were determined by the multidisciplinary team assembled at Birmingham Women and Children's hospital and in accordance with the RCPCH guidance(*Paediatric multisystem inflammatory syndrome temporally associated with COVID-19 (PIMS) - guidance for clinicians*, no date). Intravenous immunoglobulin (IVIG) was given to both KD patients as standard of care(McCrindle Brian W. *et al.*, 2017) and to 12 out of 16 patients (81%) of the MIS-C patients (Figure 5.1C and 5.2). Second IVIG was offered to one KD patient and to three MIS-C patients due to persistent inflammation (Figure 5.1C and 5.2). IV methylprednisolone was administered over the course of three days, in eight MIS-C patients who exhibited signs of relapse or persistent inflammation. In one case (patient 13), anti-IL6 therapy (tocilizumab) was offered due to refractory disease. The majority of patients (88%) required admission to paediatric intensive care unit (PICU) to manage their disease (Figure 5.1C and 5.2). The overall hospital length of stay ranged between five to 16 days (Figure 5.2). All 18 patients survived without long term health complications at the time of last clinical follow up.

Research samples were taken pre-IVIG administration from eight patients (seven MIS-C and one KD) with the exception of patient 14 where the first sample was taken a few hours post-IVIG administration (Figure 5.2). Subsequent research samples post IVIG were taken in

seven patients (six MIS-C and one KD) and at the time of discharge in three patients (two MIS-C and one KD) in order to assess the immune responses to treatment (Figure 5.2).

ID	Age (years)	Sex	Ethnicity	Fever	Rash	Lymph-adenopathy	Conjunctivitis non-exudated	Mucosal changes	Peripheral changes	GI features	Cardiac involvement	PCR for SARS-CoV-2	Serology for SARS-CoV-2	Diagnosis
1	0-4	M	Asian British	Yes	Yes	No	No	No	No	No	NO	Neg x3	Not done	KD
2	0-4	M	White British	Yes	Yes	Yes	Yes	Yes	Yes	Yes, V	NO	Neg x1	Negative	KD
3	5-10	M	Black British-African	Yes	No	No	No	No	No	Yes, V	YES	Neg x3	Positive	MIS-C
4	5-10	M	Asian British-Pakistani	Yes	Yes	No	Yes	Yes	Yes	Yes, abdominal pain, V	NO	Neg x1	Positive	MIS-C
5	5-10	M	Asian British-Pakistani	Yes	Yes	Yes	Yes	Yes	No	Yes, acute abdomen, pain, V	Yes	Neg x3	Positive	MIS-C
6	5-10	F	Black British	Yes	Yes	No	Yes	Yes	No	Yes, amdominal pain, D	Yes	Pos x1 Neg x2	Positive	MIS-C
7	5-10	F	Asian British-Indian	Yes	Yes	No	No	No	No	Yes, abdominal pain, V	NO	Pos x2	Positive	MIS-C
8	5-10	M	Asian British-Indian	Yes	No	No	No	No	No	Yes, acute abdomen, pain, D&V	YES	Neg x3	Positive	MIS-C
9	5-10	F	Asian British-Pakistani	Yes	Yes	No	No	No	No	Yes, pain, D&V	YES	Negx2	Positive	MIS-C
10	5-10	F	Black British-African	Yes	Yes	No	Yes	Yes	Yes	Yes,D&V	YES	Neg x2	Positive	MIS-C
11	5-10	M	Black British-Carribean	Yes	Yes	No	Yes	Yes	Yes	Yes, abdominal pain, D&V	YES	Neg x2	Positive	MIS-C
12	5-10	M	Asian British-Baghladeshi	Yes	No	No	Yes	No	Yes	Yes, abdominal pain, D&V	YES	Neg x2	Positive	MIS-C
13	5-10	F	Black British-African	Yes	Yes	Yes	No	Yes	No	Yes, acute abdomen, D&V	YES	Neg x2	Positive	MIS-C
14	11-15	F	Mixed White Black-Caribbean	Yes	No	No	No	No	No	Yes, admominal pain, D	YES	Neg x3	Positive	MIS-C
15	11-15	M	Mixed White Black- Afro Caribbean	Yes	No	No	No	No	No	Yes, abdominal pain, D&V	YES	Neg x2	Positive	MIS-C
16	11-15	F	White-Romanian	Yes	Yes	Yes	Yes	No	No	Yes, abdominal pain, V	YES	Neg x2	Positive	MIS-C
17	11-15	F	Black British-Caribbean	Yes	Yes	No	No	No	No	Yes, D&V	YES	Neg x3	Positive	MIS-C
18	11-15	M	Asian British-Pakistani	Yes	Yes	No	Yes	No	No	Yes, abdominal pain	NO	Neg x3	Positive	MIS-C

Table 5-1 Clinical characteristics of MIS-C and KD cohort.

Demographic and clinical data for the 16 patients with MIS-C and 2 patients with Kawasaki disease (KD) recruited to the study. KD patients are indicated by grey background. PCR: polymerase chain reaction. D=Diarrhoea, V=Vomiting, Neg= Negative, Pos= Positive, M=Male, F=Female. Cardiac involvement includes abnormal ECG and/or echocardiography findings.

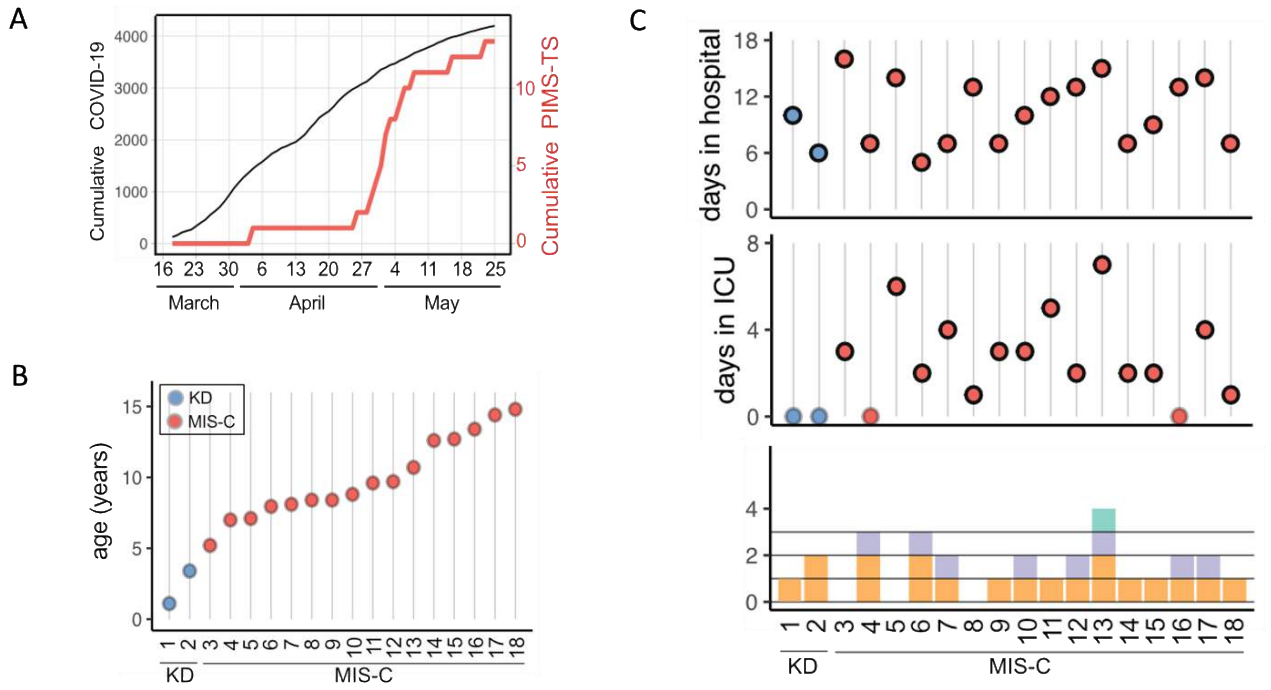

Figure 5-1 Cohort characteristics and disease severity indicators

(A) Cumulative SARS-CoV-2 positive cases identified by PCR testing within the Birmingham area compared to MIS-C cases admitted to Birmingham Children's Hospital PICU. (B)Age of KD and MIS-C patients recruited to this study. (C) Disease severity indicators shown as days hospitalised, days in PICU and treatment cycles of IVIG, intravenous steroids and Tocilizumab

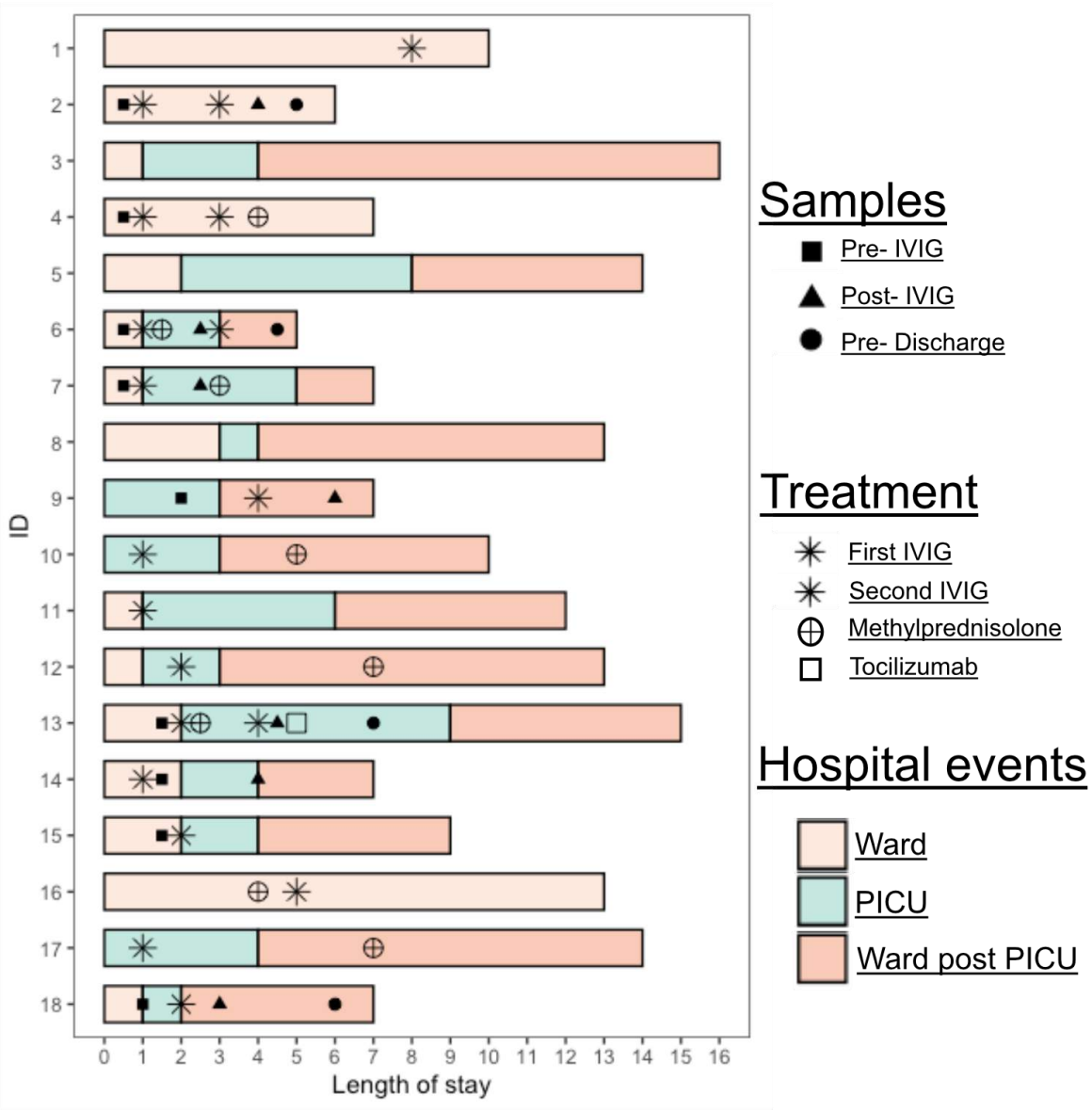

Figure 5-2 Key hospital events shown for each individual in the form of swimmer plot.

Length of stay in hospital is shown in days. Treatments received and sample collection timings are annotated accordingly. Hospital events are coloured in each patient's bar. Patients 1 and 2 represent the KD patients while 3-18 the MIS-C patients.

5.3 Clinical laboratory data of MIS-C and KD patients show patients present with hyperinflammation

5.3.1 Antibody responses suggest MIS-C develops weeks after primary SARS-CoV-2 infection

To confirm reports that MIS-C occurs several weeks after primary SARS-CoV-2 infection(Feldstein *et al.*, 2020; Godfred-Cato *et al.*, 2020) antibodies against the spike glycoprotein S of the virus were measured by ELISA from the plasma of eight MIS-C patients. Analysing the individual anti-SARS-CoV-2 antibodies showed that all eight MIS-C patients had raised IgG and IgA antibodies but lacked IgM antibodies (figure 5.3). Since antibody responses can reflect recent infection (with the presence of IgM antibodies) or past infection (with the presence of IgG and IgA antibodies), these data confirm that MIS-C develops weeks after primary virus infection occurred.

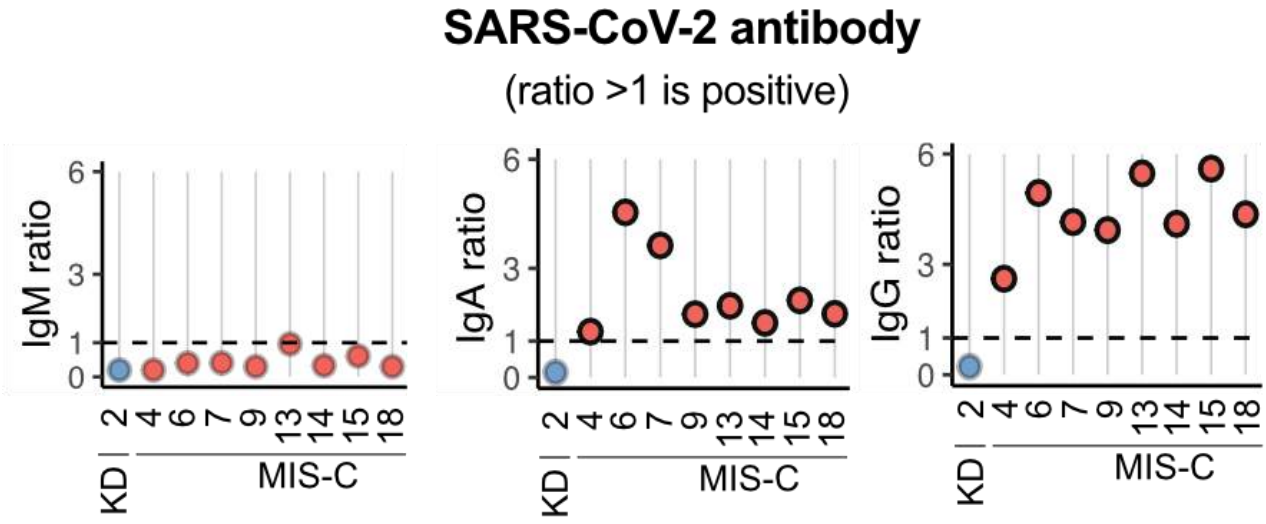

Figure 5-3 SARS-CoV-2 antibody responses for IgM, IgA and IgG.

5.3.2 Clinical laboratory data of MIS-C patients

Multiple reports have described the clinical laboratory characteristics of MIS-C patients (Ahmed *et al.*, 2020; Hoste, Van Paemel and Haerynck, 2021). Affected children have elevated markers of inflammation such as erythrocyte sedimentation rate (ESR), C-reactive protein (CRP) and ferritin, elevated neutrophils and reduced lymphocytes. To investigate whether our cohort also had elevated markers of inflammation the clinical laboratory profile of 16 MIS-C and two KD patients was investigated.

Confirming the findings of previous reports, elevated ESR, CRP and ferritin were detected in both KD and MIS-C children (figure 5.4A). Almost all MIS-C patients had high troponin and pro-B-type natriuretic peptide (NT pro-BNP), suggesting cardiac involvement (figure 5.4B). Interestingly, all MIS-C patients were deficient in Vitamin D but not the KD patients (figure 5.4B). In addition, both KD and all MIS-C patients acutely presented with lymphopaenia and neutrophilia (figure 5.4C). The absolute numbers of monocytes were normal for the KD patients but at the lower limit of normal for almost all MIS-C patients (figure 5.4C). KD patients had normal or high platelets but MIS-C patients had normal or low platelets (figure 5.4C). Finally, additional clinical laboratory assays were performed in a subset of patients, using the BD Trucount^{TM} tubes. In accordance with low lymphocytes the absolute counts of CD4, CD8 T-cells and B-cells were decreased however, the relative proportion of these within the lymphocyte pool were generally unaltered (Figure 5.5). All of these clinical laboratory findings are consistent with other clinical MIS-C cohorts published by other groups(Ahmed *et al.*, 2020; Feldstein *et al.*, 2020; Hoste, Van Paemel and Haerynck, 2021).

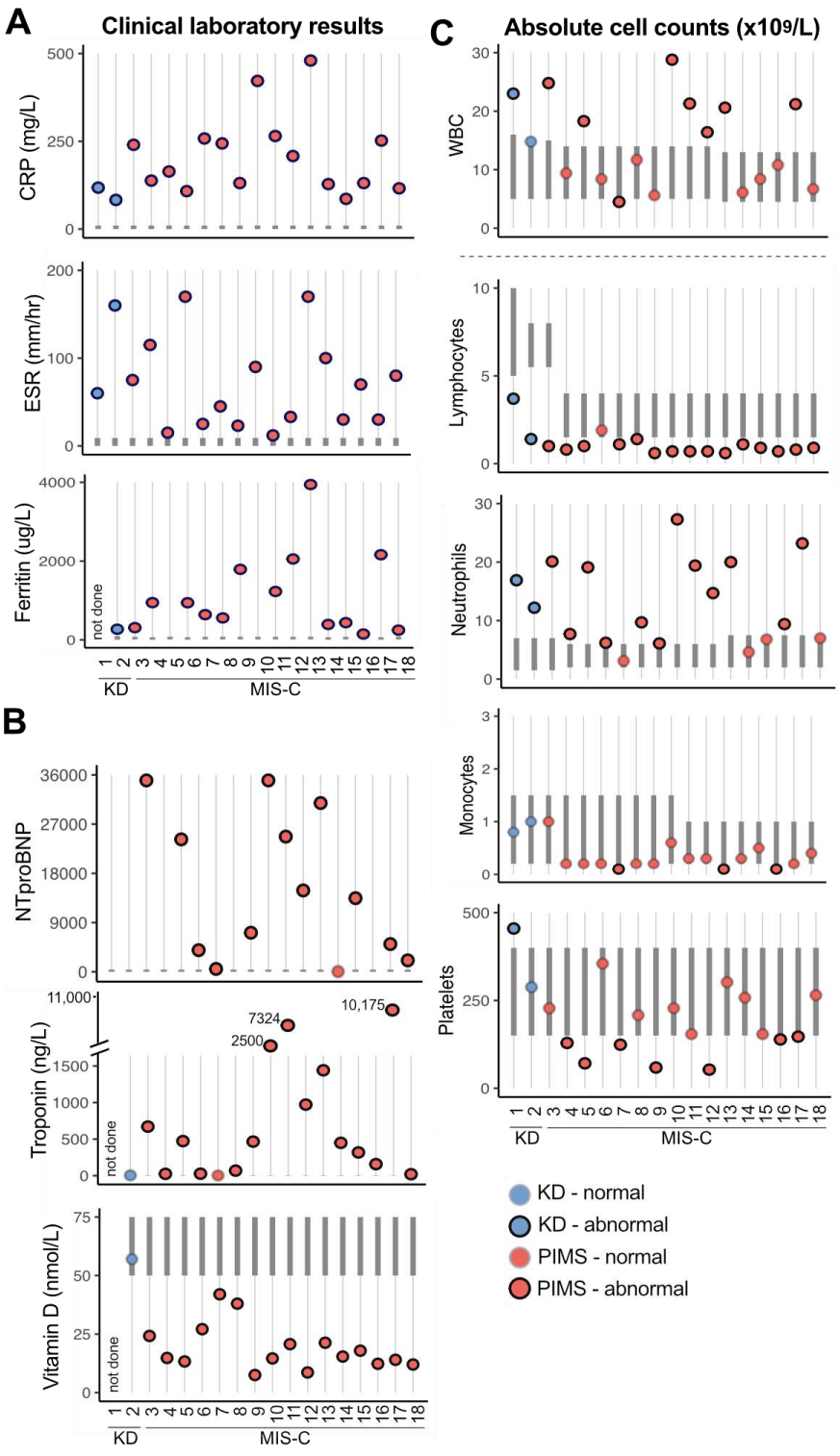

Figure 5-4 Clinical laboratory data for acute MIS-C and KD.

(A) Clinical laboratory results shown for C-reactive protein (CRP), erythrocyte sedimentation rate (ESR) and ferritin. (B) Clinical laboratory results shown for pro-B-type natriuretic peptide (NTproBNP), troponin and vitamin D. (C) Pre-treatment absolute count of different immune cell subsets expressed as 10^9 cells/L, White Blood Cell (WBC). Grey bars represent the normal values range for each patient's age and sex.

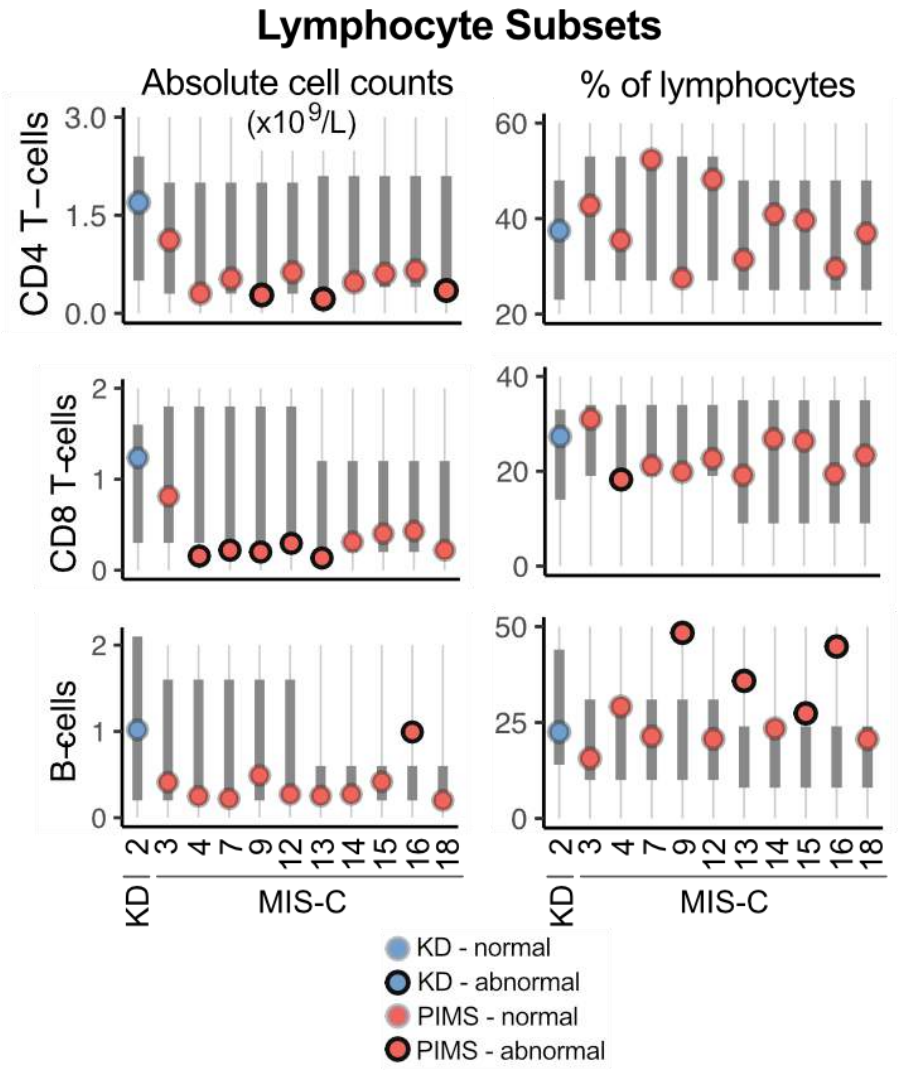

Figure 5-5 Trucount data for acute MIS-C and KD

Pre-treatment frequency of lymphocyte subsets expressed as the absolute number of cells x10^9/L (left column) or percentage of total lymphocytes (right column). Grey bars represent the normal values range for each patient's age and sex.

5.3.3 Neutrophilia is associated with more severe disease in MIS-C

To further explore the clinical laboratory data principal component analysis was performed to reduce the dimensionality of the data and to gain a better overview of the clinical dataset. For healthy controls synthetic data were generated using values from normal ranges widely available for each parameter. For each patient ten controls were used by randomly selecting the values taking into account patient's age and sex. Neutrophil count, CRP and ESR correlated with each other while monocyte and lymphocyte counts were linearly uncorrelated (Figure 5.6A- Right panel). All patients fell outside the normal region consisting of the synthetic healthy values, to varying degrees and consistent with laboratory results this was driven by the ESR, CRP, neutrophils and WBC (Figure 5.6A- Left panel). These results indicate that elevated ESR, CRP, neutrohpils and WBC differentiate MIS-C patients from healthy children.

To investigate the relationships between clinical features, absolute immune cell counts and demographics for the MIS-C patients a correlation matrix was constructed (Figure 5.6B). As expected, clinical markers of cardiac and kidney dysfunction (troponin, pericardial effusion, urea and creatinine) positively correlated with the need for inotrope support suggesting these patients presented with cardiogenic shock. The most striking result emerging from this analysis was the positive correlations between absolute neutrophil count and markers of inflammation (CRP), cardiac dysfunction (presence of pericardial effusion, levels of troponin, creatinine kinase and NTpro-BNP) but also the overall length of hospital stay, suggesting neutrophilia can be a predictive factor of severe disease.

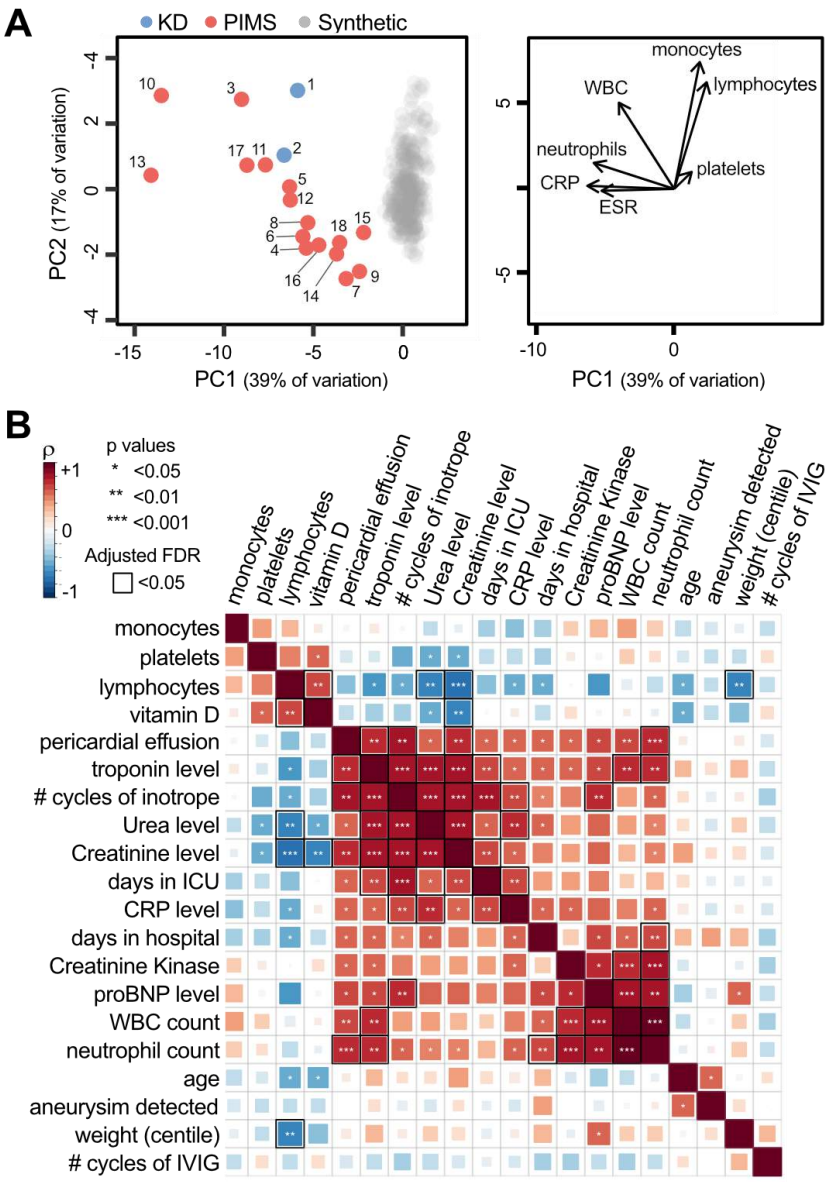

Figure 5-6 Unsupervised analysis of acute clinical data.

(A) Left: Principal component analysis biplot of clinical laboratory features for patients with MIS-C or KD and synthetic healthy controls derived from normal range data. Right: Loading plot showing the top 7 features contributing to principal components one and two. (B) Correlation matrix of clinical features, immune parameters and demographics for the 16 MIS-C patients. The strength of each correlation is indicated by colour and statistical significance by asterisks: *p<0.05, **P<0.01, ***P<0.001. Black outline indicates a significant result after 5% false discovery rate correction using the Benjamini-Hochberg method.

5.4 Mass cytometry shows that both innate and adaptive immune cells are activated in acute MIS-C

To explore in more detail the immune changes occurring in MIS-C patients, high-dimensional approaches were deployed. Preliminary single cell RNA (scRNA) sequencing data of pre-treatment samples from two MIS-C patients (P13 and P14) and one KD patient (KD2), showed monocytes were profoundly altered in both diseases (Syrimi, Fennell, Richter, Vrljicak, Stark, Ott, Murray, Al-Abadi, Chikermane, Dawson, Hackett, Jyothish, Kanthimathinathan, Monaghan, Nagakumar, Scholefield, Welch, Khan, Faustini, Kearns, *et al.*, 2021)**.** These data were exploited to inform a 38 marker mass cytometry panel (Table 2.4) that was used to investigate fixed whole blood samples from seven patients (six MIS-C and one KD) and seven healthy children.

5.4.1. Manual gated data show CD8 T cell activation with concomitant phenotypic changes in B-cells, NK and monocytes.

Agranulocytes were manually gated by first excluding the platelets using the marker CD41/42a61 and then granulocytes using the marker CD66b (figure 5.7). Next, the CD3+CD4+ T-cells, CD3+CD8+ T-cells and CD19+ B-cells were identified (figure 5.7). Further manual gating was performed for the main T- and B-cells subsets. Based on CD45RA and CD27 expression (Sallusto *et al.*, 1999), CD4+ and CD8+ T-cells were divided into naïve (Tn, CD45RA+CD27+), central memory (Tcm, CD45RA-CD27+), effector memory (Tem, CD45RA-CD27-) and terminally differentiated effector memory (TEMRA, CD45RA+CD27-). Activated CD4+ and CD8+T cells were defined by their HLA-DR+ expression(Maecker, McCoy and Nussenblatt, 2012). B-cell main subsets were also identified by gating plasmablasts as CD19+

$CD38^{high}$CD27+ (Cossarizza *et al.*, 2019) and based on their IgD and CD27 expression non-plasmablasts were divided into four subsets: IgD-CD27+ class-switch B-cells, IgD+CD27+ Non-Switch memory B-cells, IgD+CD27- naïve B-Cells and IgD-CD27- B-cells (Blomberg and Frasca, 2013).

Furthermore, monocytes were identified from the CD3-CD19-HLA-DR+ population (figure 5.7). Based on the canonical monocyte markers CD14 and CD16 the three circulating monocyte(Ziegler-Heitbrock *et al.*, 2010b) subsets were gated as: classical monocytes (CM, CD14+Cd16-), transitional monocytes (TM, CD14+CD16+) and non-classical monocytes (NCM, CD14-CD16+). Natural Killer (NK) cells were identified from the CD3-CD19-HLA-DR- population based on their CD56 expression and CD57+ NK cells(Lopez-Vergès *et al.*, 2010) were subsequently identified. Finally, plasmacytoid and myeloid dendritic cells (pDCs and mDCs) were identified from the CD3-CD19-HLA-DR+CD14-CD16- population and gated as CD123+CD11c- for pDCs and CD11C+CD123+ for mDCs (Della Bella *et al.*, 2008)(figure 5.7). No statistically significant difference was observed within the main subsets of MIS-C and healthy children with the exception of pDCs (figure 5.8).

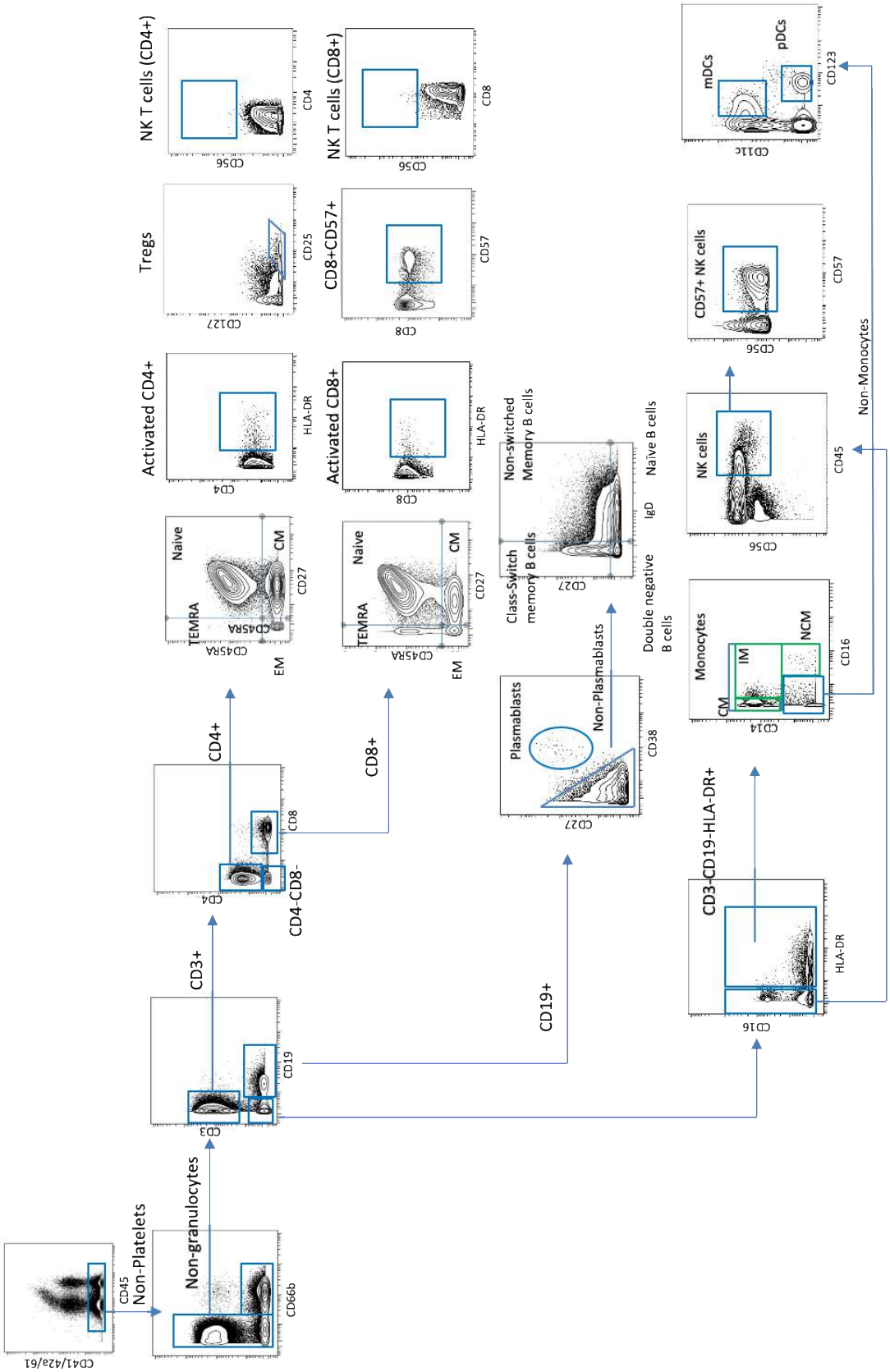

Figure 5-7 Manual gating strategy of non-granulocytes.

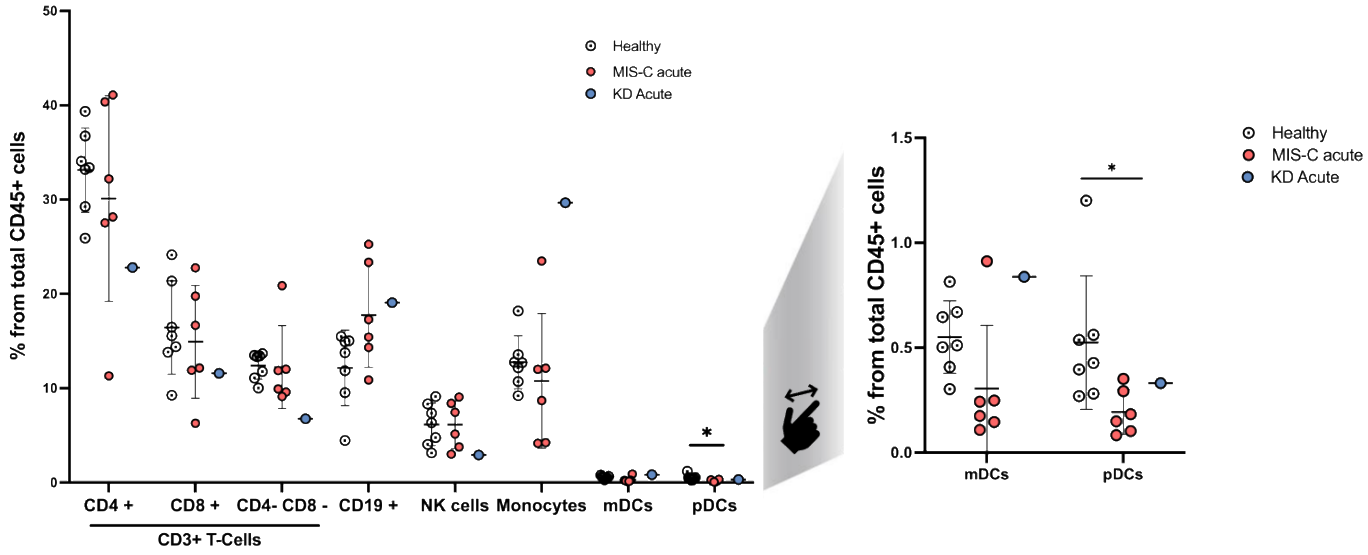

Figure 5-8 Frequencies of immune cell subsets in acute MIS-C and KD.

Frequency of the main immune subsets for healthy children and MIS-C patients expressed as a percentage of total CD45+ cells. The mean +/- SD is shown. Significant results are indicated: * p<0.05, ** p<0.01, *** p<0.001P values that are not significant are not shown. The results of Wilcoxon ranked sum tests with false discovery rate correction using the Benjamini-Hochberg method are shown.

Turning now to T- cells, there was no significant difference in the distribution of the four main subsets of CD4+ and CD8+ T-cells between MIS-C and healthy children (figure 5.9 A and B). The KD patient had the highest proportion of CD4+ and CD8+ naïve T-cells likely due to their younger age (Taylor *et al.*, 2019; Lakshmikanth *et al.*, 2020) (figure 5.9 A and B). Next, manual gating of HLA-DR+ cells was performed, to investigate whether these cells were activated (figure 5.9C). Only a small proportion of the Tcm CD4+ T-cells had evidence of activation in MIS-C patients (figure 5.9D). In contrast, within the CD8+ T-cells, MIS-C patients had a significantly higher proportion of HLA-DR+ CD8+ T-cells at their pre-treatment samples. More specifically, 2% of the naïve, 35% of Tcm and 30% of Tem CD8+ T-cells were HLA-DR positive (Figure 5.9D). Similarly, the KD patient showed the same pattern of CD8 T-cell activation (Figure 5.9D). Finally, manual gating of Tregs, CD8+CD57+, NK T-cells showed no significant differences between MIS-C patients and healthy children (figure 5.9E). Moving on to B-cells even though there was no significant difference in the frequencies of total B-cells (figure 5.8), when B-cells subsets were analysed, marked differences were identified between the MIS-C and healthy children (figure 5.10). More specifically, the MIS-C patients had higher plasmablasts and IgD-CD27- B- cells compared to healthy children and had significantly lower abundance of non-switch and class-switch memory B-cells. These results are in agreement with previous reports of plasmablast expansion in MIS-C but also provided additional insights into the abnormalities of B-cell subsets in MIS-C disease. Finally, monocytes and NK cells subsets were explored in more detail. MIS-C patients had significant lower abundance of classical monocytes (figure 5.11) with a similar pattern observed for CD57+ NK cells (figure 5.12).

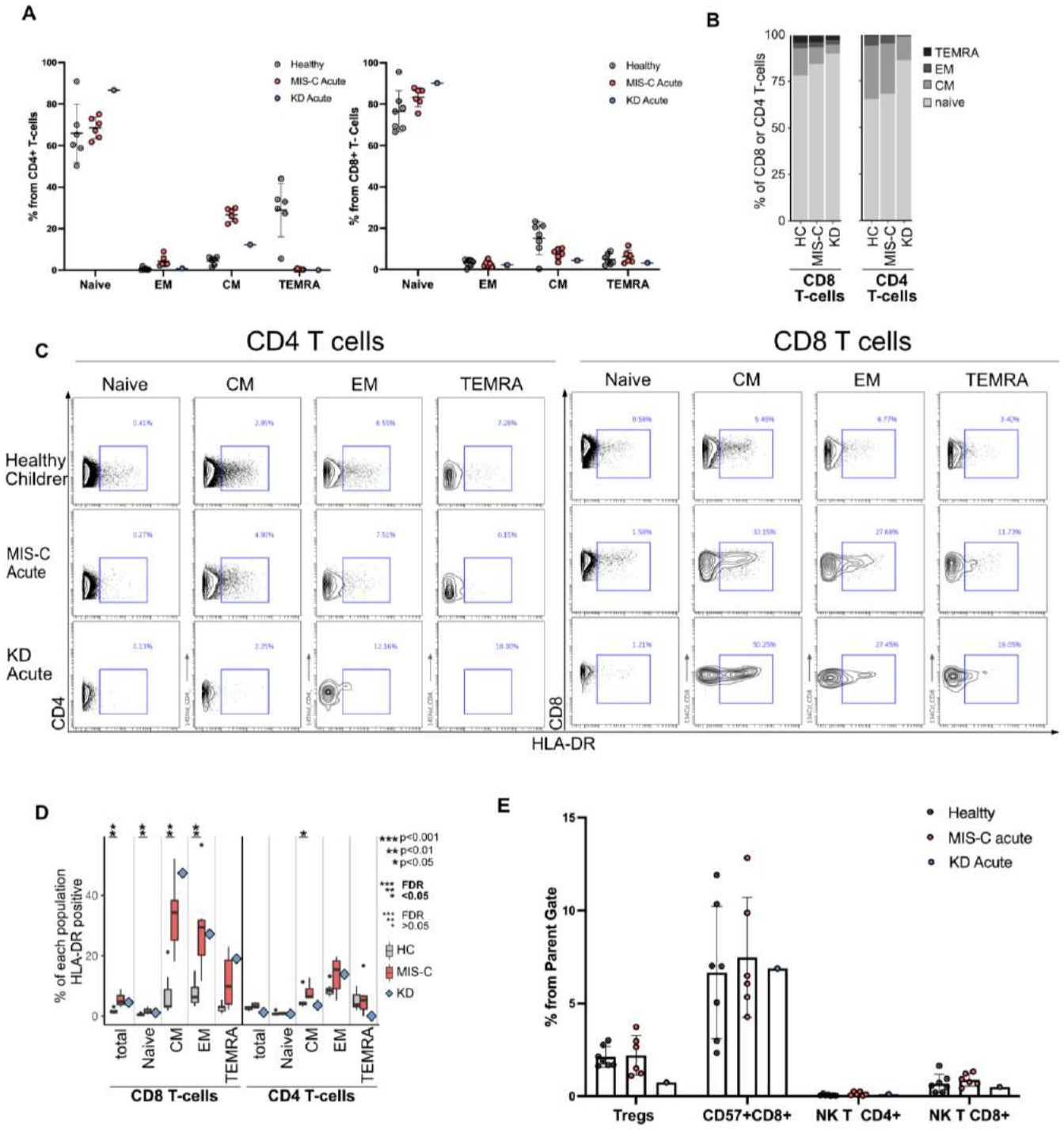
A
% from CD4+ T-cells
% from CD8+ T- Cells
Healthy
MIS-C Acute
KD Acute
Naive
EM
CM
TEMRA
B
% of CD8 or CD4 T-cells
TEMRA
EM
CM
naive
HC
MIS-C
KD
CD8 T-cells
CD4 T-cells
C
CD4 T cells
CD8 T cells
Naive
CM
EM
TEMRA
Healthy Children
MIS-C Acute
KD Acute
CD4
CD8
HLA-DR
D
% of each population HLA-DR positive
***p<0.001
**p<0.01
*p<0.05
FDR <0.05
FDR >0.05
HC
MIS-C
KD
total
Naive
CM
EM
TEMRA
CD8 T-cells
CD4 T-cells
E
% from Parent Gate
Healtty
MIS-C acute
KD Acute
Tregs
CD57+CD8+
NK T CD4+
NK T CD8+

Figure 5-9 T-cells analysis in acute MIS-C and KD.

(A)Frequency of CD4+ and CD8+ T-cells within each of the four subsets for each individual healthy control and MIS-C acute patient. Statistical significance was determined by Wilcoxon test between healthy children and MIS-C patients at the acute stage of disease. ns: no significant difference. (B) Percentage of CD8+ and CD4+ T-cells in each of the four canonical T-cell sub-populations for healthy children, and patients at the acute stage of their disease. (C) Gating strategy for HLA-DR+ cells in the four subsets of CD4+ and CD8+ T-cells. (D) Percentage of each T-cell subpopulation from the same donors that were positive for HLA-DR. (E) Frequency of other CD4 and CD8 subpopulations. The results of Wilcoxon ranked sum tests comparing the frequency of each cluster in healthy children to acute MIS-C patients are shown. For all panels the data were from seven healthy children, a single KD patient or six acute MIS-C patients. Significant results are indicated: * p<0.05, ** p<0.01, *** p<0.001. Emboldened p value symbols indicate significant results after 5% false discovery rate correction using the Benjamini-Hochberg method. No significant results are not shown.

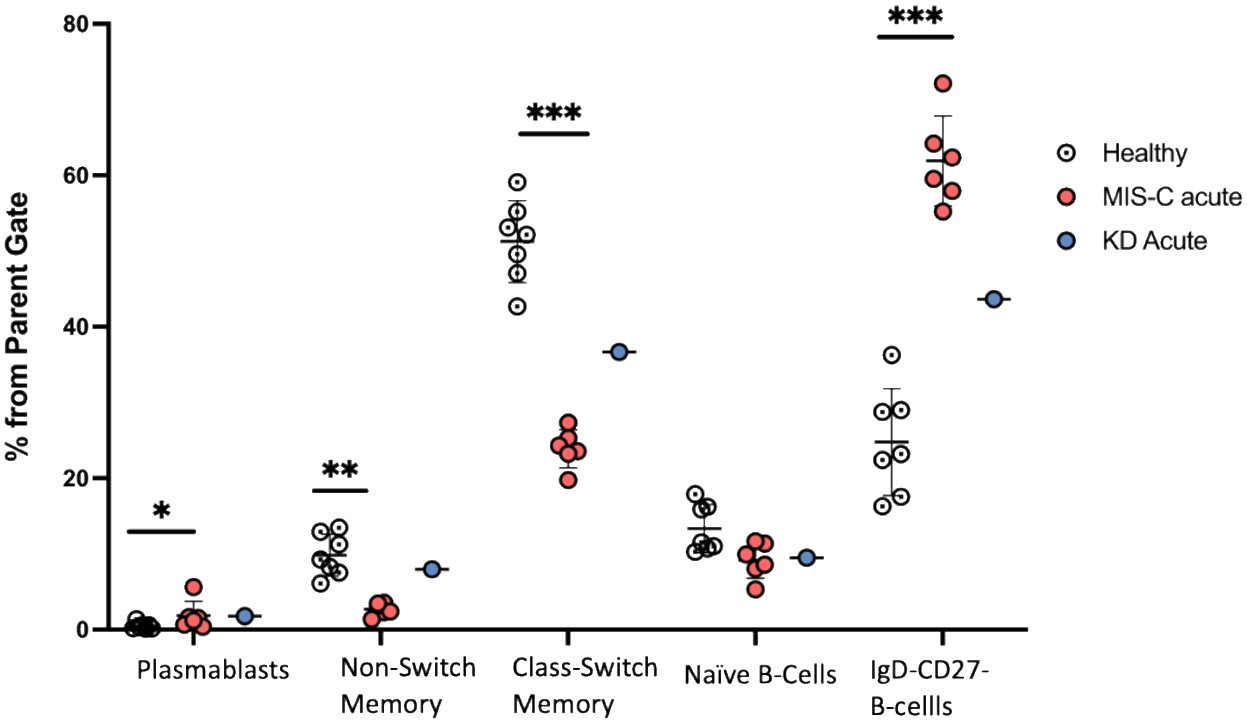

Figure 5-0-10 B-cells analysis in acute MIS-C and KD.

Frequency of the main B-Cells subsets for healthy children, MIS-C and KD patients expressed as a percentage from their parent gate as shown in figure 5.6. The mean +/- SD is shown. Significant results are indicated: * p<0.05, ** p<0.01, *** p<0.001. The results of Wilcoxon ranked sum tests with false discovery rate correction using the Benjamini-Hochberg method are shown.

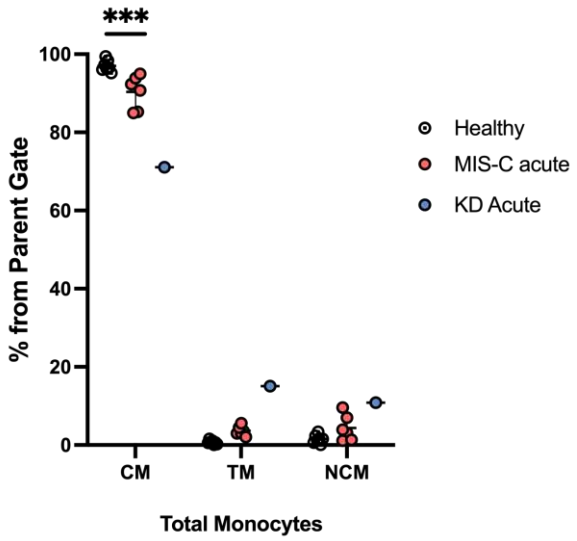

Figure 5-0-11 Monocytes analysis in acute MIS-C and KD.

Frequency of the main monocyte's subsets for healthy children, MIS-C and KD patients expressed as a percentage from their parent gate as shown in figure 5.6. The mean +/- SD is shown. Significant results are indicated: * p<0.05, ** p<0.01, *** p<0.001. The results of Wilcoxon ranked sum tests with false discovery rate correction using the Benjamini-Hochberg method are shown.

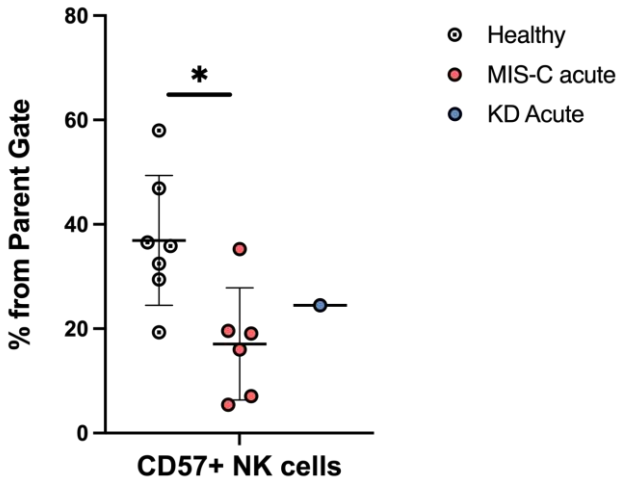

Figure 5-12 CD57 NK cells analysis in acute MIS-C and KD.

Frequency of the CD56+CD57+ NK cells for healthy children and MIS-C patients expressed as a percentage from their parent gate as shown in figure 5.6. The mean +/- SD is shown. Significant results are indicated: * p<0.05, ** p<0.01, *** p<0.001. The results of Wilcoxon ranked sum tests.

5.4.2 Unsupervised clustering of mass cytometry data corroborates the manual gated findings and further demonstrates monocyte activation.

In order to aid data visualisation, flow cytometry standard (fcs) files from MIS-C patients and healthy children were concatenated (using an equal number of cells from each individual) and analysed in parallel with the individuals' fcs files. Next, to analyse and display these high-dimensional data on a two-dimensional space, 224,000 agranulocytes as gated in figure 5.7 (16,000 from each of the seven healthy children, six MIS-C patients and one KD patient) were configured using the viSNE algorithm in Cytobank and were plotted onto the two t-distributed stochastic neighbour embedding (t-SNE) axis. Unsupervised clustering on the t-SNE projected cells was then performed using the FlowSOM algorithm and 24 clusters were revealed constituting of T-cells, B-cells, NK-cells, monocytes plasmacytoid dendritic cells (pDCs, Figure 5.13A). Perhaps the most striking result observed when the two-dimensional map of MIS-C patients was compared to those of healthy children, was the marked difference of the monocyte cellular distribution on the tsne axis (figure 5.13A).

Next, the data for each individual were assessed and seven clusters were significantly different in frequency between MIS-C patients and healthy children (Figure 5.13B). The KD patient is not included in this statistical analysis but results are shown on the plot as a representative of the disease. Based on marker expression reviewed on heatmaps generated for each cluster (figure 5.13C), the frequency of activated CM (cluster 20) defined as CD64+ and CD36+ was significantly increased in MIS-C accompanied by a decrease of non-activated CM (cluster 17). Exploring the rest of the immune cell types, MIS-C patients showed a small but significant increase in $CD19^{+}$ $CD38^{hi}$ $CD27^{hi}$ B-cell plasmablasts (cluster 5) and a larger

increase in IgD-CD27- double negative (DN) B-cells (cluster 2) confirming the manual gated data in figure 5.10. These DN B-cells were CD11c negative consistent with them being the recently proposed DN1 B-cell subset in patients with inactive systemic lupus erythematosus (SLE, Sanz *et al.*, 2019). Furthermore, B-cell cluster 3 also noted to be increased in MIS-C patients. This subset was IgD +CD27- for the healthy children and KD patient suggesting this could represent the non-switch memory B-cells, however, was IgD-CD27- for the MIS-C patients. Turning to T-cells, CD8 naïve cluster 8, was noted to be reduced in MIS-C patients relative to healthy children. It is worth noting that even though there was not a specific cluster assigned for CD8 activated T-cells, cluster 13 expressed HLA-DR only in MIS-C and KD patients. Cluster 13 had a varied expression of CD45RA between the compared groups and therefore for healthy children cluster 13 was defined as CD8 TEMRA while in MIS-C and KD CD8 Tem. Lastly, pDCs (cluster 11) were reduced in MIS-C patients compared to healthy children.

To confirm whether the phenotypic changes of monocytes activation existed in the manual gated data as well, the expression of CD64 was used to manually gate activated monocytes in total monocytes, CM, TM and NCM (figure 5.14). MIS-C patients had significantly increased activation in all subsets of monocytes when compared to the healthy children (figure 5.14B). The KD patient exhibited the same phenotypes as the MIS-C patients however this patient was not included in the statistical analysis. Similarly, IgD-CD27-CD11c - and IgD-CD27-CD11c + B-cells were manually gated and confirmed the findings of mass cytometry data with DN1 CD11c- B-cells increased in MIS-C patients. In contrary, the DN2 CD11c+ B-cells population was found to be decreased in MIS-C patients (figure 5.15).

In summary, unsupervised analysis of the multidimensional data corroborated the manual gated data and further highlighted important phenotypical changes in monocytes, CD8 T-cells and B-cells.

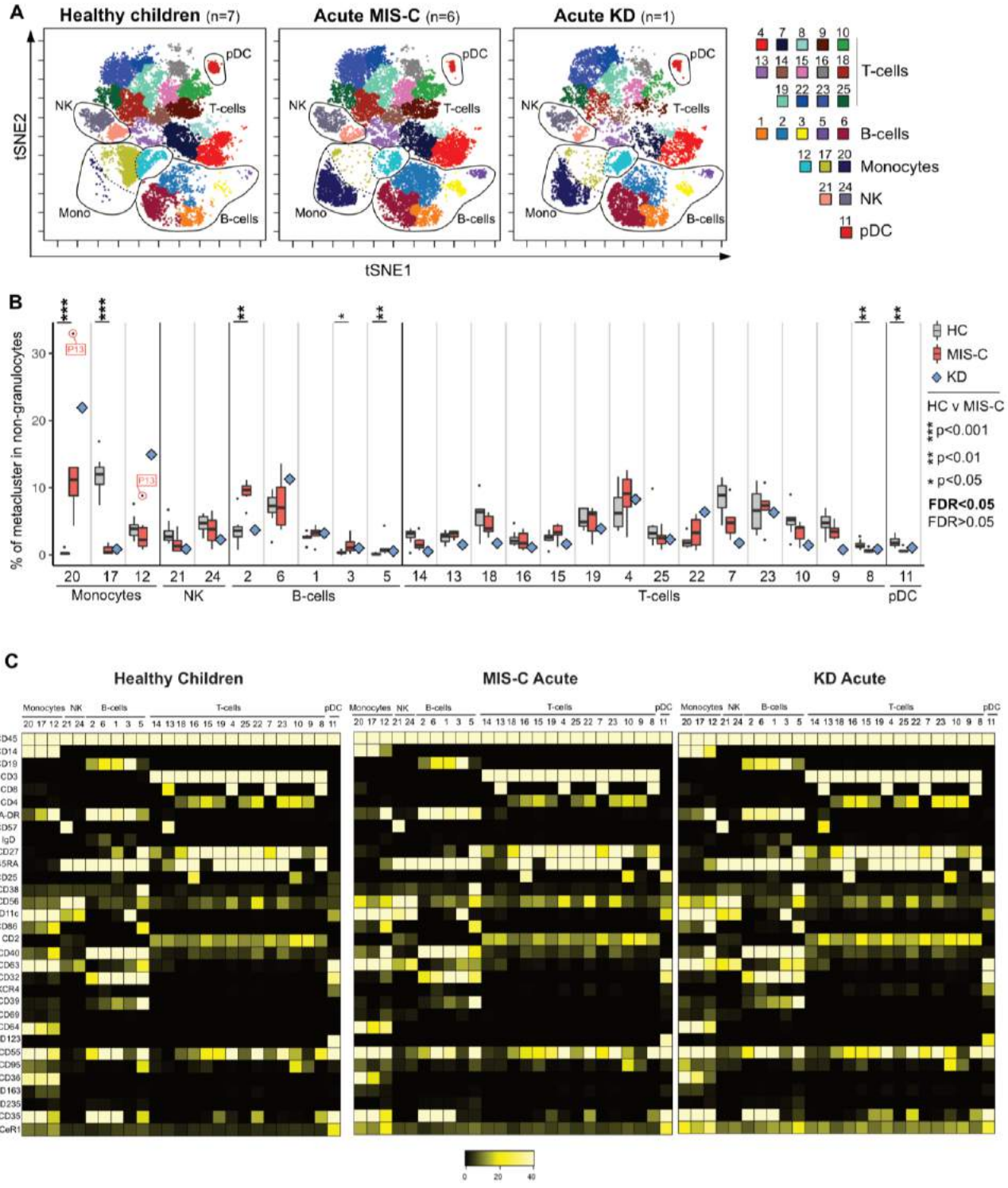
A
Healthy children (n=7)
Acute MIS-C (n=6)
Acute KD (n=1)
tSNE2
tSNE1
pDC
NK
T-cells
Mono
B-cells
T-cells
B-cells
Monocytes
NK
pDC
B
% of metacluster in non-granulocytes
HC
MIS-C
KD
HC v MIS-C
p<0.001
p<0.01
p<0.05
FDR<0.05
FDR>0.05
Monocytes
NK
B-cells
T-cells
pDC
C
Healthy Children
MIS-C Acute
KD Acute

Figure 5-13 Unsupervised analysis of agranulocytes in acute MIS-C and KD

(A) tSNE plots of concatenated flow cytometry data from six MIS-C patients or one KD patient at the acute stage of their disease alongside seven healthy children (HC). Each meta-cluster is represented by a different colour and key populations are indicated on the plots. Results from these concatenated datafiles are shown throughout this figure. (B) The frequency of each FlowSOM metacluster in the same donors expressed as a percentage of total non-granulocyte mononuclear cells are shown as box and whisker plots (healthy volunteer children and MIS-C) or a blue diamond (KD). Results of Wilcoxon rank-sum tests comparing the frequency of each cluster in healthy children and MIS-C patients are indicated by: * $p<0.05$, ** $p<0.01$, *** $p<0.001$. Non-significant results are not shown and emboldened p value symbols indicate significant results after 5% false discovery rate correction using the Benjamini-Hochberg method. (C) Heatmaps of the concatenated fcs files shown in (A) for healthy children, MIS-C and KD patients. Each column is a FlowSOM meta-cluster shown in (A) and each row is a marker. The median intensity of each marker is shown from 0 to 40.

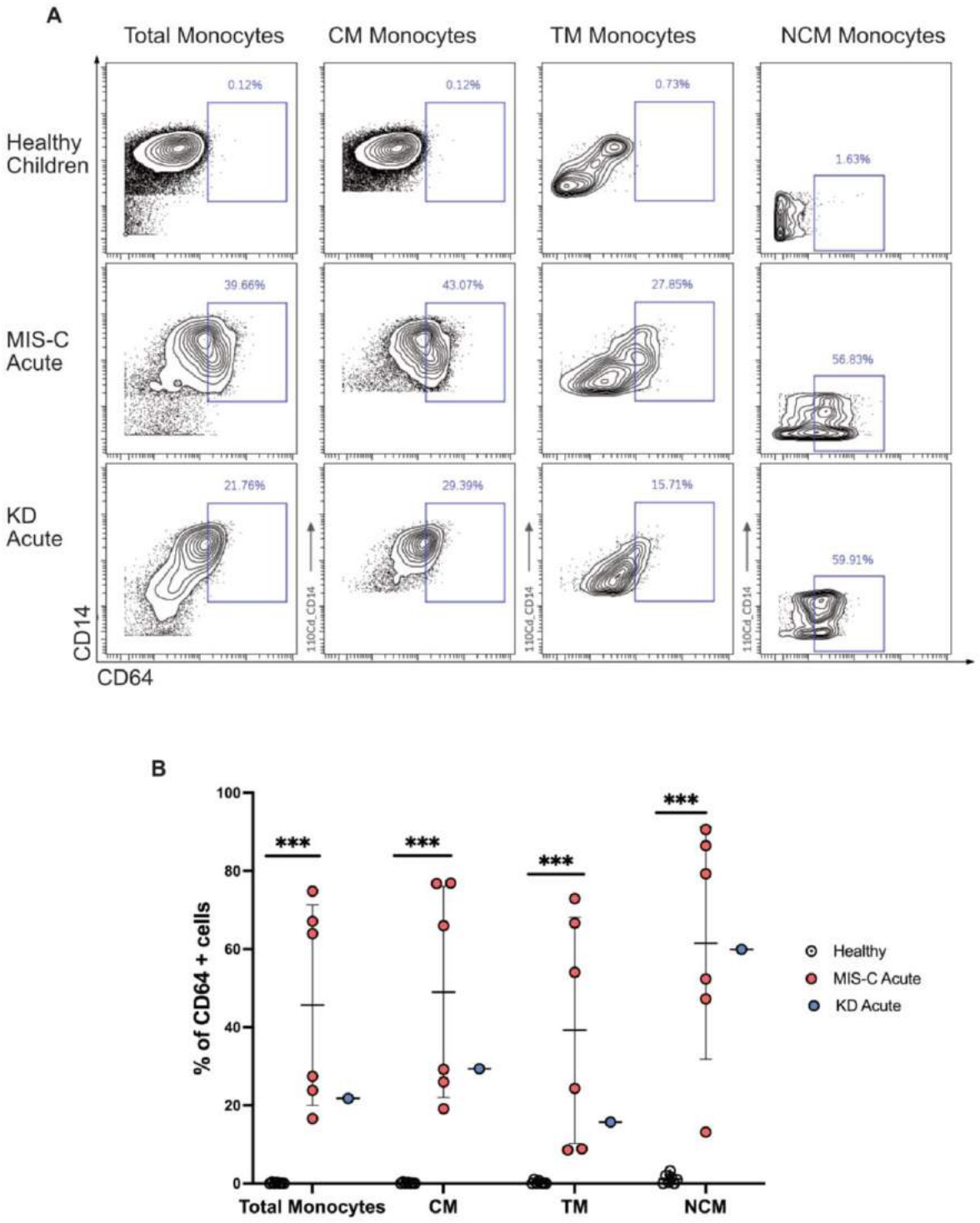

Figure 5-14 Activated monocytes in acute MIS-C and KD

(A) Manual gated data of CD64+ (activated) monocytes in total monocytes, classical monocytes (CM) , transitional monocytes (TM) and non-classical monocytes (NCM).
(B) The frequency of CD64+ cells within total monocytes, CM, TM and NCM is shown for each individual for healthy, MIS-C and KD. Results of Wilcoxon rank-sum tests after 5% false discovery rate correction using the Benjamini-Hochberg method are indicated by: * $p<0.05$, ** $p<0.01$, *** $p<0.001$.

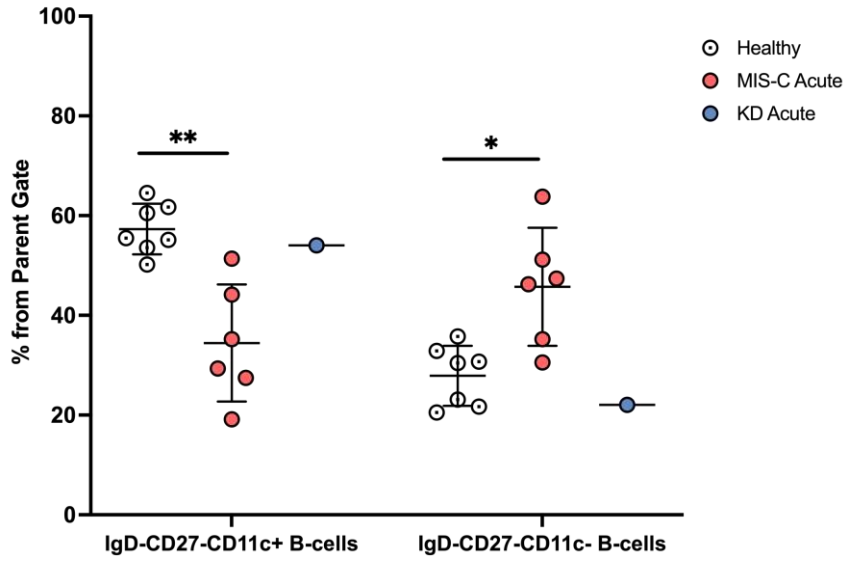

Figure 5-15 Double negative B-cells and CD11c expression in acute MIS-C and KD.

Manual gated data of IgD-CD27-CD11c- and IgD-CD27-CD11c+ B-cells are shown for healthy, MIS-C and KD. Results of Wilcoxon rank-sum tests after 5% false discovery rate correction using the Benjamini-Hochberg method are indicated by: * $p<0.05$, ** $p<0.01$, *** $p<0.001$.

5.5 Mass cytometry show granulocytes are immature and activated in acute MIS-C

5.5.1 Manual gating data show both activated and immature neutrophils are increased in acute MIS-C

Having defined the perturbations occurring in the agranulocytes of the acute MIS-C patients, next the granulocytes were investigated. Platelets were gated using the platelet marker CD41/42a/61 and subsequently activated platelets were gated based on their CD63 expression (Gerdsen *et al.*, 2005)figure 5.16). Granulocytes were then identified from the platelet negative population (CD41/42a/61-) by gating on the CD66b positive cells (figure 5.16A). Neutrophils were then gated as CD16+ and CD66b+(Lakschevitz *et al.*, 2016) figure 5.16A). Activated neutrophils were gated based on their CD64 expression (Hoffmann, 2009)figure 5.16A). Then, from the CD16- granulocytes, basophils were gated as CD45+CD11c+HLA-DR-CD38+CD123+ (Han *et al.*, 2008) and eosinophils were gated CD45+CD11c+HLA-DR-CD62L+CD11b+(Hassani *et al.*, 2020)figure 5.16A). The frequency of these subsets is shown in figure 5.16B. MIS-C and KD patients had a significantly increased frequency of activated neutrophils, eosinophils and a significant decreased frequency of basophils (figure 5.16B).

Heatmaps of median metal intensity were next generated for neutrophils, basophils and eosinophils for healthy children, acute MIS-C and KD patients (figure 5.17). Neutrophils displayed higher CD64 expression and decreased CD10 and CD16 expression in both MIS-C and KD patients (figure 5.16A and 5.17). For neutrophils, CD64 is a marker of activation (Hoffmann, 2009) while CD16 and CD10 are markers of maturity (Dransfield *et al.*, 1994; Marini *et al.*, 2017). Similar phenotypic changes were evident for the eosinophils where

CD64 expression was increased in MIS-C and KD patients. CD64 has also been reported to be a marker of activation in eosinophils. In summary, manual gated data show that both MIS-C and KD patients possessed higher frequencies of activated immature neutrophils and activated eosinophils.

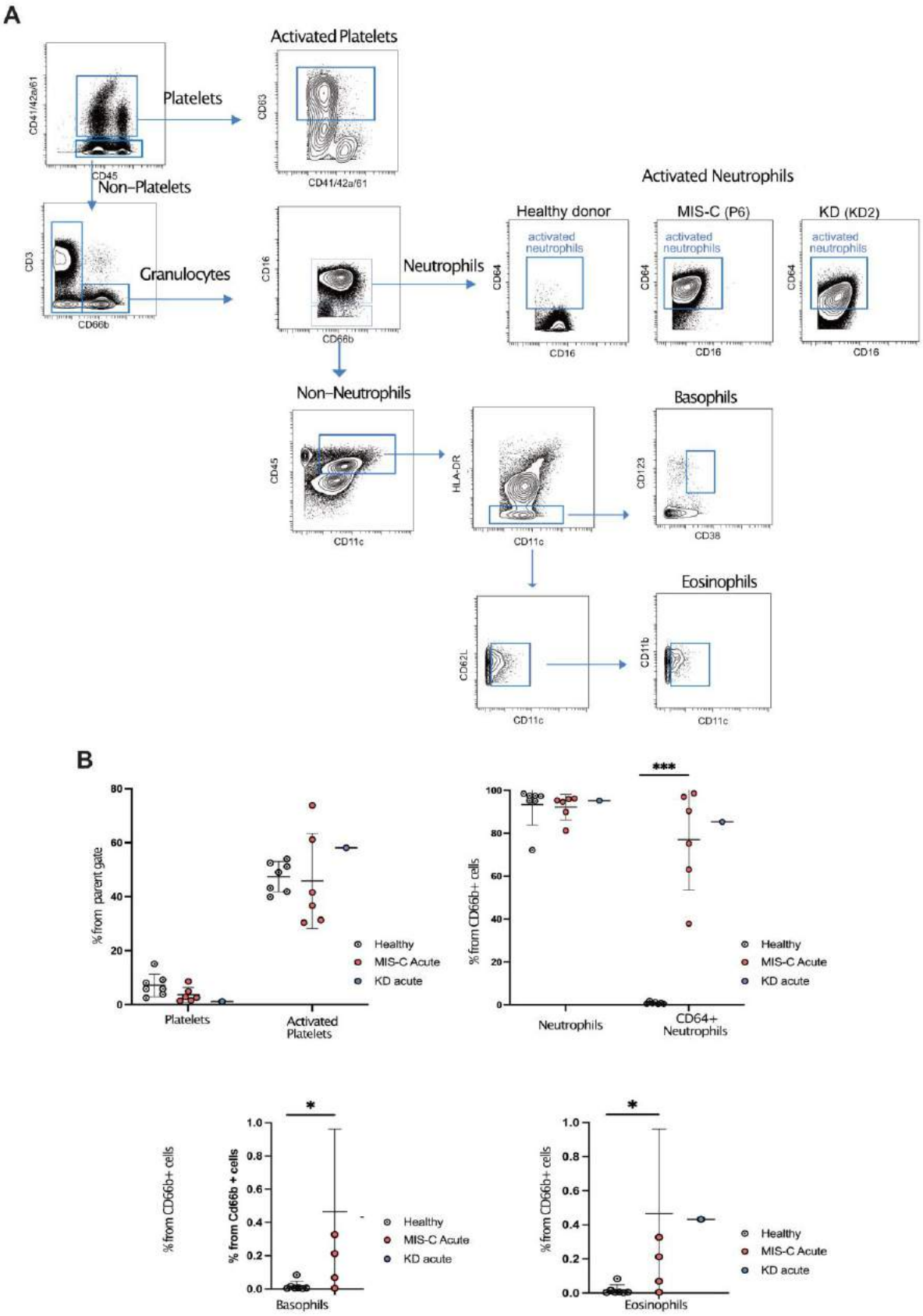
A
Activated Platelets
Platelets
CD41/42a/61
CD63
CD45
Non–Platelets
Activated Neutrophils
Healthy donor
MIS-C (P6)
KD (KD2)
activated neutrophils
CD3
Granulocytes
CD66b
CD16
Neutrophils
CD64
Non–Neutrophils
Basophils
HLA-DR
CD11c
CD123
CD38
Eosinophils
CD62L
CD11b
B
% from parent gate
Healthy
MIS-C Acute
KD acute
Platelets
Activated Platelets
***
% from CD66b+ cells
Neutrophils
CD64+ Neutrophils
*
% from Cd66b + cells
Basophils
Eosinophils

Figure 5-16 Gating strategy for non-granulocytes and frequency of main subsets in acute MIS-C and KD.

A) Gating strategy for the main granulocytes subsets including neutrophils, activated neutrophils, basophils and eosinophils. (B) Frequency of granulocytes subsets gated in A is shown. Results of Wilcoxon rank-sum tests after 5% false discovery rate correction using the Benjamini-Hochberg method are indicated by: * $p<0.05$, ** $p<0.01$, *** $p<0.001$.

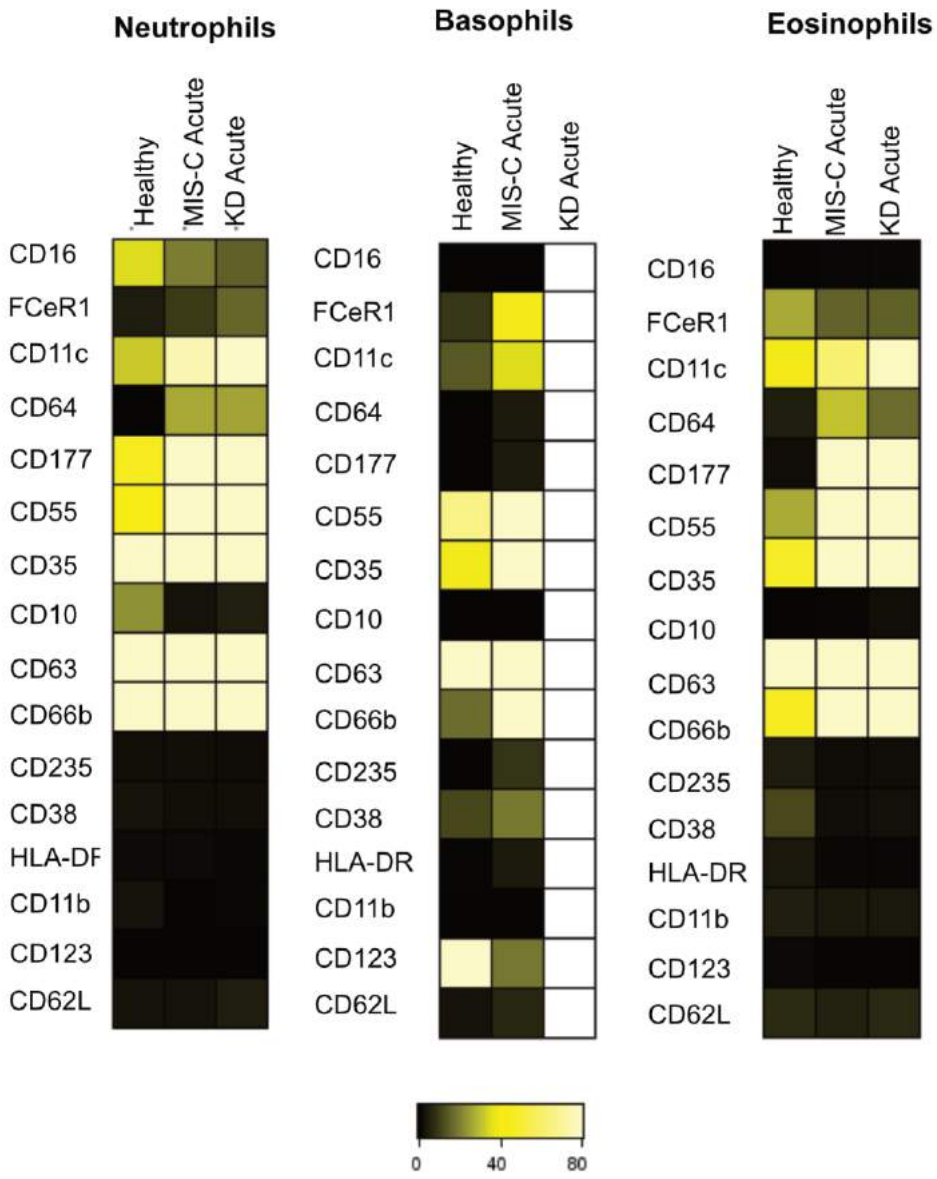

Figure 5-17 Heatmaps showing median metal intensity (MMI) for the main granulocytes subsets

Markers expressed for neutrophils, basophils and eosinophils. As KD acute had zero basophils no marker expression is shown for this patient and therefore is blank.

5.5.2 Unsupervised analysis of mass cytometry data confirms the manual gated data

To investigate granulocytes in more depth, unsupervised analysis of total CD66b+ cells was performed using the phenotypical and lineage markers for granulocytes. Equal numbers of cells (22,000) were sampled from fcs files of seven healthy children and seven patients (six MIS-C and one KD). First, dimensionality reduction was performed using the ViSNE implementation of t-SNE in Cytobank and high-dimensional data were plotted onto the two t-SNE axes. This was then followed by unsupervised clustering using the FLowSOM algorithm which generated nine clusters (figure 5.18A). Cluster one represented eosinophils and basophils, based on the expression of the high-affinity IgE receptor (FceR1), CD38 and lack of CD16 and CD10 as shown in the heatmaps generated (figure 5.18C). The other eight clusters were all CD16 positive and therefore assigned to neutrophils (figure 5.18C). These clusters appeared to be dramatically different in cellular abundance in healthy children and MIS-C patients (figure 5.18B). More specifically, clusters 4,5,8 and 9 were mostly present in acute MIS-C and KD patients whereas clusters 2,6 and 7 were largely present in healthy children. The neutrophil distribution in MIS-C was driven by a marked decrease in CD10 and an increase in CD64 expression on patients' neutrophils (figure 5.18 A). This finding was also confirmed when heatmaps from the same clusters were analysed (figure 5.18C). MIS-C and KD patients' clusters 4,5,8 and 9 had increased expression of CD64 as well as reduced expression of CD10 and CD16, assigning these cells to immature activated neutrophils. In contrary, clusters 2,6 and 7 were mature resting neutrophils as they expressed CD10 and CD16 and lacked CD64. In summary, unsupervised analysis of granulocytes demonstrated an increase of immature activated neutrophils in MIS-C and KD patients but failed to identify differences in eosinophils and basophils.

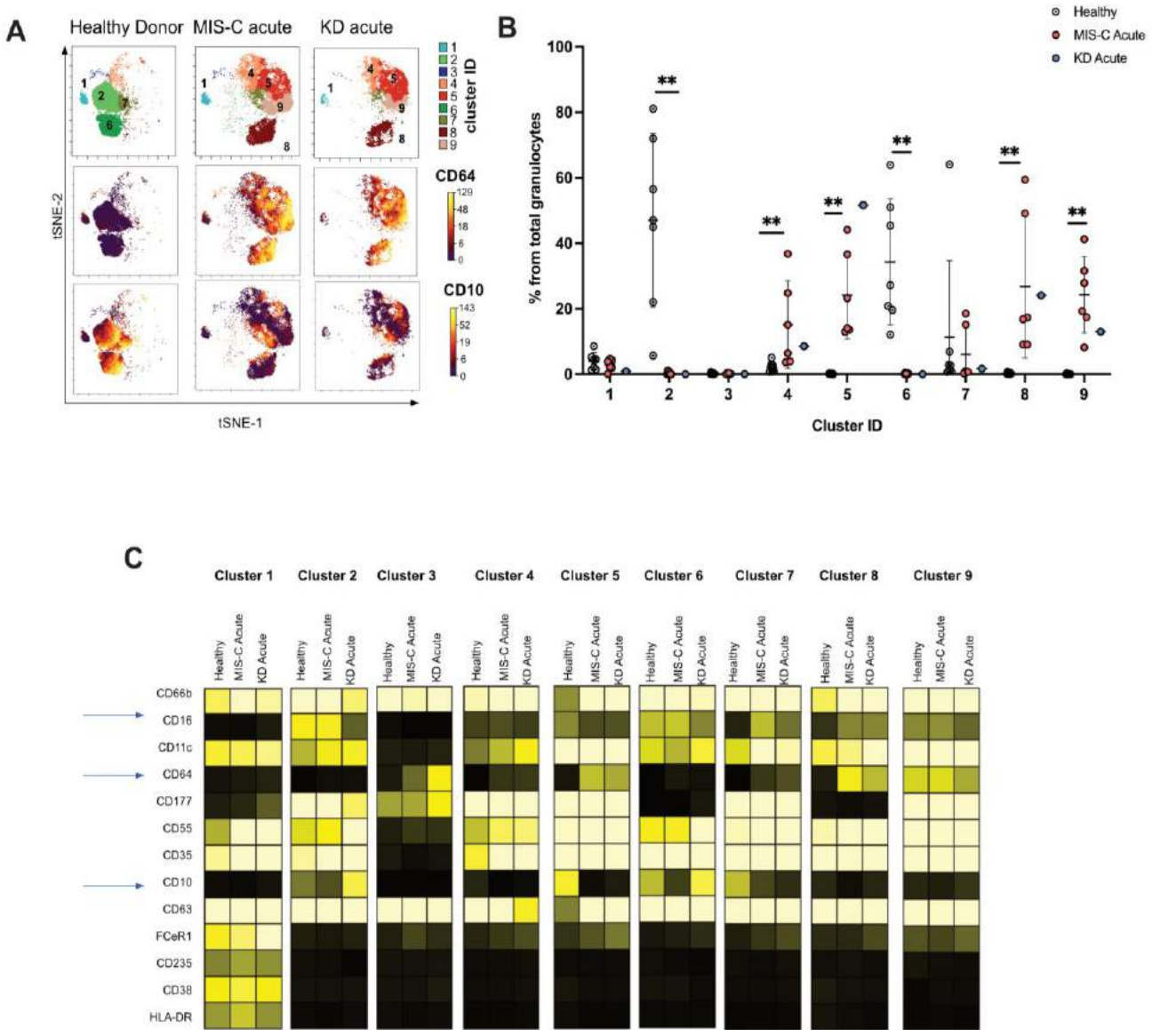

Figure 5-18 Unsupervised analysis of granulocytes in acute MIS-C and KD.

(A) tSNE plots of granulocytes from the same donors analysed by unsupervised clustering. Top row: FlowSom metaclusters. Middle row: CD64 expression. Bottom row: CD10 expression. (B) Frequency of granulocytes clusters shown in A. Results of Wilcoxon rank-sum tests after 5% false discovery rate correction using the Benjamini-Hochberg method are indicated by: * p<0.05, ** p<0.01, *** p<0.001. (C) Heatmaps showing expression level of different markers in each metacluster for healthy children, MIS-C and KD patients.

5.6 Pro- and anti- inflammatory cytokines are elevated in MIS-C and KD patients

Having demonstrated the hyperinflammatory immune state in acute MIS-C, the cytokine profile of acute MIS-C patients was next examined. Using the LEGENDplex multiplex kit, analysis of 32 cytokines and chemokines in plasma samples from nine patients (eight MIS-C, one KD) and seven healthy children was performed. These plasma proteins were selected based on the immune changes identified by the mass cytometry data, as well as published studies in KD and MIS-C (Carter *et al.*, 2020; C. Gruber *et al.*, 2020; Consiglio *et al.*, 2020; Diorio *et al.*, 2020; Esteve-Sole *et al.*, 2021; Rodríguez-Rubio *et al.*, 2021).

Comparison of cytokine levels between MIS-C and healthy children showed statistically significant differences for 16 out of the 32 soluble plasma proteins (figure 5.18). More specifically, MIS-C patients had statistically significantly raised levels of the monocyte chemoattractant protein 1 (MCP-1/CCL2), interferon gamma-induced protein 10 (IP10/CXCL10), pro-inflammatory cytokines IL-6 and IL-18 but also, higher levels of anti-inflammatory cytokine IL-10 (figure 5.18). Moreover, soluble receptors of tumour necrosis factor alpha (sTNF-R1 and sTNFR2), soluble CD40 ligand (sCD40L) and IL-2 (sCD25), and Interleukin-1 receptor antagonist (IL-1RA), a member of the IL1 family that binds the IL1-receptor to inhibit this pathway, were also elevated in MIS-C patients (figure 5.18). Finally, plasminogen activator inhibitor 1 (PAI-1), pentraxin-3 (PTX3), myeloperoxidase (MPO) and IL-18 were also found to be higher in MIS-C patients. Surprisingly no difference was observed among these groups for several key pro-inflammatory cytokines and chemokines, including: IL1-β, IL-8 (CXCL8), IL-17A, interferon-alpha2 (IFN-α2) interferon-gamma (IFN-γ)

and TNFα. The KD patient was not included in the statistical analysis, but their acute sample had the same cytokine profile as the acute MIS-C patients (figure 5.18).

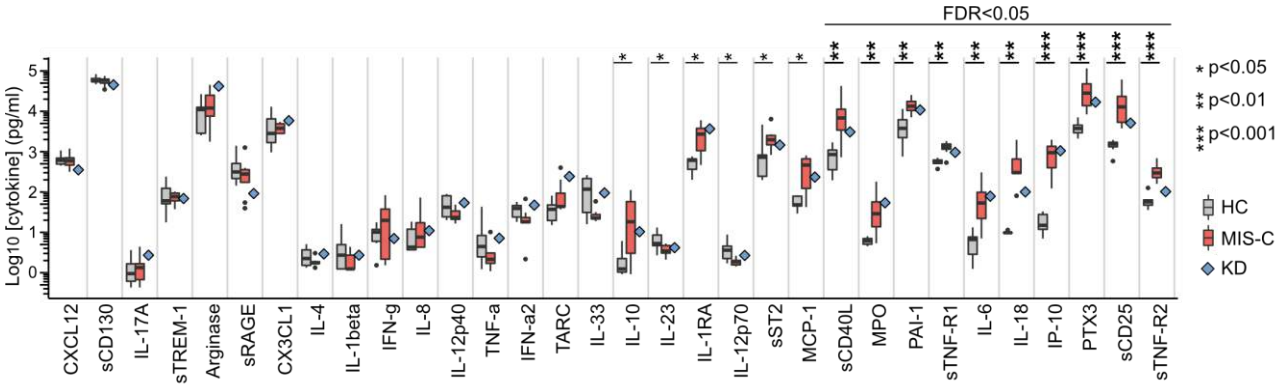

Figure 5-19 Cytokines profile of acute MIS-C and KD

Levels of cytokines in plasma from seven healthy children or six MIS-C patients at the acute stage of disease are shown as box and whisker alongside a blue diamond indicating results from a single KD patient also at the acute stage. Results of Wilcoxon rank-sum tests comparing the frequency of each cluster in healthy children and MIS-C patients are indicated by: * p<0.05, ** p<0.01, *** p<0.001. Non-significant results are not shown and emboldened p value symbols indicate significant results after 5% false discovery rate correction using the Benjamini-Hochberg method.

5.7 Longitudinal immune analysis of MIS-C patients

5.7.1 Analysis of the longitudinal clinical data in MIS-C patients show that the acute hyperinflammatory state normalises following treatment administration.

Next, the effects of MIS-C treatment in the immune system were investigated. The clinical parameters available for both MIS-C and KD patients were examined during the course of the hospital stay. Monocyte, lymphocyte, granulocyte absolute counts and CRP were plotted for each patient over time (figure 5.20). Following IVIG administration, inflammation was resolved in the majority of patients, and this was evident by the marked reduction of their CRP (figure 5.20). Although at the time of discharge all markers returned back to normal, interestingly granulocytes were the slowest to recover. Another interesting observation was the fact that for some patients their granulocytes did not follow the CRP trend. More specifically, for patient P13 despite the gradual drop of their CRP, the granulocytes continued to rise until day four. This was despite the patient receiving two IVIG cycles and a course of high dose methylprednisolone. In this patient, granulocyte recovery was only noted following tocilizumab administration. The persistent granulocytosis in this patient who had severe MIS-C disease refractory to conventional treatment, could further support our observation that granulocytes correlate with severe disease. To determine whether this can be used as a marker of MIS-C disease severity and resistance to conventional treatment strategies, future larger studies will need to be undertaken.

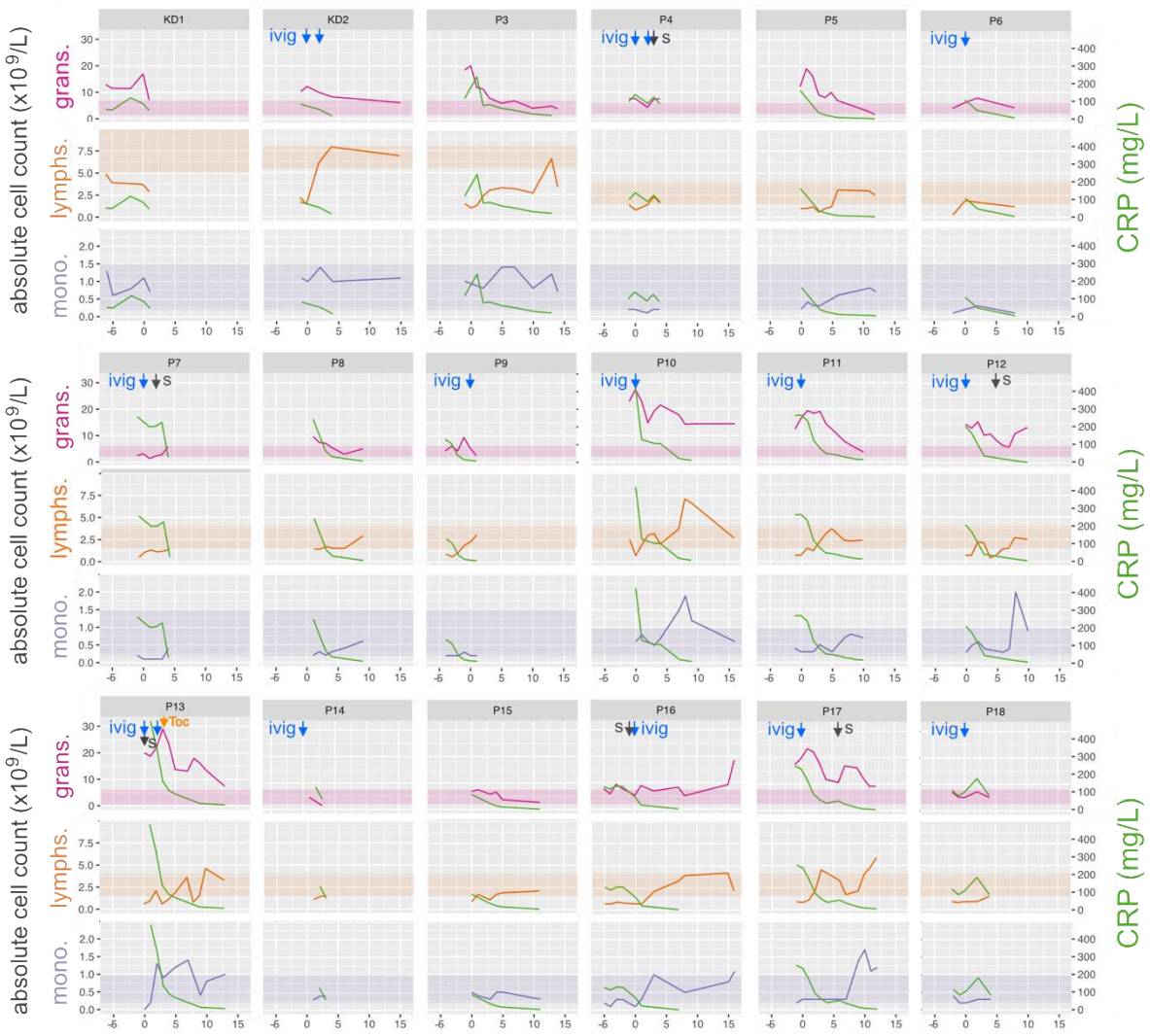

Figure 5-20 Longitudinal analysis of clinical laboratory data.

Monocytes, Lymphocytes, Granulocytes absolute counts and CRP is shown for each individual patient over the course of time in the hospital. Highlighted in each box is the normal range for each parameter taking into account normal ranges for each patient's age. Treatment is indicated as follows: ivig= Intravenous Immunoglobulin, S= IV Methylprednisolone and Toc=Tocilizumab. The x axis represents time in the hospital in days.

5.7.2 Mass cytometry analysis of longitudinal manual gated data reveals that activation of the innate and adaptive immune system resolves with treatment

Having characterised the immune system during acute MIS-C, we next sought to investigate the immune status of patients over the course of disease. We were particularly interested at the timepoint when IVIG was administered as this agent is known to offer rapid resolution of symptoms in inflammatory conditions. To do this samples collected from three key disease stages, acute, post IVIG administration and at hospital discharge, were analysed. More specifically, four patients samples were received post IVIG administration, and for two of these patients' further samples were collected at the time of discharge. Post IVIG and discharge samples were also received for the KD patient. The same pipeline of analysis used earlier to define the acute MIS-C perturbations was applied.

First the main lymphocyte subsets were analysed (figure 5.21). Post IVIG administration the frequencies of mDCs, pDCs and NK cells in MIS-C were significantly lower when compared to healthy children. At the time of discharge several significant changes occurred. MIS-C patients had lower frequencies of CD4+ T-cells and monocytes. In addition, the frequencies of mDCs and pDCs remained low at discharge for MIS-C patients even though a trend towards recovery was noted for the mDCs. The KD patient mostly followed the trends of MIS-C patients at all three timepoints (figure 5.21).

Moving on to T-cells, the four main CD4+ and CD8+ subsets were analysed. These remained relatively unchanged throughout the three different timepoints, with the exception of patient P7 for whom the naïve subsets decreased and memory subsets expanded for both the CD4 and CD8 compartment (figure 5.22A). Next, the activation of CD4 and CD8 T-cell subsets were investigated using once again HLA-DR as a hallmark of activation. Interestingly,

the proportion of HLA-DR positive CD8 T-cells remained high post IVIG, and, for patient P7, this proportion increased markedly in keeping with the expansion seen in their memory subsets (figure 5.22 A and B). The HLA-DR positivity was mainly observed in the Tcm, Tem and TEMRA CD8 subsets (figure 5.22B). At discharge the proportion of activated cells had declined dramatically but were still higher than healthy children. In contrast, only a small proportion of Tcm CD4 T-cells expressed HLA-DR at the acute stage and post IVIG. A similar pattern of HLA-DR expression was also observed with the KD patient. Finally, manual gated data on Tregs, CD8+CD57+, NK T-cell showed no significant differences between MIS-C patients and healthy children at any disease stage(figure 5.23). However, it's worth noting that Tregs increased in frequency at discharge for the two MIS-C patients (P6 and P13) but not for the KD patient. It is also worth mentioning that patient P7 showed a dramatic increase of the CD8+CD57+ population post IVIG administration (figure 5.23).

Turning to B-cells, the five main subsets were investigated at different timepoints. The changes seen acutely in plasmablasts, non-switch memory, class-switch memory and IgD-CD27- persisted post IVIG for all the MIC-S and KD patients. In addition, the naïve B-cells significantly decreased, potentially contributing to the recovery of the other B-cells subsets. At discharge all of the B-cells subsets recovered however levels were still different from those observed in healthy children (figure 5.24A). The IgD-CD27-CD11c+ and CD11c- populations were also investigated at the different timepoints. Post IVIG the significant decrease of the IgD-CD27-CD11c+ and significant increase of IgD-CD27-CD11c- populations persisted when compared to healthy children (figure 5.24B). At the time of discharge both frequencies were similar to those of healthy children with the exception of the KD patient (figure 5.24B).

Next, monocyte subsets were investigated at the three key disease stages. The decrease in the CM abundance seen in acute MIS-C was no longer present post IVIG or at discharge (figure 5.25A). Similarly, the TM and NCM subset frequencies also returned to levels comparable of those of healthy children (figure 5.25A). As described in acute MIS-C, the majority of monocytes were CD64+ indicating activation. To investigate whether this activation persisted throughout the course of illness the CD64+ monocytes were manually gated at different timepoints (figure 5.25B). The percentage of CD64+ monocytes gradually decreased in numbers for all the subsets post IVIG and returned to normal levels at the time of discharge (figure 5.25B).

Finally, CD57+ NK cells were investigated. This population was decreased in acute MIS-C when compared to healthy children. Interestingly, this decrease persisted and did not recover neither post IVIG nor at the time of discharge (figure 5.26).

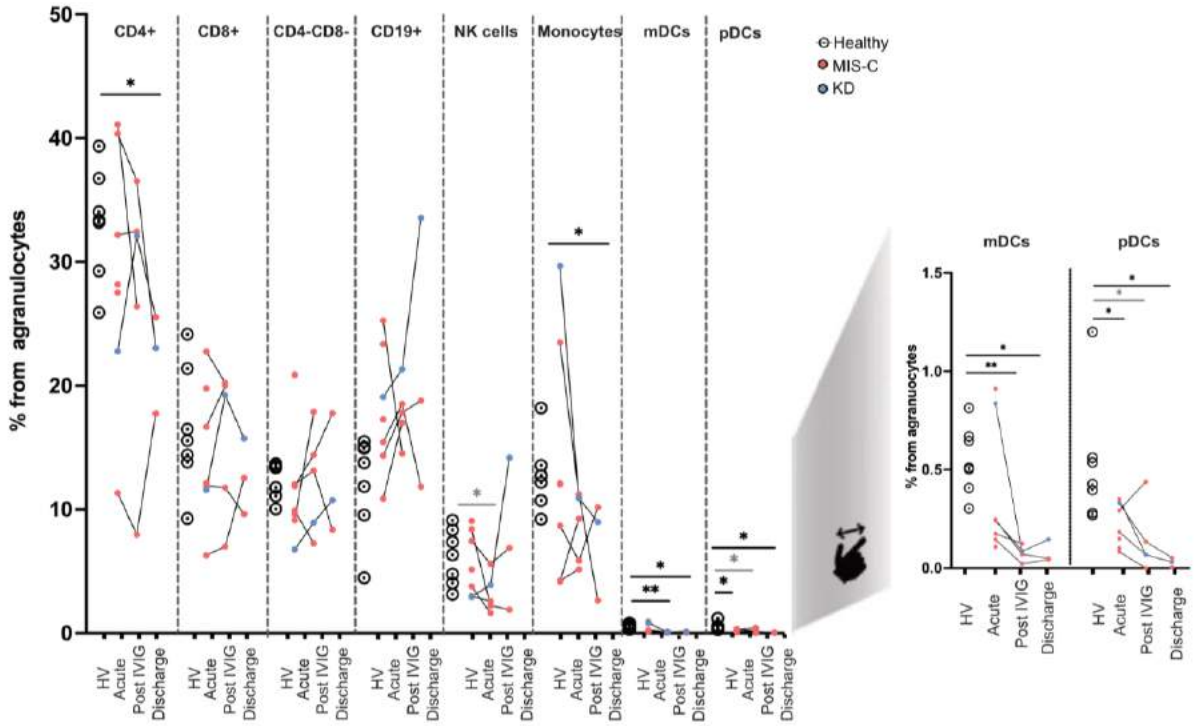

Figure 5-21 Longitudinal analysis of main immune subsets.

The frequencies of the main lymphocytes subsets are shown for MIS-C (red) and KD (Blue) at different timepoints. Healthy children are also shown. Results of Wilcoxon rank-sum tests comparing the frequency of each cluster in healthy children and MIS-C patients are indicated by: * p<0.05, ** p<0.01, *** p<0.001. Non-significant results are not shown and p values in black indicate significant results after 5% false discovery rate correction using the Benjamini-Hochberg method while p values in grey indicated a greater than 5% false discovery rate.

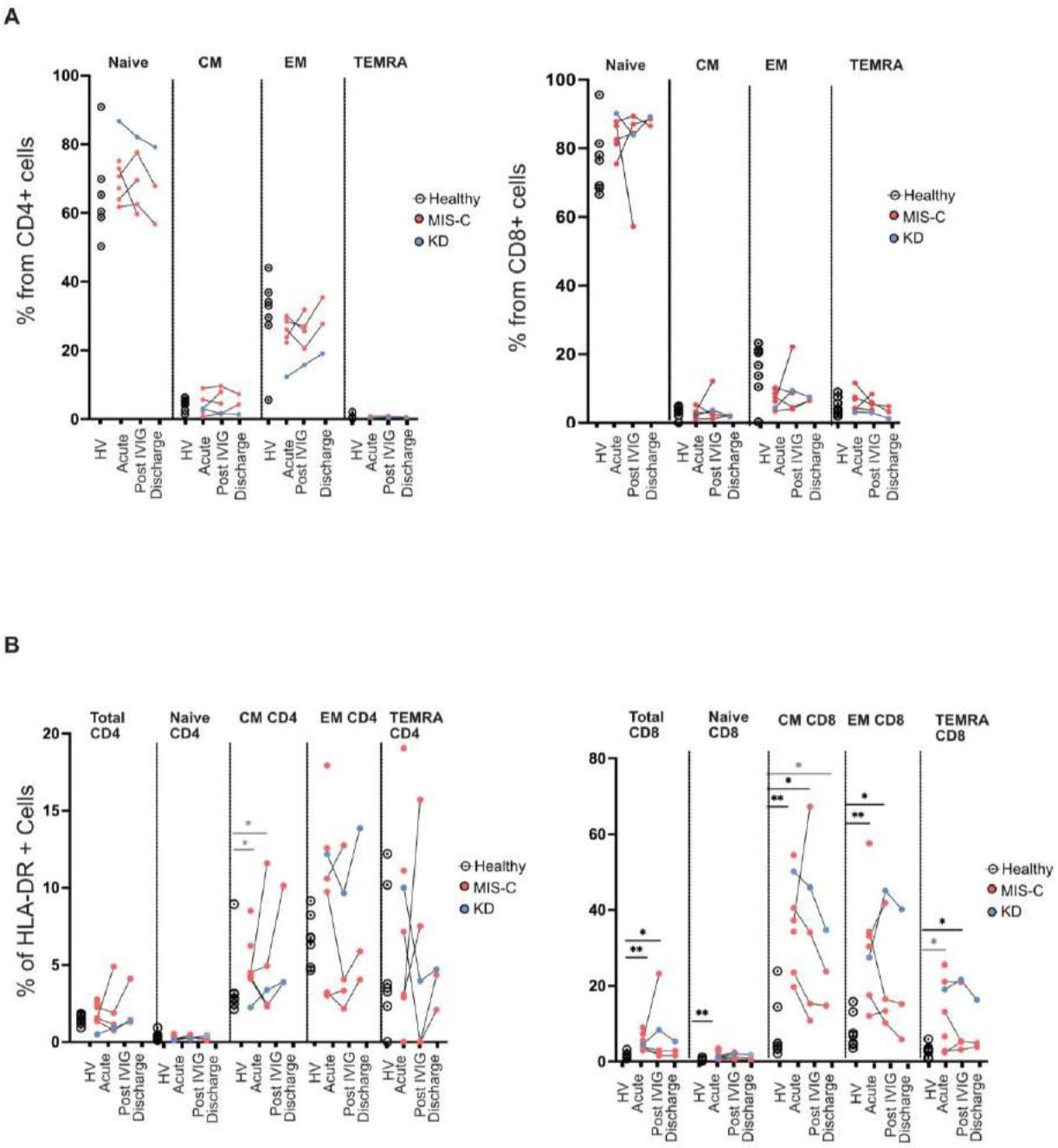

Figure 5-22 Longitudinal T-cells analysis (main subsets).

(A) The frequencies of the main CD4 and CD8 subsets are shown for MIS-C (red) and KD (Blue) at different timepoints. Healthy children are also shown. (B) Percentage of each T-cell sub-population positive for HLA-DR over the course of disease. Results of Wilcoxon rank-sum tests comparing the frequency of each cluster in healthy children and MIS-C patients are indicated by: * $p<0.05$, ** $p<0.01$, *** $p<0.001$. Non-significant results are not shown and p values in black indicate significant results after 5% false discovery rate correction using the Benjamini-Hochberg method while p values in grey indicated a greater than 5% false discovery rate.

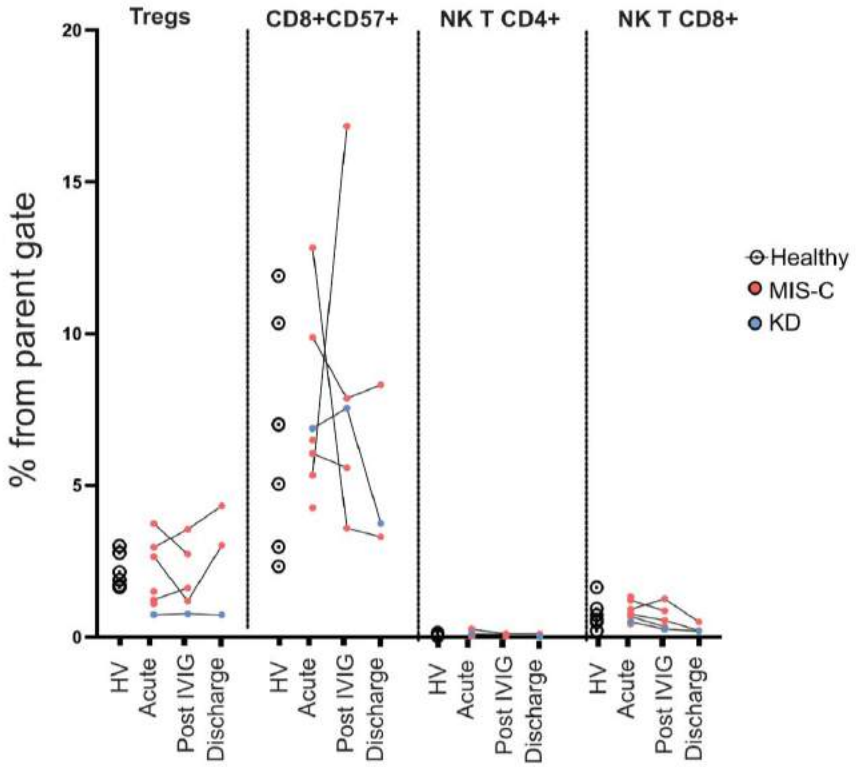

Figure 5-23 Longitudinal T-cells analysis (CD4/CD8 Subsets).

The frequencies of the CD4 and CD8 subsets are shown for MIS-C (red) and KD (Blue) at different timepoints. Healthy children are also shown. Results of Wilcoxon rank-sum tests comparing the frequency of each cluster in healthy children and MIS-C patients. Non-significant results are not shown.

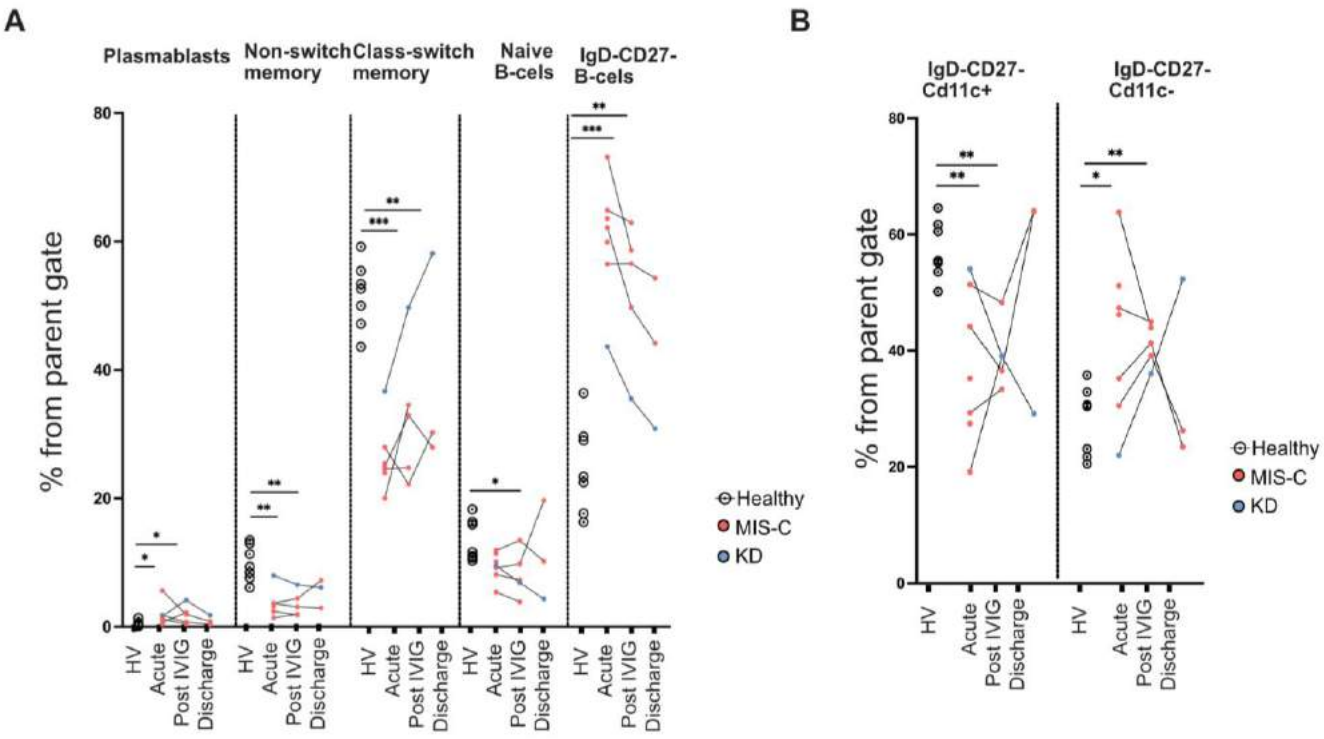

Figure 5-24 Longitudinal B-cells analysis

(A) The frequencies of the B-cell subsets are shown for MIS-C (red) and KD (Blue) at different timepoints. Healthy children are also shown. (B) The frequencies of the IgD-CD27-CD11c+ and CD11c- subsets are shown for MIS-C (red) and KD (Blue) at different timepoints. Healthy children are also shown. Results of Wilcoxon rank-sum tests comparing the frequency of each cluster in healthy children and MIS-C patients are indicated by: * $p<0.05$, ** $p<0.01$, *** $p<0.001$. Non-significant results are not shown and p values in black indicate significant results after 5% false discovery rate correction using the Benjamini-Hochberg method while p values in grey indicated a greater than 5% false discovery rate.

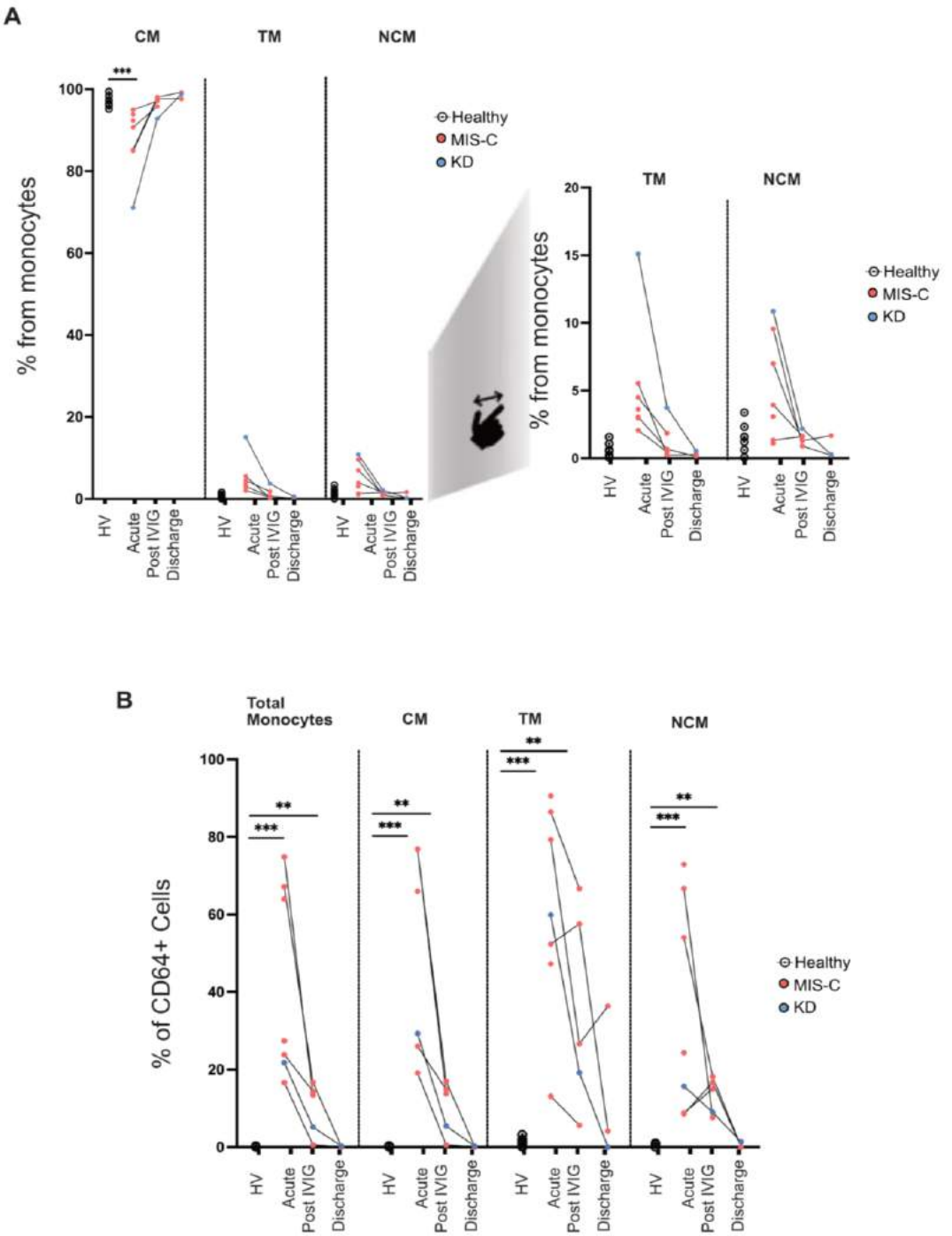

Figure 5-25 Longitudinal Monocytes analysis.

(A) The frequencies of the monocytes subsets are shown for MIS-C (red) and KD (Blue) at different timepoints. Healthy children are also shown. (B) The frequencies of CD64+ Monocytes and their subsets are show for MIS-C (red) and KD (blue) at different timepoints. Healthy children are also shown. Results of Wilcoxon rank-sum tests comparing the frequency of each cluster in healthy children and MIS-C patients are indicated by: * $p<0.05$, ** $p<0.01$, *** $p<0.001$. Non-significant results are not shown and p values in black indicate significant results after 5% false discovery rate correction using the Benjamini-Hochberg method while p values in grey indicated a greater than 5% false discovery rate.

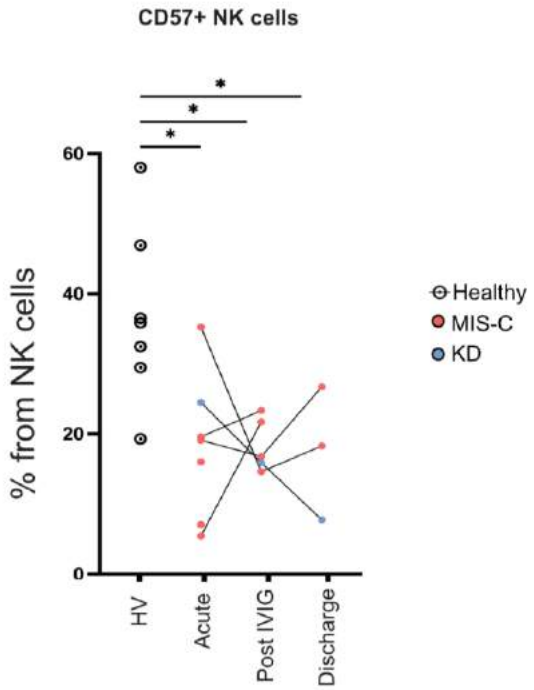

Figure 5-26 Longitudinal CD57 NK cells analysis.

The frequencies of the CD57+ NK cells is shown for MIS-C (red) and KD (Blue) at different timepoints. Healthy children are also shown. Results of Wilcoxon rank-sum tests comparing the frequency of each cluster in healthy children and MIS-C patients are indicated by: * $p<0.05$, ** $p<0.01$, *** $p<0.001$. P values in black indicate significant results after 5% false discovery rate correction using the Benjamini-Hochberg method while p values in grey indicated a greater than 5% false discovery rate.

5.7.3 Unsupervised analysis of the agranulocytes mass cytometry longitudinal data confirms the manual gated data and further reveals an anti-inflammatory monocyte population

Next, unsupervised analysis of the longitudinal data was also performed to further investigate the longitudinal immune perturbations in MIS-C. Investigating the 25 lymphocyte clusters reported in acute MIS-C (figure 5.27A), most of the differences observed acutely persisted post IVIG with the exceptions of monocytes clusters 20, 17 and T-cell cluster 8, the levels of which were now comparable to those of healthy children (figure 5.27B). At the time of discharge the changes in frequencies observed in acute MIS-C were no longer present and clusters frequencies were similar to those of healthy children (figure 5.27B).

Turning our focus to monocytes, we noted that the CM cells started to normalise in the post IVIG samples (figure 5.28A). More specifically the activated CM cluster 20 that expanded in acute MIS-C, reduced in frequency post IVIG with a concomitant increase in the CM cluster 17 seen in healthy children (figure 5.28 A and C). This reversion to normality continued further to discharge, at which point the patients' classical monocyte cluster t-SNE distributions resembled those of healthy children (figure 5.28 A and C). Reversion proceeded rapidly for patient P13, who had the highest frequency of activated CM (cluster 20) at the acute stage. Examining the phenotype of each monocyte cluster over time, increased CD64 and CD163 co-expression on non-activated CM (cluster 17) after IVIG was observed (figure 5.28B and D). These dual positive cells were present in 3 of the 4 MIS-C patients who received IVIG and from whom we obtained post-IVIG samples (figure 5.28E). At discharge these changes persisted for the 2 MIS-C patients however, not as profound (figure 5.28E). Once again the KD patient followed the same pattern as the MIS-C patients

(figure 5.28D). In summary, unsupervised analysis of the mass cytometry data confirmed the immune recovery observed with the manual gated data and further revealed the presence of CD64+CD163+ CM post IVIG and discharge in both MIS-C and KD.

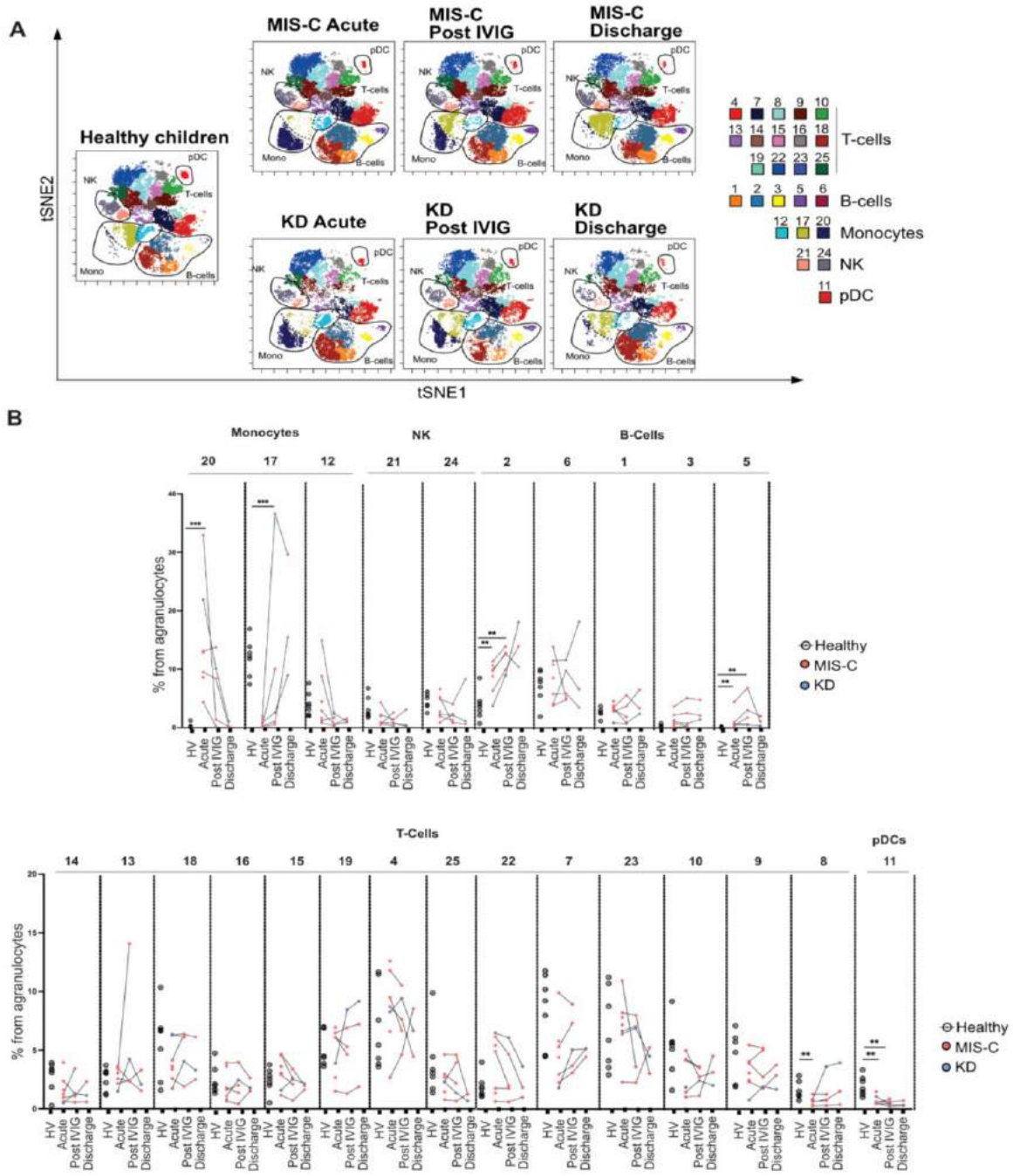

Figure 5-27 Unsupervised longitudinal analysis of agranulocytes.

(A) tSNE plots of concatenated fcs files from MIS-C patients or one KD patient at the acute stage of their disease, post IVIG and at discharge alongside seven healthy children. Each meta-cluster is represented by a different colour and key populations are indicated on the plots. (B) The frequency of each FlowSOM metacluster in the same donors expressed as a percentage of total non-granulocyte mononuclear cells are shown as box and whisker plots (healthy volunteer children and MIS-C) or a blue diamond (KD). Results of Wilcoxon rank-sum tests after 5% false discovery rate correction using the Benjamini-Hochberg method comparing the frequency of each cluster in healthy children and MIS-C patients are indicated by: * p<0.05, ** p<0.01, *** p<0.001. Non-significant results are not shown.

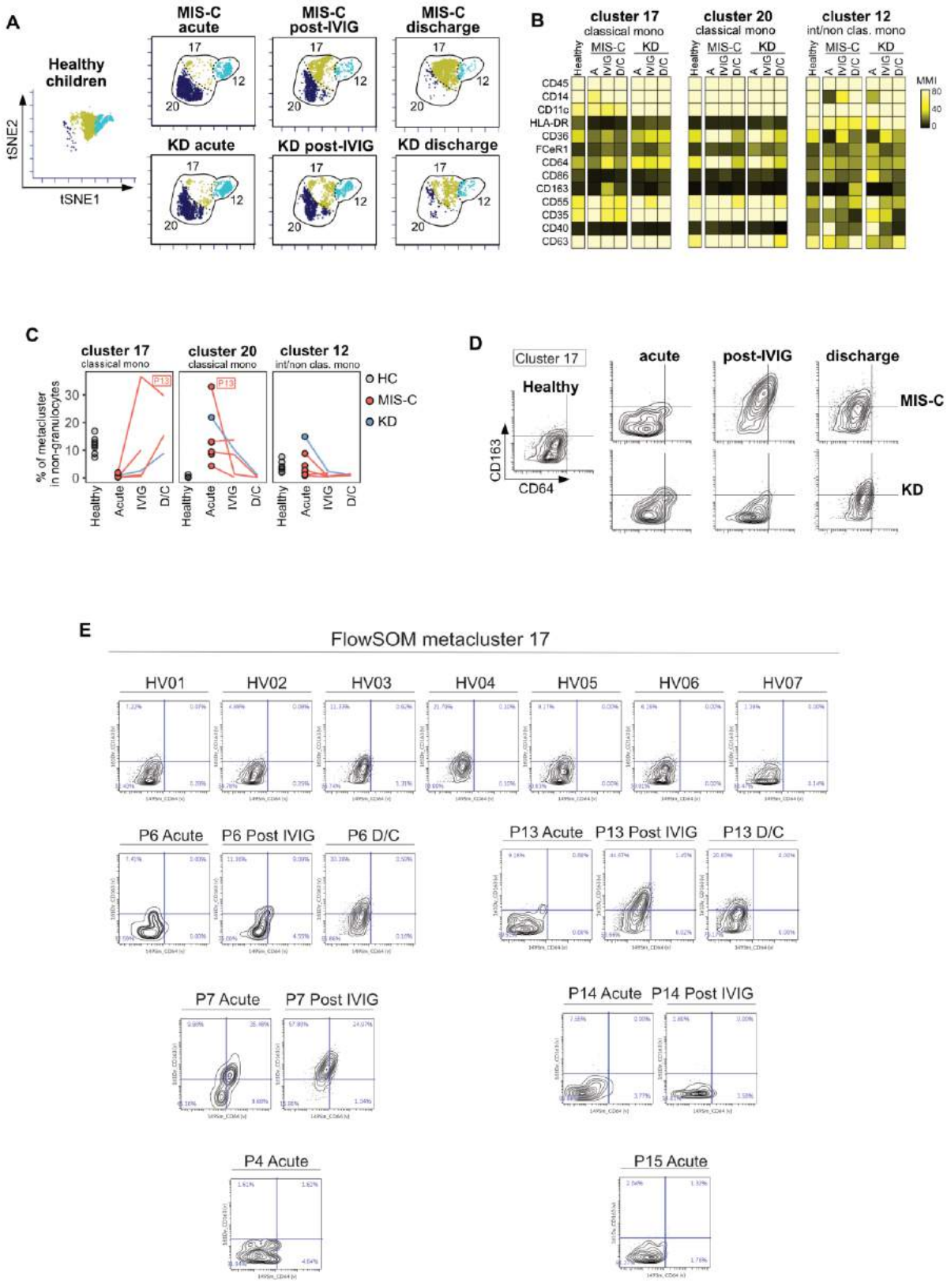
A
Healthy children
tSNE2
tSNE1
MIS-C acute
MIS-C post-IVIG
MIS-C discharge
KD acute
KD post-IVIG
KD discharge
17
12
20
B
cluster 17
classical mono
cluster 20
classical mono
cluster 12
int/non clas. mono
Healthy
MIS-C
KD
A
IVIG
D/C
CD45
CD14
CD11c
HLA-DR
CD36
FCeR1
CD64
CD86
CD163
CD55
CD35
CD40
CD63
MMI
80
40
0
C
cluster 17
classical mono
cluster 20
classical mono
cluster 12
int/non clas. mono
% of metacluster in non-granulocytes
30
20
10
0
P13
HC
MIS-C
KD
Healthy
Acute
IVIG
D/C
D
Cluster 17
Healthy
acute
post-IVIG
discharge
MIS-C
KD
CD163
CD64
E
FlowSOM metacluster 17
HV01
HV02
HV03
HV04
HV05
HV06
HV07
P6 Acute
P6 Post IVIG
P6 D/C
P13 Acute
P13 Post IVIG
P13 D/C
P7 Acute
P7 Post IVIG
P14 Acute
P14 Post IVIG
P4 Acute
P15 Acute

Figure 5-28 Unsupervised longitudinal analysis of monocytes.

(A) tSNE plots showing cells within monocyte clusters 17, 20 and 12 for MIS-C patients at the acute stage (n=6), post IVIG (n=4) and at discharge (n=2) alongside a single KD patient and healthy children (n=7). (B) Heatmaps showing the median metal intensity (MMI) of markers expressed on monocyte clusters 17, 20 and 12. (C) Trajectory of each of the three monocyte clusters over time in seven healthy children or patients over time (acute stage, post IVIG and discharge). Data from patient P13 is indicated on the plots. (D) Biaxial plots of CD64 and CD163 expression on cluster 17 monocytes cells in concatenated fcs files form healthy children or patients with MIS-C or KD at the acute, post-IVIG or discharge stages of disease. (E) Biaxial plots of CD64 and CD163 expression on cluster 17 monocytes cells showed at the level of individual for healthy and MIS-C patient at the acute, post IVIG or discharge stages of disease.

5.7.4 Mass cytometry analysis of longitudinal data reveals that immature activated granulocytes resolve with treatment

In acute MIS-C granulocytes appeared to be immature and activated. To investigate whether this also persisted at the different key stages of the disease the same manual gating strategy as described previously (figure 5.16A) was applied at samples received from MIS-C and KD post IVIG and discharge. Following the pattern seen in the adaptive immune system, neutrophil activation also persisted post IVIG however at discharge this reverted to normal (figure 5.29). Basophils recovered post IVIG and interestingly for P14 the basophils increased dramatically, while eosinophils normalised at discharge (figure 5.29). No changes were observed in platelets at any stage of disease (figure 5.29).

Next, unsupervised analysis of granulocytes was also performed as described earlier, and the nine granulocytes identified in acute MIS-C analysis were explored during the different stages of MIS-C. Focusing on the neutrophils (clusters 2-9), it was evident that the redistribution of maturity marker CD10 and activation marker CD64 begun to decrease towards healthy children's levels after IVIG administration and further decreased at discharge (figure 5.30A). Interestingly, the frequencies of all four activated clusters (clusters 4, 5, 8, 9) were still significantly higher at the time of discharge in MIS-C patients (figure 5.30 B). However, when marker expression analysis was performed on the relevant heatmaps a marked reduction of their CD64 expression and a marked increase of the CD10 expression was seen, suggesting these cells have reverted to a more mature non-activated phenotype (figure 5.30 B).

Finally, granulocyte cluster 3 was present at very low frequency in healthy children (0.16% of granulocytes), in acutely MIS-C (0.11%) and KD (0.04%) patients. However, post IVIG the

frequency of this cluster increased 5 to 12-fold over pre-treatment values in MIS-C patients (median frequency 0.81% range 0.30-2.7%) and 30-fold (frequency 1.6%) in the KD patient. These cells continued to increase in frequency and at discharge their frequency was 70-fold to 204-fold higher than at the acute stage, comprising 2.79% and 29.05% of total granulocytes in P6 and P13 respectively. Similar results were also observed in the KD patient with the frequency of cluster 3 cells being 280-fold higher in the discharge sample compared to the acute sample, comprising 14.0% of this patient's granulocytes at the time of discharge. Cluster 3 cells also possessed an unusual phenotype. Based on the strong expression of the canonical marker CD66b and the lack of CD16 and CD10, cluster 3 can be assigned to an immature granulocyte phenotype. This puzzling cluster differed from other immature granulocytes clusters as they lacked expression of CD11c, CD35 and CD55 but expressed CD64 indicating activation (figure 5.30).

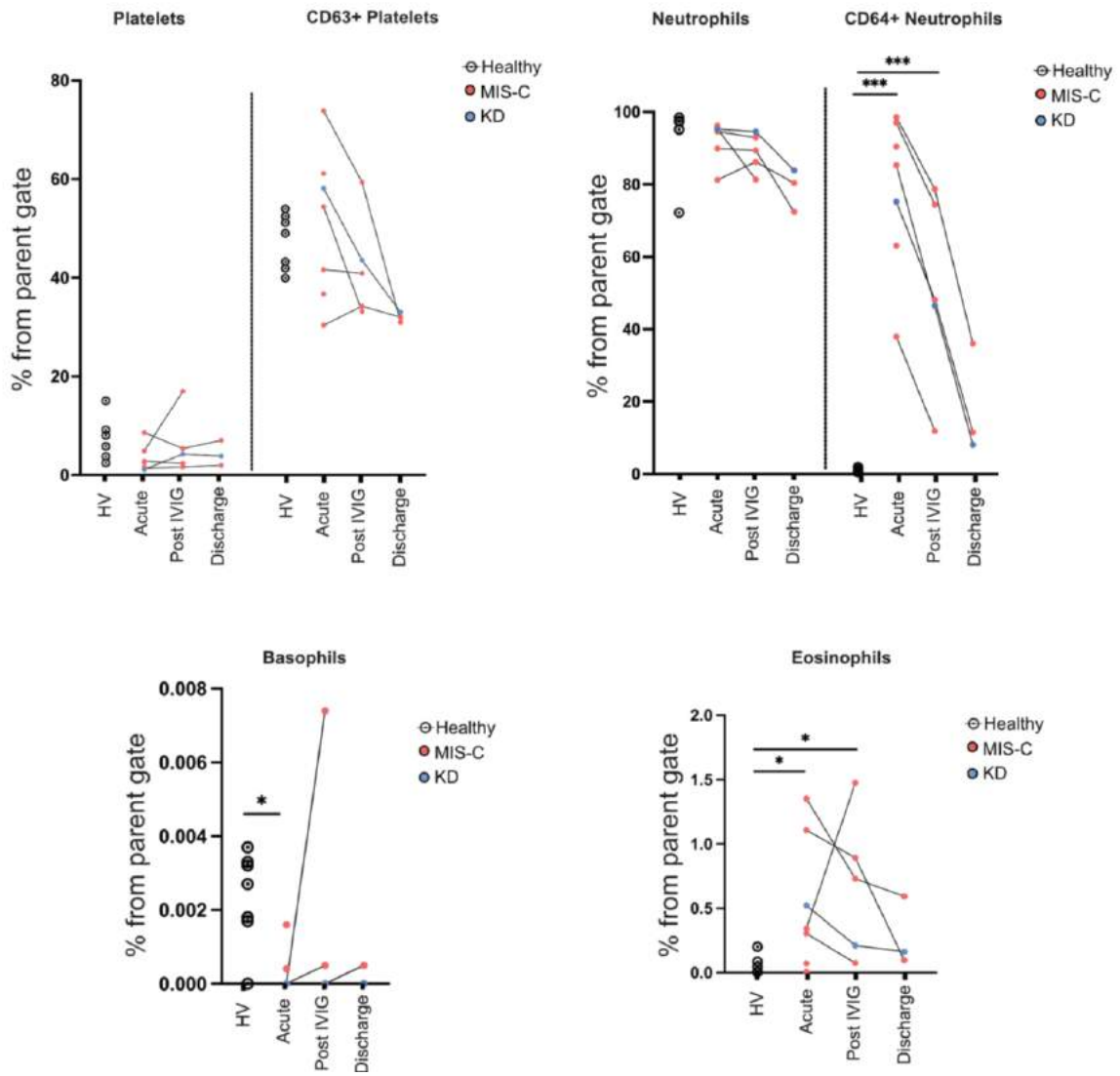

Figure 5-29 Longitudinal analysis of granulocytes subsets.

The frequency of each platelets, CD63+ platelets, neutrophils, CD64+ neutrophils, basophils and eosinophils is shown for MIS-C (red), KD (blue) and healthy children. Results of Wilcoxon rank-sum tests after 5% false discovery rate correction using the Benjamini-Hochberg method comparing the frequency of each cluster in healthy children and MIS-C patients are indicated by: * $p<0.05$, ** $p<0.01$, *** $p<0.001$. Non-significant results are not shown.

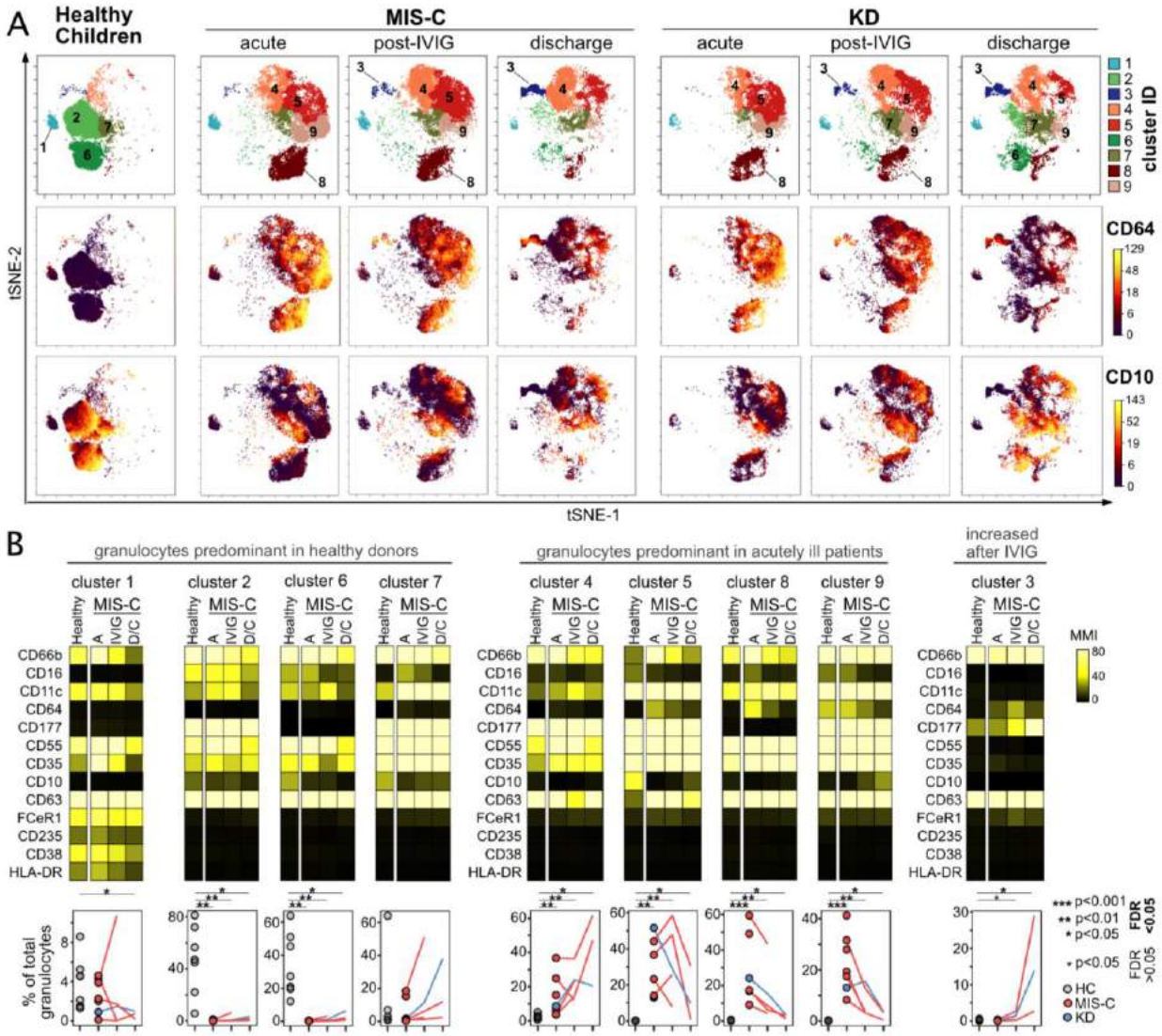

Figure 5-30 Unsupervised longitudinal analysis of granulocytes.

(A) tSNE plots of granulocytes from the healthy children, MIS-C and KD patients at different stages of the disease. Top row: FlowSom metaclusters. Middle row: CD64 expression. Bottom row: CD10 expression. (B) Upper panels: heatmaps showing expression level of different markers in each metacluster for the same donors. Lower panels: Trajectory of each metacluster over time, expressed as a percentage of total granulocytes, for each of the healthy children and patients. The results of Wilcoxon ranked sum tests comparing the frequency of each cluster in healthy children to all patients (six MIS-C and one KD patient) at the acute, post-IVIG and discharge timepoints as indicated: * p<0.05, ** p<0.01, *** p<0.001. Non-significant results are not shown and emboldened p value symbols indicate significant results after 5% false discovery rate correction using the Benjamini-Hochberg method.

5.7.6 Longitudinal analysis of cytokine profile of MIS-C patients noted an increase in arginase post IVIG administration

Finally, analysis of the cytokine profile of MIS-C and KD at different stages of disease was performed. In order to compare the cytokine profile across the different groups principal component analysis was performed and patients were divided into two groups (figure 5.31A). Acute MIS-C samples were the most distant from healthy children and almost all patients shifted towards the healthy post IVIG, with the exception of P13, a patient with particularly severe disease. The main features contributing to the principal components and therefore explaining the differences among the groups were investigated (figure 5.31A). IP10, IL1RA, sCD25 and sTNF-R2 contributed to the first group while MPO and PAI-1 contributed to the second group.

Next, each soluble protein over the disease course was examined. It was evident many decreased following treatment and all returned to normal at the time of discharge (figure 5.31B). These included both proinflammatory (IL-6, IP-10, MCP-1) and anti-inflammatory (IL-10, IL-1Ra) molecules. A notable exception was arginase, levels of which in the acute phase of disease were comparable to those of healthy children but increased dramatically post IVIG for KD and MIS-C P13 patients. Patient P13 received IVIG and then steroids before this sample was taken but patient KD2 received IVIG alone. The increased quantity of arginase in these patients' plasma was confirmed to be enzymatically active in an independent assay (figure 5.31C). Finally, across all patients a significant positive correlation between post-IVIG arginase levels and pre-treatment absolute number of neutrophils ($r=0.91$, $R^2=0.822$, $p=0.008$) was noted (figure 5.31 D). Arginase levels were not correlated with lymphocytes or monocytes (figure 5.31 D). It has been reported that arginase can be

released by activated neutrophils(Munder *et al.*, 2005). Therefore, increased arginase in high granulocyte patients is consistent with granulocytes being the main source although this would need experimental validation. In summary, longitudinal cytokine profile analysis of MIS-C and KD patients, showed a reduction of the hyperinflammation state seen in the acute stage and also revealed that this immune tapering could have been assisted by the post IVIG transient production of the immunosuppressive molecule arginase.

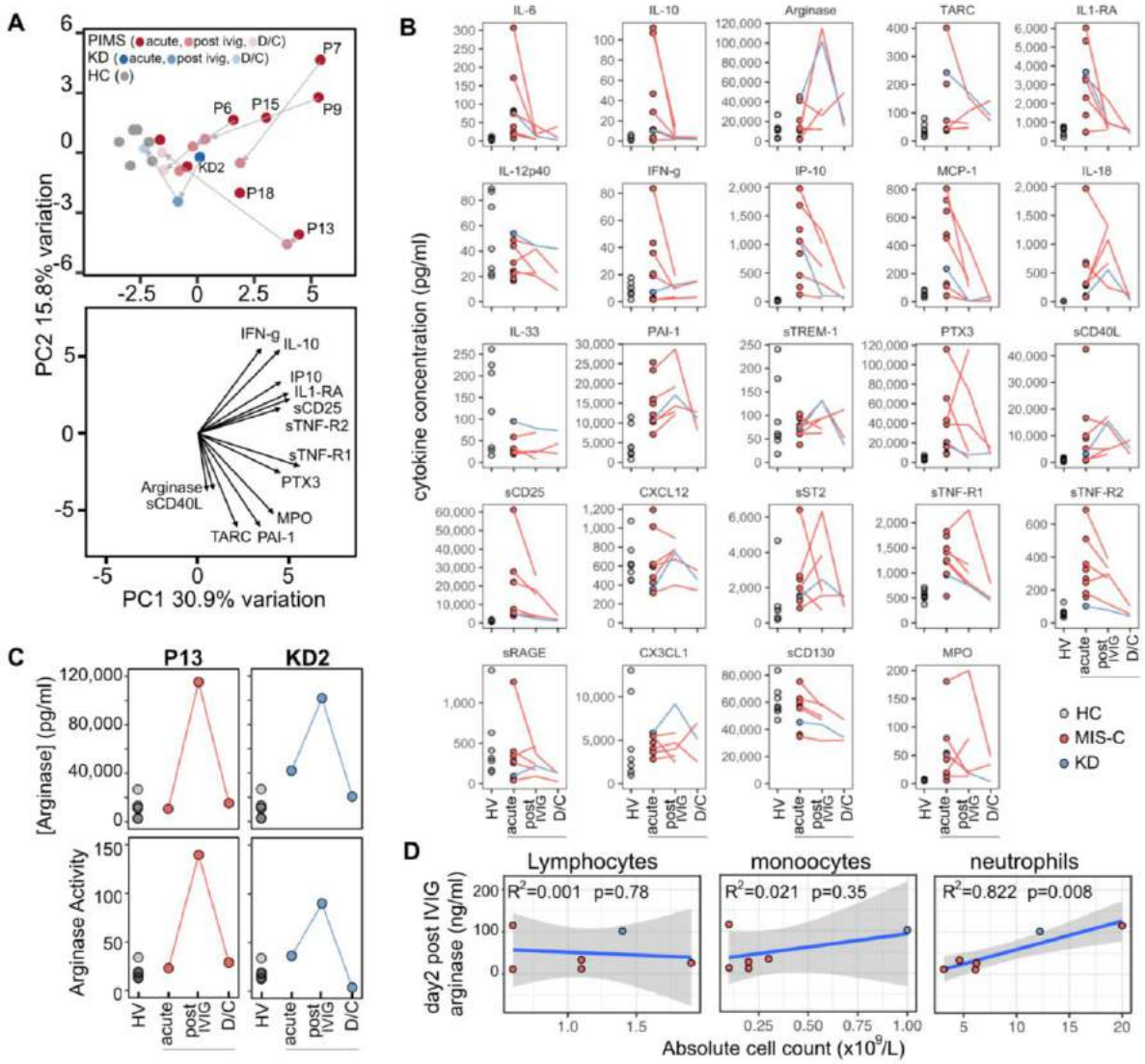

Figure 5-31 Longitudinal analysis of cytokines.

(A) Upper panel: principal component analysis biplot of cytokines. Lower panel: loading plot showing the top 13 features contributing to principal components one and two. (B) Trajectory of cytokines over time for the same healthy children and patients shown in panel A at the acute, post-IVIG and discharge timepoints. (C)Plots showing the concentration (upper panel) and enzyme activity (lower panel) of arginase over time in plasma samples from seven healthy children, MIS-C patient P13 and KD patient. (D) Results of linear regression analysis of the acute disease stage absolute counts of lymphocytes, monocytes or neutrophils against the plasma arginase concentration after IVIG treatment. The R^2 and statistical significance of each regression model is shown on the plot with the shaded area indicating the 95% confidence interval.

5.8 Conclusions

Reports of children presenting with a rare severe hyperinflammatory syndrome that shares clinical characteristics with KD, were raised a few months after the declaration of the global pandemic of coronavirus disease 2019, COVID-19 (Cabrero-Hernández *et al.*, 2020; Chiotos *et al.*, 2020; Feldstein *et al.*, 2020; Riphagen *et al.*, 2020; Verdoni *et al.*, 2020; Whittaker *et al.*, 2020). Several studies have since emerged describing the immunological changes of MIS-C, however the mixed results and conclusions provided made it difficult to decipher the immunopathology of MIS-C. Clinically all the studies agree that hyperinflammatory shock is a common feature of MIS-C. On the other hand, while most of the studies reported positive IgG antibodies against SARS-CoV-2 in their cohorts, others described cohorts of MIS-C patients lacking SARS-CoV-2 specific antibodies(Carter *et al.*, 2020; C. Gruber *et al.*, 2020).

Furthermore, the immunological responses described by several studies are contradictory. Some groups reported activation of the adaptive immune system (Consiglio *et al.*, 2020) whereas others reported both innate and T-cell activation in acute MIS-C (Carter *et al.*, 2020; C. Gruber *et al.*, 2020). In addition, the cytokine profile of MIS-C evaluated by several studies also generated conflicting results. For example, (Consiglio *et al.*, 2020)reported normal levels of IL-6 while(Carter *et al.*, 2020)reported elevated levels of IL-6. In general, these previous studies failed to achieve comprehensive immune characterisation of MIS-C and to address whether MIS-C lies along a spectrum of KD or whether it is a distinct disease.

To elucidate the immunological processes characterising MIS-C, we studied a cohort of 16 MIS-C and 2 KD patients. Using high-dimensional approaches we performed deep immune

profiling and combined this with clinical data to better understand the relationships between the immune responses and disease clinical characteristics. This approach has identified several key findings. First, when we evaluated the clinical characteristics we identified that increased neutrophil count was positively correlated with cardiac dysfunction, inflammation, and disease severity in MIS-C. It has been previously suggested that neutrophilia can be used as a predictor of IVIG resistance in KD(Cho *et al.*, 2017) and neutrophilia has been associated with more severe disease in adult COVID-19 studies(Guan *et al.*, 2020). Therefore, our data suggest that neutrophils could be used as a potential marker of severe or refractory MIS-C disease. Neutrophils can be measured simply in every hospital laboratory as part of the full blood count result. Therefore, a simple bedside test can provide an insight of disease severity and perhaps can help stratify patients in the future. In addition, MIS-C patients were deficient for vitamin D. Vitamin D modulates both the innate and adaptive immune responses and in severe infections intracellular consumption of Vitamin D has been described(Shirvani *et al.*, 2019)**.** Based on observational studies performed in adult COVID-19 patients, it has been hypothesised that Vitamin D can be used as a potential biomarker of severe MIS-C and correction of Vitamin D levels could contribute to reducing the severity of MIS-C (Yılmaz and Şen, 2020; Feketea *et al.*, 2021).

This result should be interpreted with caution since in the UK, vitamin D deficiency is common in the black and ethnic minority groups (Uday *et al.*, 2018), who are also at risk of developing MIS-C disease (E. H. Lee *et al.*, 2020). Whether low Vitamin D is a cause or effect of MIS-C disease and whether neutrophils and Vitamin D could be used as a biomarker of severe or refractory disease, remains to be determined in larger prospective studies.

Second, high dimensional immune analysis revealed that the acute stage of the disease is characterised by activation of monocytes, CD8+ memory T-cells and neutrophils. In acute MIS-C, both monocytes and neutrophils strongly expressed CD64, a marker of activation but also a known Fc receptor binding IgG antibody with high affinity(Nimmerjahn and Ravetch, 2008). Two studies reported the presence of autoantibodies in MIS-C patients (C. Gruber *et al.*, 2020; Consiglio *et al.*, 2020). Thus, it can be postulate that these cells could be activated by autoantibodies binding to Fc Receptors and play a pivotal role to the pathogenesis of MIS-C. Furthermore, the reduction of the CD57+ NK cells throughout all stages of the disease was interesting, considering that this subset is highly mature with potent cytotoxic potential and play a crucial role in viral clearance. In a recent study investigating dengue virus infection in children, the authors reported increased CD57 expression on NK cells as an immediate response to the virus(McKechnie *et al.*, 2020), a result opposite to that observed in MIS-C. Given that primary SARS-CoV2 infection occurred several weeks prior to MIS-C disease, depletion of these cells could be a result of their role in viral clearance at the time of primary infection. In keeping with findings from other groups including adult covid studies(Carter *et al.*, 2020; Mathew *et al.*, 2020), acute MIS-C patients had lower levels of class-switch and non-class switch memory B-cells with a concomitant increase of plasmablasts and DN B-cells. The marked expansion of plasmablasts has been described in adult COVID-19 cases as well as in acute Ebola(McElroy *et al.*, 2015). Plasmablasts are short-lived antibody-secreting cells produced by activated B-cells in the germinal centres and provide the initial humoral immune response to an infection(Balagué and Martínez, 2015).

As all of the patients made SARS-CoV-2 specific antibodies, this finding suggests that at least the plasmablasts' response was antigen specific. Furthermore, given the timing of MIS-C

development, the lack of memory B-cells in the periphery was striking. This could perhaps reflect the lack of robust B-cell activation in germinal centres (Wang *et al.*, 2017). Finally, the expansion of the DN B-cells subsets has been described in chronic viral infections such as HIV(Rinaldi *et al.*, 2017), malaria(Weiss *et al.*, 2009) and Hepatitis C (Chang, Li and Kaplan, 2017)and they have been associated with an impaired B-cell phenotype. Whether these cells also carry the same phenotype in MIS-C remains unclear and further functional studies are needed to address this issue.

Moreover, acute MIS-C patients had elevated circulating levels of both pro- and anti-inflammatory cytokines. As expected all patients had raised IL-6, an important mediator of fever and one that plays an important role in the acute phase response (Heinrich, Castell and Andus, 1990). Furthermore, the chemokines IP10 (Devaraj and Jialal, 2009), MCP1 (Deshmane *et al.*, 2009) and IL-18 (Ruth *et al.*, 2010) all of which are secreted mainly by monocytes and the pro-inflammatory cytokines PTX-3 another acute phase protein that activates the innate immune system(Ching *et al.*, 2020) were all significantly elevated. Interestingly, anti-inflammatory cytokines regulating inflammatory responses such as IL-10(Sabat *et al.*, 2010), sTNF-R1(Vandenabeele *et al.*, 1995), sTNFR2(Vandenabeele *et al.*, 1995) and IL-1RA (Seckinger *et al.*, 1987) were also raised. The increased level of MPO, a cytotoxic enzyme expressed both by neutrophils and monocytes (Strzepa, Pritchard and Dittel, 2017) was consistent with the strong activation seen in these subsets. PAI-1, a protein that has been linked to endothelium dysfunction(Ren *et al.*, 2015) was also found to be elevated in MIS-C. Raised PAI-1 levels have been seen in multiple inflammatory conditions and it has been reported to amplify neutrophil-mediated inflammation via multiple mechanisms (Zmijewski *et al.*, 2011). Levels of IL-17A, TNFα, IFNγ or IL1-β were not

increased, results that differ from some groups(Carter *et al.*, 2020; C. Gruber *et al.*, 2020; Diorio *et al.*, 2020; Esteve-Sole *et al.*, 2021) but agree with others (Consiglio *et al.*, 2020; P. Y. Lee *et al.*, 2020). These differences may be due to differences in patient cohorts or assay sensitivity. Collectively, these results indicate that cytokines related to inflammatory monocytes and neutrophils were the main contributors of acute MIS-C inflammation.

In this study we were able to investigate the disease trajectory with samples collected over three key stages of MIS-C. The post IVIG stage of disease was characterised by the presence of classical monocytes expressing decreased levels of CD64 and high levels of CD163, a phenotype marker of monocytes with anti-inflammatory potential (Etzerodt *et al.*, 2010; West *et al.*, 2012). Similar changes were also observed in neutrophils and CD8 T-cells post IVIG with a progressive decrease of their activation state. The decreases in immune cell activation post IVIG were accompanied by decreases in levels of both proinflammatory and anti-inflammatory cytokines. An exception was the immunosuppressive enzyme arginase, with levels and enzymatic activity increasing substantially in MIS-C patient 13 and KD patient 2 after treatment. Although these patients had different diseases both presented with profound neutrophilia and received IVIG as part of their treatment. Although the source of arginase in these patients cannot be identified, neutrophils are known to produce arginase in different inflammatory situations(Pillay *et al.*, 2012; Tak *et al.*, 2017) and are therefore the main suspect. The arginase increase seen shortly after IVIG administration could suggest a potential new mode of action for this widely used drug however, further validation in larger cohorts is needed.

Furthermore, a direct comparison was made between MIS-C and KD to identify similarities and key differences. Our KD patient had classic features reported in multiple KD studies(Weng *et al.*, 2013; Ko *et al.*, 2015; Hokibara *et al.*, 2016; Stagi *et al.*, 2016; Takeshita *et al.*, 2017; Ching *et al.*, 2020) allowing them to be used as a direct comparison. MIS-C patients shared many features in common with KD. More specifically both MIS-C and KD presented with hyperinflammation, lymphopaenia, neutrophilia, innate and adaptive activation and elevated circulating pro-and anti-inflammatory cytokines. Disease recovery was associated with resolution of hyperinflammation through similar mechanisms including the presence of CD163+ classical monocytes and progressive decrease of activation in neutrophils and CD8 memory T-cells. Despite all the similarities, they did however have some notable differences. The B-cell changes observed in MIS-C were not present in KD. Furthermore, the expansion of intermediate and non-classical monocytes, a hallmark of KD(Katayama *et al.*, 2000; Hokibara *et al.*, 2016), was not as profound in MIS-C. The function of these monocyte subsets, is still being defined but they are generally considered to be involved in tissue repair(Olingy *et al.*, 2017), interact with the vasculature(Auffray *et al.*, 2007) and perhaps play a role into the pathogenesis of KD vasculitis. Finally, IL-18 was not raised in KD, a pro-inflammatory cytokine produced mainly by macrophages able to induce severe inflammatory reactions(Ruth *et al.*, 2010). Whether the differences observed in MIS-C is the reason why these patients present with shock, which is rare in KD, requires further investigation.

Lastly, treatment strategies for MIS-C have been adapted from protocols used to treat KD and include IVIG as well as targeted therapies that inhibit IL-1beta (Anakinra), TNF- a (Infliximab) or IL-6 (Tocilizumab)(Ahmed *et al.*, 2020; Consiglio *et al.*, 2020; Hoste, Van

Paemel and Haerynck, 2021). In this cohort, MIS-C patients presented with low levels of IL1-b and TNF-a but high levels of their antagonists, IL1-RA and sTNF-R1 and R2. Therefore, targeting these pathways may have limited benefit and perhaps IL-6 inhibition should be preferred. Although results from observational studies should be interpreted with caution, the immune changes seen in both MIS-C and KD post IVIG were striking, supporting the use of IVIG in MIS-C.

In summary, this study showed that acute MIS-C was characterised by activation of both innate and adaptive immunity as well as raised levels of pro- and anti-inflammatory cytokines. Almost all of these features were also present in the KD patient and have been previously reported in KD studies. In addition, the differences seen between MIS-C and KD could explain the differences in the clinical presentation, with cardiac dysfunction and life-threatening shock being a hallmark of MIS-C. Occasionally KD can present atypically with shock (Kawasaki Disease Shock Syndrome -- KDSS) and more severe laboratory markers, similar to MIS-C patients. Therefore, our data suggest that MIS-C falls across the severe end of the KD spectrum, resembling KDSS.

CHAPTER 6 - Final Conclusions and future directions

Investigating the paediatric immune system in the context of paediatric cancer, MIS-C and healthy physiology has provided novel insights regarding the immune responses present in each condition. Importantly, these insights are relevant to the clinical management of these diseases. For paediatric cancer patients the marked NK cell alterations that are present in a large number of patients with a range of cancers provides an overarching mechanism by which cancer escapes the developing paediatric immune system. This could explain why therapies such as checkpoint inhibition have had limited benefit in paediatric cancer patients.

Furthermore, it identifies new avenues for future research into paediatric oncology. Firstly, my data suggest that NK cell alterations in paediatric cancer could arise from systemic effects upon bone marrow microenvironment. Thus, future studies investigating the interplay between paediatric tumours and the bone marrow are urgently needed to further understand the cancer biology and identify novel pathways that could potentially be targeted. Secondly, deep immune analysis of paediatric cancer patients' immune systems identified an additional potential therapeutic target. The inhibitory NK receptor NKG2A was increased in cancer patients and this can be targeted with monalizumab, which is currently being trialled in adult cancers (Creelan and Antonia, 2019). Thirdly, the enhanced NK cell cytotoxicity that occurred after in vitro expansion of NK cells from a paediatric cancer patient provides another route by which NK function could be enhanced. Notably, the protocol I used has already been validated in adult cancer patients. Fourthly, this study identified several potential cancer biomarkers for paediatric cancers such as sCD40L and

MMP9. These could be used for disease monitoring and assessment of treatment response. Going forward, further analysis of the tumour microenvironment (TME) in direct comparison with the same patient's immune system is needed to identify ways to enhance the presence of TILs and their immune responses in the TME. Fifthly, the fact that CD4 Tcm were expanded in paediatric cancer patients may indicate an anti-tumour response in a subgroup of patients. Although I was unable to investigate whether these cells were indeed tumour specific, further analysis of these cells is crucial as could lead to the discovery of novel tumour antigens that could be therapeutically targeted through adoptive immune therapies such as CAR T-cells. If on the other hand these cells are suppressing anti-tumour CD8 T-cell responses then this could be overcome via anti-CD40 antibodies or CpG (Boer *et al.*, 2005)

Future studies should monitor how the above immune perturbations, ocurring in the acute phase of paediatric cancer, change longitudinally in response to treatment. This will provide further insights of the effects of chemotherapy and immune modulating agents in the immune system of children with cancer throughout the disease trajectory. In addition, this could provide further insights as to why some patients respond to treatment and others do not, potentially identifying treatment pathways that can be targeted in patients that relapse or who become refractory to treatment.

Turning to MIS-C, multidimensional immune analysis of patients and healthy children provided novel insights into the immunopathology of MIS-C. Overall, adaptive and innate immune activation, particularly in the case of neutrophils and monocytes, associated with an increase in both pro- and anti- inflammatory cytokines, were the main features of acute MIS-C. Furthermore, the positive correlation of neutrophil count with disease severity was a

novel finding that could be further explored in future studies as a potential biomarker of both disease severity and treatment response. Clinical and immunological parameters could be further explored in larger cohorts through computational approaches and machine learning methods to identify distinct clusters of clinical phenotypes and disease severity patterns among MIS-C patients. Furthermore, investigating the disease trajectory, we identified that IVIG resulted in decrease inflammation. This was associated with the presence of monocytes with anti-inflammatory potential, appearance of a novel population of granulocytes and increased plasma arginase activity. Further investigation of the granulocytes and identifying the phenotype of this novel granulocyte population is crucial in understanding the immune mechanisms underpinning MIS-C. In addition, investigating the role of arginase post IVIG administration in larger cohorts could identify the mode of action of this commonly used drug. Finally, MIS-C shares many similarities with KD in clinical presentation, laboratory markers and immune profile. Published studies have been conflicting when it comes to whether MIS-C is a different disease or a spectrum of KD (Carter *et al.*, 2020; C. N. Gruber *et al.*, 2020; Consiglio *et al.*, 2020). Our findings suggest that MIS-C is immunologically similar to KD with some differences for example the lack of non-classical monocyte expansion in MIS-C (a hallmark of KD) and the normal levels of IL-18 observed in KD. The differences I observed could be responsible for the differences seen in the clinical pictures of MIS-C and KD. Nevertheless, the question remains as to whether MIS-C falls into the severe end of the spectrum of KD or is a different disease. Future multi-centre studies recruiting both MIS-C and KD to directly compare the two diseases are needed to answer this question.

For future work in the paediatric cancer area, I propose the following:

1. Investigate the interplay between the tumour and the bone marrow microenvironment. In particular, analysis of cytokines and chemokines that might be involved in bone marrow dysfunction such as IL-12 (Schett, 2011).
2. Investigating the expanded population of CD4 Tcm that are present in patients by sorting these cells and performing TCR receptor sequence analysis comparing these sequences to those identified in the VDJDB and MCPAS databases could potentially identify novel tumour antigens. In addition, the functional role of CD4 Tcm of paediatric cancer patient should be further explored.
3. Investigate the cytotoxic potential of in vitro expanded NK cells in larger cohorts and assess whether the anti-NKG2A antibody monalizumab could enhance the activity of NK cells from paediatric cancers. The latter approach is more scalable and therefore potentially more impactful.
4. Deep immune analysis of paediatric cancer patients' peripheral blood with high-plex analysis of their tumour microenvironment. This will allow a direct comparison of the immune cells in the periphery and the tumour infiltrating lymphocytes, identifying novel pathways that can potentially be therapeutically targeted.

For future work in MIS-C, I propose the following:

1. Explore the role of neutrophils as a biomarker of disease severity and treatment response in a larger cohort.
2. Using computational approaches and machine learning methods to correlate immunological and clinical parameters from data collected in larger cohorts to

identify distinct clusters of clinical phenotypes and disease severity patterns among patients with MIS-C.

3. Identify the mode of action of IVIG by sampling pre- and post-treatment blood from patients receiving IVIG in different settings.
4. Directly compare the immune profile of MIS-C with KD in larger numbers of patients to determine the generalisability of the observations made in my study by recruiting patients with both MIS-C and KD especially KDSS.

Appendix 1

Paediatric Cancer Young <5 years

Cytokine	Mean values intensity healthy	Mean values intensity cancer	Fold Change	p value
Vitamin D BP	80.14	62.61	-0.2187422	<0.000001
PAI-1	117.5	124.8	0.06212766	0.000042
IL-1R1	5.03	12.8	1.54473161	0.000013
RBP-4	93.07	74.07	-0.2041474	<0.000001
mmp-9	22.77	29.72	0.30522617	0.000091
IGFBP-2	19.13	36.06	0.88499739	<0.000001
ENDOGLIN	41.05	30.54	-0.2560292	<0.000001
COMPEMENT FACTROR D	43.87	38.89	-0.1135172	0.004605
CRP	196.5	169.3	-0.1384224	<0.000001
DPPIV	86.95	59.46	-0.3161587	<0.000001
ADIPONECTIN	88.18	71.49	-0.1892719	<0.000001
APOPOLIPOPROTEIN A-1	58.77	53.47	-0.0901821	0.002593

Paediatric Cancer Old >5 years

Cytokine	Mean values intensity healthy	Mean values intensity cancer	Fold Change	p value
PAI-1	54.42	153.1	1.81330393	<0.000001
RBP-4	80.81	98.18	0.21494864	0.000657
mmp-9	31.53	47.37	0.50237869	0.001833
CRP	149.2	186.7	0.25134048	<0.000001
DPPIV	74.97	46.57	-0.3788182	<0.000001
EGF	46.67	3.995	-0.914399	<0.000001
ANGIOGENIN	144.8	123.8	-0.1450276	0.000044

Human XL Cytokine array results shown for both paediatric cancer young group (n=3,< 5 years old) and old group (n=3, >5 years old). Young healthy (n=4, <5 years) and older healthy children (n=4,>5 years) were used as controls. Mean values of intensity and fold changes are shown. Statistical analysis was performed using unpaired t-test and correcting for multiple comparisons. Only statistically significant results are shown.

Appendix 2

Paediatric Cancer Young <5 years

Cytokine	Mean values intensity healthy	Mean values intensity cancer	Fold Change	p value
ADAM 10	6.175	0.8891	-0.8560162	0.000002
ALCAM/CD166	3.491	0.8485	-0.7569464	0.01283
AMPHIREGULIN	4.515	0.3582	-0.9206645	0.000121
APP	2.704	0	-1	0.010934
BACE-1	2.961	0	-1	0.00544
CD58/LFA-3	5.727	9.079	0.58529771	0.001731
ENDOGLIN/CD105	4.087	1.343	-0.6713971	0.009825
IL-15 RA	3.657	0.07584	-0.9792617	0.000845
INTEGRIN B1/CD29	11.07	14.23	0.28545619	0.003078
INTEGRIN B3/ CD61	0.7927	3.419	3.3131071	0.013379
INTEGRIN B4/ CD104	0.7406	3.9	4.26600054	0.003085
NCAM-L1	8.886	11.48	0.29191987	0.014546
OSTEOPONTIN	21.8	26.15	0.19954128	0.000059
RECK	15.06	22.61	0.50132802	<0.000001
TIMP-1	18.24	22.18	0.21600877	0.000256
TIMP-2	27.59	32.4	0.17433853	0.00001
IGM	34.32	37.9	0.10431235	0.000843
A2-MACROGLOBULIN	36.16	40.1	0.10896018	0.000253

Cytokine	Mean values intensity healthy	Mean values intensity cancer	Fold Change	p value
CD30/TNFRSF8	10.38	5.566	-0.4637765	0.011085
CD40/TNFRSF5	11.4	3.167	-0.722193	0.000024
CD43	12.54	4.086	-0.6741627	0.000015
CD48/SLAMF2	13	5.162	-0.6029231	0.000055
CD59	16.67	8.357	-0.4986803	0.00002
CD84/SLAMF5	10.68	2.145	-0.7991573	0.000013
CD97	8.258	3.12	-0.6221845	0.006868
CRTAM	9.83	4.863	-0.5052899	0.008894
CXCL16	7.751	1.44	-0.8142175	0.000996
DNAM-1	5.592	1.099	-0.8034692	0.017643
DPPIV/CD26	107.2	86.58	-0.1923507	<0.000001
INTEGRIN A4/CD49D	8.215	1.774	-0.7840536	0.000792
INTEGRIN A4/CD49E	9.771	0	-1	<0.000001
INTEGRIN AE/ CD103	5.512	0.7775	-0.8589441	0.01252
INTEGRIN AL/CD11A	8.687	2.17	-0.7502015	0.000692
MMR	16.69	26.12	0.56500899	0.000002
RESISTIN	8.943	1.693	-0.8106899	0.000176
L-SELECTIN	79.78	63.89	-0.1991727	<0.000001
TLR4	4.333	0	-1	0.02198
TRANCE/TNFS11	5.889	1.6	-0.728307	0.0233

Human Soluble receptor array heamotopoietic panel performed only in the paediatric cancer young group (n=3, < 5 years old) and healthy children (n=4, <5 years). Mean values of intensity and fold changes are shown. Statistical analysis was performed using unpaired t-test and correcting for multiple comparisons. Only statistically significant results are shown.

References

Abel, A.M. *et al.* (2018) 'Natural Killer Cells: Development, Maturation, and Clinical Utilization', *Frontiers in Immunology*, 9. doi:10.3389/fimmu.2018.01869.

Adkins, B. (2007) 'Heterogeneity in the CD4 T Cell Compartment and the Variability of Neonatal Immune Responsiveness', *Current Immunology Reviews*, 3(3), pp. 151–159. doi:10.2174/157339507781483496.

Aggarwal, S. *et al.* (2003) 'Interleukin-23 promotes a distinct CD4 T cell activation state characterized by the production of interleukin-17', *The Journal of Biological Chemistry*, 278(3), pp. 1910–1914. doi:10.1074/jbc.M207577200.

Ahmed, M. *et al.* (2020) 'Multisystem inflammatory syndrome in children: A systematic review', *EClinicalMedicine*, 26. doi:10.1016/j.eclinm.2020.100527.

Alberts, B. *et al.* (2002) 'Lymphocytes and the Cellular Basis of Adaptive Immunity', *Molecular Biology of the Cell. 4th edition* [Preprint]. Available at: https://www.ncbi.nlm.nih.gov/books/NBK26921/ (Accessed: 14 July 2021).

Allen, C.D.C. *et al.* (2004) 'Germinal center dark and light zone organization is mediated by CXCR4 and CXCR5', *Nature Immunology*, 5(9), pp. 943–952. doi:10.1038/ni1100.

Allen, G. and Hicks, J. (2021) 'A Century of Change: Trends in UK Statistics Since 1900'. Available at: https://commonslibrary.parliament.uk/research-briefings/rp99-111/ (Accessed: 9 July 2021).

Ambrose, A.R. *et al.* (2020) 'Synaptic secretion from human natural killer cells is diverse and includes supramolecular attack particles', *Proceedings of the National Academy of Sciences*, 117(38), pp. 23717–23720.

'An Introduction to Spectral Overlap and Compensation Protocols in Flow Cytometry' (2016) *Bitesize Bio*, 9 July. Available at: https://bitesizebio.com/13696/introduction-to-spectral-overlap-and-compensation-flow-cytometry-protocol/ (Accessed: 28 July 2021).

Anderson, J.L. *et al.* (2012) 'Pediatric Sarcomas: Translating Molecular Pathogenesis of Disease to Novel Therapeutic Possibilities', *Pediatric research*, 72(2), pp. 112–121. doi:10.1038/pr.2012.54.

Ansell, S.M. *et al.* (2015) 'PD-1 blockade with nivolumab in relapsed or refractory Hodgkin's lymphoma', *The New England Journal of Medicine*, 372(4), pp. 311–319. doi:10.1056/NEJMoa1411087.

Aranburu, A. *et al.* (2017) 'Human B-cell memory is shaped by age- and tissue-specific T-independent and GC-dependent events', *European Journal of Immunology*, 47(2), pp. 327–344. doi:10.1002/eji.201646642.

Astuti, I. and Ysrafil (2020) 'Severe Acute Respiratory Syndrome Coronavirus 2 (SARS-CoV-2): An overview of viral structure and host response', *Diabetes & Metabolic Syndrome*, 14(4), pp. 407–412. doi:10.1016/j.dsx.2020.04.020.

Auffray, C. *et al.* (2007) 'Monitoring of blood vessels and tissues by a population of monocytes with patrolling behavior', *Science (New York, N.Y.)*, 317(5838), pp. 666–670. doi:10.1126/science.1142883.

Aygun, N. (2018) 'Biological and Genetic Features of Neuroblastoma and Their Clinical Importance', *Current Pediatric Reviews*, 14(2), pp. 73–90. doi:10.2174/1573396314666180129101627.

Bagatell, R. and Cohn, S.L. (2016) 'Genetic discoveries and treatment advances in neuroblastoma', *Current Opinion in Pediatrics*, 28(1), pp. 19–25. doi:10.1097/MOP.0000000000000296.

Bakouny, Z. and Choueiri, T.K. (2020) 'IL-8 and cancer prognosis on immunotherapy', *Nature Medicine*, 26(5), pp. 650–651. doi:10.1038/s41591-020-0873-9.

Balagué, O. and Martínez, A. (2015) 'What is a plasmablast? A commentary to: "Plasmablastic lymphoma versus diffuse large B-cell lymphoma with plasmablastic differentiation: proposal for a novel diagnostic scoring system" by Sonja Catharina Boy et al., J. Hematopathol 2015', *Journal of Hematopathology*, 8(2), pp. 51–52. doi:10.1007/s12308-015-0239-2.

Bandura, D.R. *et al.* (2009) 'Mass Cytometry: Technique for Real Time Single Cell Multitarget Immunoassay Based on Inductively Coupled Plasma Time-of-Flight Mass Spectrometry', *Analytical Chemistry*, 81(16), pp. 6813–6822. doi:10.1021/ac901049w.

Barrow, A.D. and Colonna, M. (2019) 'Exploiting NK Cell Surveillance Pathways for Cancer Therapy', *Cancers*, 11(1). doi:10.3390/cancers11010055.

Bassani, B. *et al.* (2019) 'Natural Killer Cells as Key Players of Tumor Progression and Angiogenesis: Old and Novel Tools to Divert Their Pro-Tumor Activities into Potent Anti-Tumor Effects', *Cancers*, 11(4). doi:10.3390/cancers11040461.

Becht, E. *et al.* (2019) 'Dimensionality reduction for visualizing single-cell data using UMAP', *Nature Biotechnology*, 37(1), pp. 38–44. doi:10.1038/nbt.4314.

Bernards, R., Dessain, S.K. and Weinberg, R.A. (1986) 'N-myc amplification causes down-modulation of MHC class I antigen expression in neuroblastoma', *Cell*, 47(5), pp. 667–674. doi:10.1016/0092-8674(86)90509-x.

Berry, D.C., Levi, L. and Noy, N. (2014) 'Holo-retinol-binding protein and its receptor STRA6 drive oncogenic transformation', *Cancer research*, 74(21), pp. 6341–6351. doi:10.1158/0008-5472.CAN-14-1052.

Björklund, Å.K. *et al.* (2016) 'The heterogeneity of human CD127(+) innate lymphoid cells revealed by single-cell RNA sequencing', *Nature Immunology*, 17(4), pp. 451–460. doi:10.1038/ni.3368.

Blomberg, B.B. and Frasca, D. (2013) 'Age effects on mouse and human B cells', *Immunologic research*, 57(1–3), pp. 354–360. doi:10.1007/s12026-013-8440-9.

Blum, J.S., Wearsch, P.A. and Cresswell, P. (2013) 'Pathways of Antigen Processing', *Annual Review of Immunology*, 31(1), pp. 443–473. doi:10.1146/annurev-immunol-032712-095910.

Board, I. of M. (US) and N.R.C. (US) N.C.P. *et al.* (2003) *The Epidemiology of Childhood Cancer*. National Academies Press (US). Available at: https://www.ncbi.nlm.nih.gov/books/NBK221740/ (Accessed: 27 January 2020).

Boer, A.T. den *et al.* (2005) 'CD4+ T Cells Are Able to Promote Tumor Growth through Inhibition of Tumor-Specific CD8+ T-Cell Responses in Tumor-Bearing Hosts', *Cancer Research*, 65(15), pp. 6984–6989. doi:10.1158/0008-5472.CAN-04-3344.

Bokemeyer, C., Oechsle, K. and Hartmann, J.-T. (2005) 'Anaemia in cancer patients: pathophysiology, incidence and treatment', *European Journal of Clinical Investigation*, 35 Suppl 3, pp. 26–31. doi:10.1111/j.1365-2362.2005.01527.x.

Borthwick, G.M. *et al.* (1988) 'Expression of class I and II major histocompatibility complex antigens in Wilms' tumour and normal developing human kidney.', *British Journal of Cancer*, 58(6), pp. 753–761.

Brahmer, J. *et al.* (2015) 'Nivolumab versus Docetaxel in Advanced Squamous-Cell Non–Small-Cell Lung Cancer', *The New England journal of medicine*, 373(2), pp. 123–135. doi:10.1056/NEJMoa1504627.

Brodeur, G.M. and Bagatell, R. (2014) 'Mechanisms of neuroblastoma regression', *Nature reviews. Clinical oncology*, 11(12), pp. 704–713. doi:10.1038/nrclinonc.2014.168.

Brodin, P. *et al.* (2015) 'Variation in the human immune system is largely driven by non-heritable influences', *Cell*, 160(0), pp. 37–47. doi:10.1016/j.cell.2014.12.020.

Bromage, E.S. *et al.* (2004) 'Plasmablast and Plasma Cell Production and Distribution in Trout Immune Tissues', *The Journal of Immunology*, 173(12), pp. 7317–7323. doi:10.4049/jimmunol.173.12.7317.

Brown, C.E. *et al.* (2016) 'Regression of Glioblastoma after Chimeric Antigen Receptor T-Cell Therapy', *The New England Journal of Medicine*, 375(26), pp. 2561–2569. doi:10.1056/NEJMoa1610497.

Bruggner, R.V. *et al.* (2014) 'Automated identification of stratifying signatures in cellular subpopulations', *Proceedings of the National Academy of Sciences of the United States of America*, 111(26), pp. E2770-2777. doi:10.1073/pnas.1408792111.

Cabrero-Hernández, M. *et al.* (2020) 'Severe SARS-CoV-2 Infection in Children With Suspected Acute Abdomen: A Case Series From a Tertiary Hospital in Spain', *The Pediatric Infectious Disease Journal*, 39(8), pp. e195–e198. doi:10.1097/INF.0000000000002777.

Caligiuri, M.A. (2008) 'Human natural killer cells', *Blood*, 112(3), pp. 461–469. doi:10.1182/blood-2007-09-077438.

Campbell, B.B. *et al.* (2017) 'Comprehensive Analysis of Hypermutation in Human Cancer', *Cell*, 171(5), pp. 1042-1056.e10. doi:10.1016/j.cell.2017.09.048.

Carr, E.J. *et al.* (2016) 'The cellular composition of the human immune system is shaped by age and cohabitation', *Nature immunology*, 17(4), pp. 461–468. doi:10.1038/ni.3371.

Carrega, P. *et al.* (2008) 'Natural killer cells infiltrating human nonsmall-cell lung cancer are enriched in CD56 bright CD16(-) cells and display an impaired capability to kill tumor cells', *Cancer*, 112(4), pp. 863–875. doi:10.1002/cncr.23239.

Carsetti, R. *et al.* (2020) 'The immune system of children: the key to understanding SARS-CoV-2 susceptibility?', *The Lancet Child & Adolescent Health*, 4(6), pp. 414–416. doi:10.1016/S2352-4642(20)30135-8.

Carter, M.J. *et al.* (2020) 'Peripheral immunophenotypes in children with multisystem inflammatory syndrome associated with SARS-CoV-2 infection', *Nature Medicine*, 26(11), pp. 1701–1707. doi:10.1038/s41591-020-1054-6.

Castagnoli, R. *et al.* (2020) 'Severe Acute Respiratory Syndrome Coronavirus 2 (SARS-CoV-2) Infection in Children and Adolescents: A Systematic Review', *JAMA pediatrics*, 174(9), pp. 882–889. doi:10.1001/jamapediatrics.2020.1467.

Castriconi, R. *et al.* (2004) 'Natural killer cell-mediated killing of freshly isolated neuroblastoma cells: critical role of DNAX accessory molecule-1-poliovirus receptor interaction', *Cancer Research*, 64(24), pp. 9180–9184. doi:10.1158/0008-5472.CAN-04-2682.

Chan, W.K. *et al.* (2013) 'Multiplex and genome-wide analyses reveal distinctive properties of KIR+ and CD56+ T cells in human blood', *Journal of Immunology (Baltimore, Md.: 1950)*, 191(4), pp. 1625–1636. doi:10.4049/jimmunol.1300111.

Chang, L.-Y., Li, Y. and Kaplan, D.E. (2017) 'Hepatitis C viraemia reversibly maintains subset of antigen-specific T-bet+ tissue-like memory B cells', *Journal of Viral Hepatitis*, 24(5), pp. 389–396. doi:10.1111/jvh.12659.

Chanvillard, C. *et al.* (2013) 'The Role of Natural Killer Cells in Multiple Sclerosis and Their Therapeutic Implications', *Frontiers in Immunology*, 4, p. 63. doi:10.3389/fimmu.2013.00063.

Charles A Janeway, J. *et al.* (2001) 'T cell-mediated cytotoxicity', *Immunobiology: The Immune System in Health and Disease. 5th edition* [Preprint]. Available at: https://www.ncbi.nlm.nih.gov/books/NBK27101/ (Accessed: 6 November 2021).

Chen, C. *et al.* (2019) 'Current and Future Treatment Strategies for Rhabdomyosarcoma', *Frontiers in Oncology*, 9. doi:10.3389/fonc.2019.01458.

Chen, C. *et al.* (2021) 'Immunotherapy for osteosarcoma: Fundamental mechanism, rationale, and recent breakthroughs', *Cancer Letters*, 500, pp. 1–10. doi:10.1016/j.canlet.2020.12.024.

Ching, L.L. *et al.* (2020) 'Elevated Levels of Pentraxin 3 Correlate With Neutrophilia and Coronary Artery Dilation During Acute Kawasaki Disease', *Frontiers in Pediatrics*, 8. doi:10.3389/fped.2020.00295.

Chiotos, K. *et al.* (2020) 'Multisystem Inflammatory Syndrome in Children During the Coronavirus 2019 Pandemic: A Case Series', *Journal of the Pediatric Infectious Diseases Society*, 9(3), pp. 393–398. doi:10.1093/jpids/piaa069.

Cho, H.-J. *et al.* (2017) 'High neutrophil : lymphocyte ratio is associated with refractory Kawasaki disease', *Pediatrics International: Official Journal of the Japan Pediatric Society*, 59(6), pp. 669–674. doi:10.1111/ped.13240.

Chung, H.W. and Lim, J.-B. (2014) 'Clinical significance of elevated serum soluble CD40 ligand levels as a diagnostic and prognostic tumor marker for pancreatic ductal adenocarcinoma', *Journal of Translational Medicine*, 12(1), p. 102. doi:10.1186/1479-5876-12-102.

Cohnen, A. *et al.* (2013) 'Surface CD107a/LAMP-1 protects natural killer cells from degranulation-associated damage', *Blood*, 122(8), pp. 1411–1418. doi:10.1182/blood-2012-07-441832.

Consiglio, C.R. *et al.* (2020) 'The Immunology of Multisystem Inflammatory Syndrome in Children with COVID-19', *Cell*, 183(4), pp. 968-981.e7. doi:10.1016/j.cell.2020.09.016.

Cooper, M.A., Fehniger, T.A. and Caligiuri, M.A. (2001) 'The biology of human natural killer-cell subsets', *Trends in Immunology*, 22(11), pp. 633–640. doi:10.1016/s1471-4906(01)02060-9.

Cossarizza, A. *et al.* (2019) 'Guidelines for the use of flow cytometry and cell sorting in immunological studies (second edition)', *European Journal of Immunology*, 49(10), pp. 1457–1973. doi:10.1002/eji.201970107.

COVID-19 Map (no date) *Johns Hopkins Coronavirus Resource Center*. Available at: https://coronavirus.jhu.edu/map.html (Accessed: 26 July 2021).

Creelan, B.C. and Antonia, S.J. (2019) 'The NKG2A immune checkpoint - a new direction in cancer immunotherapy', *Nature Reviews. Clinical Oncology*, 16(5), pp. 277–278. doi:10.1038/s41571-019-0182-8.

Crotty, S. (2015) 'A brief history of T cell help to B cells', *Nature Reviews Immunology*, 15(3), pp. 185–189. doi:10.1038/nri3803.

Cunningham, R.M., Walton, M.A. and Carter, P.M. (2018) 'The Major Causes of Death in Children and Adolescents in the United States', *New England Journal of Medicine*, 379(25), pp. 2468–2475. doi:10.1056/NEJMsr1804754.

Davey, M.S. *et al.* (2018) 'The human Vδ2 + T-cell compartment comprises distinct innate-like Vγ9 + and adaptive Vγ9 - subsets', *Nature Communications*, 9(1), p. 1760. doi:10.1038/s41467-018-04076-0.

David, J.M. *et al.* (2016) 'The IL-8/IL-8R Axis: A Double Agent in Tumor Immune Resistance', *Vaccines*, 4(3), p. E22. doi:10.3390/vaccines4030022.

Della Bella, S. *et al.* (2008) 'Application of six-color flow cytometry for the assessment of dendritic cell responses in whole blood assays', *Journal of Immunological Methods*, 339(2), pp. 153–164. doi:10.1016/j.jim.2008.09.009.

Della Chiesa, M. *et al.* (2008) 'Evidence that the KIR2DS5 gene codes for a surface receptor triggering natural killer cell function', *European Journal of Immunology*, 38(8), pp. 2284–2289. doi:10.1002/eji.200838434.

Deshmane, S.L. *et al.* (2009) 'Monocyte Chemoattractant Protein-1 (MCP-1): An Overview', *Journal of Interferon & Cytokine Research*, 29(6), pp. 313–326. doi:10.1089/jir.2008.0027.

Devaraj, S. and Jialal, I. (2009) 'Increased Secretion of IP-10 from Monocytes Under Hyperglycemia is via the TLR 2 and TLR 4 Pathway', *Cytokine*, 47(1), pp. 6–10. doi:10.1016/j.cyto.2009.02.004.

Dhar, P. and Wu, J.D. (2018) 'NKG2D and its ligands in cancer', *Current opinion in immunology*, 51, pp. 55–61. doi:10.1016/j.coi.2018.02.004.

Diggins, K.E. *et al.* (2017) 'Characterizing cell subsets using marker enrichment modeling', *Nature Methods*, 14(3), pp. 275–278. doi:10.1038/nmeth.4149.

Diggins, K.E. *et al.* (2018) 'Generating Quantitative Cell Identity Labels with Marker Enrichment Modeling (MEM)', *Current protocols in cytometry*, 83, p. 10.21.1-10.21.28. doi:10.1002/cpcy.34.

Diorio, C. *et al.* (2020) 'Multisystem inflammatory syndrome in children and COVID-19 are distinct presentations of SARS–CoV-2', *The Journal of Clinical Investigation*, 130(11), pp. 5967–5975. doi:10.1172/JCI140970.

Dowling, D.J. and Levy, O. (2014) 'Ontogeny of early life immunity', *Trends in Immunology*, 35(7), pp. 299–310. doi:10.1016/j.it.2014.04.007.

Dransfield, I. *et al.* (1994) 'Neutrophil apoptosis is associated with a reduction in CD16 (Fc gamma RIII) expression', *Journal of Immunology (Baltimore, Md.: 1950)*, 153(3), pp. 1254–1263.

Dunn, G.P., Old, L.J. and Schreiber, R.D. (2004) 'The Three Es of Cancer Immunoediting', *Annual Review of Immunology*, 22(1), pp. 329–360. doi:10.1146/annurev.immunol.22.012703.104803.

Enderlin, M. *et al.* (2009) 'TNF-alpha and the IFN-gamma-inducible protein 10 (IP-10/CXCL-10) delivered by parvoviral vectors act in synergy to induce antitumor effects in mouse glioblastoma', *Cancer Gene Therapy*, 16(2), pp. 149–160. doi:10.1038/cgt.2008.62.

Erdmann, F. *et al.* (2021) 'Childhood cancer: Survival, treatment modalities, late effects and improvements over time', *Cancer Epidemiology*, 71(Pt B), p. 101733. doi:10.1016/j.canep.2020.101733.

Erokhina, S.A. *et al.* (2018) 'HLA-DR+ NK cells are mostly characterized by less mature phenotype and high functional activity', *Immunology and Cell Biology*, 96(2), pp. 212–228. doi:10.1111/imcb.1032.

Esteve-Sole, A. *et al.* (2021) 'Similarities and differences between the immunopathogenesis of COVID-19-related pediatric multisystem inflammatory syndrome and Kawasaki disease', *The Journal of Clinical Investigation*, 131(6). doi:10.1172/JCI144554.

Etzerodt, A. *et al.* (2010) 'Tumor necrosis factor α-converting enzyme (TACE/ADAM17) mediates ectodomain shedding of the scavenger receptor CD163', *Journal of Leukocyte Biology*, 88(6), pp. 1201–1205. doi:10.1189/jlb.0410235.

Federico, S.M. *et al.* (2017) 'A Pilot Trial of Humanized Anti-GD2 Monoclonal Antibody (hu14.18K322A) with Chemotherapy and Natural Killer Cells in Children with Recurrent/Refractory Neuroblastoma', *Clinical Cancer Research: An Official Journal of the American Association for Cancer Research*, 23(21), pp. 6441–6449. doi:10.1158/1078-0432.CCR-17-0379.

Fehniger, T.A. *et al.* (2003) 'CD56bright natural killer cells are present in human lymph nodes and are activated by T cell-derived IL-2: a potential new link between adaptive and innate immunity', *Blood*, 101(8), pp. 3052–3057. doi:10.1182/blood-2002-09-2876.

Feketea, G. *et al.* (2021) 'Vitamin D in Corona Virus Disease 2019 (COVID-19) Related Multisystem Inflammatory Syndrome in Children (MIS-C)', *Frontiers in Immunology*, 12. doi:10.3389/fimmu.2021.648546.

Feldstein, L.R. *et al.* (2020) 'Multisystem Inflammatory Syndrome in U.S. Children and Adolescents', *New England Journal of Medicine*, 383(4), pp. 334–346. doi:10.1056/NEJMoa2021680.

Fernández, A. *et al.* (2021) 'Optimizing the Procedure to Manufacture Clinical-Grade NK Cells for Adoptive Immunotherapy', *Cancers*, 13(3), p. 577. doi:10.3390/cancers13030577.

Fidler, M.M. *et al.* (2016) 'Long term cause specific mortality among 34 489 five year survivors of childhood cancer in Great Britain: population based cohort study', *BMJ*, 354, p. i4351. doi:10.1136/bmj.i4351.

Filias, A. *et al.* (2011) 'Phagocytic ability of neutrophils and monocytes in neonates', *BMC pediatrics*, 11, p. 29. doi:10.1186/1471-2431-11-29.

Fink, K. (2012) 'Origin and Function of Circulating Plasmablasts during Acute Viral Infections', *Frontiers in Immunology*, 3. doi:10.3389/fimmu.2012.00078.

Flood, J. *et al.* (2021) 'Paediatric multisystem inflammatory syndrome temporally associated with SARS-CoV-2 (PIMS-TS): Prospective, national surveillance, United Kingdom and Ireland, 2020', *The Lancet Regional Health – Europe*, 3. doi:10.1016/j.lanepe.2021.100075.

Gadalla, R. *et al.* (2019) 'Validation of CyTOF Against Flow Cytometry for Immunological Studies and Monitoring of Human Cancer Clinical Trials', *Frontiers in Oncology*, 9. doi:10.3389/fonc.2019.00415.

Gassen, S.V. *et al.* (2015) 'FlowSOM: Using self-organizing maps for visualization and interpretation of cytometry data', *Cytometry Part A*, 87(7), pp. 636–645. doi:10.1002/cyto.a.22625.

Gayoso, I. *et al.* (2011) 'Immunosenescence of human natural killer cells', *Journal of Innate Immunity*, 3(4), pp. 337–343. doi:10.1159/000328005.

Geherin, S.A. *et al.* (2012) 'The Skin, a Novel Niche for Recirculating B Cells', *The Journal of Immunology*, 188(12), pp. 6027–6035. doi:10.4049/jimmunol.1102639.

Gerdsen, F. *et al.* (2005) 'Platelet activation markers in patients with venous thromboembolism without predisposing factors', *Pathophysiology of Haemostasis and Thrombosis*, 34(1), pp. 1–5. doi:10.1159/000088540.

Godfred-Cato, S. *et al.* (2020) 'COVID-19-Associated Multisystem Inflammatory Syndrome in Children - United States, March-July 2020', *MMWR. Morbidity and mortality weekly report*, 69(32), pp. 1074–1080. doi:10.15585/mmwr.mm6932e2.

Goodridge, J.P., Önfelt, B. and Malmberg, K.-J. (2015) 'Newtonian cell interactions shape natural killer cell education', *Immunological Reviews*, 267(1), pp. 197–213. doi:10.1111/imr.12325.

Grabow, D. *et al.* (2018) 'The PanCareSurFup cohort of 83,333 five-year survivors of childhood cancer: a cohort from 12 European countries', *European Journal of Epidemiology*, 33(3), pp. 335–349. doi:10.1007/s10654-018-0370-3.

Grattan-Smith, J.D. (2011) 'Nephroblastomatosis: imaging challenges', *Pediatric Radiology*, 41(1), pp. 198–199. doi:10.1007/s00247-011-1997-3.

Greaves, M. (2018) 'A causal mechanism for childhood acute lymphoblastic leukaemia', *Nature Reviews Cancer*, 18(8), pp. 471–484. doi:10.1038/s41568-018-0015-6.

Greaves, M., Cazzaniga, V. and Ford, A. (2021) 'Can we prevent childhood Leukaemia?', *Leukemia*, 35(5), pp. 1258–1264. doi:10.1038/s41375-021-01211-7.

Gruber, C. *et al.* (2020) 'Mapping Systemic Inflammation and Antibody Responses in Multisystem Inflammatory Syndrome in Children (MIS-C)', *medRxiv* [Preprint]. doi:10.1101/2020.07.04.20142752.

Gruber, C.N. *et al.* (2020) 'Mapping Systemic Inflammation and Antibody Responses in Multisystem Inflammatory Syndrome in Children (MIS-C)', *Cell*, 183(4), pp. 982-995.e14. doi:10.1016/j.cell.2020.09.034.

Grzywa, T.M. *et al.* (2020) 'Myeloid Cell-Derived Arginase in Cancer Immune Response', *Frontiers in Immunology*, 11, p. 938. doi:10.3389/fimmu.2020.00938.

Guan, W.-J. *et al.* (2020) 'Clinical Characteristics of Coronavirus Disease 2019 in China', *The New England Journal of Medicine*, 382(18), pp. 1708–1720. doi:10.1056/NEJMoa2002032.

Gullaksen, S.-E. *et al.* (2019) 'Titrating Complex Mass Cytometry Panels', *Cytometry Part A*, 95(7), pp. 792–796. doi:10.1002/cyto.a.23751.

Haanen, J.B. and Cerundolo, V. (2018) 'NKG2A, a New Kid on the Immune Checkpoint Block', *Cell*, 175(7), pp. 1720–1722. doi:10.1016/j.cell.2018.11.048.

de la Haba-Rodríguez, J. *et al.* (2002) 'Soluble dipeptidyl peptidase IV (CD-26) in serum of patients with colorectal carcinoma', *Neoplasma*, 49(5), pp. 307–311.

Hamann, D. *et al.* (1997) 'Phenotypic and functional separation of memory and effector human CD8+ T cells', *The Journal of Experimental Medicine*, 186(9), pp. 1407–1418. doi:10.1084/jem.186.9.1407.

Hamann, I. *et al.* (2011) 'Analyses of phenotypic and functional characteristics of CX3CR1-expressing natural killer cells', *Immunology*, 133(1), pp. 62–73. doi:10.1111/j.1365-2567.2011.03409.x.

Han, X. *et al.* (2008) 'Immunophenotypic study of basophils by multiparameter flow cytometry', *Archives of Pathology & Laboratory Medicine*, 132(5), pp. 813–819. doi:10.1043/1543-2165(2008)132[813:ISOBBM]2.0.CO;2.

Hanns, P. *et al.* (no date) 'Stress and catecholamines modulate the bone marrow microenvironment to promote tumorigenesis', *Cell Stress*, 3(7), pp. 221–235. doi:10.15698/cst2019.07.192.

Harwood, N.E. and Batista, F.D. (2010) 'Early Events in B Cell Activation', *Annual Review of Immunology*, 28(1), pp. 185–210. doi:10.1146/annurev-immunol-030409-101216.

Hasmim, M. *et al.* (2015) 'Critical Role of Tumor Microenvironment in Shaping NK Cell Functions: Implication of Hypoxic Stress', *Frontiers in Immunology*, 6, p. 482. doi:10.3389/fimmu.2015.00482.

Hassani, M. *et al.* (2020) 'Characterization of the phenotype of human eosinophils and their progenitors in the bone marrow of healthy individuals', *Haematologica*, 105(2), pp. e52–e56. doi:10.3324/haematol.2019.219048.

He, Y. and Tian, Z. (2017) 'NK cell education via nonclassical MHC and non-MHC ligands', *Cellular & Molecular Immunology*, 14(4), pp. 321–330. doi:10.1038/cmi.2016.26.

Heinrich, P.C., Castell, J.V. and Andus, T. (1990) 'Interleukin-6 and the acute phase response.', *Biochemical Journal*, 265(3), pp. 621–636.

Henderson, L.A. and Yeung, R.S.M. (2021) 'MIS-C: early lessons from immune profiling', *Nature Reviews Rheumatology*, 17(2), pp. 75–76. doi:10.1038/s41584-020-00566-y.

Hilton, H.G. *et al.* (2015) 'Polymorphic HLA-C receptors balance the functional characteristics of KIR haplotypes', *Journal of immunology (Baltimore, Md. : 1950)*, 195(7), pp. 3160–3170. doi:10.4049/jimmunol.1501358.

Hoang, A. *et al.* (2020) 'COVID-19 in 7780 pediatric patients: A systematic review', *EClinicalMedicine*, 24. doi:10.1016/j.eclinm.2020.100433.

Hodi, F.S. *et al.* (2010) 'Improved survival with ipilimumab in patients with metastatic melanoma', *The New England Journal of Medicine*, 363(8), pp. 711–723. doi:10.1056/NEJMoa1003466.

Hoffmann, J.J.M.L. (2009) 'Neutrophil CD64: a diagnostic marker for infection and sepsis', *Clinical Chemistry and Laboratory Medicine*, 47(8), pp. 903–916. doi:10.1515/CCLM.2009.224.

Hokibara, S. *et al.* (2016) 'Markedly elevated CD64 expression on neutrophils and monocytes as a biomarker for diagnosis and therapy assessment in Kawasaki disease', *Inflammation Research: Official Journal of the European Histamine Research Society ... [et Al.]*, 65(7), pp. 579–585. doi:10.1007/s00011-016-0942-1.

Hoste, L., Van Paemel, R. and Haerynck, F. (2021) 'Multisystem inflammatory syndrome in children related to COVID-19: a systematic review', *European Journal of Pediatrics* [Preprint]. doi:10.1007/s00431-021-03993-5.

Howie, S.R.C. (2011) 'Blood sample volumes in child health research: review of safe limits', *Bulletin of the World Health Organization*, 89(1), pp. 46–53. doi:10.2471/BLT.10.080010.

Huang, H. (2018) 'Matrix Metalloproteinase-9 (MMP-9) as a Cancer Biomarker and MMP-9 Biosensors: Recent Advances', *Sensors (Basel, Switzerland)*, 18(10), p. 3249. doi:10.3390/s18103249.

Huang, J. *et al.* (2012) 'Elevated serum soluble CD40 ligand in cancer patients may play an immunosuppressive role', *Blood*, 120(15), pp. 3030–3038. doi:10.1182/blood-2012-05-427799.

Huang, S. *et al.* (2002) 'Fully humanized neutralizing antibodies to interleukin-8 (ABX-IL8) inhibit angiogenesis, tumor growth, and metastasis of human melanoma', *The American Journal of Pathology*, 161(1), pp. 125–134. doi:10.1016/S0002-9440(10)64164-8.

Huang, W.-C. *et al.* (2019) 'Less circulating mucosal-associated invariant T cells in patients with cervical cancer', *Taiwanese Journal of Obstetrics & Gynecology*, 58(1), pp. 117–121. doi:10.1016/j.tjog.2018.11.022.

Hunka, J., Riley, J.T. and Debes, G.F. (2020) 'Approaches to overcome flow cytometry limitations in the analysis of cells from veterinary relevant species', *BMC Veterinary Research*, 16(1), p. 83. doi:10.1186/s12917-020-02299-2.

Hutzen, B., Ghonime, M., *et al.* (2019) 'Immunotherapeutic Challenges for Pediatric Cancers', *Molecular Therapy Oncolytics*, 15, pp. 38–48. doi:10.1016/j.omto.2019.08.005.

Hutzen, B., Paudel, S.N., *et al.* (2019) 'Immunotherapies for pediatric cancer: current landscape and future perspectives', *Cancer and Metastasis Reviews*, 38(4), pp. 573–594. doi:10.1007/s10555-019-09819-z.

'Infections in child care centres' (2000) *Paediatrics & Child Health*, 5(8), pp. 495–496.

Ivarsson, M.A. *et al.* (2013) 'Differentiation and functional regulation of human fetal NK cells', *The Journal of Clinical Investigation*, 123(9), pp. 3889–3901. doi:10.1172/JCI68989.

Ivarsson, M.A., Michaëlsson, J. and Fauriat, C. (2014) 'Activating Killer Cell Ig-Like Receptors in Health and Disease', *Frontiers in Immunology*, 5, p. 184. doi:10.3389/fimmu.2014.00184.

de Jonge, K. *et al.* (2019) 'Circulating CD56 bright NK cells inversely correlate with survival of melanoma patients', *Scientific Reports*, 9(1), p. 4487. doi:10.1038/s41598-019-40933-8.

Kärre, K. (2002) 'NK cells, MHC class I molecules and the missing self', *Scandinavian Journal of Immunology*, 55(3), pp. 221–228. doi:10.1046/j.1365-3083.2002.01053.x.

Katayama, K. *et al.* (2000) 'CD14+CD16+ monocyte subpopulation in Kawasaki disease', *Clinical and Experimental Immunology*, 121(3), pp. 566–570. doi:10.1046/j.1365-2249.2000.01321.x.

Khailany, R.A., Safdar, M. and Ozaslan, M. (2020) 'Genomic characterization of a novel SARS-CoV-2', *Gene Reports*, 19, p. 100682. doi:10.1016/j.genrep.2020.100682.

Khan, N. *et al.* (2002) 'Cytomegalovirus seropositivity drives the CD8 T cell repertoire toward greater clonality in healthy elderly individuals', *Journal of Immunology (Baltimore, Md.: 1950)*, 169(4), pp. 1984–1992. doi:10.4049/jimmunol.169.4.1984.

Kimball, A.K. *et al.* (2018) 'A Beginner's Guide To Analyzing and Visualizing Mass Cytometry Data', *Journal of immunology (Baltimore, Md. : 1950)*, 200(1), pp. 3–22. doi:10.4049/jimmunol.1701494.

Kliegman RM, S. Geme J (no date) *Nelson textbook of Pediatrics*. 21st edn. Elsevier Health Sciences.

Ko, T.-M. *et al.* (2015) 'CXCL10/IP-10 is a biomarker and mediator for Kawasaki disease', *Circulation Research*, 116(5), pp. 876–883. doi:10.1161/CIRCRESAHA.116.305834.

Koch, S. *et al.* (2008) 'Multiparameter flow cytometric analysis of CD4 and CD8 T cell subsets in young and old people', *Immunity & Ageing: I & A*, 5, p. 6. doi:10.1186/1742-4933-5-6.

Kollmann, T.R. *et al.* (2012) 'Innate immune function by Toll-like receptors: distinct responses in newborns and the elderly', *Immunity*, 37(5), pp. 771–783. doi:10.1016/j.immuni.2012.10.014.

Korbecki, J. *et al.* (2020) 'CC Chemokines in a Tumor: A Review of Pro-Cancer and Anti-Cancer Properties of the Ligands of Receptors CCR1, CCR2, CCR3, and CCR4', *International Journal of Molecular Sciences*, 21(21), p. 8412. doi:10.3390/ijms21218412.

Kordasti, S. *et al.* (2016) 'Deep phenotyping of Tregs identifies an immune signature for idiopathic aplastic anemia and predicts response to treatment', *Blood*, 128(9), pp. 1193–1205. doi:10.1182/blood-2016-03-703702.

Krzewski, K. and Coligan, J.E. (2012) 'Human NK cell lytic granules and regulation of their exocytosis', *Frontiers in Immunology*, 3, p. 335. doi:10.3389/fimmu.2012.00335.

Krzywinska, E. *et al.* (2016) 'CD45 Isoform Profile Identifies Natural Killer (NK) Subsets with Differential Activity', *PLOS ONE*, 11(4), p. e0150434. doi:10.1371/journal.pone.0150434.

Kumar, S. (2018) 'Natural killer cell cytotoxicity and its regulation by inhibitory receptors', *Immunology*, 154(3), pp. 383–393. doi:10.1111/imm.12921.

Kumari, N. *et al.* (2016) 'Role of interleukin-6 in cancer progression and therapeutic resistance', *Tumor Biology*, 37(9), pp. 11553–11572. doi:10.1007/s13277-016-5098-7.

Kuo, P.T. *et al.* (2018) 'The Role of CXCR3 and Its Chemokine Ligands in Skin Disease and Cancer', *Frontiers in Medicine*, 5. doi:10.3389/fmed.2018.00271.

Kurioka, A. *et al.* (2018) 'CD161 Defines a Functionally Distinct Subset of Pro-Inflammatory Natural Killer Cells', *Frontiers in Immunology*, 9. doi:10.3389/fimmu.2018.00486.

Lai, L. *et al.* (2015) 'A CD45-based barcoding approach to multiplex mass-cytometry (CyTOF)', *Cytometry*, 87(4), pp. 369–374. doi:10.1002/cyto.a.22640.

Lakschevitz, F.S. *et al.* (2016) 'Identification of neutrophil surface marker changes in health and inflammation using high-throughput screening flow cytometry', *Experimental Cell Research*, 342(2), pp. 200–209. doi:10.1016/j.yexcr.2016.03.007.

Lakshmikanth, T. *et al.* (2020) 'Human Immune System Variation during 1 Year', *Cell Reports*, 32(3). doi:10.1016/j.celrep.2020.107923.

Lancashire, E.R. *et al.* (2010) 'Educational attainment among adult survivors of childhood cancer in Great Britain: a population-based cohort study', *Journal of the National Cancer Institute*, 102(4), pp. 254–270. doi:10.1093/jnci/djp498.

Lasek, W., Zagożdżon, R. and Jakobisiak, M. (2014) 'Interleukin 12: still a promising candidate for tumor immunotherapy?', *Cancer Immunology, Immunotherapy*, 63(5), pp. 419–435. doi:10.1007/s00262-014-1523-1.

Le Dréan, E. *et al.* (1998) 'Inhibition of antigen-induced T cell response and antibody-induced NK cell cytotoxicity by NKG2A: association of NKG2A with SHP-1 and SHP-2 protein-tyrosine phosphatases', *European Journal of Immunology*, 28(1), pp. 264–276. doi:10.1002/(SICI)1521-4141(199801)28:01<264::AID-IMMU264>3.0.CO;2-O.

Le Garff-Tavernier, M. *et al.* (2010) 'Human NK cells display major phenotypic and functional changes over the life span', *Aging Cell*, 9(4), pp. 527–535. doi:10.1111/j.1474-9726.2010.00584.x.

Le Gars, M. *et al.* (2019) 'Pregnancy-Induced Alterations in NK Cell Phenotype and Function', *Frontiers in Immunology*, 10. doi:10.3389/fimmu.2019.02469.

LeBien, T.W. and Tedder, T.F. (2008) 'B lymphocytes: how they develop and function', *Blood*, 112(5), pp. 1570–1580. doi:10.1182/blood-2008-02-078071.

Lee, B.H. and Rahman, A.H. (2019) 'Acquisition, Processing, and Quality Control of Mass Cytometry Data', in McGuire, H.M. and Ashhurst, T.M. (eds) *Mass Cytometry: Methods and Protocols*. New York, NY: Springer (Methods in Molecular Biology), pp. 13–31. doi:10.1007/978-1-4939-9454-0_2.

Lee, E.H. *et al.* (2020) 'Race/Ethnicity Among Children With COVID-19–Associated Multisystem Inflammatory Syndrome', *JAMA Network Open*, 3(11). doi:10.1001/jamanetworkopen.2020.30280.

Lee, P.-I. *et al.* (2020) 'Are children less susceptible to COVID-19?', *Journal of Microbiology, Immunology and Infection*, 53(3), pp. 371–372. doi:10.1016/j.jmii.2020.02.011.

Lee, P.Y. *et al.* (2020) 'Distinct clinical and immunological features of SARS–CoV-2–induced multisystem inflammatory syndrome in children', *The Journal of Clinical Investigation*, 130(11), pp. 5942–5950. doi:10.1172/JCI141113.

Lee, S.-H., Fragoso, M.F. and Biron, C.A. (2012) 'Cutting edge: a novel mechanism bridging innate and adaptive immunity: IL-12 induction of CD25 to form high-affinity IL-2 receptors on NK cells', *Journal of Immunology (Baltimore, Md.: 1950)*, 189(6), pp. 2712–2716. doi:10.4049/jimmunol.1201528.

Levine, J.H. *et al.* (2015) 'Data-Driven Phenotypic Dissection of AML Reveals Progenitor-like Cells that Correlate with Prognosis', *Cell*, 162(1), pp. 184–197. doi:10.1016/j.cell.2015.05.047.

Li, S. *et al.* (2018) 'Plasminogen activator inhibitor-1 in cancer research', *Biomedicine & Pharmacotherapy*, 105, pp. 83–94. doi:10.1016/j.biopha.2018.05.119.

Libri, V. *et al.* (2011) 'Cytomegalovirus infection induces the accumulation of short-lived, multifunctional CD4+CD45RA+CD27+ T cells: the potential involvement of interleukin-7 in this process', *Immunology*, 132(3), pp. 326–339. doi:10.1111/j.1365-2567.2010.03386.x.

Lieberman, J. (2003) 'The ABCs of granule-mediated cytotoxicity: new weapons in the arsenal', *Nature Reviews. Immunology*, 3(5), pp. 361–370. doi:10.1038/nri1083.

Lim, S.P. *et al.* (2020) 'Treg sensitivity to FasL and relative IL-2 deprivation drive idiopathic aplastic anemia immune dysfunction', *Blood*, 136(7), pp. 885–897. doi:10.1182/blood.2019001347.

Lin, R.J., Afshar-Kharghan, V. and Schafer, A.I. (2014) 'Paraneoplastic thrombocytosis: the secrets of tumor self-promotion', *Blood*, 124(2), pp. 184–187. doi:10.1182/blood-2014-03-562538.

Lin, Y. and Okada, H. (2016) 'Cellular immunotherapy for malignant gliomas', *Expert opinion on biological therapy*, 16(10), pp. 1265–1275. doi:10.1080/14712598.2016.1214266.

Liu, W. *et al.* (2006) 'CD127 expression inversely correlates with FoxP3 and suppressive function of human CD4+ T reg cells', *The Journal of Experimental Medicine*, 203(7), pp. 1701–1711. doi:10.1084/jem.20060772.

Liu, X. *et al.* (2019) 'A comparison framework and guideline of clustering methods for mass cytometry data', *Genome Biology*, 20, p. 297. doi:10.1186/s13059-019-1917-7.

Lopez-Vergès, S. *et al.* (2010) 'CD57 defines a functionally distinct population of mature NK cells in the human CD56dimCD16+ NK-cell subset', *Blood*, 116(19), pp. 3865–3874. doi:10.1182/blood-2010-04-282301.

Louis, D.N. *et al.* (2007) 'The 2007 WHO classification of tumours of the central nervous system', *Acta Neuropathologica*, 114(2), pp. 97–109. doi:10.1007/s00401-007-0243-4.

Maaten, L. van der and Hinton, G. (2008) 'Visualizing Data using t-SNE', *Journal of Machine Learning Research*, 9(86), pp. 2579–2605.

Mace, E.M. *et al.* (2014) 'Cell biological steps and checkpoints in accessing NK cell cytotoxicity', *Immunology and Cell Biology*, 92(3), pp. 245–255. doi:10.1038/icb.2013.96.

Maecker, H.T., McCoy, J.P. and Nussenblatt, R. (2012) 'Standardizing immunophenotyping for the Human Immunology Project', *Nature Reviews. Immunology*, 12(3), pp. 191–200. doi:10.1038/nri3158.

Majzner, R.G., Heitzeneder, S. and Mackall, C.L. (2017) 'Harnessing the Immunotherapy Revolution for the Treatment of Childhood Cancers', *Cancer Cell*, 31(4), pp. 476–485. doi:10.1016/j.ccell.2017.03.002.

Mamessier, E. *et al.* (2013) 'Peripheral blood NK cells from breast cancer patients are tumor-induced composite subsets', *Journal of Immunology (Baltimore, Md.: 1950)*, 190(5), pp. 2424–2436. doi:10.4049/jimmunol.1200140.

Marini, O. *et al.* (2017) 'Mature CD10+ and immature CD10- neutrophils present in G-CSF-treated donors display opposite effects on T cells', *Blood*, 129(10), pp. 1343–1356. doi:10.1182/blood-2016-04-713206.

Maris, J.M. and Denny, C.T. (2002) 'Focus on embryonal malignancies', *Cancer Cell*, 2(6), pp. 447–450. doi:10.1016/S1535-6108(02)00206-4.

Marshall, G.M. *et al.* (2014) 'The prenatal origins of cancer', *Nature Reviews. Cancer*, 14(4), pp. 277–289. doi:10.1038/nrc3679.

Martín-Fontecha, A. *et al.* (2004) 'Induced recruitment of NK cells to lymph nodes provides IFN-gamma for T(H)1 priming', *Nature Immunology*, 5(12), pp. 1260–1265. doi:10.1038/ni1138.

Massini, G., Siemer, D. and Hohaus, S. (2009) 'EBV in Hodgkin Lymphoma', *Mediterranean Journal of Hematology and Infectious Diseases*, 1(2), p. e2009013. doi:10.4084/MJHID.2009.013.

Masuzawa, Y. *et al.* (2015) 'Elevated D-dimer level is a risk factor for coronary artery lesions accompanying intravenous immunoglobulin-unresponsive Kawasaki disease', *Therapeutic Apheresis and Dialysis: Official Peer-Reviewed Journal of the International Society for Apheresis, the Japanese Society for Apheresis, the Japanese Society for Dialysis Therapy*, 19(2), pp. 171–177. doi:10.1111/1744-9987.12235.

Mathew, D. *et al.* (2020) 'Deep immune profiling of COVID-19 patients reveals distinct immunotypes with therapeutic implications', *Science*, 369(6508). doi:10.1126/science.abc8511.

McCrindle Brian W. *et al.* (2017) 'Diagnosis, Treatment, and Long-Term Management of Kawasaki Disease: A Scientific Statement for Health Professionals From the American Heart Association', *Circulation*, 135(17), pp. e927–e999. doi:10.1161/CIR.0000000000000484.

McDowell, H. (2003) 'Update on childhood rhabdomyosarcoma', *Archives of Disease in Childhood*, 88(4), pp. 354–357. doi:10.1136/adc.88.4.354.

McElroy, A.K. *et al.* (2015) 'Human Ebola virus infection results in substantial immune activation', *Proceedings of the National Academy of Sciences*, 112(15), pp. 4719–4724. doi:10.1073/pnas.1502619112.

McGinty, L. and Kolesar, J. (2017) 'Dinutuximab for maintenance therapy in pediatric neuroblastoma', *American journal of health-system pharmacy: AJHP: official journal of the American Society of Health-System Pharmacists*, 74(8), pp. 563–567. doi:10.2146/ajhp160228.

McInnes, L. *et al.* (2018) 'UMAP: Uniform Manifold Approximation and Projection', *Journal of Open Source Software*, 3(29), p. 861. doi:10.21105/joss.00861.

McInnes, L., Healy, J. and Melville, J. (2020) 'UMAP: Uniform Manifold Approximation and Projection for Dimension Reduction', *arXiv:1802.03426 [cs, stat]* [Preprint]. Available at: http://arxiv.org/abs/1802.03426 (Accessed: 28 July 2021).

McKechnie, J.L. *et al.* (2020) 'Mass Cytometry Analysis of the NK Cell Receptor–Ligand Repertoire Reveals Unique Differences between Dengue-Infected Children and Adults', *ImmunoHorizons*, 4(10), pp. 634–647. doi:10.4049/immunohorizons.2000074.

McKinnon, K.M. (2018) 'Flow Cytometry: An Overview', *Current protocols in immunology*, 120, p. 5.1.1-5.1.11. doi:10.1002/cpim.40.

Mellman, I., Coukos, G. and Dranoff, G. (2011) 'Cancer immunotherapy comes of age', *Nature*, 480(7378), pp. 480–489. doi:10.1038/nature10673.

Mengos, A.E., Gastineau, D.A. and Gustafson, M.P. (2019) 'The CD14+HLA-DRlo/neg Monocyte: An Immunosuppressive Phenotype That Restrains Responses to Cancer Immunotherapy', *Frontiers in Immunology*, 10, p. 1147. doi:10.3389/fimmu.2019.01147.

Michel, T. *et al.* (2016) 'Human CD56bright NK Cells: An Update', *The Journal of Immunology*, 196(7), pp. 2923–2931. doi:10.4049/jimmunol.1502570.

Mittal, D. *et al.* (2014) 'New insights into cancer immunoediting and its three component phases — elimination, equilibrium and escape', *Current opinion in immunology*, 27, pp. 16–25. doi:10.1016/j.coi.2014.01.004.

Mohamadian, M. *et al.* (2021) 'COVID-19: Virology, biology and novel laboratory diagnosis', *The Journal of Gene Medicine*, 23(2), p. e3303. doi:10.1002/jgm.3303.

Molfetta, R. *et al.* (2017) 'Regulation of NKG2D-Dependent NK Cell Functions: The Yin and the Yang of Receptor Endocytosis', *International Journal of Molecular Sciences*, 18(8). doi:10.3390/ijms18081677.

Monaco, E.L. *et al.* (2011) 'Human Leukocyte Antigen E Contributes to Protect Tumor Cells from Lysis by Natural Killer Cells', *Neoplasia (New York, N.Y.)*, 13(9), pp. 822–830.

Morales, E. *et al.* (2020) 'Role of immunotherapy in Ewing sarcoma', *Journal for ImmunoTherapy of Cancer*, 8(2), p. e000653. doi:10.1136/jitc-2020-000653.

Moretta, A. *et al.* (2001) 'Activating receptors and coreceptors involved in human natural killer cell-mediated cytolysis', *Annual Review of Immunology*, 19, pp. 197–223. doi:10.1146/annurev.immunol.19.1.197.

Mosmann, T.R. *et al.* (1986) 'Two types of murine helper T cell clone. I. Definition according to profiles of lymphokine activities and secreted proteins', *Journal of Immunology (Baltimore, Md.: 1950)*, 136(7), pp. 2348–2357.

Mosmann, T.R. (1992) 'T lymphocyte subsets, cytokines, and effector functions', *Annals of the New York Academy of Sciences*, 664, pp. 89–92. doi:10.1111/j.1749-6632.1992.tb39751.x.

Mosmann, T.R. and Coffman, R.L. (1989) 'TH1 and TH2 cells: different patterns of lymphokine secretion lead to different functional properties', *Annual Review of Immunology*, 7, pp. 145–173. doi:10.1146/annurev.iy.07.040189.001045.

Multisystem inflammatory syndrome in children and adolescents temporally related to COVID-19 (no date). Available at: https://www.who.int/news-

room/commentaries/detail/multisystem-inflammatory-syndrome-in-children-and-adolescents-with-covid-19 (Accessed: 27 July 2021).

Munder, M. *et al.* (2005) 'Arginase I is constitutively expressed in human granulocytes and participates in fungicidal activity', *Blood*, 105(6), pp. 2549–2556. doi:10.1182/blood-2004-07-2521.

Murphy, K. and Weaver, C. (2016) *Janeway's Immunobiology*. 9th edition. New York, NY: Garland Science.

Nagel, J.E., Collins, G.D. and Adler, W.H. (1981) 'Spontaneous or natural killer cytotoxicity of K562 erythroleukemic cells in normal patients', *Cancer Research*, 41(6), pp. 2284–2288.

Nakagawa, K., Lokugamage, K.G. and Makino, S. (2016) 'Viral and Cellular mRNA Translation in Coronavirus-Infected Cells', *Advances in Virus Research*, 96, pp. 165–192. doi:10.1016/bs.aivir.2016.08.001.

Neelapu, S.S. *et al.* (2020) 'Society for Immunotherapy of Cancer (SITC) clinical practice guideline on immunotherapy for the treatment of lymphoma', *Journal for Immunotherapy of Cancer*, 8(2), p. e001235. doi:10.1136/jitc-2020-001235.

Nimmerjahn, F. and Ravetch, J.V. (2008) 'Fcgamma receptors as regulators of immune responses', *Nature Reviews. Immunology*, 8(1), pp. 34–47. doi:10.1038/nri2206.

Niu, C. *et al.* (2020) 'PD-1-positive Natural Killer Cells have a weaker antitumor function than that of PD-1-negative Natural Killer Cells in Lung Cancer', *International Journal of Medical Sciences*, 17(13), pp. 1964–1973. doi:10.7150/ijms.47701.

Oghumu, S. *et al.* (2015) 'CXCR3 expression defines a novel subset of innate CD8+ T cells that enhance immunity against bacterial infection and cancer upon stimulation with IL-15', *The FASEB Journal*, 29(3), pp. 1019–1028. doi:10.1096/fj.14-264507.

Okada, T. and Cyster, J.G. (2006) 'B cell migration and interactions in the early phase of antibody responses', *Current Opinion in Immunology*, 18(3), pp. 278–285. doi:10.1016/j.coi.2006.02.005.

Olin, A. *et al.* (2018) 'Stereotypic Immune System Development in Newborn Children', *Cell*, 174(5), pp. 1277-1292.e14. doi:10.1016/j.cell.2018.06.045.

Olingy, C.E. *et al.* (2017) 'Non-classical monocytes are biased progenitors of wound healing macrophages during soft tissue injury', *Scientific Reports*, 7(1), p. 447. doi:10.1038/s41598-017-00477-1.

Paediatric multisystem inflammatory syndrome temporally associated with COVID-19 (PIMS) - guidance for clinicians (no date) *RCPCH*. Available at: https://www.rcpch.ac.uk/resources/paediatric-multisystem-inflammatory-syndrome-temporally-associated-covid-19-pims-guidance (Accessed: 23 May 2021).

Peck, A. and Mellins, E.D. (2010) 'Plasticity of T-cell phenotype and function: the T helper type 17 example', *Immunology*, 129(2), pp. 147–153. doi:10.1111/j.1365-2567.2009.03189.x.

Pegram, H.J. *et al.* (2011) 'Activating and inhibitory receptors of natural killer cells', *Immunology and Cell Biology*, 89(2), pp. 216–224. doi:10.1038/icb.2010.78.

Penack, O. *et al.* (2005) 'CD56 dim CD16 neg cells are responsible for natural cytotoxicity against tumor targets', *Leukemia*, 19(5), pp. 835–840. doi:10.1038/sj.leu.2403704.

Pesce, S. *et al.* (2016) 'Human NK Cell Subsets Redistribution in Pathological Conditions: A Role for CCR7 Receptor', *Frontiers in Immunology*, 7. doi:10.3389/fimmu.2016.00414.

Pfeiffer, M. *et al.* (2011) 'CD155 is involved in NK-cell mediated lysis of human hepatoblastoma in vitro', *Frontiers in Bioscience (Elite Edition)*, 3, pp. 1456–1466. doi:10.2741/e346.

Piątosa, B. *et al.* (2010) 'B cell subsets in healthy children: reference values for evaluation of B cell maturation process in peripheral blood', *Cytometry. Part B, Clinical Cytometry*, 78(6), pp. 372–381. doi:10.1002/cyto.b.20536.

Pillay, J. *et al.* (2012) 'A subset of neutrophils in human systemic inflammation inhibits T cell responses through Mac-1', *The Journal of Clinical Investigation*, 122(1), pp. 327–336. doi:10.1172/JCI57990.

Pinti, M. *et al.* (2016) 'Aging of the immune system – focus on inflammation and vaccination', *European journal of immunology*, 46(10), pp. 2286–2301. doi:10.1002/eji.201546178.

Pinto, N.R. *et al.* (2015) 'Advances in Risk Classification and Treatment Strategies for Neuroblastoma', *Journal of Clinical Oncology*, 33(27), pp. 3008–3017. doi:10.1200/JCO.2014.59.4648.

Pistoia, V. *et al.* (2013) 'Immunosuppressive microenvironment in neuroblastoma', *Frontiers in Oncology*, 3, p. 167. doi:10.3389/fonc.2013.00167.

Postow, M.A. *et al.* (2015) 'Nivolumab and ipilimumab versus ipilimumab in untreated melanoma', *The New England Journal of Medicine*, 372(21), pp. 2006–2017. doi:10.1056/NEJMoa1414428.

Pritchard-Jones, K. (2007) 'Childhood cancer in Britain: incidence, survival and mortality', *British Journal of Cancer*, 96(12), p. 1927. doi:10.1038/sj.bjc.6603800.

Qiu, P. *et al.* (2011) 'Extracting a cellular hierarchy from high-dimensional cytometry data with SPADE', *Nature Biotechnology*, 29(10), pp. 886–891. doi:10.1038/nbt.1991.

Raffaghello, L. *et al.* (2007) 'Expression and Functional Analysis of Human Leukocyte Antigen Class I Antigen-Processing Machinery in Medulloblastoma', *Cancer Research*, 67(11), pp. 5471–5478. doi:10.1158/0008-5472.CAN-06-4735.

Raphael, I. *et al.* (2015) 'T cell subsets and their signature cytokines in autoimmune and inflammatory diseases', *Cytokine*, 74(1), pp. 5–17. doi:10.1016/j.cyto.2014.09.011.

Ren, W. *et al.* (2015) 'Plasminogen activator inhibitor-1 regulates LPS-induced TLR4/MD-2 pathway activation and inflammation in alveolar macrophages', *Inflammation*, 38(1), pp. 384–393. doi:10.1007/s10753-014-0042-8.

Reulen, R.C. *et al.* (2010) 'Long-term cause-specific mortality among survivors of childhood cancer', *JAMA*, 304(2), pp. 172–179. doi:10.1001/jama.2010.923.

Rinaldi, S. *et al.* (2017) 'Paradoxical aging in HIV: immune senescence of B Cells is most prominent in young age', *Aging (Albany NY)*, 9(4), pp. 1307–1322. doi:10.18632/aging.101229.

Riphagen, S. *et al.* (2020) 'Hyperinflammatory shock in children during COVID-19 pandemic', *The Lancet*, 395(10237), pp. 1607–1608. doi:10.1016/S0140-6736(20)31094-1.

Robert, C. *et al.* (2015) 'Pembrolizumab versus Ipilimumab in Advanced Melanoma', *The New England Journal of Medicine*, 372(26), pp. 2521–2532. doi:10.1056/NEJMoa1503093.

Rodríguez-Rubio, M. *et al.* (2021) 'Cytokine Profile in Children with Severe Multisystem Inflammatory Syndrome Related to the Coronavirus Disease 2019', *Journal of Pediatric Intensive Care* [Preprint]. doi:10.1055/s-0041-1724101.

Ruth, J.H. *et al.* (2010) 'Interleukin-18 as an in vivomediator of monocyte recruitment in rodent models of rheumatoid arthritis', *Arthritis Research & Therapy*, 12(3), p. R118. doi:10.1186/ar3055.

Sabat, R. *et al.* (2010) 'Biology of interleukin-10', *Cytokine & Growth Factor Reviews*, 21(5), pp. 331–344. doi:10.1016/j.cytogfr.2010.09.002.

Sadeghi, H.M. *et al.* (1999) 'Phenotypic and functional characteristics of circulating monocytes of elderly persons', *Experimental Gerontology*, 34(8), pp. 959–970. doi:10.1016/s0531-5565(99)00065-0.

Sáez de Guinoa, J. *et al.* (2011) 'CXCL13/CXCR5 signaling enhances BCR-triggered B-cell activation by shaping cell dynamics', *Blood*, 118(6), pp. 1560–1569. doi:10.1182/blood-2011-01-332106.

Salam, N. *et al.* (2013) 'T cell ageing: Effects of age on development, survival & function', *The Indian Journal of Medical Research*, 138(5), pp. 595–608.

Sallusto, F. *et al.* (1999) 'Two subsets of memory T lymphocytes with distinct homing potentials and effector functions', *Nature*, 401(6754), pp. 708–712. doi:10.1038/44385.

Sanz, I. *et al.* (2019) 'Challenges and Opportunities for Consistent Classification of Human B Cell and Plasma Cell Populations', *Frontiers in Immunology*, 10. doi:10.3389/fimmu.2019.02458.

Schatorjé, E.J.H. *et al.* (2012) 'Paediatric reference values for the peripheral T cell compartment', *Scandinavian Journal of Immunology*, 75(4), pp. 436–444. doi:10.1111/j.1365-3083.2012.02671.x.

Schett, G. (2011) 'Effects of inflammatory and anti-inflammatory cytokines on the bone', *European Journal of Clinical Investigation*, 41(12), pp. 1361–1366. doi:10.1111/j.1365-2362.2011.02545.x.

Schuyler, R.P. *et al.* (2019) 'Minimizing Batch Effects in Mass Cytometry Data', *Frontiers in Immunology*, 10, p. 2367. doi:10.3389/fimmu.2019.02367.

Scoville, S.D., Freud, A.G. and Caligiuri, M.A. (2017) 'Modeling Human Natural Killer Cell Development in the Era of Innate Lymphoid Cells', *Frontiers in Immunology*, 8. doi:10.3389/fimmu.2017.00360.

Sebire, N.J. *et al.* (2005) 'Immunohistochemical findings in embryonal small round cell tumors with molecular diagnostic confirmation', *Applied immunohistochemistry & molecular morphology: AIMM*, 13(1), pp. 1–5. doi:10.1097/00129039-200503000-00001.

Seckinger, P. *et al.* (1987) 'A urine inhibitor of interleukin 1 activity that blocks ligand binding', *Journal of Immunology (Baltimore, Md.: 1950)*, 139(5), pp. 1546–1549.

Shimodaira, S. *et al.* (2016) 'Dendritic Cell-Based Cancer Immunotherapy Targeting Wilms' Tumor 1 for Pediatric Cancer', in van den Heuvel-Eibrink, M.M. (ed.) *Wilms Tumor*. Brisbane (AU): Codon Publications. Available at: http://www.ncbi.nlm.nih.gov/books/NBK373368/ (Accessed: 14 July 2021).

Shirvani, S.S. *et al.* (2019) 'The molecular and clinical evidence of vitamin D signaling as a modulator of the immune system: Role in Behçet's disease', *Immunology Letters*, 210, pp. 10–19. doi:10.1016/j.imlet.2019.03.017.

Shlomchik, M.J. (2008) 'Sites and stages of autoreactive B cell activation and regulation', *Immunity*, 28(1), pp. 18–28. doi:10.1016/j.immuni.2007.12.004.

Simon, A.K., Hollander, G.A. and McMichael, A. (2015) 'Evolution of the immune system in humans from infancy to old age', *Proceedings of the Royal Society B: Biological Sciences*, 282(1821), p. 20143085. doi:10.1098/rspb.2014.3085.

Sims, G.P. *et al.* (2005) 'Identification and characterization of circulating human transitional B cells', *Blood*, 105(11), pp. 4390–4398. doi:10.1182/blood-2004-11-4284.

Somersalo, K. *et al.* (1992) 'Involvement of beta 2-integrins in the migration of human natural killer cells.', *The Journal of Immunology*, 149(2), pp. 590–598.

Stagi, S. *et al.* (2016) 'Severe vitamin D deficiency in patients with Kawasaki disease: a potential role in the risk to develop heart vascular abnormalities?', *Clinical Rheumatology*, 35(7), pp. 1865–1872. doi:10.1007/s10067-015-2970-6.

Statement on the second meeting of the International Health Regulations (2005) Emergency Committee regarding the outbreak of novel coronavirus (2019-nCoV) (no date). Available at: https://www.who.int/news/item/30-01-2020-statement-on-the-second-meeting-of-the-international-health-regulations-(2005)-emergency-committee-regarding-the-outbreak-of-novel-coronavirus-(2019-ncov) (Accessed: 26 July 2021).

Stein, J.V. and Nombela-Arrieta, C. (2005) 'Chemokine control of lymphocyte trafficking: a general overview', *Immunology*, 116(1), pp. 1–12. doi:10.1111/j.1365-2567.2005.02183.x.

Steliarova-Foucher, E. *et al.* (2005) 'International Classification of Childhood Cancer, third edition', *Cancer*, 103(7), pp. 1457–1467. doi:10.1002/cncr.20910.

Steliarova-Foucher, Eva *et al.* (2017) 'International incidence of childhood cancer, 2001–10: a population-based registry study', *The Lancet Oncology*, 18(6), pp. 719–731. doi:10.1016/S1470-2045(17)30186-9.

Stoeckius, M. *et al.* (2017) 'Large-scale simultaneous measurement of epitopes and transcriptomes in single cells', *Nature methods*, 14(9), pp. 865–868. doi:10.1038/nmeth.4380.

Strzepa, A., Pritchard, K.A. and Dittel, B.N. (2017) 'Myeloperoxidase: A new player in autoimmunity', *Cellular immunology*, 317, pp. 1–8. doi:10.1016/j.cellimm.2017.05.002.

Sundar, R. *et al.* (2015) 'Nivolumab in NSCLC: latest evidence and clinical potential', *Therapeutic Advances in Medical Oncology*, 7(2), pp. 85–96. doi:10.1177/1758834014567470.

Syrimi, E., Fennell, E., Richter, A., Vrljicak, P., Stark, R., Ott, S., Murray, P.G., Al-Abadi, E., Chikermane, A., Dawson, P., Hackett, S., Jyothish, D., Kanthimathinathan, H.K., Monaghan, S., Nagakumar, P., Scholefield, B.R., Welch, S., Khan, N., Faustini, S., Davies, K., *et al.* (2021) 'The immune landscape of SARS-CoV-2-associated Multisystem Inflammatory Syndrome in Children (MIS-C) from acute disease to recovery', *iScience*, 24(11), p. 103215. doi:10.1016/j.isci.2021.103215.

Syrimi, E., Fennell, E., Richter, A., Vrljicak, P., Stark, R., Ott, S., Murray, P.G., Al-Abadi, E., Chikermane, A., Dawson, P., Hackett, S., Jyothish, D., Kanthimathinathan, H.K., Monaghan, S., Nagakumar, P., Scholefield, B.R., Welch, S., Khan, N., Faustini, S., Kearns, P., *et al.* (2021) *The innate and adaptive immune landscape of SARS-CoV-2-associated Multisystem Inflammatory Syndrome in Children (MIS-C) from acute disease to recovery*, p. 2020.08.06.20164848. doi:10.1101/2020.08.06.20164848.

Tak, T. *et al.* (2017) 'Neutrophil-mediated Suppression of Influenza-induced Pathology Requires CD11b/CD18 (MAC-1)', *American Journal of Respiratory Cell and Molecular Biology*, 58(4), pp. 492–499. doi:10.1165/rcmb.2017-0021OC.

Takahashi, C. *et al.* (2017) 'Mass cytometry panel optimization through the designed distribution of signal interference', *Cytometry Part A*, 91(1), pp. 39–47. doi:10.1002/cyto.a.22977.

Takeshita, S. *et al.* (2017) 'The Role of Neutrophil Activation in the Pathogenesis of Kawasaki Disease', *Pediatric Infectious Diseases: Open Access*, 3(1). doi:10.21767/2573-0282.100057.

Tay, R.E., Richardson, E.K. and Toh, H.C. (2021) 'Revisiting the role of CD4 + T cells in cancer immunotherapy—new insights into old paradigms', *Cancer Gene Therapy*, 28(1), pp. 5–17. doi:10.1038/s41417-020-0183-x.

Taylor, D.M. *et al.* (2019) 'The Pediatric Cell Atlas: Defining the Growth Phase of Human Development at Single-Cell Resolution', *Developmental Cell*, 49(1), pp. 10–29. doi:10.1016/j.devcel.2019.03.001.

Teng, M.W.L. *et al.* (2010) 'IL-23 suppresses innate immune response independently of IL-17A during carcinogenesis and metastasis', *Proceedings of the National Academy of Sciences*, 107(18), pp. 8328–8333. doi:10.1073/pnas.1003251107.

Terry, R.L. *et al.* (2020) 'Immune profiling of pediatric solid tumors', *The Journal of Clinical Investigation*, 130(7), pp. 3391–3402. doi:10.1172/JCI137181.

Topham, N.J. and Hewitt, E.W. (2009) 'Natural killer cell cytotoxicity: how do they pull the trigger?', *Immunology*, 128(1), pp. 7–15. doi:10.1111/j.1365-2567.2009.03123.x.

Trapani, J.A. and Bird, P.I. (2008) 'A renaissance in understanding the multiple and diverse functions of granzymes?', *Immunity*, 29(5), pp. 665–667. doi:10.1016/j.immuni.2008.10.002.

Tulla, M. *et al.* (2015) 'Incidence, Trends, and Survival of Children With Embryonal Tumors', *Pediatrics*, 136(3), pp. e623–e632. doi:10.1542/peds.2015-0224.

Uday, S. *et al.* (2018) 'Cardiac, bone and growth plate manifestations in hypocalcemic infants: revealing the hidden body of the vitamin D deficiency iceberg', *BMC Pediatrics*, 18(1), p. 183. doi:10.1186/s12887-018-1159-y.

van Unen, V. *et al.* (2016) 'Mass Cytometry of the Human Mucosal Immune System Identifies Tissue- and Disease-Associated Immune Subsets', *Immunity*, 44(5), pp. 1227–1239. doi:10.1016/j.immuni.2016.04.014.

Van Gassen, S. *et al.* (2015) 'FlowSOM: Using self-organizing maps for visualization and interpretation of cytometry data', *Cytometry. Part A: The Journal of the International Society for Analytical Cytology*, 87(7), pp. 636–645. doi:10.1002/cyto.a.22625.

Vandenabeele, P. *et al.* (1995) 'Two tumour necrosis factor receptors: structure and function', *Trends in Cell Biology*, 5(10), pp. 392–399. doi:10.1016/s0962-8924(00)89088-1.

Vella, L.A. *et al.* (2020) 'Deep Immune Profiling of MIS-C demonstrates marked but transient immune activation compared to adult and pediatric COVID-19', *medRxiv*, p. 2020.09.25.20201863. doi:10.1101/2020.09.25.20201863.

Vella, L.A. *et al.* (2021) 'Deep immune profiling of MIS-C demonstrates marked but transient immune activation compared to adult and pediatric COVID-19', *Science Immunology*, 6(57). doi:10.1126/sciimmunol.abf7570.

Verdoni, L. *et al.* (2020) 'An outbreak of severe Kawasaki-like disease at the Italian epicentre of the SARS-CoV-2 epidemic: an observational cohort study', *The Lancet*, 395(10239), pp. 1771–1778. doi:10.1016/S0140-6736(20)31103-X.

Vivier, E. *et al.* (2008) 'Functions of natural killer cells', *Nature Immunology*, 9(5), pp. 503–510. doi:10.1038/ni1582.

Voss, D. *et al.* (2009) 'Studies on membrane topology, N-glycosylation and functionality of SARS-CoV membrane protein', *Virology Journal*, 6, p. 79. doi:10.1186/1743-422X-6-79.

Wang, H.-W. *et al.* (2019) 'Diagnosis of Hodgkin Lymphoma in the Modern Era', *British journal of haematology*, 184(1), pp. 45–59. doi:10.1111/bjh.15614.

Wang, Y. *et al.* (2017) 'Germinal-center development of memory B cells driven by IL-9 from follicular helper T cells', *Nature Immunology*, 18(8), pp. 921–930. doi:10.1038/ni.3788.

Wedekind, M.F. *et al.* (2018) 'Pediatric Cancer Immunotherapy: Opportunities and Challenges', *Paediatric Drugs*, 20(5), pp. 395–408. doi:10.1007/s40272-018-0297-x.

Weiss, G.E. *et al.* (2009) 'Atypical memory B cells are greatly expanded in individuals living in a malaria-endemic area', *Journal of Immunology (Baltimore, Md.: 1950)*, 183(3), pp. 2176–2182. doi:10.4049/jimmunol.0901297.

Wendel, M. *et al.* (2008) 'Natural killer cell accumulation in tumors is dependent on IFN-gamma and CXCR3 ligands', *Cancer Research*, 68(20), pp. 8437–8445. doi:10.1158/0008-5472.CAN-08-1440.

Weng, K.-P. *et al.* (2013) 'Interleukin-18 and coronary artery lesions in patients with Kawasaki disease', *Journal of the Chinese Medical Association*, 76(8), pp. 438–445. doi:10.1016/j.jcma.2013.04.005.

West, S.D. *et al.* (2012) 'Transforming growth factor-β, macrophage colony-stimulating factor and C-reactive protein levels correlate with CD14(high)CD16+ monocyte induction and activation in trauma patients', *PloS One*, 7(12), p. e52406. doi:10.1371/journal.pone.0052406.

White, M.K. *et al.* (2005) 'Human polyomaviruses and brain tumors', *Brain Research. Brain Research Reviews*, 50(1), pp. 69–85. doi:10.1016/j.brainresrev.2005.04.007.

Whittaker, E. *et al.* (2020) 'Clinical Characteristics of 58 Children With a Pediatric Inflammatory Multisystem Syndrome Temporally Associated With SARS-CoV-2', *JAMA*, 324(3), pp. 259–269. doi:10.1001/jama.2020.10369.

WHO Director-General's opening remarks at the media briefing on COVID-19 - 11 March 2020 (no date). Available at: https://www.who.int/director-general/speeches/detail/who-director-general-s-opening-remarks-at-the-media-briefing-on-covid-19---11-march-2020 (Accessed: 26 July 2021).

Why children die - research and recommendations (2014) (no date) *RCPCH*. Available at: https://www.rcpch.ac.uk/resources/why-children-die-research-recommendations (Accessed: 27 January 2020).

Willis RA (no date) *The pathology of the tumours of children*. Edinburgh, UK: Oliver and Boyd.

Winter, D. *et al.* (2007) 'Down-modulation of CXCR3 surface expression and function in CD8+ T cells from cutaneous T cell lymphoma patients', *Journal of Immunology (Baltimore, Md.: 1950)*, 179(6), pp. 4272–4282. doi:10.4049/jimmunol.179.6.4272.

Wollmann, M. *et al.* (2014) 'Reticulocyte maturity indices in iron deficiency anemia', *Revista Brasileira de Hematologia e Hemoterapia*, 36(1), pp. 25–28. doi:10.5581/1516-8484.20140009.

Wu, J. *et al.* (2019) 'IL-6 and IL-8 secreted by tumour cells impair the function of NK cells via the STAT3 pathway in oesophageal squamous cell carcinoma', *Journal of Experimental & Clinical Cancer Research*, 38(1), p. 321. doi:10.1186/s13046-019-1310-0.

Yabuhara, A., Kawai, H. and Komiyama, A. (1990) 'Development of natural killer cytotoxicity during childhood: marked increases in number of natural killer cells with adequate cytotoxic abilities during infancy to early childhood', *Pediatric Research*, 28(4), pp. 316–322. doi:10.1203/00006450-199010000-00002.

Yan, J., Smyth, M.J. and Teng, M.W.L. (2018) 'Interleukin (IL)-12 and IL-23 and Their Conflicting Roles in Cancer', *Cold Spring Harbor Perspectives in Biology*, 10(7), p. a028530. doi:10.1101/cshperspect.a028530.

Yılmaz, K. and Şen, V. (2020) 'Is vitamin D deficiency a risk factor for COVID-19 in children?', *Pediatric Pulmonology*, 55(12), pp. 3595–3601. doi:10.1002/ppul.25106.

Yokoyama, W.M. and Kim, S. (2006) 'Licensing of natural killer cells by self-major histocompatibility complex class I', *Immunological Reviews*, 214, pp. 143–154. doi:10.1111/j.1600-065X.2006.00458.x.

Yu, J.C. *et al.* (2018) 'Innate Immunity of Neonates and Infants', *Frontiers in Immunology*, 0. doi:10.3389/fimmu.2018.01759.

Zalocusky, K.A. *et al.* (2018) 'The 10,000 Immunomes Project: Building a Resource for Human Immunology', *Cell Reports*, 25(2), pp. 513-522.e3. doi:10.1016/j.celrep.2018.09.021.

Zhang, Y. *et al.* (2007) 'In vivo kinetics of human natural killer cells: the effects of ageing and acute and chronic viral infection', *Immunology*, 121(2), pp. 258–265. doi:10.1111/j.1365-2567.2007.02573.x.

Zhao, Z. *et al.* (2019) 'Delivery strategies of cancer immunotherapy: recent advances and future perspectives', *Journal of Hematology & Oncology*, 12. doi:10.1186/s13045-019-0817-3.

Zhen, Z. *et al.* (2016) 'Involvement of IL-10 and TGF-β in HLA-E-mediated neuroblastoma migration and invasion', *Oncotarget*, 7(28), pp. 44340–44349. doi:10.18632/oncotarget.10041.

Ziegler-Heitbrock, L. *et al.* (2010a) 'Nomenclature of monocytes and dendritic cells in blood', *Blood*, 116(16), pp. e74–e80. doi:10.1182/blood-2010-02-258558.

Ziegler-Heitbrock, L. *et al.* (2010b) 'Nomenclature of monocytes and dendritic cells in blood', *Blood*, 116(16), pp. e74–e80. doi:10.1182/blood-2010-02-258558.

Zmijewski, J.W. *et al.* (2011) 'Inhibition of neutrophil apoptosis by PAI-1', *American Journal of Physiology. Lung Cellular and Molecular Physiology*, 301(2), pp. L247-254. doi:10.1152/ajplung.00075.2011.